Spring 2018

A new signal processing method for acoustic emission/microseismic data analysis

Charles Mborah

Recommended Citation

A NEW SIGNAL PROCESSING METHOD FOR ACOUSTIC

EMISSION/MICROSEISMIC DATA ANALYSIS

by

CHARLES MBORAH

A DISSERTATION

Presented to the Faculty of the Graduate School of the

MISSOURI UNIVERSITY OF SCIENCE AND TECHNOLOGY

In Partial Fulfillment of the Requirements for the Degree

DOCTOR OF PHILOSOPHY

in

MINING ENGINEERING

2018

Approved by:

Dr. Moachen Ge, Advisor
Dr. Samuel Frimpong, Co-advisor
Dr. Galecki Grzegorz
Dr. Nassib Aouad
Dr. Stephen S. Gao
Dr. Xiaoming He

ABSTRACT

The acoustic emission/microseismic technique (AE/MS) has emerged as one of the most important techniques in recent decades and has found wide applications in different fields. Extraction of seismic event with precise timing is the first step and also the foundation for processing AE/MS signals. However, this process remains a challenging task for most AE/MS applications. The process has generally been performed by human analysts. However, manual processing is time consuming and subjective. These challenges continue to provide motivation for the search for new and innovative ways to improve the signal processing needs of the AE/MS technique. This research has developed a highly efficient method to resolve the problems of background noise and outburst activities characteristic of AE/MS data to enhance the picking of P-phase onset time. The method is a hybrid technique, comprising the characteristic function (CF), high order statistics, stationary discrete wavelet transform (SDWT), and a phase association theory. The performance of the algorithm has been evaluated with data from a coal mine and a 3-D concrete pile laboratory experiment. The accuracy of picking was found to be highly dependent on the choice of wavelet function, the decomposition scale, CF, and window size. The performance of the algorithm has been compared with that of a human expert and the following pickers: the short-term average to long-term average (STA/LTA), the Baer and Kradolfer, the modified energy ratio, and the short-term to long-term kurtosis. The results show that the proposed method has better picking accuracy (84% to 78% based on data from a coal mine) than the STA/LTA. The introduction of the phase association theory and the SDWT method in this research provided a novelty, which has not been seen in any of the previous algorithms.

ACKNOWLEDGMENTS

TABLE OF CONTENTS

LIST OF ILLUSTRATIONS

LIST OF TABLES

NOMENCLATURE

Symbol	Description
AE/MS	Acoustic Emission/Microseismic
NIOSH	National Institute for Occupational Safety and Health
USBM	U.S. Bureau of Mines
WT	Wavelet transform
SDWT	Stationary discrete wavelet transform
HOS	High order statistics
SNR	Signal-to-noise ratio
CF	Characteristic function
FFT	Fast Fourier transform
STFT	windowed or short-time Fourier transform
DWT	Discrete wavelet transform
CWT	Continuous wavelet transform
AR	Autoregressive
AIC	Akaike Information Criteria
AR-AIC	Autoregressive two-model Akaike Information Criterion
STA/LTA	Short-term average to long-term average ratio
WCEDS	Waveform correlation event-detection and location system
ER	Energy ratio
MER	Modified energy ratio picker
STK	Short-term kurtosis
LTK	Long-term kurtosis
S/L-Kurt	Short-term kurtosis and long-term kurtosis ratio picker
PAI-S/K	Phase arrival identification-skewness/kurtosis picker

1. INTRODUCTION

■ BACKGROUND OF RESEARCH PROBLEM

The acoustic emission/microseismic technique (AE/MS) has emerged as one of the most important techniques in recent decades and has found wide applications in the mining and petroleum industries as well as aerospace engineering. In the mining industry, for instance, the technique has been used in applications involving slope stability analysis (surface mining). In underground mining, it has been used for ground control, rockburst, and coal bump monitoring. Uncertainties associated with rock mass stability are generally high in regions affected by mining operations. Therefore, the AE/MS monitoring technique is usually employed to provide a means of establishing zones of instability. In general, when solid bodies/materials are under stress, they emit low-level seismic signals. The AE/MS technique uses the signals generated as a result of a material being under stress to study fracture/failure processes [1].

The AE/MS monitoring technique has three unique advantages over other monitoring techniques: its source location capabilities, global monitoring capabilities, and real-time monitoring capabilities [2]. Implementing and achieving the objectives of the AE/MS monitoring system requires the design of an efficient and robust system to withstand the environment in which it operates. In a mine environment, for example, successful implementation of the system hinges on the following factors:

- planning and optimization of the monitoring system;
- data/signal processing;
- event location; and
- evaluating the location solutions [3].

Planning is essential for achieving and providing a robust monitoring system to ensure long-term performance. According to Ge [3], a diligent engineering assessment of the monitoring objectives and monitoring conditions, the establishment of the number of channels in the monitoring system, and sensor array layout optimization are essential processes required in the early stages of planning.

Practically, event source location remains the most valuable feature of the AE/MS technique due to its ability to delineate the unstable areas of the monitored system. The

accuracy and stability of source location depend on many factors. The quality of data used in the determination of phase arrival remains one of the most important factors if reliable source location is to be achieved [1, 3, 4]. From a source location point of view, data processing is comprised of two interrelated tasks: a rapid extraction of AE/MS events from the recorded data and accurate timing of arrivals of the signals defining each event. The final goal is to provide a set of arrival times that can be used directly for the source location.

The most widely used technique in the detection of phase arrival on AE/MS data is based on the simple amplitude threshold signal detector method. In this technique, separation of the signal of interest ("useful signal") from background noise ("useless signal") is achieved by comparing the AE/MS amplitude with a predetermined threshold level. For cases where the signal to noise ratio (SNR) is high, the technique has been found to be effective [5]. A major challenge with this technique, however, is that the threshold is chosen arbitrarily and therefore could lead to errors in the accuracies of the AE/MS source location. If the AE/MS data is acquired in a noisy environment (for example, in or near a mine operation), the data can be severely affected by excessive background noise leading to low SNRs. Data affected by background noise can be very complex and will ultimately result in unrealistic data analysis. The output signals of the systems used at mines, for instance, are often partly suppressed by the surrounding background noises. This situation makes automatic identification of phase arrival of incoming signals a major challenge in signal processing [3]. Therefore, for an efficient monitoring system, extensive planning should be done to ensure a set-up that can prevent the acquisition of excessive background noise. However, if the noise levels are still high after the acquisition, data processing techniques capable of minimizing noise impact must be adopted to enhance the accuracy of the AE/MS source location. The planning must, therefore, address technical concerns desirable for any efficient AE/MS monitoring system that will ensure that the acquisition and processing stages result in clean data as much as possible [3].

◼◼ STATEMENT OF THE PROBLEM

The quantum of energy normally associated with rockburst can be enormous. Rockburst with a local magnitude of 5.2 ML has been recorded in the past at the Solvay trona mine in Wyoming. The coal mining industry in the United States has in the past

experienced coal bumps with magnitudes up to 4.5 dating back to the 1920s [6]. Catastrophic failures of mine openings, mine equipment damages, halting of mining operations, and many others are some of the different effects of these phenomena. For example, seventy-five (75) lives were reported lost in 1958 due to a rockburst incidence at the Springhill Coal mine in Nova Scotia. Also, there were twenty (20) deaths of miners reported on average every year in South Africa 1997. The main causes of deaths were identified as roof and wall collapses resulting from rockburst [7]. Before 2003, there were about 100 rockburst related fatalities reported in the United States alone [6]. The issues of safety and the cost associated with the occurrence of such events can be enormous. In the United States, statistics from the National Institute for Occupational Safety and Health, [NIOSH] [8] indicate that the fall of ground (e.g., roof fall) constituted about 25% of the fatalities in underground mines from 2009 to 2013 (Figure 1.1).
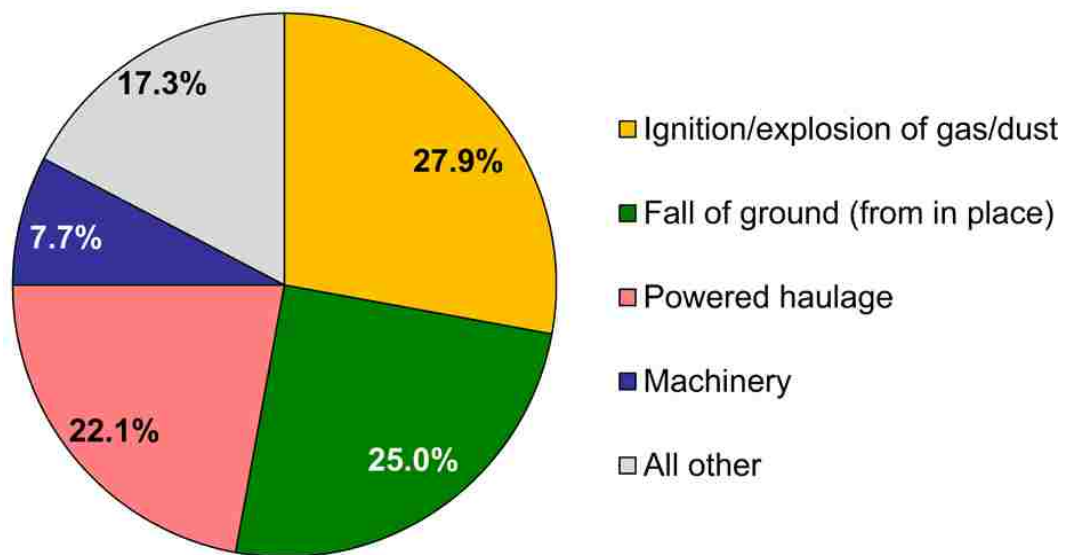
NOTE: "Fall of ground (from in place)" includes MSHA's Accident/Injury/Illness classifications for "Fall of face, rib, pillar, side, or highwall (from in place)" and "Fall of roof, back, or brow (from in place)."

Figure 1.1 Occupational fatalities by accident class, underground mining locations, 2009-2013, excludes office employees [8]

The activities associated with rockbursts are widely monitored by the AE/MS monitoring technique [3, 9]. In fact, the phenomena of mining-induced seismicity and rockbursting have long been key issues in underground hard rock mining. The trend

towards highly mechanized mining operations in Australia, with high extraction ratios operating at increasingly greater depth, led to an increased prevalence and awareness of the problem [10]. The need for an improved understanding of rockbursts and mine seismicity has been driven by their increased occurrence and severity on a worldwide basis due to greater depths of mining and expanded mineral exploration and production [9]. Ge [3] reported a case of spontaneous severe rockburst problems in Canadian mines from the middle of the 1980s to the early 1990s resulting in more than 20 rockburst-prone mines installing AE/MS systems for constant monitoring.

Hasegawa et al [11] provided an account of mine-induced seismicity in Canada with emphasis on potash, coal, and hard-rock mines. Zhang et al [12], on the other hand, reported the utilization of AE/MS monitoring in studying the stability of a crown pillar at Shirengou iron mine in Hebei Province, China during a transition from open pit to underground mining. The activities of underground mining, fault activation, and water seepage had resulted in unstable failure risk of the crown pillar. Using the temporal and spatial distribution of AE/MS events and deformation mechanism, the authors found that the propagation of a buried fault caused the failure of the crown pillar. This, according to the authors, resulted in increased water seepage into the underground drifts. They concluded that the AE/MS method was a useful tool for understanding the damage and fracture process of the crown pillar.

The real-time monitoring ability of the AE/MS method, in terms of event source location, magnitude, and source mechanism, makes it an ideal tool for studying mine seismicity and related underground control problems [3]. In the late 1930s, Obert and Duvall of the U.S. Bureau of Mines (USBM) discovered the release of micro-level sounds by stressed rocks when they were performing sonic studies in deep hard rock mines [13]. Researchers began to utilize the phenomena in the early 1960s for rockburst problems. And for the most part, much of our knowledge has stemmed from the extensive research performed in the Deep South African gold mines and, to a lesser extent, in the coal and metalliferous mines of Eastern Europe [9, 14]. The results obtained by these early researchers further echoed the applicability and great potentials of the use of the AE/MS method for locating rockburst, a fundamental concern of mine AE/MS monitoring [3].

The findings from USBM's research program in the 1960s on the efficiency of the AE/MS technique as a tool for mine safety monitoring set the platform for adopting the AE/MS technique for industrial use. Some of the major findings that revolutionized the technique included the development of hardware and software, as well as field research initiatives [15, 16]. Subsequently, the AE/MS technique has not only found application in hard rock mines but in coal mines as well. The system has been used in coal mines to further understand the ground failures and rock mechanics involved in longwall mining especially in the United States and Australia [17-20]. The AE/MS technique has been transferred from the research paradigm into industry applications for mine safety and ground control monitoring [3].

A successful implementation of the AE/MS monitoring system in any field of application is influenced by several factors. AE/MS signals are usually very weak, rendering data acquisition a challenge in a service environment that is generally very noisy. Signal discrimination and noise reduction are very difficult, yet extremely important for the successful application of the AE/MS technique [21]. Even clean signals can also be extremely complex. These complexities are due to other activities unrelated to the event under consideration. Furthermore, a good portion of these signals may be caused by S-wave arrivals instead of P-wave arrivals as would normally be assumed. If these signals are used without discrimination, it will result in significant contamination of the database, leading to the wrong source location. The Canadian experience of daily monitoring has shown that effective monitoring is dependent on the ability to process AE/MS data [3].

NOISH, in its effort to minimize hazardous ground conditions and provide safer working conditions for miners, has over the years pioneered and embraced the AE/MS technique, installing monitoring systems in some mines. Wang and Ge [22] provided a study that analyzed the performance of one such system located in an underground limestone mine in southwestern Pennsylvania. The authors emphasized the fact that the system performance was greatly affected by two main problems: background noise caused by the different mining activities and the source location accuracy. The background noises were responsible for many of the triggered events detected by the system. Also, the background noise was said to have partly or completely buried the AE/MS signals making it extremely difficult or impossible to determine the actual signal arrival. When these

challenges occur, they will result in inaccurate determination of the first P-wave phase arrival time, which is the fundamental data required for accurate source location determination. The authors report that signal processing (digital filtering), among other processes, was used to resolve the problem. The recovery of signals completely masked by background noises was achieved by the use of a low-pass filtering device. The authors recommended, among other things, that future studies should include the development of a reliable automatic signal detection system to further improve the monitoring efficiency of the system.

From the above discussions, it is evident that the detection and onset time picking of AE/MS events are paramount processing steps for accurately determining AE/MS event location. In other words, the reliable and accurate estimation of onset time of a detected P-wave phase is considered a fundamental requirement for any successful source location algorithm. Traditionally, these processes are performed visually by human experts called the analysts [23]. In most cases, the useful signal is buried by the surrounding noises, as noted by Ge [3]. This makes the visual detection of phase arrival impossible resulting in different identification by different analysts or even the same analysts picking different onset times at different moments in time. Manual analysis is therefore subjective and time-consuming. These factors, coupled with the huge volume of recorded AE/MS data, therefore require the development of a fast and efficient automatic algorithm for the detection and picking of the first P-wave onset time.

The need and reasons for the urgent need for automated systems were long emphasized by Stewart [24]. A number of algorithms have been proposed for seismic event detection and picking of P- and S-waves onset time in the field of seismology and petroleum engineering [5, 25-34]. In the mining environment, however, little can be said in terms of automation with regard to event detection and first P-wave onset time picking. In an effort to contribute toward a safe mining environment and to provide a means of enhancing research, teaching, and learning at the Department of Mining and Nuclear Engineering of the Missouri University of Science and Technology, a new signal processing method for acoustic AE/MS data analysis is being developed. Thus, this research study will open and advance the frontiers in automatic detection and the first P-

wave onset time picking of AE/MS events in mining and related fields and provide a strong foundation for students and researchers at the department.

██ OBJECTIVES AND SCOPE OF STUDY

For every operation, the safety of personnel and equipment and the economies of scale remain paramount, and the AE/MS technique has provided a reliable means of achieving this goal. The method has found wide application in all fields of engineering. The most difficult part of the AE/MS technique is signal processing. Among various signal processing issues, the most important one is seismic event extraction with precise timing. In addition to the fact that this is the first step and also the foundation for signal processing, data processing remains a challenging task for most AE/MS applications. On the other hand, the basic processing of AE/MS data is normally accomplished using proprietary commercial software packages. In most cases, however, such commercial software packages might not be readily available to academic institutions for research purposes. Therefore, the AE/MS research group in the Department of Mining and Nuclear Engineering at Missouri University of Science and Technology (Missouri S&T) aims to develop a processing software to fill this gap and to aid in research and teaching in the field of AE/MS data processing.

The main objective of this research is, therefore, to develop a highly efficient method to resolve the problems of background noise and outburst activities characteristic of AE/MS data. The proposed method is a hybrid technique that encompasses four recent and sophisticated techniques, including the characteristic function, high order statistics, wavelet analysis, and a phase association theory. The specific objectives shall include the following:

- the design and development of an algorithm for filtering AE/MS data using the stationary discrete wavelet transform (SDWT);
- the formulation of a characteristic function derived from high order statistics [35];
- the design/adoption of a phase association theory; and
- the calibration and testing of the algorithm using datasets consisting of real data from both geotechnical and nondestructive industries.

The scope of this research is limited to the development of a signal processing method that can be used to automatically detect and pick the first P-wave onset arrivals on AE/MS data.

■ RESEARCH METHODOLOGY

This research will combine the use of an analytical survey of relevant literature, mathematical, and numerical modeling techniques to build an algorithm for processing AE/MS data. The survey of literature will assess the methods available for defining the characteristic function (CF), automatic and non-automatic seismic data filtering in the fields of seismology, petroleum, and mining. Critical review and analysis of the relevant literature will provide the current body of knowledge in defining the CF, the use of the wavelet technique, and high order statistics method for detecting and picking accurate arrival times of AE/MS events. Verification process by way of using actual field data and comparing the results to existing methods will be used to prove the suitability, accuracy, stability, convergence, and reliability of the method for achieving the research objectives and potential industry use. The process of validation will be performed using AE/MS data from geotechnical and nondestructive testing industries.

Appropriate mathematical and numerical models will be developed to capture and deal with the special characteristics of mine noise that is normally acquired during the acquisition phase of the AE/MS monitoring process. The models shall include the following: (i) the statistical model formulation (capable of minimizing the noise effects and amplifying the amplitude and frequency content of meaningful signals) of the CF; (ii) model for data filtering; (iii) a model for event detection and arrival time picking; and (iv) a phase association theory. The filtering model is determined based on its ability to ensure that false picks are eliminated or minimized to guarantee reliable arrival time picks, for accurate source location determination. The performance evaluation of the models and solutions shall be tested with actual AE/MS data from a mine. These processes ultimately place the research study at the frontiers of this research paradigm and provide a rationale for the PhD research. The research results will be analyzed to draw relevant conclusions and make necessary recommendations.

■ **SCIENTIFIC AND INDUSTRIAL CONTRIBUTIONS**

The research will advance the understanding and application of automatic signal processing in underground mining and contribute immensely to the existing body of knowledge on automatic picking techniques. It is also expected that the results obtained by this automation will provide reliable arrival time and hence ensure accurate location of events. This, in turn, will provide mine operators with critical information. This information will then be used to estimate the deformation and relative stress state of the rock mass in the presence of excavations. Also, mine operators can use the information to evaluate the hazards associated with ground instability.

This research contributes immensely to the body of knowledge on signal processing and automatic picking of first arrivals in AE/MS data in the underground mining industry. It is used to formulate the governing equation and numerical models, as well as to provide a reliable algorithm based on established statistical parameters to ensure accurate picks, leading to successful source locations. Also, it will reduce the human input and the time required for data processing and analysis in this modern world of digital data. This research will promote health and safety in surface and underground mining, as well as the mechanical, electrical, civil, and geological engineering industries.

This research will contribute significantly towards the training of undergraduate and graduate students at Missouri S&T. The knowledge gained in the course of this research will be a strong case to integrate the monitoring of mine AE/MS techniques, signal processing and source location, and numerical modeling into the curricula of underground mining and rock mechanics courses. Also, students will be introduced to issues with data acquisition and processing challenges in underground AE/MS studies at seminar presentations conducted periodically.

Particularly, this research initiative applies a host of numerical methods and software application and simulation techniques to solve pertinent mining engineering problems. These techniques have not been traditionally taught to mining engineering students and their application will initiate an interest in them.

This research program is closely linked with other research initiatives being conducted by other graduate students under the research advisor. The completion of this component is essential to the programs required in the AE/MS research group. This

research will thus, contribute indirectly to the expansion of existing and the development of new research facilities at Missouri S&T.

The knowledge gained through this research will be largely distributed through conference presentations and scholarly and journal publications to encourage other initiatives, promote public education, and create interest in college students. In addition, the results will be broadly disseminated to enhance industrial and academic understanding into automatic time picking of seismic events in underground mine AE/MS monitoring.

■■■ STRUCTURE OF DISSERTATION

This dissertation report contains six (6) sections. Section 1 begins by providing background information on the research; highlighting the applicable areas of the AE/MS monitoring technique and its challenges. This is then followed by a discussion of the research problem/statement of the problem, the objectives and scope of the research, the methodology adopted for the research, the scientific and academic contributions of the research, and finally a discussion of the research outline.

In Section 2, a detailed review of the literature covering the techniques for seismic or AE/MS signal filtering/denoising to improve data quality is provided. The section also discusses the various automatic phase arrival detectors and pickers relevant to the study. This discussion included the theories underpinning these methods and their advantages and disadvantages where applicable. Finally, conclusions derived from these reviews are provided to close the section.

Section 3 provides detailed discussions on the new signal processing technique being proposed in this research. The necessary mathematical concepts adopted and assumptions made in the algorithm development are provided. A flowchart of the algorithm is also provided in this section, followed by some concluding remarks.

The testing and verification of the algorithm are provided in Section 4. To ensure that the proposed method is robust and reliable, three real datasets from a coal mine exhibiting different background noise characteristics were used to test and verify the model.

In Section 5, various simulation tests and discussions were performed to assess the performance of the proposed algorithm. To ensure that the proposed method is robust and

reliable in different environment, datasets from a coal mine and a 3-D concrete pile laboratory experiment were used as case studies to validate the proposed model.

The last section, Section 6, provides a discussion on the summary of the research study, research conclusions, research contributions, and recommendations for future work.

2. LITERATURE REVIEW

This section covers a comprehensive review of the relevant literature underlying the research in seismic or emission/microseismic (AE/MS) data filtering and automatic arrival phase detection and picking. The review covers the previous work on algorithms for improving the signal-to-noise ratio (SNR) of AE/MS data to enhance picking accuracy. Various detector and picker algorithms relevant to the study are reviewed, and where necessary, the strengths and weaknesses of these techniques are discussed. Symbols, signs, and abbreviations used in the section are defined in the Nomenclature section of this dissertation.

■ NOISE FILTERING/ATTENUATION

One of the fundamental challenges in any acoustic emission/microseismic (AE/MS) monitoring is the acquisition of high-quality data from a body under stress or undergoing deformation. Geophysicists manning these systems continually strive to acquire AE/MS signals with high signal-to-noise ratio (SNR) as much as possible. However, achieving this objective remains a challenge because AE/MS signals emitted from bodies under stress are usually weakened by the presence of several factors. These factors may include attenuation, reflection, diffraction, transmission loss, background noise, and many other factors. According to Ge [3], AE/MS signals acquired in mines, for example, are often buried by the surrounding noises, making it difficult to detect phase/event arrivals. As such, obtaining signals with high SNR is critical in the automatic processing of AE/MS data in any field of application. The importance of this step is highlighted by Cai et al. [21]. In the study, the authors indicated that AE/MS signals are usually very weak; as such, background noise reduction is a very vital process if reliable results are desired. On the other hand, Bormann [36] indicated that SNR enhancement can be achieved at the acquisition and processing stages. The success of the AE/MS monitoring system is therefore dependent on a variety of factors. Obtaining accurate event arrivals on AE/MS data with low SNR is a difficult task. Therefore, attenuating noise or reducing their impacts accompanied by the corresponding increase in the SNR is essential in AE/MS data processing.

Software denoising/filtering of AE/MS has become the most reliable means of enhancing the SNR of data acquired in noisy environments. The attractiveness of this technique is in part due to the improved capacity of modern computers to handle and process large volumes of data within a short period. Bandpass filtering was considered satisfactory in reducing noise in some applications in the recent past. However, application of complex transforms achieved in adapting windows and multiple iterations are now a norm in modern-day signal processing. Fundamentally, the technique of seismic data denoising/filtering has become an integral part of nearly all processing flows. In general, the three main steps needed to achieve success in seismic data denoising include (i) data transformation from a time domain into a different domain to separate the signal and background noise; (ii) reducing the effect of background noise in the new domain; and finally (iii) converting the data back into the time domain. The major challenge in these processes, however, is being able to identify the appropriate domain for the separation of background noise and the signal of interest [37]. The principal idea in the study of time series with time-dependent frequencies of real problems is to transform and represent the raw signal so that its frequency characteristics can be achieved locally in time. Capilla [32] noted that for real-life problems involving time-varying frequencies, such as AE/MS signals, time-frequency analyses are more reliable compared with analyses in either time or frequency domain alone. Popular among the methods available for performing such analysis is the windowed or short-time Fourier transform (STFT) and wavelet transforms [32].

◼ FOURIER AND WAVELET TRANSFORMS AND THEIR PROPERTIES

Acoustic emission/microseismic signals are generally characterized by variations in time and in frequency. Different AE/MS events arrive at the monitoring sensors at different times and with different frequency bands. In the following section, the mathematical theories of the Fourier and wavelet transforms are discussed. In the course of these discussions, the challenges making each of these techniques appropriate or otherwise for AE/MS data filtering are highlighted in relation to the present study.

2.2.1. Fourier Transform and its Limitations in Time-frequency Analysis.

The mathematical expression for the Fourier transform $\hat{f}(\omega)$, of a signal $f(t)$ is given by Equation (2.1).

$$\hat{f}(\omega) = \left\langle f(t), e^{j\omega t} \right\rangle = \int_{-\infty}^{\infty} f(t) e^{-j\omega t} \tag{2.1}$$

$e^{j\omega t}$ is a sinusoidal wave.

Performing the inner product of the signal $f(t)$ with the sinusoidal wave $e^{j\omega t}$ transforms the signal from the time domain into the frequency domain ω. Frequency domain analysis of signal remains one of the most popular techniques used in AE/MS signal processing. The Fourier transform expression in Equation (2.1) requires the integration of the signal for all times. The fact that the Fourier transform integral must be performed globally makes it difficult to obtain local properties of the signal. In order to address the challenges faced by the regular Fourier transform function, the STFT was introduced [38]. The expression for the STFT is given by Equation (2.2).

$$(STFT)(f(t)) = \left\langle f(t), \phi_{u,\omega} \right\rangle = \int_{-\infty}^{\infty} f(t) g(t-u) e^{-j\omega t} dt \tag{2.2}$$

$\phi_{u,\omega}(t) = e^{j\omega t} g(t-u)$ is the localized time-frequency function.

STFT has limitations that make it inappropriate for some applications. One of its limitations is that the STFT precision in time and frequency in a given window function is fixed. Thus, it is impossible to detect the arrival time of transient components with different levels [32]. As demonstrated in Figure 2.1, the original signal has an infinite resolution in time (Figure 2.1a) but no frequency information. Also, the Fourier transform of the signal has an infinite resolution in frequency but provides no time information (Figure 2.1b). Figure 2.1c, on the other hand, represents the time-frequency resolution of the windowed transform, which is constant [39].

Until the advent of the theory of wavelets, the classical Wiener filter operating in the Fourier domain remained one of the most widely used denoising/filtering methods [40]. Among all linear estimators, the Wiener filter is considered the optimal. However, the assumption that the real signal is circular stationary remains a major disadvantage of the Wiener filter. Again, the method of frequency filtering enhances the removal of some specific incoherent noise types. However, it is not amplitude preserving, an important consideration in signal processing. A specific problem is that prediction filters affect signals that do not appear along a straight line, commonly found in areas of complex geology [37, 40]. The mining environment, for example, remains one such area where geological complexities are dominant.
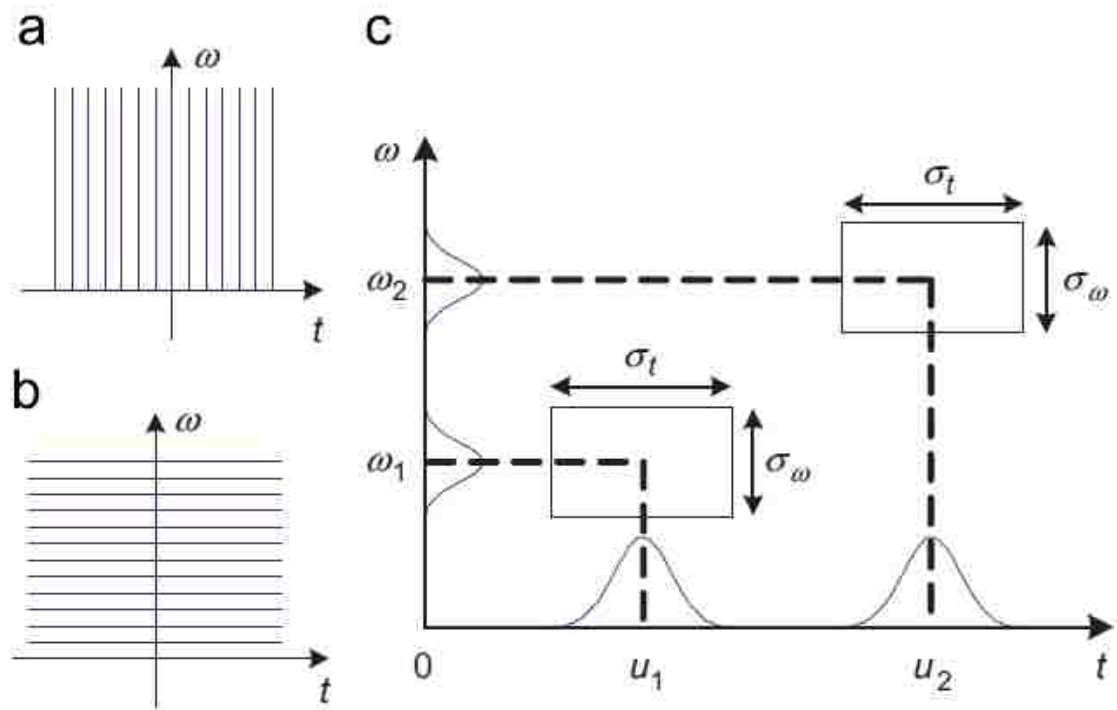
Figure 2.1 Time-frequency resolutions of the Fourier transform [39]

The wavelet transform, on the other hand, has been widely used in different scientific areas. The wavelet method continues to be an attractive tool for analyzing nonstationary and transient events, such as AE/MS signals because of its unique properties,

including localization, orthogonality, and multi-rate filtering, or space-scale analysis [32]. It provides a means to overcome the disadvantages associated with the Fourier methods.

2.2.2. Wavelet Transforms (WT), Types, and Signal Processing. Wavelet transforms are linear transforms that use a series of oscillating functions with different frequencies as window functions $\mu_{s,u}(t)$ to scan and translate the signal $f(t)$. The s and u in the window function are scaling and position parameters, respectively.

According to Goupillaud et al. [41], geophysical exploration was one area that influenced the application of the wavelet technique in its early days of development. The continuous existence of random noise and the need to remove these noises during the processing of seismic data to achieve good SNR remains a very challenging task in the field of geophysical exploration. The wavelet technique is regarded as a reliable method for removing random noise during seismic data processing [42]. For instance, using the discrete wavelet transform (DWT) method, Botella et al. [31] removed stationary noise at all stations in a network. The main purpose of employing the DWT was to assess its influence on the detection of seismic activities. Using the DWT process to pre-filter the seismic signal, the authors noted that they achieved an increase in detection and a reduction in false alarm rate in comparison with two other detectors not using wavelet filters. They also indicated that no meaningful event was lost as a result of using this technique.

The wavelet technique has also been used by many other authors for the determination and picking of the arrival of seismic phases in the past. For example, Capilla [32] demonstrated the use of the Haar wavelet in a DWT as a tool for the time-frequency (scale) representation of raw seismic data and for establishing the presence of events. Using the localization properties of the wavelet, the author extracted characteristics of importance (energy and predominant time scales), which were then examined for seismic events detection. Also, Gendron et al. [43] extracted key features from the discrete wavelet coefficients of a seismic record and then, using the Bayes theorem, provided a joint detection and classification of seismic events. Authors such as Zhang et al. [44] and Ahmed et al. [26], on the other hand, employed different forms of the wavelet transform together with the Akaike Information Criteria (AIC) auto picker to detect and pick P-wave arrivals. While Zhang et al. [44] employed the continuous wavelet transform (CWT) technique on

3-component broadband seismological data, Ahmed et al. [26] used the DWT method on a single-component recording. Both authors report strong agreements of their results with that obtained by analyst picks and other auto picks as well.

Continuous Wavelet Transform (CWT)

The ability of CWT and all wavelet types to construct a time-frequency representation of a signal remains its major advantage over the Fourier transform methods. The CWT involves the division of a continuous-time function into equal time and frequency intervals. In this process, the signal is multiplied by the wavelets and the transform is calculated independently for various parts of the time-domain signal. To derive the mathematical expression for the CWT, let $\mu_{s,u}(t), s, u \in R, s > 0$, belong to the group of functions expressed as translations and rescaling of an individual function $\mu_{s,u}(t) \in L^2(R)$ [45] given by Equation (2.3).

$$\mu_{s,u}(t) = \frac{1}{\sqrt{s}} \mu\left(\frac{t-u}{s}\right) \tag{2.3}$$

The properties of $\mu_{s,u}(t)$ are as expressed in Equation (2.4) [39].

$$\int_{-\infty}^{\infty} \psi(t)dt = 0, \int_{-\infty}^{\infty} \psi^2(t)dt = 1 \tag{2.4}$$

The above properties are an indication that the wavelet has a zero mean and has finite energy (see Figure 2.2a). For a given signal $f(t)$, the CWT of the signal can be expressed as in Equation (2.5) [46]:

$$W_\psi f(s,u) = \langle f(t), \psi_{s,u}(t) \rangle = \frac{1}{\sqrt{s}} \int_{-\infty}^{\infty} f(t)\psi\left(\frac{t-u}{s}\right)dt \tag{2.5}$$

The equation for the CWT is similar to the Fourier transform; the exception is that the sine and cosine functions in the Fourier transform have been replaced by the family of wavelets as the basis functions. Also, while a Fourier transform of a signal will project the signal into a one-dimensional domain, the use of two parameters (scaling and positioning parameters) in the wavelet family means transforming a signal with the wavelet technique will project the signal into a two-dimensional domain (time-scale domain).

Shown in Figure 2.2b is the time-frequency resolution associated with the wavelet transform. The localized section of the signal is defined by the area of the graph bounded by the time and frequency widths of $\left[u_0 - \left(\frac{1}{2}\right) a_0 \sigma_t, u_0 + \left(\frac{1}{2}\right) a_0 \sigma_t \right]$ and $\left[\left(\frac{\eta}{a_0}\right) - \left(\frac{\sigma_\omega}{2a_0}\right), \left(\frac{\eta}{\eta}\right) + \left(\frac{\sigma_\omega}{2a_0}\right) \right]$, respectively. While time-frequency resolution associated with STFT is constant, that of the wavelet transform (WT) is dependent on the signal frequency [39]. According to Zhu et al. [39], the quality factor in the time-frequency domain is constant for the WT. The mathematical expressions for this factor in the case of the mother WT, $\psi\left(\frac{t}{a}\right)$ is given as in Equation (2.6).

$$Q_a = \text{Central frequency} \Big/ \text{bandwidth} = \left(\frac{\eta}{a}\right) \Big/ \left(\frac{\sigma_\omega}{a}\right) = \frac{\eta}{\sigma_\omega} \tag{2.6}$$

and for $\psi\left(\frac{t}{a_0}\right)$ the expression is given by Equation (2.7).

$$Q_{a_0} = \text{Central frequency} \Big/ \text{bandwidth} = \left(\frac{\eta}{a_0}\right) \Big/ \left(\frac{\sigma_\omega}{a_0}\right) = Q_a \tag{2.7}$$

The variation of bandwidth and frequency with the scale factor u makes it beneficial for processing signals across scales.

Discrete Wavelet Transform (DWT)

In spite of its preference over the STFT, CWT is found to be slow computationally compared to DWT. DWT is mainly based on using low- and high-pass filters and down-

sampling. For the mathematical expressions of the DWT, let $h_0[n]$, $h_1[n]$ be the analysis filters, and $g_0[n]$, $g_1[n]$ be the synthesis filters of a 2-channel orthogonal filter bank. The zero represents the low-pass filter and one represents the high-pass filter. From the equations provided by Botella et al. [31], the input signal for a single level decomposition process can be written as in Equations (2.8) and (2.9).

$$x[n] = \sum_{k \in Z} X^{(1)}[2k+1] g_1^{(1)}[n - 2^1 k] + \sum_{k \in Z} X^{(1)}[2k] g_0^{(1)}[n - 2^1 k] \qquad (2.8)$$

$$X^{(1)}[2k] = \left\langle h_0^{(1)}[2^1 k - l], x[l] \right\rangle \text{ and } X^{(1)}[2k+1] = \left\langle h_1^{(1)}[2^1 k - l], x[l] \right\rangle \qquad (2.9)$$

In Equations (2.8) and (2.9), $X^{(1)}[2k]$ gives the scaling coefficients of DWT obtained by the convolution of the input signal with the low-pass filter $h_0[n]$. This is followed by a down-sampling by a factor of 2, whereas $X^{(1)}[2k+1]$ gives the wavelet coefficients also obtained by the convolution of the input signal with the high-pass filter $h_1[n]$, followed by a down-sampling by a factor of 2. The superscript (1) represents the scales or levels of the wavelet decomposition while h_0 and h_1 represent the scale and wavelet functions, respectively. Finally, $h_1^{(1)}$ is called the mother wavelet, which is the basis of the wavelet analysis based on shifts and scales of this mother wavelet.

The low-pass section can be further split by low-pass/high-pass filtering and down-sampling as is the case in an octave-band filter. If the process are repeated *J* times, then a discrete wavelet series over *J* scales plus the final scale containing the output of the last low-pass filter will be obtained. Thus, Equation (2.8) becomes Equations (2.10) and (2.11).

$$x[n] = \sum_{j=1}^{J} \sum_{k \in Z} X^{(j)}[2k+1] g_1^{(j)}[n - 2^j k] + \sum_{k \in Z} X^{(J)}[2k] g_0^{(J)}[n - 2^J k] \qquad (2.10)$$

$$X^{(j)}[2k+1] = \left\langle h_1^{(j)}[2^j k - l], x[l] \right\rangle, j = 1,...,J , \text{ and } X^{(J)}[2k] = \left\langle h_0^{(J)}[2^J k - l], x[l] \right\rangle \qquad (2.11)$$
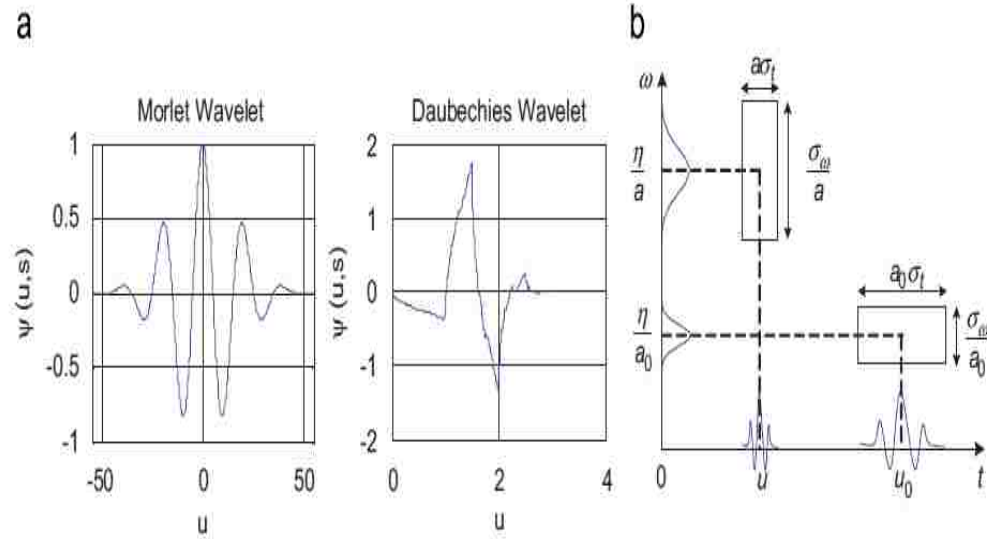
Figure 2.2 Typical wavelets and adaptive time-frequency resolution of wavelet transform
(u and s have the same meanings as explained above) [39]

Once again, $X^{(J)}[2k]$ are the scaling coefficients and $X^{(j)}[2k+1]$ are the wavelet coefficients for scale j. According to Vetterli and Kovacevic [47], since any input sequence can be decomposed as in Equation (2.10), the family of functions $\{g_1^{(j)}[2^j k - n], g_0^{(J)}[2^J k - n]\}, j = 1,..., J$ and $k, n \in Z$ is an orthonormal basis for $l_2(Z)$.

Generally, with the scaling and wavelet coefficients at an obtained j scale, the scaling coefficients at a scale j-1 can also be determined. This process is referred to as the decomposition of the discrete wavelet transform. The decomposition terms can therefore be expressed as in Equations (2.12) and (2.13).

$$X^{(j)}[2k] = \sum_{k \in Z} h_0[2^j k - l] X^{(j-1)}[l] \tag{2.12}$$

$$X^{(j)}[2k+1] = \sum_{k \in Z} h_1[2^j k - l] X^{(j-1)}[l] \tag{2.13}$$

To obtain the original signal, the process of reconstruction with the estimated wavelet coefficients for scales from $j = 1,..., J$ and the last scaling coefficients at J are used

and are expressed as in Equation (2.14). Figure 2.3 shows an example of a single level decomposition and reconstruction.

$$X^{(j-1)}[2k] = \sum_{k \in Z} g_0 [n - 2^j k] X^{(j)}[2k] + \sum_{k \in Z} g_1 [n - 2^j k] X^{(j)}[2k+1] \qquad (2.14)$$

■■■ AUTOMATIC PHASE ARRIVAL DETECTION AND PICKING

Due to the large volumes of recorded AE/MS data and the subjective nature of manual analysis, the processes of detecting and picking of event arrival times are mainly performed automatically. The algorithms used for these tasks may operate in either the time or the frequency domain.
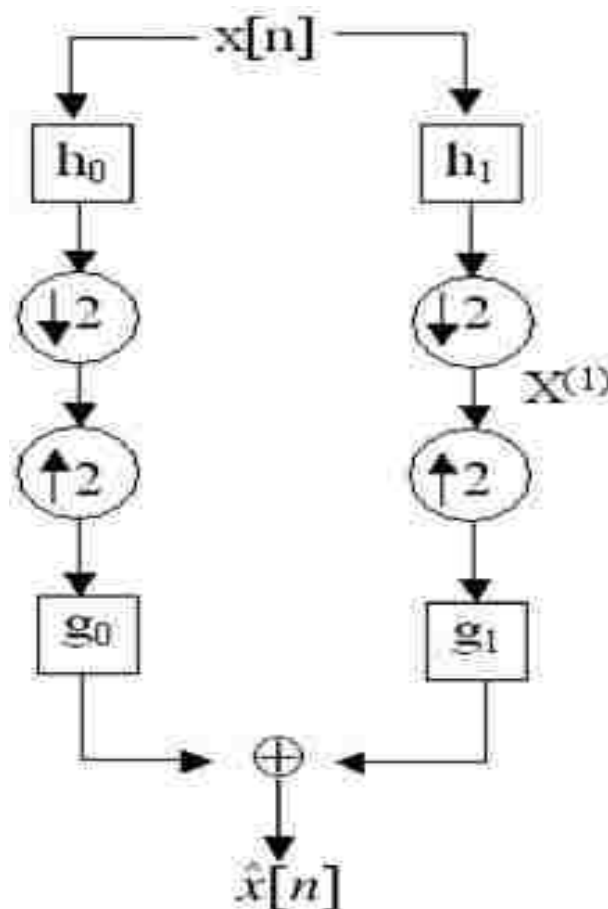
Figure 2.3 A single level decomposition and reconstruction of a signal x[n] using DWT [31]

The first mathematically-based signal detector was introduced in 1963 by the application of an approximate contrast of spectral densities for the identification of Gaussian-based signals in Gaussian noise [48]. The method is appropriate and efficient for the processes of signal detection rather than estimating signal onset times. Stewart [24], on the other hand, developed an automatic system (on-line system) for the detection and location of local seismic events in central California. The characteristics required of the system included the determination of onset time, maximum amplitude, the direction of first motion, and the coda length. Using three moving windows for computing "moving-time noise averages" from the original seismic trace verifies whether the seismic station is operating within acceptable limits of noise or not. For a single trace, the input seismic signal is processed in one of three different modes, namely, the P-phase detection mode, P-phase processing mode, and coda-processing mode. A P-phase is detected if the threshold exceeds 2.9 times the noise level. Also, the Walsh transform, a method very similar to the Fourier transform but less expensive in terms of computation has been used to develop an automatic seismic signal detector by Goforth and Herrin [49] and used by Micheal et al. (Micheal et al., 1982) for real-time event detection and recording system at MIT. However, the precision of these algorithms is limited.

The classic short-term average to long-term average ratio (STA/LTA) technique by Allen [25, 27] remains one of the most widely used techniques in global seismology for event detection and onset time picking [50]. The concept of a characteristic function (CF) was first introduced by Allen in 1978. In this algorithm, a CF, which is devised to enhance the signal changes and its averages in the STA/LTA windows, is computed to detect the advent of a phase arrival. After detection, the processed data is subjected to various logical and arithmetic tests for phase onset timing. The use of functions based on absolute value and the square of the seismic input signal as CF are well discussed in the literature [27]. The algorithm by Allen has undergone various modifications over the years [5, 25, 51-53].

Many of the modifications to the method by Allen were necessitated by the desire to rectify the challenges that made the use of the STA/LTA picker ineffective under some specific conditions. The method has been shown to be ineffective in noisy environments [5]. On the other hand, Evans and Allen [54] emphasized the computational impact of the method of squaring the data as used by the Allen picker as one of its challenges. Also, Chen

and Stewart [55] stated that inaccurate arrival times due to the length of the STA window and difficulty in distinguishing between high amplitude noise and actual events were a major weakness generally associated with the STA/LTA methods.

Withers et al. [56], in the development of their automated near-real-time waveform correlation event-detection and location system (WCEDS), also provided a study involving an STA/LTA method with a detector based on Z-statistics. The method fundamentally involved the estimation of the deviation of the data from the mean of the standard deviation. The other methods involved frequency transient algorithm and a polarization algorithm. When testing these algorithms under different cases of source, receiver, path, and noise conditions, no single algorithm was found most favorable. However, an STA/LTA algorithm operating with adaptive window lengths controlled by nonstationary seismogram spectral characteristics was found to give the best output. This, the authors noted, was because the output obtained met the requirements of a global correlation-based event-detection and location system.

Beside the STA/LTA detector/picker algorithms, there exist a large number of detectors and pickers that have been developed based on the desire to minimize the deficiencies associated with the STA/LTA method. For example, the autoregressive (AR) techniques are widely used. Based on the Akaike Information Criterion (AIC), Takanami and Kitagawa [57] developed a procedure for the fitting of a locally stationary AR model to seismograms. They implemented this procedure in an online system and called it FUNIMAR (fast univariate case of minimum AIC method of AR model fitting). Leonard and Kennett [58], on the other hand, proposed an autoregressive method that detects increases in the AR-model order due to the higher complexity of signals compared to preceding noise. The standard autoregressive two-model Akaike Information Criterion (AR-AIC) was also used by Sleeman and van Eck [59] to estimate the AR coefficients from predefined noise and signal windows. The use of the AIC method in other forms can also be found in the following studies [44, 60-62].

The use of artificial neural networks for phase determination studies is reported in studies, including [63, 64]. A typical example can be found in a study by Gentili and Michelini [65]. In this study, the authors used the artificial neural network approach for the determination of P- and S-phase onset time. They referred to the technique as an innovative

model of neural network (IUANT2). To realize their objectives, they used variance, skewness, kurtosis, and a combination of skewness and kurtosis and their time derivatives as the basis of picking a phase.

Zhang et al. [44] and Bai and Kennett [28] developed their automatic phase-detection algorithms by employing different methods and using the different advantages of these methods to help improve detection. For example, Nippress et al. [66] applied the STA/LTA picker while Saragiotis et al. [67] used high order statistics [HOS] to estimate the P-arrival times of seismic data. The HOS methods have also been used by authors, including [23, 50, 68], for the estimation of arrival times. Though only amplitude based, HOS are quite sensitive even to emergent P onsets.

Again, in an effort to improve the efficiency of picking, algorithms for estimating the relative travel times instead of absolute ones have also been developed. Examples are multi-station and array approaches using cross-correlation methods [69-72] or adaptive stacking techniques [73]. These methods require high waveform coherence at neighboring stations and high signal-to-noise ratios (SNR), as is observed in the case of low-pass filtered teleseismic waveforms. Also, Molyneux and Schmitt [72] and Raymer et al. [71] have employed the use of the cross-correlation techniques for estimating the arrival time picking, while Plenkers et al. [74] used it for detecting events.

Other detector methods based on polarization, time-frequency analysis, and wavelet-transformation have also been proposed and used by several researchers [29, 31, 33, 75, 76]. Many other time-picking algorithms, such as the modified energy-ratio [77], modified Coppen's method [53], and algorithms based on fractals [30, 78] have been reported in the literature.

Many of the present onset time pickers, however, have used events with high SNR or those with high SNR obtained by the application of suitable bandpass filters, thereby making the pickers perform well. The AIC picker is one of the most popular algorithms in modern times to out-perform the STA/LTA picker in high SNR environment [61]. Zhang et al. [44], however, noted that the AIC method is sometimes affected by the SNR in the seismogram. There will always be a global minimum in a given time window, and thus, the picker always picks onset time whether there is a true phase or not. Küperkoch et al. [50] noted that for best results, recent automatic pickers try to combine the advantages of

different approaches. Below, we provide brief descriptions of some of the automatic algorithms mentioned above that are relevant to the present study. Where necessary, the strengths and weaknesses of these methods will be highlighted.

2.3.1. The Allen's Algorithm. In this algorithm, the CF is achieved by the nonlinear transformations of the seismogram. The presence of a phase arrival is generally characterized by an increase in the CF. After the determination of the CF, the picking algorithm uses the CF to estimate the arrival time and then finally performs quality estimation of the pick. Figure 2.4 shows the flowchart of the algorithm.

Now, assume x_i to be the time series with a first difference of d_i, the CF defined by Allen [25] is as shown in Equation (2.22).

$$CF_i = x_i^2 + C_i d_i^2 \tag{2.22}$$

C_i is a weighting constant to control the relative contributions of amplitude and derivative and defined as in Equation (2.23).

$$C_i = \frac{\sum_{j=1}^{i} |x_j|}{\sum_{j=1}^{i} |x_j - x_{j-1}|} \tag{2.23}$$

With the CF, an STA and an LTA (approximately 100*STA) are computed. An initial time is stored as a potential pick if the ratio, STA/LTA, exceeds the reference level γ. At this point, the reference level γ is frozen. The amplitudes of the raw seismogram are then taken through a series of tests to confirm or reject the initial onset time. If the STA values exceed the continuation level, δ (low amplitudes), the system assumes a temporary increase of noise and discards the initial onset. If the STA values go above the continuation level, δ (high amplitudes), the system assumes a real seismic phase and estimates the duration. To establish the difference between short-range increases of noise and actual seismic phase, the algorithm searches for the next zero crossing in the seismic trace. When

the next zero crossing is achieved, the automatic picker starts counting the number, M, of all peaks, which is increased by 1 at each zero crossing. With M, the δ is computed as $\delta = \beta(j) * M$ and a "termination number" $L = 3 + 3/M$ is also calculated. The values for δ and L are constantly increasing and are therefore used as parameters for the identification of the signal length and confirmation of the provisional pick. Again, if STA exceeds δ, a counter s (referred to as a "small count counter"), counting the number of successive zero crossings occurring since STA drops below δ, is reset. If STA does not exceed δ, s is increased by one. If s > L, the event is said to be over otherwise, the processing continues. The duration for which L > s serves as an approximation of the signal length. If the signal length exceeds a certain threshold, tmin, the signal is said to be a seismic event, the pick is stored and optional post-processing starts. The pick is removed if the signal length is too short and s, L, M, δ are then reset. A new γ is also recalculated.

The system has a weighting scheme introduced to account for automatic quality and error assessment, which is based on the seismogram and the CF. To perform these weighting assignments, one requires the following:

- B, a measure of the noise level at the detection time;
- A_0, the trace amplitude at the detection time;
- D, the trace first difference at the detection time;
- A_1, A_2, A_3, the first three amplitude peaks.

For example, for a weight-0 P onset ("excellent"), the detection has to meet the following criteria [25]:

1. $D > \sqrt{B}$,
2. $A_1 > 450$,
3. $A_1/\sqrt{B} > 4$,
4. $A_2 > 6\sqrt{B}$ or $A_3 > 6$.

These criteria are to be successively relaxed to obtain lower weights 1, 2, and 3.

Pros and Cons of the Method

Most pickers developed based on the concept of CF have their performance tied to the appropriateness of such functions to describe the type of signal expected and the required performance. The STA/LTA method by Allen has been described as simple, efficient, and effective in most environments and regarded as the major foundation for automatic detection processes [43]. It is also a fast and robust algorithm equipped with efficient automatic quality assessment criteria, as shown in the description.
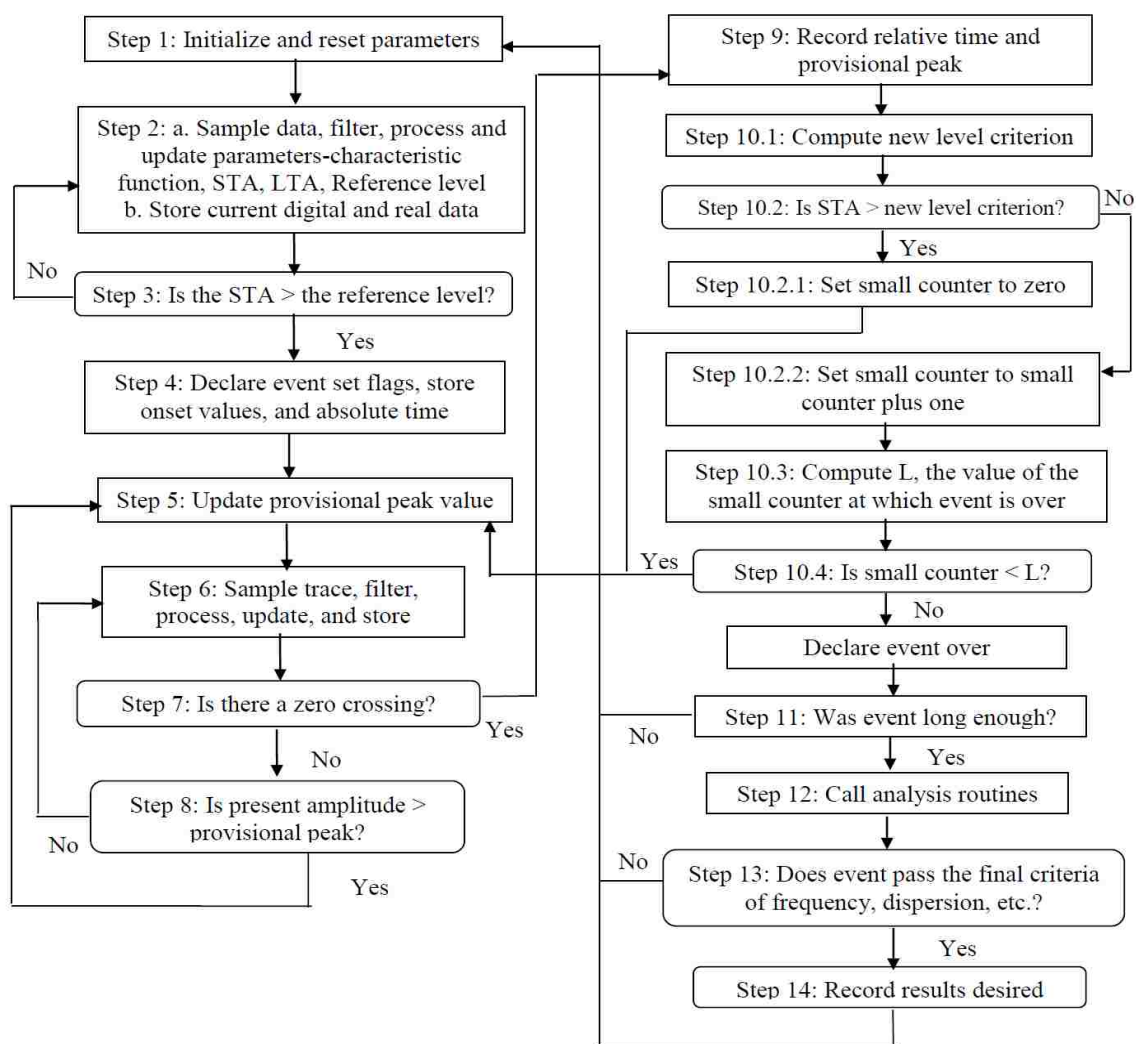
Figure 2.4 Allen's automatic picker program flow chart (adapted from [25])

However, the algorithm has been reported to perform unsatisfactorily under some specific conditions, leading to several modifications. For example, Baer and Kradolfer [5] reported a modified version of Allen's picker used for their system. The study noted that the picker performed excellently for local events as a result of its sensitivity to changes in frequency, but was unable to detect weak signals in high-noise environments. The use of fixed thresholds contributed to the inability of the method to detect phase arrival in weak signals. Gendron et al. [43], in their study, highlighted the many positive attributes of the STA/LTA detector. However, the authors also noted that it was the undesirable manner of false detection and issues of missed events on a wideband network that led to interest in multiband methods building on the STA/LTA detector. A comparative study by Küperkoch et al. [50] also showed that Allen's algorithm picks arrivals early compared to that of an analyst. These challenges have restricted the use of the algorithm in some applications with confidence.

2.3.2. The Baer and Kradolfer Picker. The Baer and Kradolfer [5] algorithm represents one of the early modifications made to the picker by Allen [25]. The motivation for the development of this method was the inability of Allen's picker to detect weak signals in high-noise environments. Also, the use of fixed thresholds, which contributed to the inability of the method to detect phase arrival in weak signals, was identified as a key factor for the modifications [5]. To address the challenges encountered using the picker by Allen, the authors first modified the CF used by Allen to obtain an envelope function (EF(t)) given in Equation (2.24).

$$E_i = x_i^2 + d_i^2 \frac{\sum_{j=1}^{i} x_j^2}{\sum_{j=1}^{i} d_j^2} \tag{2.24}$$

With the EF(t), a function with a more distinct SNR, which is the fourth power of the EF(t), was defined. The CF used for the method was then defined as in Equation (2.25).

$$CF_i = \frac{\left(SF_i - \overline{SF_i}\right)}{S_i} \tag{2.25}$$

$SF_i = E_i^4$, $\overline{SF_i}$ is the average of SF_i and S_i is the variance taken from the beginning of the series to the present point.

A pick flag is set if $CF_i >$ (threshold S1 = 10). To prevent the detection of short-term increases due to noise, a signal is accepted if the CF is equal to or greater than the signal threshold for times greater than the dominating period. The variance is updated continuously until CF_i exceeds a dynamic threshold given by S2 = 2S1. The provisional pick is cleared if the CF decreases within a given time, "tup". At the same time, a provision is made to accommodate the complexity of seismic signals by the inclusion of the "tdown" when the CF drop below the threshold S1.

The Baer and Kradolfer picker is a fast and robust routine, making it ideal for online detection. The algorithm is user-friendly due to the low number of parameters required to be set by the user. However, unlike the Allen picker, the method proposes no automatic quality assessment. Other comparative studies [50, 59] showed that the algorithm tends to pick arrival time late in comparison with that of a human expert (analyst).

2.3.3. The Modified Energy Ratio (MER) Picker. The MER algorithm was proposed by Han et al. [77]. The algorithm is fundamentally an extension of the STA/LTA method. The main feature of the MER method that distinguishes it from the STA/LTA method is that the pre- and post-sample windows are of equal size [79, 80]. The expression for the energy ratio (ER) at the ith time sample is given by Equation (2.26).

$$ER_{\{i\}} = \frac{\displaystyle\sum_{j=i}^{i+w} x_j^2}{\displaystyle\sum_{j=i-w}^{i} x_j^2} \tag{2.26}$$

w is the window length and x is the input series. The MER is then given by Equation (2.27).

$$MER_{\{i\}} = \left(ER_i |x_i|\right)^3 \tag{2.27}$$

In this method, the time index corresponding to the maximum of the MER value represents the arrival-time pick on the trace [80]. Because the ER function is computed using post- and pre-sample windows, the arrival-time pick by the method is usually reliable.

To achieve reliable and better results with this algorithm, careful selection of window size is required. The window size should be long enough (greater than a few periods of the microseismic signal) so as to avoid false picks as a result of noise fluctuations. Also, properly selecting the window size ensures that signal changes are accurately picked. Gaci [80] observed that the MER method yields results that are more reliable since it has superior accuracy and is more tolerant of high background noise compared to the STA/LTA.

2.3.4. The Short-term Kurtosis and Long-term Kurtosis Ratio (S/L-Kurt). A higher order statistical method motivated by the concept of the STA/LTA technique was recently proposed by Li et al. [81]. The authors referred to this new method as the short-term kurtosis and long-term kurtosis ratio (S/L-Kurt). The S/L-Kurt method was effectively used to detect the P- and S-arrivals on synthetic and field data because any bias in the short-term kurtosis (STK) and long-term kurtosis (LTK) windows were reduced. The mathematical expressions for the STK and LTK windows preceding the j sample index are given by Equations (2.28) and (2.29).

$$STK_{\{j\}} = \frac{\sum_{i=j-ss}^{j}\left(X_i - \overline{X}_j\right)^4}{(ss-1)\sigma_j^4}, \tag{2.28}$$

$$\sigma_j^2 = \frac{\sum_{i=j-ss}^{j}\left(X_i - \overline{X}_j\right)^2}{(ss-1)}, \overline{X}_{\{j\}} = \frac{\sum_{i=j-ss}^{j}\left(X_i\right)}{ss}, \text{ and } ss \text{ is the size/length of the short-term window.}$$

$$LTK_{\{j\}} = \frac{\sum_{i=j-sl}^{j}\left(X_i - \overline{X}_j\right)^4}{(sl-1)\sigma_j^4}, \tag{2.29}$$

$$\sigma_j^2 = \frac{\sum_{i=j-sl}^{j}\left(X_i - \overline{X}_j\right)^2}{(sl-1)}, \quad \overline{X}_{\{j\}} = \frac{\sum_{i=j-sl}^{j}(X_i)}{sl}, \text{ and } sl \text{ is the size/length of the long-term window.}$$

Lastly, the S/L-Kurt is then defined as in Equation (2.30).

$$S/L-kurt_{\{j\}} = \frac{STK_{\{j\}}}{LTK_{\{j\}} + \varepsilon} \tag{2.30}$$

ε is a small non-zero value added to prevent division by zero.

To obtain the arrival times, the maximum slope of the local maxima in the corresponding P- and S-wave intervals is selected. Like all STA/LTA methods, its performance is greatly impacted by the window selection. Shorter window sizes will produce rapid fluctuations, while much longer windows will affect the response for later arrivals.

2.3.5. The Phase Arrival Identification-Skewness/Kurtosis (PAI-S/K Scheme) and the PAI-K Picker. The PAI-S/K method introduced by Saragiotis et al. [23, 67] is based on HOS and consists of two parts: the PAI-S (skewness-based) and the PAI-K (kurtosis-based). While the PAI-S/K scheme was used for arrival identification [67], the PAI-K was later used together with other statistical parameters for arrival time picking [23]. In these algorithms, a characteristic curve is developed from the skewness and kurtosis values on a sliding window for the entire input signal length. The expression for skewness (S) is given by Equation (2.31) [35].

$$S[s] = \frac{\sum_{n=1}^{N}\left(s(n) - \mu_s\right)^3}{(N-1)\cdot\sigma_s^3} \tag{2.31}$$

μ_s and σ_s are the estimated mean and standard deviation of the signal $s(n)$ respectively.

The kurtosis, on the other hand, is expressed as in Equation (2.32) [35].

$$K[s] = \frac{\sum_{n=1}^{N}(s(n) - \mu_s)^4}{(N-1) \cdot \sigma_s^4} - 3 \qquad (2.32)$$

In these algorithms, both the identification and arrival time picks are done on the maximum slope of the corresponding local maxima for the P- and S-wave arrivals on S and K. The statistical properties of skewness and kurtosis make them effective tools for the identification and picking of arrival phases on seismic signal if the noise distribution is close to Gaussian while the signal is non-Gaussian [23, 66, 67]. For reliable results, a window length based on the frequency characteristics of the signal is recommended [50].

2.3.6. The Akaike Information Criterion Picker (AIC). The algorithm is based on the principle that AE/MS signals are transient and can be estimated by dividing the signal waveform into locally stationary segments and then modeling each segment using an autoregressive process [59, 61]. According to Zhang et al. [44], for a given AE/MS waveform of length N, the AIC value for the kth data point is expressed as in Equation (2.33).

$$AIC(k) = (k - M)\log(\sigma_{1,max}^2) + (N - M - k)\log(\sigma_{2,max}^2) + C \qquad (2.33)$$

M is the order of the autoregressive model, $\sigma_{,max}^2$ is the variances of AE/MS waveforms in the two intervals not explained by the autoregressive process, and C is a constant. The order of the autoregressive model is approximated by trial and error on the data window containing noise. The fitness of the model is achieved by the AIC function obtained by model order, while the optimal separation of the noise and signal is shown by the time index associated with the minimum value of AIC [26, 82]. The AIC algorithm defines the onset time as a global minimum and therefore requires an approximate of arrival time windows when dealing with multiple arrivals [44].

▄▄ EXAMPLES OF AE/MS APPLICATIONS IN THE MINING INDUSTRY

The AE/MS monitoring technique since it discovery in the 1960s has been used to provide solutions to many challenging problems in the mining industry. According to [83], accurately locating events presents a wide range of benefits. Examples of these benefits are:

- it designate the position of possible rockbursts;
- it helps in all successive seismological processing (e.g. AE/MS source factors and attenuation or velocity inversion);
- it helps in all ensuing explanation of specific events (e.g. events distant from active mining or near to a shaft); and
- also, all successive explanation of seismicity are judged by their location and timing.

The AE/MS method has been ultilized in a variaty of fields to provide solution to potentially life threatening problems. In underground mine studies, it has typically been used for

- pillar stability analysis;
- assessment of roof conditions;
- examination of the influence of different support systems; and
- the processes of backfill.

For mines where rockburst incidence is dominant, the AE/MS technique remains a fundamental means for evaluating overall ground conditions. For instance, [84] discussed the conclusions of the first modern AE/MS monitoring program in Australia undertaken at the Mt Charlotte underground mine and commissioned in 1994. According to the report, the principal incentive for the installation at the time was the desire for achieving an economic and safer mining environment. The author noted that the decision in part was also impacted by an increased environmental awareness, as the mine was just 200 m away from the city of Kalgoorlie, Western Australia. It concluded that the installed AE/MS system proved very useful for the determination of the location and magnitude of AE/MS events and many other important seismic parameters. It was also concluded that for the first one and half year of operation of the system, mine operators, and engineers understanding of the rock mass response to mining was greatly enhanced. On the other

hand, [85] reported of the utilization of the technique by the National Institute for Occupational Safety and Health for the identification of the processes involve in roof fall failures and to evaluate its potential in order to provide the needed advise on flawed roof conditions. The authors concluded that by using the AE/MS signals, local rock failure processes were successfully identified. In addition, the study showed that studying the distribution of AE/MS emissions could provide a means of evaluating the extent of instability related to these rock failure processes.

Using the AE/MS technique and laboratory tests, [86] esblished that there was a relation between stress and the nature of observed AE/MS emission from rock materials. Also, [87] in a report on the recent advances in seismic monitoring technology at Canadian mines showed how different seismic techniques can be used at mine sites. The authors using the space–time distribution in microseismicity and fault plane solutions were able to evaluate active fractures at the mine site.

2.4.1. Example Case Study 1: Moonee Colliery Mine Failure. According to Hayes [88] and referenced by Iannacchione et al. [85], the mining technique used at Moonee Colliery is the longwall underground mining technology. The mine is located in the Great Northern Coalbed of the Newcastle Coal Measure. The thickness of overburden ranges from 90 m to 170 m from the north to south of the mine. Coal and claystone constitute approximately 1.6 m of the immediate roof, which are overlain by 30 to 35 m of Teralba Conglomerate.

The Teralba Conglomerate does not constantly cave as the longwall advances but hangs until wide unsupported spans exist. Iannacchione et al. [85], described the caving process of the mine roof as non-continuous caving. The authors noted that the non-continuous caving could be attributed to "low overburden, narrow panels, and strong abutment strength of the adjacent solid longwall panels". The authors also indicated that 41 cases of roof falls were experienced with a 46 m average hanging span during the period of mining of the first longwall panel.

After advancing for the opening 200 m of first longwall panel, the mine experienced it first event of roof fall caving. One of the major events of roof fall that was particularly dangerous to miners occurred on 22 January 1998 and was associated with the fifth

longwall panel roof fall event. According to Mills and Jeffrey [89], six miners were injured due to windblast event as a result. Figure 2.5 shows the nature of material fall because of this roof fall event. As shown on Figure 2.5, the roof fall failure surface is inclined at 16° over the panel from the longwall face and the two gate entries from the top. At the central portion of the panel, the thickness of the failure is about 15 m and 35 m from the longwall face. Mills and Jeffrey [89] noted that "the top of the roof fall cavity was made up of both horizontal and vertical planes that formed a step-like surface". It was indicated that the horizontal planes were potentially due to local bedding structures within the conglomerate and that of the vertical planes were because of the local jointing.

To ensure the safety of miners in the event of future caving activities, the Moonee mine installed an AE/MS monitoring system with the objective of acquiring advance information on the inception of caving activities. The said system was adopted after the roof fall incidence on January 22 and consisted of a 14 Hz three-component geophone [85, 90]. Four of the geophones were located in 10 m roof boreholes around the longwall and were constantly relocated to frame the face of the longwall. Hayes [88] and Brink an Newland [91] noted that several thousands of seismic events and roof fall caving's were observed over the year of implementation of the system [85]. Shown in Figure 2.6 is a graph of 118 rock fracture events that occurred after roof fall No. 20 and before roof fall No. 21 for an 8-day period. Of the total events recorded, 70%t of them ensued in the course of the last three days of advance. In this case, there was only a weak correlation between advance rate and seismicity. The authors indicated it was reasonable to ascribe this seismicity to the stepped fracture surface developing in the overlying conglomerate that would soon outline the fallen material for roof fall No. 21 (Figure 2.6) [85]. On the other hand, Figure 2.7 provides a distribution of the rock fracture as of April 3 of the year under consideration. The study noted that a smaller amount of rock fracture events were observed along the northwest-southeast dyke 150 m off the longwall face with an average number occurring at 16 m above the extraction horizon. An average of -0.9 was observed as the moment magnitude for the 118 rock fracture events as illustrated in Figure 2.6. The actual range was however found to be from -1.7 to 0.6. Also, it was observed that moment magnitudes within the range of 0.3 to 0.6 for three rock fracture events occurred three minutes before the roof fall No. 21 [85].

In the stability assessment, the authors indicated that constant advance of the longwall face helped to weaken the overlying roof strata above the longwall panel. It observed that most of the AE/MS activity did not cluster around the face but represented "the initiation and development of the stepped failure surface and accommodation of stress adjustment over a wide area" [85]. Moreover, as shown in Figure 2.6, this action before roof failure signified a major increase in the incidence, degree, and magnitude of microseismic events. According to Hayes [88] and referenced by Iannacchione et al. [85], the installed MS system was able to provide reliable warnings 90% of the time before any roof fall incidence. The study concluded that the information obtained from the AE/MS system helped in establishing the start and growth of the stepped failure surface that outlines the eventual roof fall material. The last surge in AE/MS activity the study noted indicated the completion of the failure of the roof. In addition, it was shown that MS information is valuable means of assessing the stability of roof rock. Finally, the authors noted that there exist a great potential for the use of the AE/MS technique for the assessment of the stability of underground structures to provide safer mine layouts, system monitoring, and support systems for miners.

assessment of the stability of underground structures to provide safer mine layouts, system monitoring, and support systems for miners.

2.4.2. Example Case Study 2: Shirengou Iron Mine [12]. The Shirengou iron mine started its operations in 1975 and is located approximately 40 km northwest of Tangshan city, Hebei province, China (Figure 2.8). Formally, an open pit mine, the mine was converted into an underground mine in the year 2005. The mining method currently used is the short-hole shrinkage slopping. Current operations at the mine include an open pit 2.8-km-long, 0.3-km-wide and 120-m-deep (Figure 2.8c) and 129-stope underground operations at the first underground level (Figure 2.8d). As a result of excessive excavation and the activities of illegal miners, actual crown pillar thickness are below the designed thickness of 25 to 30 m [12].
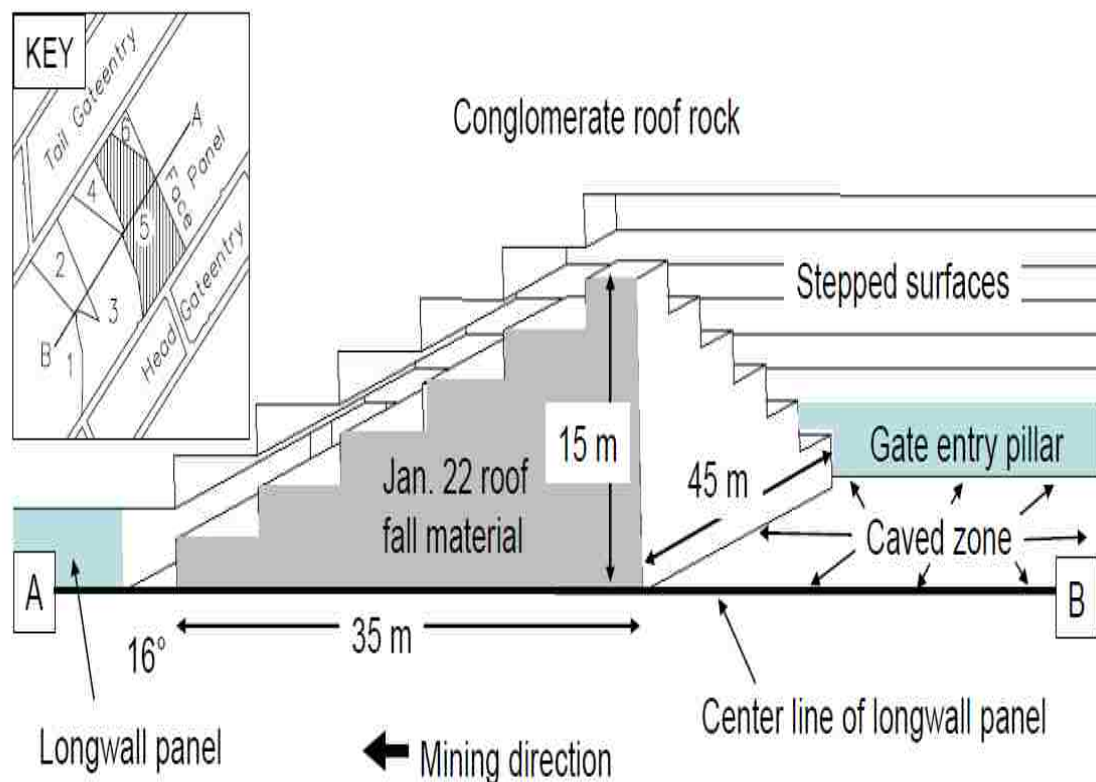
Figure 2.5 Generalized sketch of the Jan. 22 roof fall (Fall No. 5), longwall panel No.1, Moonee Mine [85]
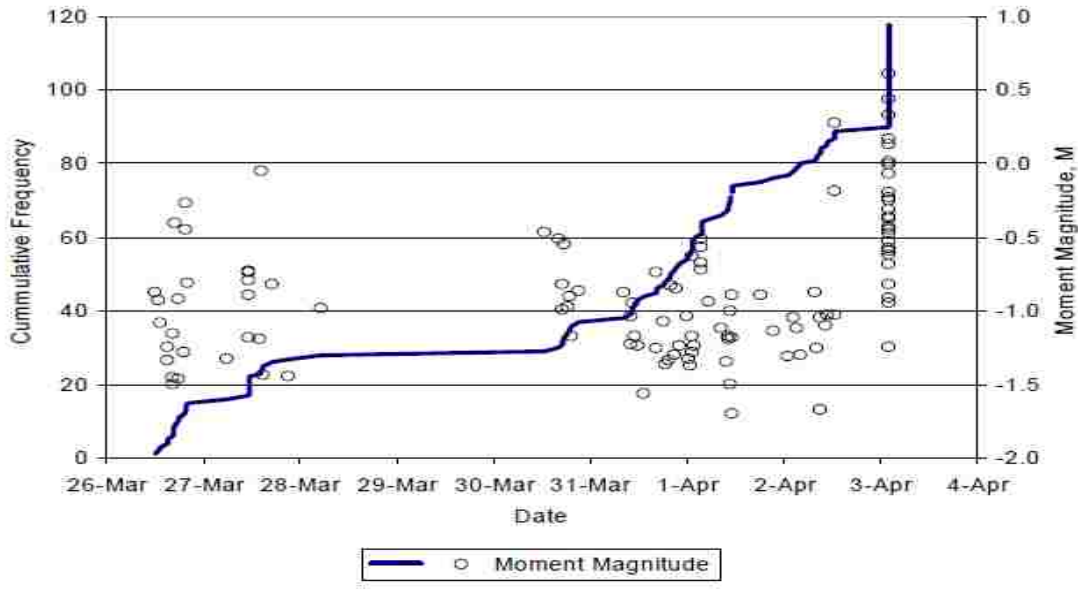
Figure 2.6 A plot of the cumulative frequency of the 118 rock fracture events associated with the period between Roof Fall No. 20 and 21 [85]
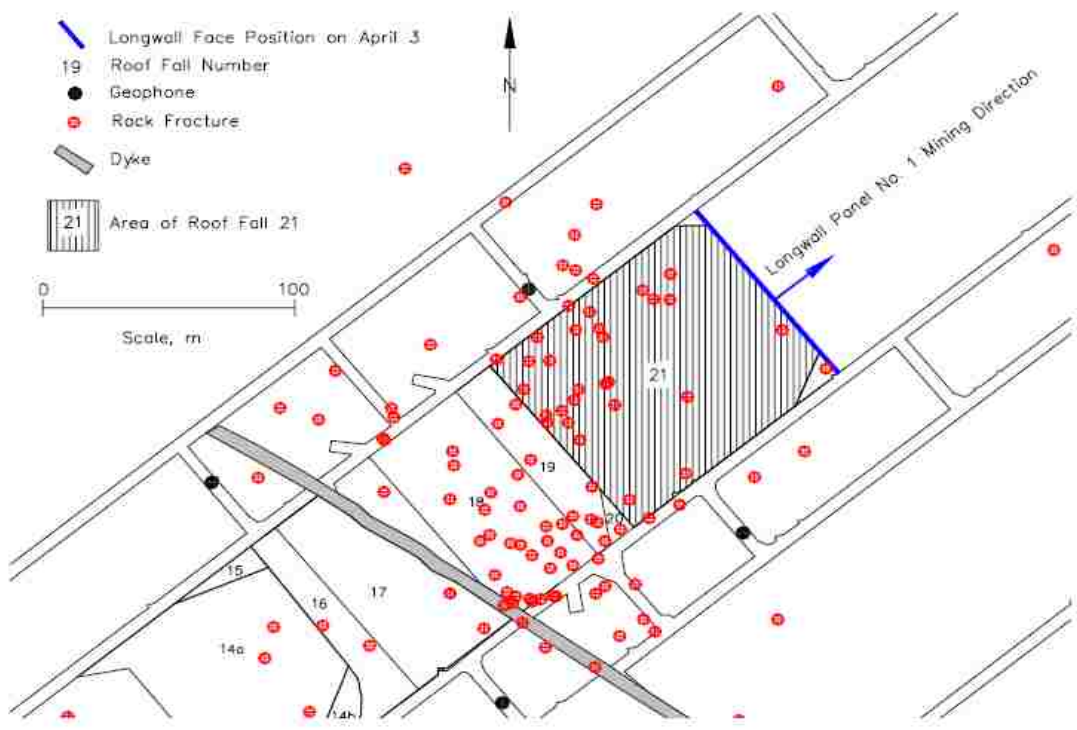
Figure 2.7 Location of the 118 rock fracture events, geophones, roof falls, longwall face, and dyke [85]

According to Nan [92] in the period of the transition, rock mass failures were observed at two locations. Of the two cases, one was caused by mining a fault to a height of 30 m, which was located at the No. 12 stope. On the other hand, case two was because of roof collapse due to water seepage at the No. 10 stope over a long period. These two incidence heighted the danger posed to the safety of miners and equipment when the rock mass is exposed to or affected by geologic structures and water seepage [12]. An MS system was therefore installed to evaluate rock mass stability at the Shirengou iron mine in 2006. The main components of the system included: a digital signal processing system, a digital signal acquisition system, thirty geophones, and a three-dimensional visualization system. The system options included both manual and automatic mode for the calculation of seismic source parameters such as event location, seismic moment, apparent stress, event magnitude, spectral parameters of waveform [12, 93].

From Figure 2.9, while stopes No. 9 and 16 were mined in accordance with mine plans stopes No. I15 and I16 were mined illegally. In the figure, the spatial distribution of the underground stopes and the AE/MS sensors (blue cylinders) are shown in Figure 2.9a. Also shown is a buried fault F15 with unclear boundaries through the region of interest. Seven geophones were installed with three at -10 m level drift and four at -60 m level drift. Figures 2.9b and 2.9c show an installed pumping station intended to help minimize the volume of water seepage and an observed water drop in the drift respectively. In order to establish the mechanisms causing the increase in water seepage, the microseismic data in the area were analyzed [12].

Temporal and Spatial Distribution of AE/MS Events

Shown in Figure 2.10 is the spatial distribution of AE/MS events obtained from October 24, 2009 to March 23, 2010. The blue spheres represent the distribution change of the microseismic events during the mining operation at the No. 16 stope. The darker colors correspond to later occurrence times. Figure 2.10a represent the side view of all the microseismic events (the gray plane represent the fault F15 plane) while 2.11b represents up to December 5, 2009. On the hand, Figures 2.10c, 2.10d, and 2.10e represent up to January 1, 2010, up to February 12, 2010, and up to March 23, 2010. The No. 16 stope was the only stope in operation at the time under consideration. The AE/MS events are shown

as blue spheres while time of occurrence is represented in different colors. The authors noted that majority of the AE/MS events were concentrated along the buried fault F15. This, the authors said according to Tezuka and Niitsuma [94] were evidence the AE/MS events were caused by fault activation. Studying the spatial-temporal relationship in the AE/MS events can help decipher the underlying details in the fault activation process [95]. The spatial-temporal distribution of AE/MS events showed that fault activation at the beginning of mining mostly occurred at the lower section of the crown pillar (Figure 2.10b). On the other hand, it was observed that fault activation during the continuous mining phase spread to the upper part of the pillar and the lower part of the open pit (Figures 2.10c to 2.10e). In addition, using the AE/MS event distribution, the direction (arrows in Figure 2.11) and range of the fault (curves in Figure 2.11) were successfully identified. Again, by means of the spatial-temporal distribution of AE/MS events, the authors established that fault movement was fundamentally because of the mining activities. It noted that with time, fault movement transformed into fault propagation resulting in the crown pillar failure. The study established that sharp increases in energy release and the apparent stress coupled with low dominant frequency and a speedily decreasing b value were characteristic features observed before any failure. The authors therefore noted that MS monitoring present a great potential for studying the failure of crown pillars in mines. The study also recommended that the minimum crown pillar thickness should be maintained at 40 m to protect the safety of personnel and equipment.

■■■ RATIONALE FOR PHD RESEARCH

The issues of accurate and reliable event detection and onset-time picking continue to engage the attention of experts in the field of seismology and related industries. When dealing with local events, the precision of event detection is of paramount interest. In the AE/MS monitoring process, event source location is the most critical information of interest to a geotechnical engineer, seismologist, or geologists. As such, errors in the picking of the onset time must be minimized as much as possible. Errors not managed properly may be amplified in the event source location computations. To ensure efficiency, consistency, and reliability in the detection and onset time picking of phases in seismic or AE/MS data, automatic processing has become the norm. These automatic algorithms

involve analysis of amplitude, frequency, and polarization combined with pre-filtering of data. They may also include autoregressive techniques and waveform correlation. The motivations for the development of these algorithms may be different and could be developed as a trigger, onset time picker, or both.
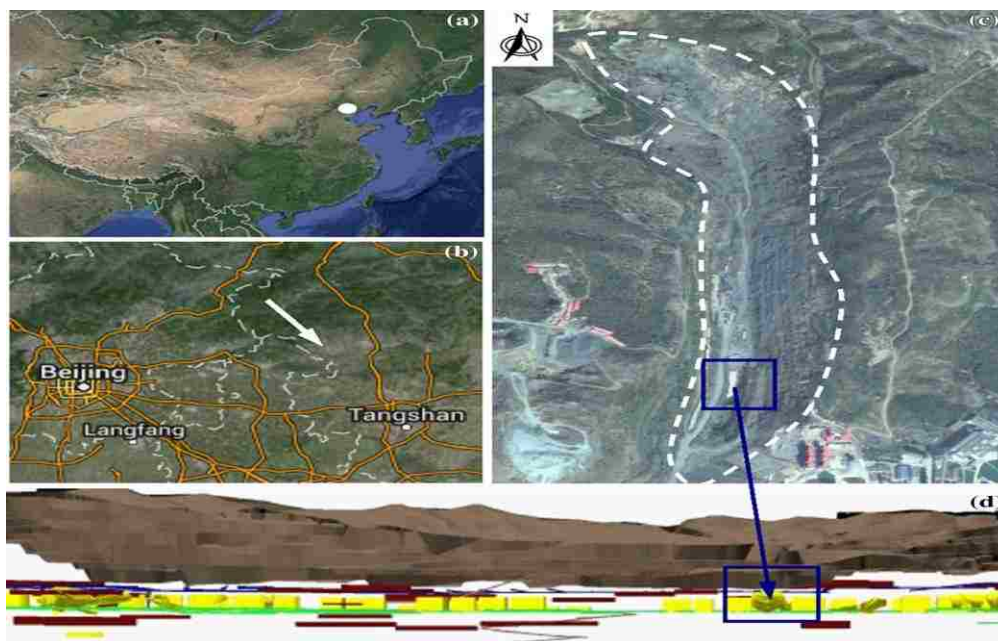
Figure 2.8 The Shirengou iron mine [12]

Energy analysis that uses the STA/LTA techniques [25, 27] for event phase detection and picking is the most widely adopted method in the processing of seismic data [50]. The concept of a characteristic function (CF) was first introduced by [25, 27] in 1978. In this algorithm, a CF, which is devised to enhance the signal changes and its averages in the STA/LTA windows, is computed to detect the advent of a phase arrival. After detection, the processed data is subjected to various logical and arithmetic tests for phase onset timing. The use of functions based on absolute value and the square of the seismic input signal as CF is well discussed in the literature [27]. Other forms of the energy-based algorithms developed as a modification to the algorithm by [25, 27] can be found in [5, 25, 51-53]. In spite of the wide application, the STA/LTA methods have been found to be ineffective and unreliable in high-noise environments [5, 43, 50]. These challenges have restricted the use of the STA/LTA algorithms in some applications with confidence.
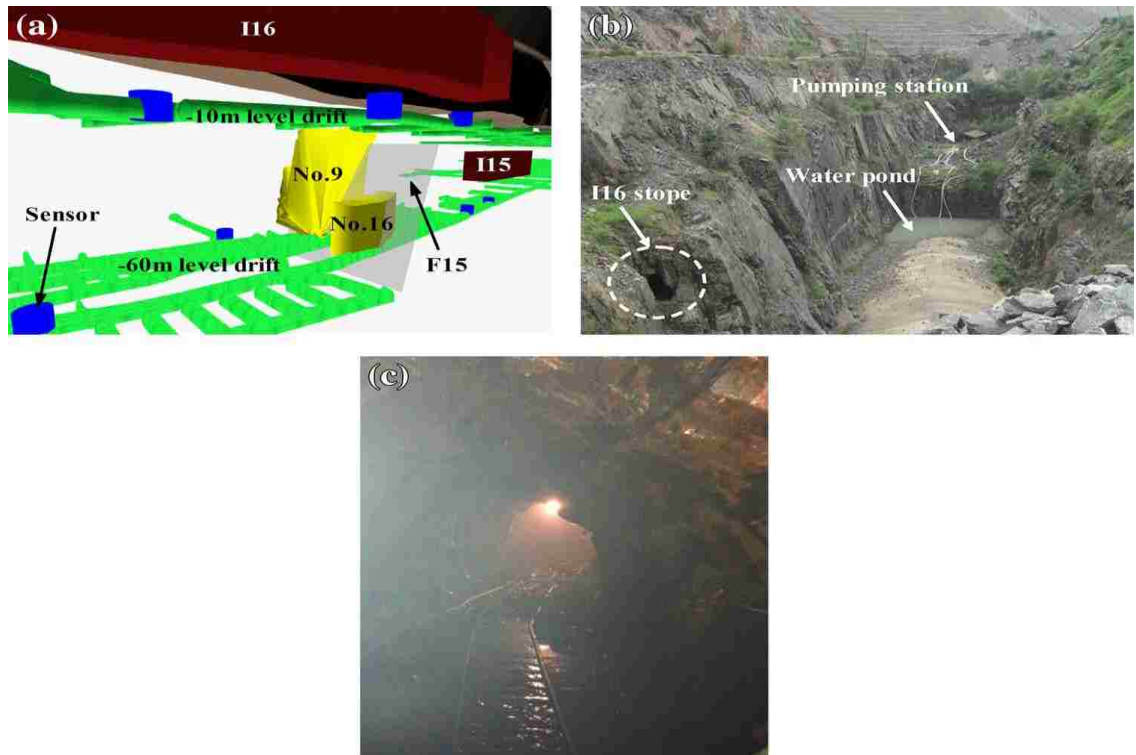
Figure 2.9 The study area [12]
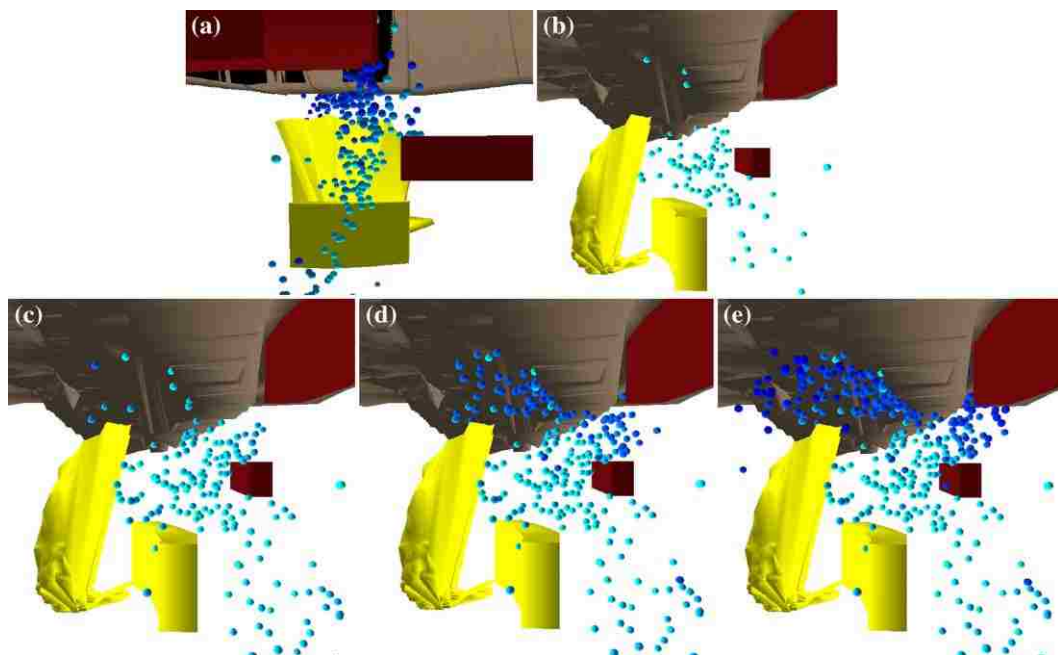
Figure 2.10 Distribution change of the AE/MS events (blue spheres) during the mining operation at the No. 16 stope [12]

Bear and Kradolfer [5], in an effort to fix some of the challenges encountered by using the STA/LTA algorithm proposed by Allen [25, 27], modified the CF in the original algorithm by introducing an envelope function EF(t). With the EF(t), a function with a more distinct SNR, which is the fourth power of the EF(t), is defined. A pick flag is set if $CF_i > $ (threshold S1 = 10). To prevent the detection of short-term increases due to noise, a signal is accepted if the CF is equal to or greater than the signal threshold for times greater than the dominating period. The variance is updated continuously until CF_i exceeds a dynamic threshold given by S2 = 2S1. The provisional pick is cleared if the CF decreases within a given time "tup." At the same time, a provision is made to accommodate the complexity of seismic signals by the inclusion of the "tdown" when the CF drops below the threshold S1. A major challenge with the method, however, is that the method proposes no automatic quality assessment. Also, other comparative studies [50, 59] showed that the algorithm tends to pick late in comparison with that of a human expert (analyst).

Figure 2.11 Direction and range of the fault activation (—Up to December 5, 2009, —Up to January 1, 2010, —Up to February 12, 2010, —Up to March 23, 2010) [12]

The use of highly complicated algorithms such the AR-AIC picker, which is based on information theory, is widely reported in [44, 57-62]. The AR-AIC algorithm introduced by Sleeman and van Eck [59] is based on the initial studies by Akaike [96] and Takanami and Kitagawa [57]. The algorithm based on this theory is found to be computationally expensive and much slower than many other algorithms. The AIC picker has been identified as one of the most popular algorithms in modern times to out-perform the STA/LTA picker in high SNR environments [61]. Zhang et al. [44], however, noted that the AIC method is sometimes affected by the SNR in the seismogram. There will always be a global minimum in a given time window, and thus, the picker always picks onset time whether there is a true phase or not. In the version of the algorithm proposed by Sleeman and van Eck [59], the initial P onset is achieved from an STA/LTA detector. In the AR-AIC algorithm, a waveform is divided into two locally stationary segments with each segment modeled by an autoregressive (AR) process.

While the first segments represent noise, the signal is contained in the second segment. In general, the major steps of the algorithm can be summarized as follows: (i) filtering of the seismogram using a Bandpass filter, (ii) using the STA/LTA detector for event phase detection, (iii) estimating the noise and signal AR parameters respectively, (iv) using the noise and signal AR parameters for the calculation of two prediction errors and finally, and (v) using the minimum of the two model AIC to estimate the arrival time. The use of the STA/LTA detector remains a major disadvantage of the algorithm. The STA/LTA algorithm as noted could miss emergent P-phase arrivals dominated by rapid variations in frequency. Also, the quality assessment technique as used in the algorithm is based on SNR only and is found not to be adequate for robust quality estimation of the P onsets. As indicated by [50], for best results, recent automatic pickers try to combine the advantages of different approaches.

In light of the disadvantages with the various methods, many of the present onset time pickers have had to use events with high SNR or those with high SNR obtained by the application of suitable bandpass filters, thereby making the pickers perform well. Software denoising/filtering of AE/MS remains the most reliable means of enhancing the SNR. Bandpass filtering was considered satisfactory in reducing noise in some applications in the recent past. One of the major processes required in seismic data denoising is the

transformation of data from a time domain into a different domain to separate the signal and background noise. The challenge, however, is being able to identify the appropriate domain for the separation of background noise and the signal of interest [37]. The principal idea in the study of time series with time-dependent frequencies of real problems is to transform and represent the raw signal so that its frequency characteristics can be achieved locally in time.

Capilla [32] noted that, for real-life problems involving time-varying frequencies (such as AE/MS signals), time-frequency analysis is more reliable compared to an analysis in either time or frequency domain alone. This property of time-frequency analysis cannot be achieved with the ordinary filtering algorithms usually employed in AE/MS data filtering. Again, the method of frequency filtering enhances the removal of some specific incoherent noise types. However, it is not amplitude preserving an important consideration in signal processing. A specific problem is that prediction filters affect signals that do not appear along a straight line, commonly found in areas of complex geology [37, 40]. The mining environment, for example, remains one such area where geological complexities are dominant. The STFT method has occasionally been employed to achieve a time-frequency domain analysis in some applications. However, precision in time and frequency in a given window function for the STFT is fixed. As such, it is impossible to detect the arrival time of transient components with different levels [32].

As is the case in seismology, the most difficult part of the AE/MS technique is signal processing. Among various signal processing issues, the most important one is seismic event extraction with precise timing. In addition to the fact that this is the first step and also the foundation for signal processing, there is no efficient method for processing AE/MS data. However, algorithms for event onset detection and picking have been extensively studied in the fields of seismology over the years. Generally, an accurate onset time is required to ensure reliable source location determination. To accomplish the objective of efficiently processing AE/MS data, algorithms originally developed for event detection and onset time pickings in the field of seismology have been adopted in some applications. In a noisy environment, AE/MS acquired data could be highly corrupted by background noises.

For instance, in a mining environment, the activities of mining machines, ventilation fans, blasting, electrical spikes, operations from nearby mines, and transportation vehicles generate noise of varying intensities that could impact the quality of the AE/MS data. Hence, the reliability of these algorithms could be affected if applied without appropriate modifications. Again, for cases where there is interference among signals (typically under burst conditions), the AE/MS signals themselves may present a major challenge. Also, most of the algorithms reported in the literature are single trace-based algorithms. As such, these algorithms provide no phase association theories critical to the identification of the physical status of an arrival pick on AE/MS data. These challenges, therefore, require the design of algorithms capable of addressing the specific and unique characteristics of AE/MS data, which are uncommon with seismic data.

The absence of algorithms specifically developed for the unique characteristics of AE/MS data remains a major concern in the AE/MS field. This PhD research study will provide appropriate insights through fundamental signal processing theory for minimizing and/or eliminating the effect of noise and thus improving the accuracy of onset time picks on AE/MS data. The research adopts a multi-trace approach, which will present an opportunity for the physical interpretation of arrival pick status leading to reliable source locations. To achieve this, the study will develop a highly efficient method capable of addressing the challenges that limit the application of present algorithms when processing AE/MS data. The proposed method is a hybrid technique that encompasses four recent and sophisticated techniques, including the characteristic function, high-order statistics, wavelet analysis, and a phase association theory.

The research combines the use of analytical survey of relevant literature, mathematical, and numerical modeling techniques to build an algorithm for processing AE/MS data. The survey of literature assesses the methods available for defining the CF, automatic, and non-automatic seismic data filtering in the fields of seismology, petroleum, and mining. Critical review and analysis of the relevant literature are done to provide the current body of knowledge in defining the CF, the use of the wavelet technique, and high-order statistics method for detecting and picking accurate arrival times of AE/MS events. Validation by way of using actual field data and comparing the results to existing methods

are used to prove the suitability, accuracy, stability, convergence, and reliability of the method for achieving the research objectives and potential industry use.

Appropriate mathematical and numerical models are developed to capture and deal with the special characteristics of AE/MS noise that is normally acquired during the acquisition phase of the AE/MS monitoring process. The models include the following: (i) the statistical model formulation (capable of minimizing the noise effects and amplifying the amplitude and frequency content of meaningful signals) of the CF, (ii) a model for data filtering, (iii) a model for event detection and arrival time picking, and finally, (iv) a phase association theory. The filtering technique model is one determined based on its ability to ensure that false picks are eliminated or minimized to guarantee reliable arrival time picks, leading to accurate source location determination. The performance evaluation of the models and solutions are tested with actual AE/MS data from a mine. These processes ultimately place the research study at the frontiers of this research paradigm and provide a rationale for the PhD research. The results from the various performance validations are analyzed to draw relevant conclusions and make necessary recommendations.

■ SUMMARY

An extensive review of literature relevant to the processes for improving and enhancing data quality, event phase arrival detection, and picking aimed at evaluating the contributions and limitations of the previous and current body of knowledge has been carried out in this section. The first part of the section provided an overview of the key techniques available for frequency and time-frequency domain analysis of seismic or AE/MS data. While the traditional Fourier transform was identified as the main tool for frequency domain analysis, the STFT and the WT were identified as primary tools for time-frequency domain analysis. However, the literature showed that the STFT is fixed in time for any given window and therefore not suitable for some applications. The WT, on the other hand, was found to be very reliable for time-frequency localization analysis of nonstationary signals such as AE/MS signals.

The second part of the section provided a review of relevant automatic phase arrival detection and picking algorithms used in seismic data processing. These algorithms were found to have been developed for the processing of seismic data in the field of seismology.

With various modifications, many of these algorithms are now being adopted for processing AE/MS data. In spite of the presence of these numerous algorithms, however, accurately detecting and picking phase arrival times on AE/MS data remains a major challenge. AE/MS data are generally characterized by low SNRs and complex waveforms making automatic phase picking difficult. As was indicated by Sharma et al. [52], no arrival time picking algorithm is optimal under all conditions, instead, they tend to become unstable under noisy conditions. This realization makes the present study relevant and critical in contributing to the knowledge bank of AE/MS signal processing.

The dilemma faced by mine operators is usually on how to efficiently extract ore without jeopardizing safety. Issues such as ore zone delineation, defining the extent of excavation influence for dilution purposes, and identifying regions of potential instability are among the concerns dealt with by mine managers. The literature reviewed also provided some case studies showing successful utilization of the AE/MS method in mines. The review showed that the discovery of the technology has gone a long way to improve safety monitoring especially in underground mines.

The rationale for this PhD research is then highlighted by way of showing the challenges encountered with present algorithms when applied to AE/MS data. Of the various signal processing steps, seismic event extraction with precise timing has been identified as the most important step. However, there is no efficient method for processing AE/MS data in the literature. Accurate onset time is required to ensure reliable source location determination. In a noisy environment, the acquired AE/MS data are highly corrupted by background noises. Hence, the reliability of present algorithms is affected if applied without appropriate modifications. Again, for cases where there is interference between signals, the AE/MS signals themselves may present a major challenge. These challenges, therefore justify this research.

3. THEORIES AND SUMMARY OF PROPOSED METHOD

This section provides a comprehensive summary of the key concepts adopted for the newly proposed acoustic emission/microseismic (AE/MS) signal processing method. The section provides a detailed discussion on the choice of the WT as a filter. Specifically, the use of the stationary discrete wavelet transform (SDWT) as a filter is explored. According to Lee and Stewart [97], seismic events can be distinguished by high frequency, impulsive onsets, exponential envelope, and decreasing signal frequency with time. On the other hand, low frequencies and low amplitudes are the main features that define background noises. However, AE/MS events characteristics are drastically different from seismic events in seismology. Hence, dealing with AE/MS data requires the use of techniques capable of separating appropriately AE/MS events from noise. Using these features, the SDWT is employed to filter raw AE/MS data to demonstrate its effectiveness in background noise reduction. The principles of operations and the mathematical background of the SDWT as well as the fundamental differences between the SDWT and the DWT method are highlighted. These discussions are then followed by the mathematical theories on coefficients thresholding to further enhance the signal-to-noise ratio (SNR). Immediately following this is the discussion on the choice of a characteristic function (CF). Again, the discussion on the CF is devoted to the mathematical theories and justification for the particular CF choice made for this research. The theories and concepts for phase identification, phase picking, and phase associations are then presented. A summary of the proposed method is then provided to conclude the section.

■■■ IMPROVING DATA QUALITY FOR PHASE RELIABILITY DETECTION

The mining environment, as well as other industrial environments, is sometimes characterized by high noise levels. As such, the AE/MS data acquired during monitoring can be very difficult to analyze. The activities of mining machines, ventilation fans, blasting, electrical spikes, operations from nearby mines, and transportation vehicles generate noise of varying intensities. The noise from these activities may drastically affect the quality of the AE/MS data. On the other hand, for cases where there is interference among signals (typically under burst conditions), the AE/MS signals themselves may

present a major challenge. Again, data recorded may have been a result of activities associated with S-wave arrivals instead of P-wave arrivals. Using this data without any preprocessing could introduce systematic errors in the database [2]. The presence of noise can extremely hinder the accurate detection of actual phase arrival, leading to wrong source location. Therefore, most applications employ the use of various techniques to help separate noise from the actual signal of interest.

As indicated by Ge et al. [98], for weak arrivals in an environment such as a mine, identifying the P-wave arrivals is sometimes impossible. Traditionally, the well-known high-pass and low-pass filtering technique have been used to filter background noise, making manual and automatic picking more reliable in the mine environment. However, for applications in which the time-frequency relations are of importance, these methods become ineffective. Even for the windowed Fourier transform, exactness in time and frequency in a given window function is fixed, making it inappropriate for detecting the arrival time of nonstationary signals with different levels [32]. In this section of the dissertation, the use of the stationary discrete wavelet transform (SDWT) technique is explored as a filter for the preprocessing of noisy AE/MS data.

3.1.1. Stationary Discrete Wavelet Transform (SDWT). The principles on which the SDWT operates are similar to that of the DWT except the process of sub-sampling. Section 2 of this dissertation gives detailed mathematical discussions on the DWT. As noted by Nason and Silverman [99], to obtain the SDWT, the filters in the SDWT are modified at each scale by introducing a zero between every adjacent pair of elements using an operator Z. The process of achieving this is as expressed in Equation (3.1):

$$h\left[2^{j+1}k-l\right]=Zh\left[2^{j}k-l\right] \Rightarrow \begin{cases} h_1\left[2^{j+1}k-l\right]=0 \\ h_0\left[2^{j}k-l\right]=h\left[2^{j}k-l\right] \end{cases} \tag{3.1}$$

$j = 0, 1 \ldots J - 2$

The detail and approximation coefficients of the stationary wavelet are then recursively calculated using Equations (3.2) and (3.3), respectively.

$$X^{(j)}[2k] = \sum_{k \in Z} h_0 [2^j k - l] X^{(j-1)}[l] \tag{3.2}$$

$$X^{(j)}[2k+1] = \sum_{k \in Z} h_1 [2^j k - l] X^{(j-1)}[l] \tag{3.3}$$

The original signal can be reconstructed by applying an algorithm similar to Equation (2.14). It is important to note that each of the coefficients obtained at the different scales in the SDWT will have the same length as the original signal rather than becoming shorter with increasing scale as is the case in the DWT. This property remains a fundamental advantage of the SDWT compared to the DWT, and therefore, a good candidate for the present study.

A diagram depicting the processes involved in the SDWT is illustrated in Figure 3.1. In Figure 3.1, the signal for which the SDWT operation is to be performed on is represented by x (k). WT^a (j, k) and WT^d (j, k), with $j = 1 \ldots J$, are the approximation and detail SDWT coefficients of the signal at any given scale j, respectively. The approximation coefficients equal the output of the low-pass filters while the output of the high-pass filters equals the detail coefficients. The values for filters H_j and G_j ($j = 2 \ldots J$) are the output resulting from the up-sampling of the filters used at the immediate past step (H_{j-1} and G_{j-1}) by 2, respectively. The h1 and g1 at the beginning are taken as the high-pass and low-pass wavelet filters, respectively, of the standard decomposition [99].

3.1.2. Fundamental Differences Between the DWT and the SDWT Algorithms.

Major advantages of the DWT include its computational efficiency and the property of orthogonality. The DWT efficiency in computation is achieved by using the Mallat algorithm. While these properties of the DWT are important for some applications, in multi-resolution analysis, this importance has not been shown [100].

A fundamental challenge with the DWT technique remains its shift-variant transform property [101]. The problem of shift variance is due to the use of down-sampling in the DWT process. With the down-sampling process, every second coefficient of the wavelet is excluded at every decomposition scale (level). The down-sampling technique ensures a reduction in the volume of data being used, as well as implementation of the

inherent time-frequency uncertainty of the process. In the end, this down-sampling produces wavelet coefficients that are reliant on their position in the sub-sampling matrix. This may result in three fundamental problems:

- minimal changes to the input waveform causing major variations in the wavelet coefficients;
- major disparities in energy distribution at various levels; and
- possibly significant variations in waveforms that is reconstructed [102].
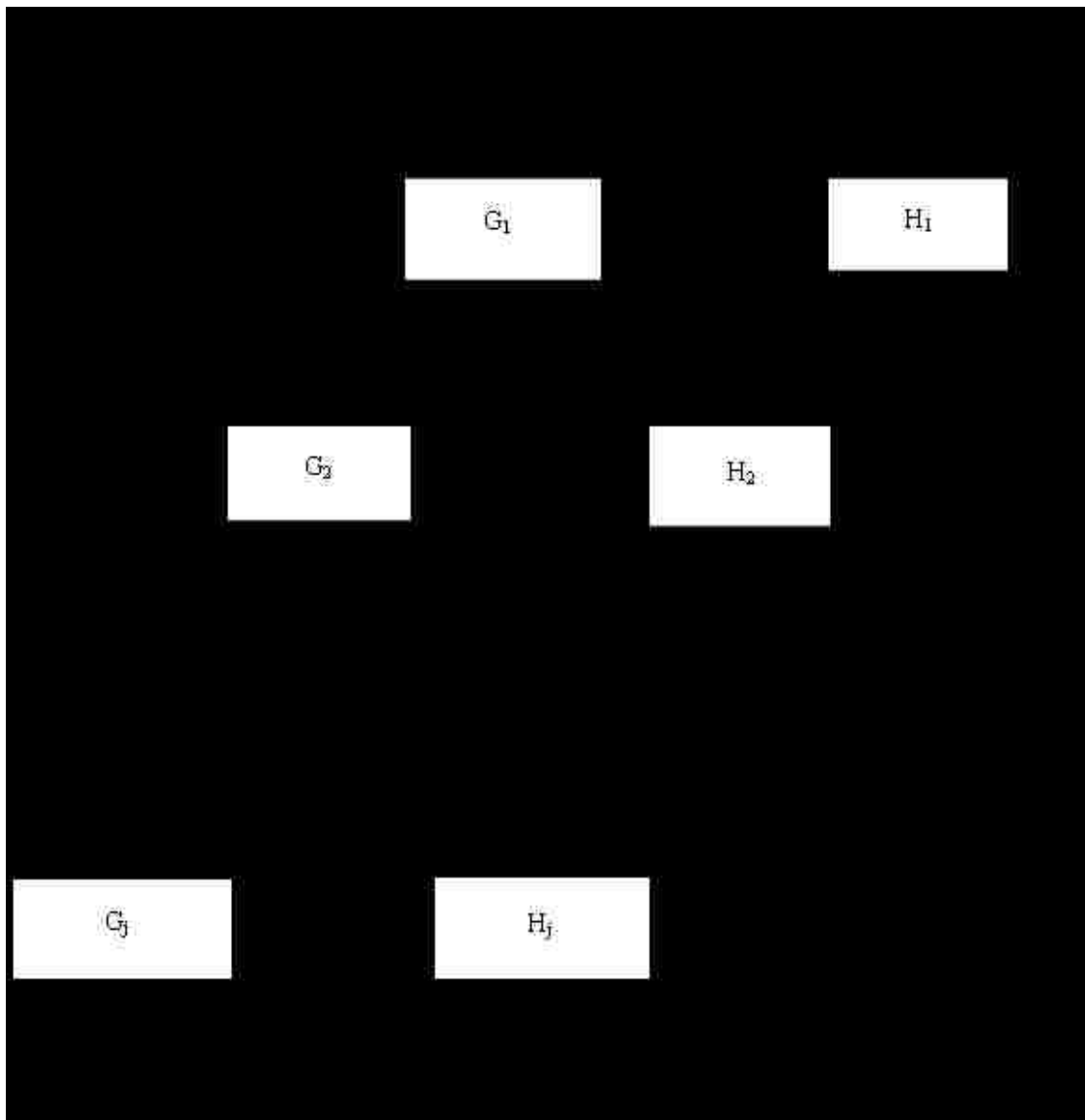
Figure 3.1 Algorithm for computing the SDWT coefficients [105]

One of the major ways to address the challenges encountered with the DWT is to employ the SDWT technique. As indicated by Mallat and Zhong [101] and Mallat [103], the DWT is unsuitable for many signal analysis applications because of its shift-variant transform property. The SDWT, on the other hand, has no translation of the signal and is obtained by modifying the original algorithm for the DWT [99]. The absence of the process of down sampling in the SDWT remains the fundamental difference between the SDWT and the DWT algorithms. Also, the SDWT provides an output (detailed and approximate coefficients) at the different scales for which the length is approximately equal to the length of the original signal instead of becoming shorter with increasing scale as is the case in the DWT algorithm. However, the filters in the SDWT are modified at each scale by introducing zero between adjacent pair of elements using an operator. The SDWT method, therefore, has the following properties: (i) redundancy; (ii) linearity; and (iii) shift invariance and therefore, the SDWT method provides better approximation than the DWT [99].

This research study intends to find the phase arrival in the wavelet domain. Therefore, the sample point corresponding to this arrival time must be determined. This requires that the transformation used is shift-invariant. The requirement for this property informed the choice of the SDWT over the DWT in the study.

3.1.3. Wavelet Thresholding. To improve the SNR of data in noisy environments, level-dependent thresholding techniques have been used in some wavelet applications to eliminate background noise [40]. In the wavelet domain, nonlinear thresholding estimators provide nearly minimax risk over a large class of functions [104]. This property, coupled with the ease of implementation and generality, has provided motivation for the development of nonlinear thresholding estimators. This has provided an amazing tool for function estimation.

The fundamental requirement in level-dependent wavelet thresholding is estimating the threshold at each scale from the wavelet coefficients of the contaminated data. It has been shown that the optimal threshold at each scale is proportional to the standard deviation of the noise estimated from the median of certain wavelet coefficients. The validity of the threshold estimation is based on the assumption that the wavelet representation of the

deterministic signal is sparse, and thus, most of the wavelet coefficients are due to noise [40].

Since the AE/MS data acquired in the mining environment is one noted for high noise levels [22], performing either soft or hard level dependent thresholding could further improve the SNR. The method of thresholding generally involves four fundamental steps. The mathematical description and steps are well described by To et al., [40]. The first step requires the computation of the wavelet coefficients. The second step involves the estimation of the noise variance σ_j^2 at each level $j = m,..., J-1$ using Equation (3.4), where med (.) represents the median.

$$\hat{\sigma}_j = \frac{med\left(\left|X^{(j)}[2k+1]\right|\right)}{0.6745} \tag{3.4}$$

After obtaining the variance at any particular level, the threshold T_j at that level j is then obtained using Equation (3.5):

$$T_j = \hat{\sigma}_j \sqrt{2In(2^j)} \tag{3.5}$$

For a soft-level dependent threshold estimator, Equation (3.6) is used, while Equation (3.7) is used for hard-level thresholding.

$$\hat{X}_S^{(j)}[2k+1] = \begin{cases} sgn\left(X^{(j)}[2k+1]\right)\left(\left|X^{(j)}[2k+1]\right|-T_j\right) & \text{if } \left|X^{(j)}\right| > T_j \\ 0 & \text{otherwise} \end{cases} \tag{3.6}$$

$$\hat{X}_H^{(j)}[2k+1] = \begin{cases} \left(X^{(j)}[2k+1]\right) & \text{if } \left|X^{(j)}\right| > T_j \\ 0 & \text{otherwise} \end{cases} \tag{3.7}$$

The parameter $\hat{X}^{(j)}[2k+1]$ represents the estimates of the wavelet coefficients $(X^{(j)}[2k+1])$ of the signal while the subscripts H and S denote hard and soft thresholding, respectively.

In an effort to enhance data quality, the process of thresholding is incorporated in the proposed new algorithm based on the theories discussed in Equation (3.4) through Equation (3.7). It is believed that this step will further ensure event arrival picks are reliable.

3.1.4. Verification and Validation Results on AE/MS Data Quality Improvement. To ascertain the suitability or otherwise of the data quality improvement methods discussed in Equations (3.1) through (3.7), the methods were applied to a real AE/MS event for which the phase arrival time and frequency contents were known. In order to achieve the set objective of cleaning up the data, the raw data was first decomposed over six (6) scales (levels) using the DSWT. The soft thresholding technique was then applied and the resulting signals are shown in Figures 3.3 to 3.5. The unfiltered raw signal is shown in Figure 3.2. In Figure 3.2, manual identification of the onset of the P-wave phase arrival will be a major challenge even for an experienced human expert. The arrival is completely buried in the background noise. By decomposing the signal over the six scales (Figures 3.3, 3.4, and 3.5), the phase arrival can easily be seen at the higher scales. The first two scales (Figure 3.3) provided no clear observation of the phase onset because the background noise levels were still very high. As a result, accurately reading and estimating the arrival times on these scales were impossible due to the presence of the high background noise. The frequency band for these scales was 241 hertz (Hz) and above.

On the other hand, the emergence of the phase arrival became clear from scale 4 and the corresponding frequency band was 120 Hz and below (see Figures 3.4b and Figure 3.5). Using these detail-coefficients, the P-wave phase arrival onset was manually found at sample number 550. The results obtained by this technique matched very accurately the results by Ge et al. [98] and demonstrated that, the filtering effect was effective.

From the frequency content distribution across the scales, it is obvious the AE/MS signal has frequencies of 120 Hz and below while that of the noise is about 240 Hz and above. These observations are well within the frequency limits defined for the noise and

AE/MS event for the dataset by Ge et al. [98]. One of the key advantages of the time-frequency method employed in this manual technique was the clear identification of the frequency contents and the time range of this frequency as the scales increased (the scale is inversely proportional to frequency). In other words, low-frequency content signals (AE/MS signal) had very good frequency resolution while high-frequency contents (background noise) had good time resolutions. A property that cannot be obtained if only time or frequency domain analysis is done. The improvement in manual picking as a result of the use of the SDWT technique indicates that its use in the automatic picking will enhance the performance of the proposed system.

■■ BRIEF MATHEMATICAL CONCEPTS ON STATISTICS

In mathematical statistics, four fundamental statistic moments, namely the first statistic moment (mean value), the second statistic moment (variance), the third statistic moment (skewness), and the fourth statistic moment (kurtosis), are used and have been widely reported in literature. In this section, the suitability of high order statistics [HOS] as functions for defining the CF for AE/MS data is investigated. This is done by using the different statistical functions to determine an optimal CF capable of amplifying the arrival of a phase in the presence of background noise. The evaluation is performed using both synthetic and actual AE/MS data in a moving time window. For accuracy and efficiency, the lengths of the window were computed based on the sampling interval and the dominant period of the signal. For each HOS function calculation, the window is moved one sample at a time. For a start, a brief review of these statistical functions is provided below.

For a given distribution, the weighted center of the distribution is commonly measured by using the mean. According to Gravetter and Wallnau [106], central tendency is "the statistical measure that identifies a single value as representative of an entire distribution." The mean generally provides a good representation of the data because it uses all data values. Mathematically, the expression of the mean (arithmetic mean) of a distribution is obtained by Equation (3.8):

$$\bar{x} = \frac{1}{n} \sum_{i=1}^{n} x_i \tag{3.8}$$

n is the number of sample points in the distribution, x_i is sample value at any given index i, and $\overline{x}$ the mean.
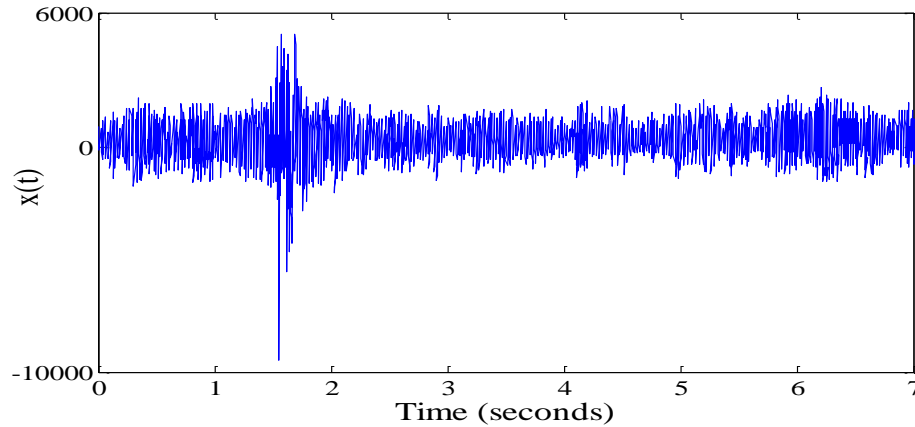
Figure 3.2 Original unfiltered signal

The variance of the distribution is then expressed as shown in Equation (3.9):

$$\sigma^2 = \frac{1}{n-1} \sum_{i=1}^{n} \left(x_i - \overline{x} \right)^2 \tag{3.9}$$

The term skewness is generally used to describe distributions in which one tail is longer than the other. The term skewness was first used by Pearson [107] to describe asymmetry in distributions. According to this statistic, if the resulting value is positive, then the distribution is said to be positively skewed. The skewness is zero for a normal distribution and therefore any symmetric data should have a near-zero skewness. If the data is skewed to the right, the skewness value will be positive, and it will be negative if it is to the left. The mathematical expression for the skewness of a distribution is obtained by Equation (3.10) [35]:

$$S[s] = \frac{\sum_{n=1}^{N} \left(s(n) - \mu_s \right)^3}{(N-1) \cdot \sigma_s^3} \tag{3.10}$$
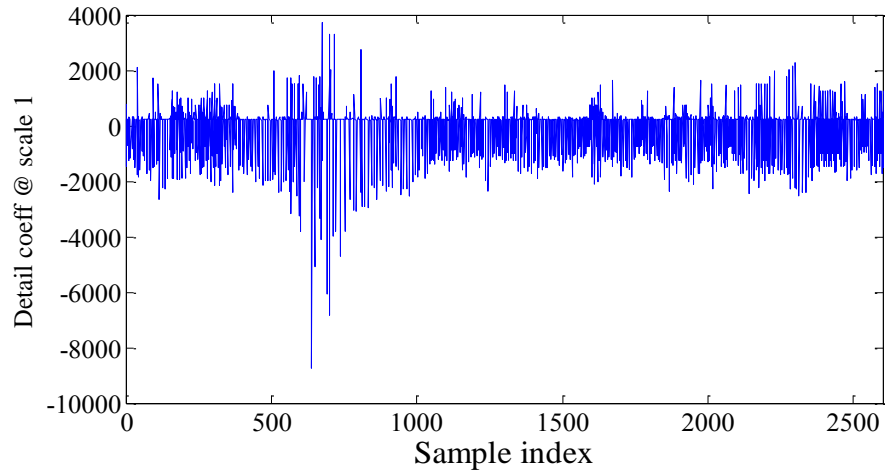
(a)
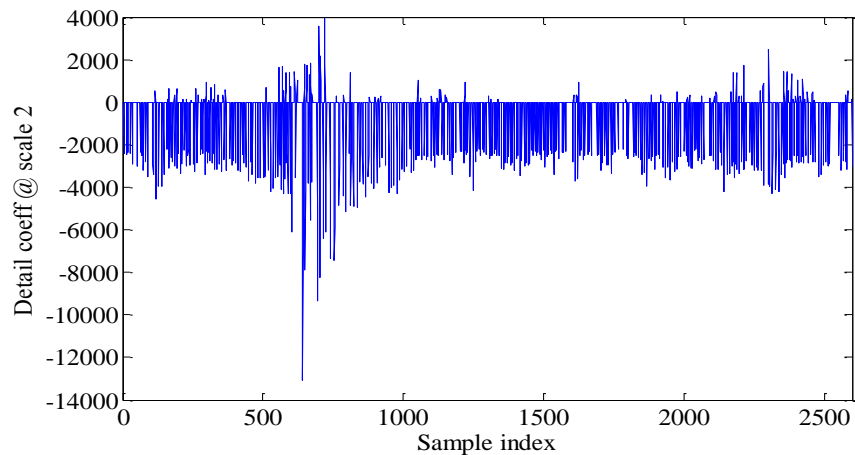
(b)

Figure 3.3 SDWT decomposition results for (a) detail coefficients at scale 1 and (b) detail coefficients at scale 2

Kurtosis, on the other hand, shows how peaked a data is distributed in relation to a normal distribution. In other words, it measures the sharpness of the distribution. Pearson [108] provided a comparative study of kurtosis and normal distribution and established three data distribution classes. The author noted that if a distribution has more values in the tails, less in the shoulders, and a peak, it was leptokurtic. The second class was platykurtic, characterized by fewer values in the tails, more in the shoulders, and less in the peak. The third and final class was mesokurtic. This type of distribution has the same values as the

normal distribution. The mathematical definition of kurtosis is given in Equation (3.11) [35]:

$$K[s] = \frac{\sum\limits_{n=1}^{N}(s(n)-\mu_s)^4}{(N-1)\cdot\sigma_s^4} - 3 \tag{3.11}$$
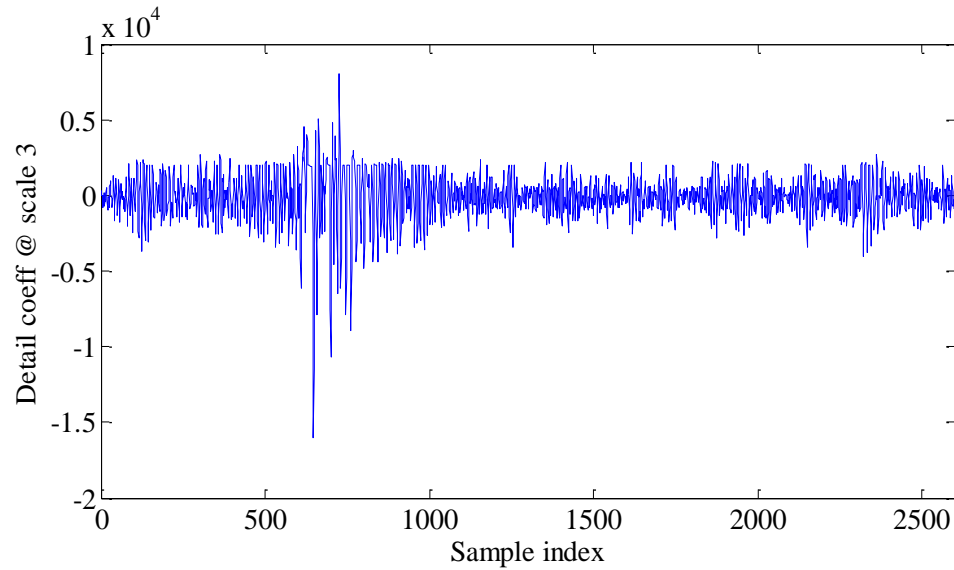
(a)
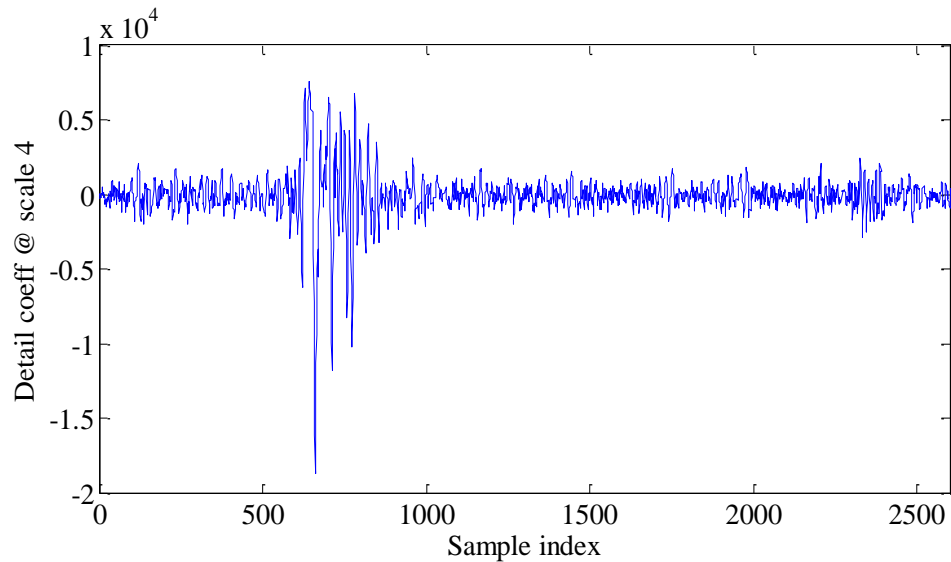
(b)

Figure 3.4 SDWT decomposition results for (a) detail coefficients at scale 3 and (b) detail coefficients at scale 4
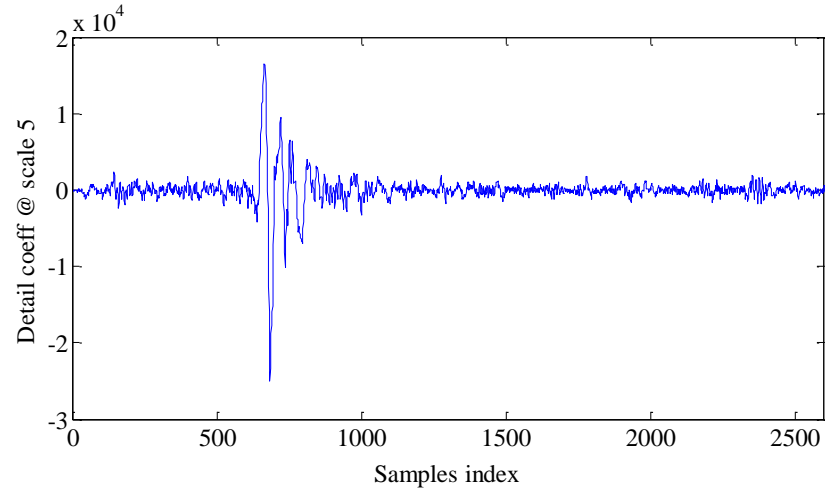
(a)
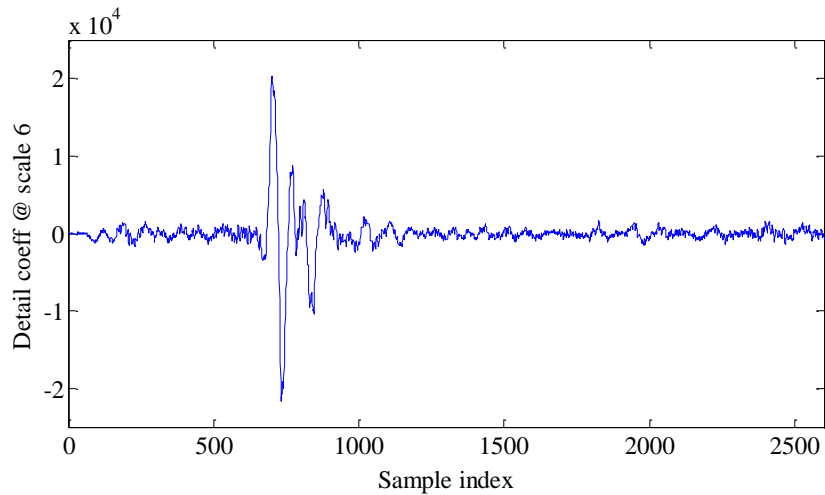
(b)

Figure 3.5 SDWT decomposition results for (a) detail coefficients at scale 5 and (b) detail coefficients at scale 6

If a dataset has high kurtosis, the data tend to have a distinct peak near the mean value and declines sharply with heavy tails. Low kurtosis datasets have a flat top near the mean in comparison to the sharp peaks obtained in high kurtosis data-sets. A positive kurtosis indicates a peaked distribution, while a negative value indicates a flat distribution.

■■ DETERMINATION OF CF AND PHASE ARRIVAL TIME PICKING

In this section, the impact of different statistical functions on accurately defining the characteristics of phase arrival in the presence of noise is examined using both synthetic and field data. The results from these functions are then compared the results from the standard STA/LTA CF. The section also presents the mathematical background for the proposed phase association algorithm. The results of these tests and the discussions are presented below.

3.3.1. Determination of Appropriate CF/Verification and Validation. The CF remains the single most important parameter that determines the performance of an automatic detector or picker. Phase arrival is usually characterized by changes in the frequency content and amplitude of the seismic or AE/MS time series. Any good CF should, therefore, respond to this change and enhance the change in a timely manner [27]. The choice of this parameter is therefore critical in the design of any new detector or picker. In this section, various CF functions are evaluated using HOS in moving time windows to determine the function that best enhances changes in AE/MS signal characteristics. Figures 3.7 to 3.8 show a demonstration of the performance of different CFs on synthetic data. For pure background noise distribution (Figure 3.6a), the mean, variance, skewness, kurtosis, as well as the standard STA/LTA CFs all showed a near constant distribution in each window (Figure 3.7). On the other hand, the presence of a phase arrival associated with an event (Figure 3.6b) causes sharp variations in the distribution of these functions (Figure 3.8). The sharpest and clearest variations are more pronounced in the case of skewness and kurtosis compared to the other functions. The sharp change in these functions demonstrates that the distribution is not a normal distribution as was shown in the case of the pure background synthetic noise (Figure 3.7).

To verify and validate further the appropriateness of these parameters for detecting and picking the P-wave phase arrivals, the various functions were applied to the field data used in Figure 3.2. The results of the performance of each function in detecting the change in distribution are shown in Figure 3.9. While there were clear changes in the shapes of each of the functions near the point of the P-wave phase arrival, the sharpest changes were once again observed in the case of the skewness and kurtosis functions (Figure 3.9b).
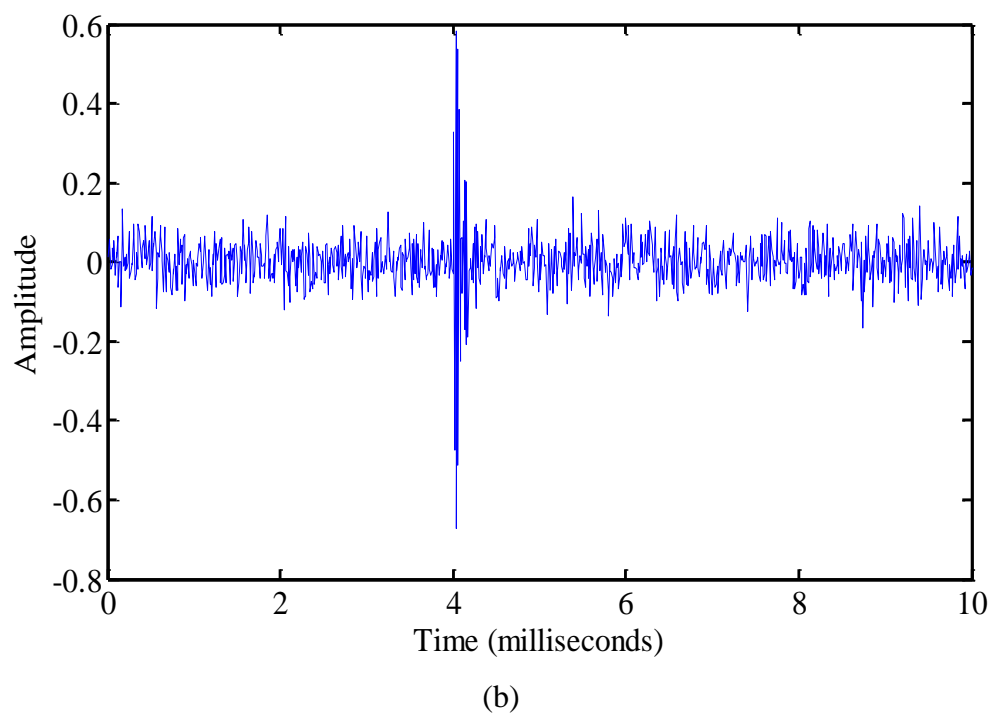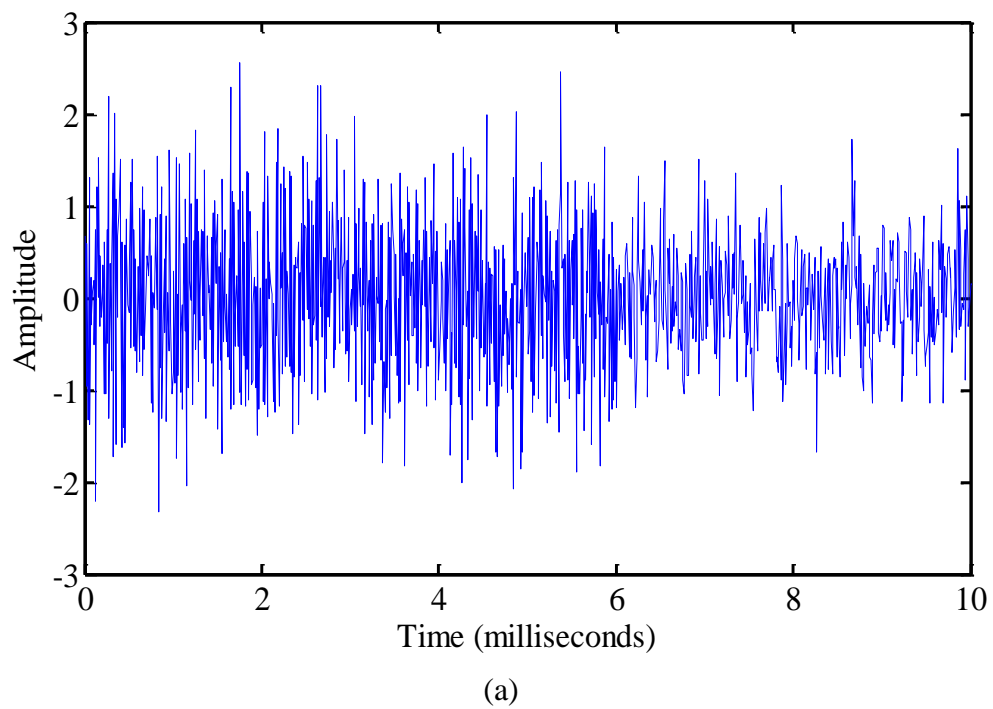
Figure 3.6 (a) Synthetic noise with no event and (b) synthetic noise with an event
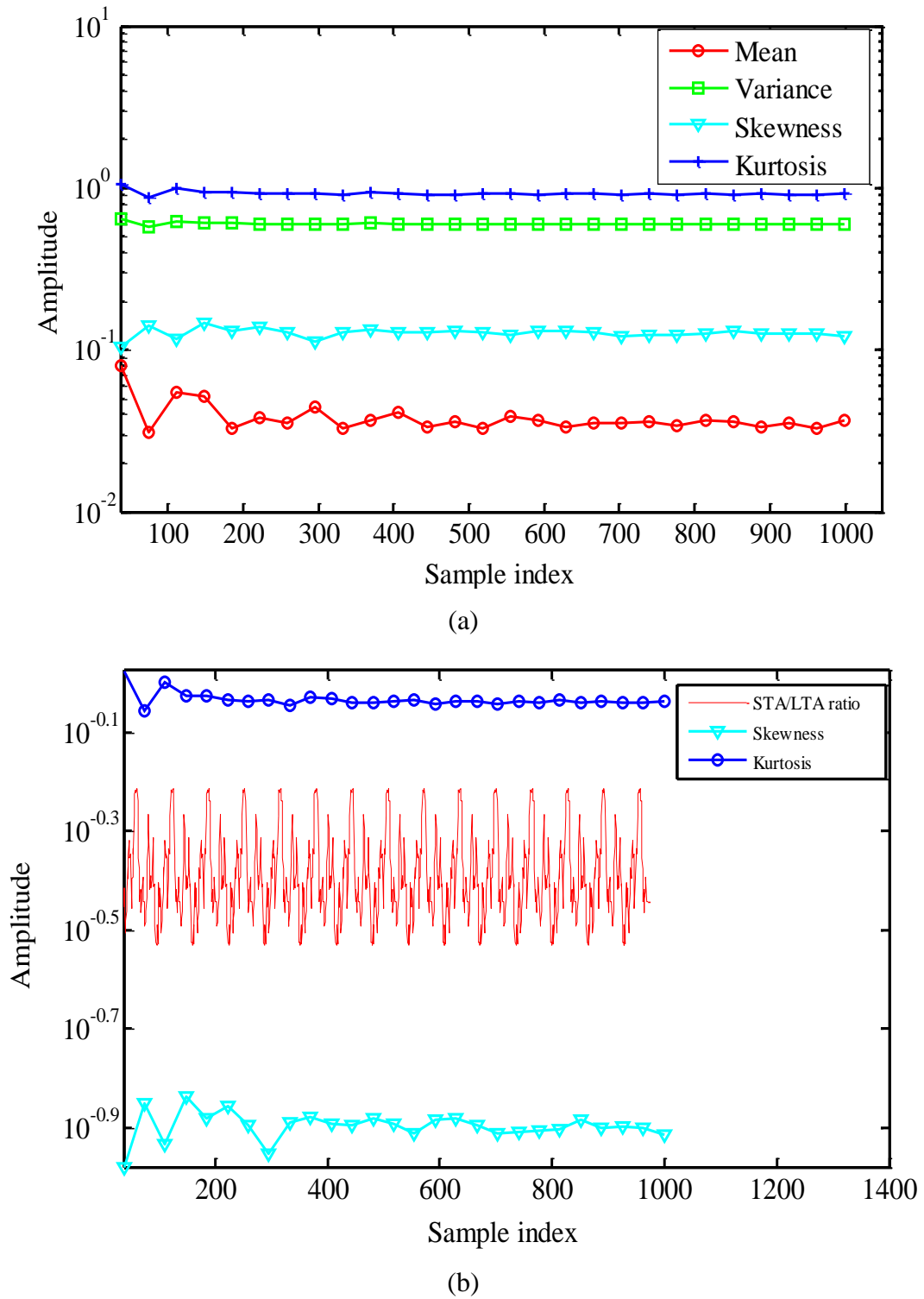
Figure 3.7 Performance of the mean, variance, skewness, kurtosis, and the standard STA/LTA on synthetic noise with no event
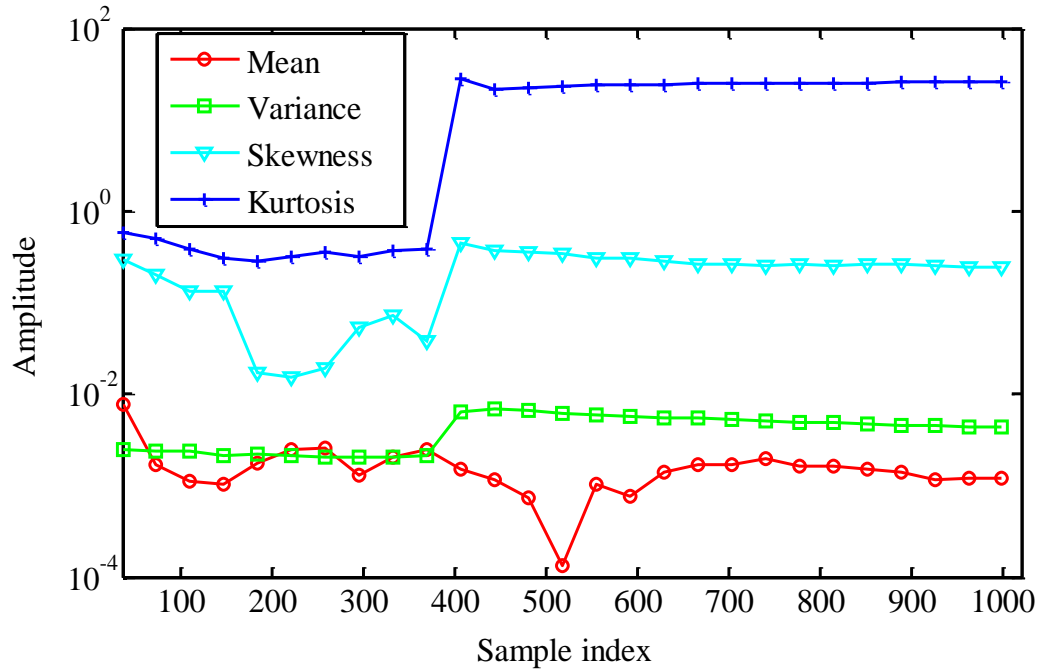
(a)
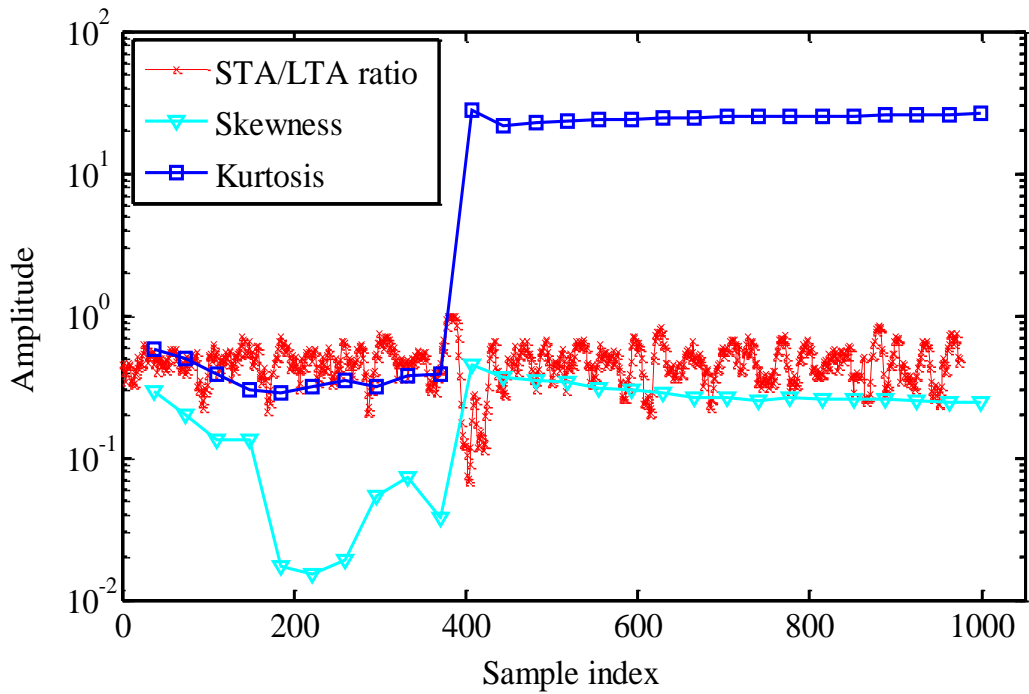
(b)

Figure 3.8 Performance of the mean, variance, skewness, kurtosis, and the standard
STA/LTA on synthetic noise with an event

(a)

(b)
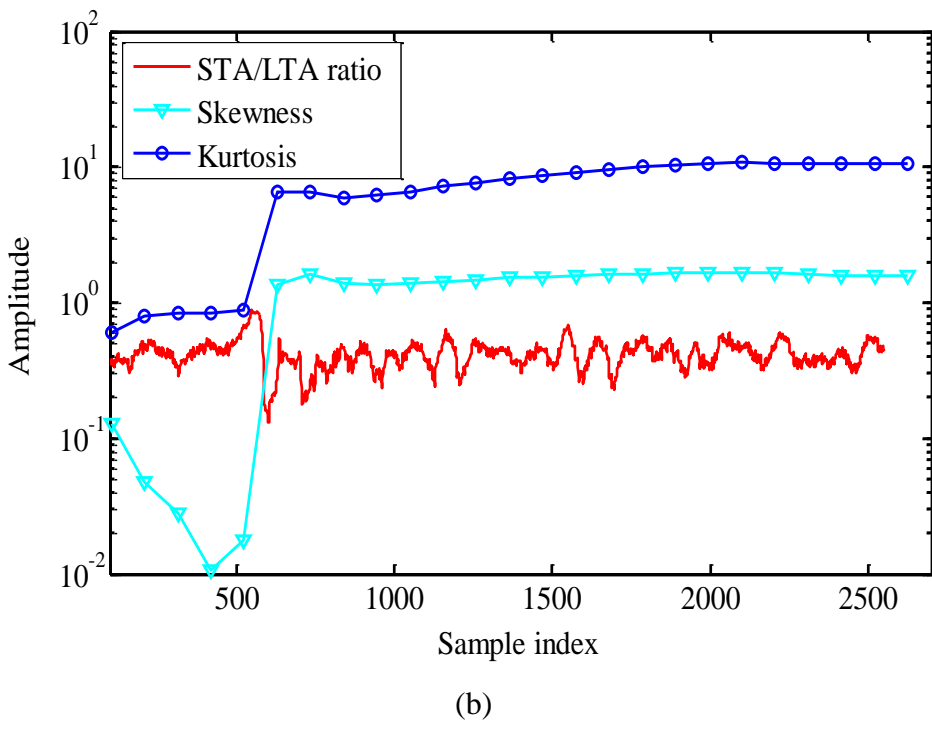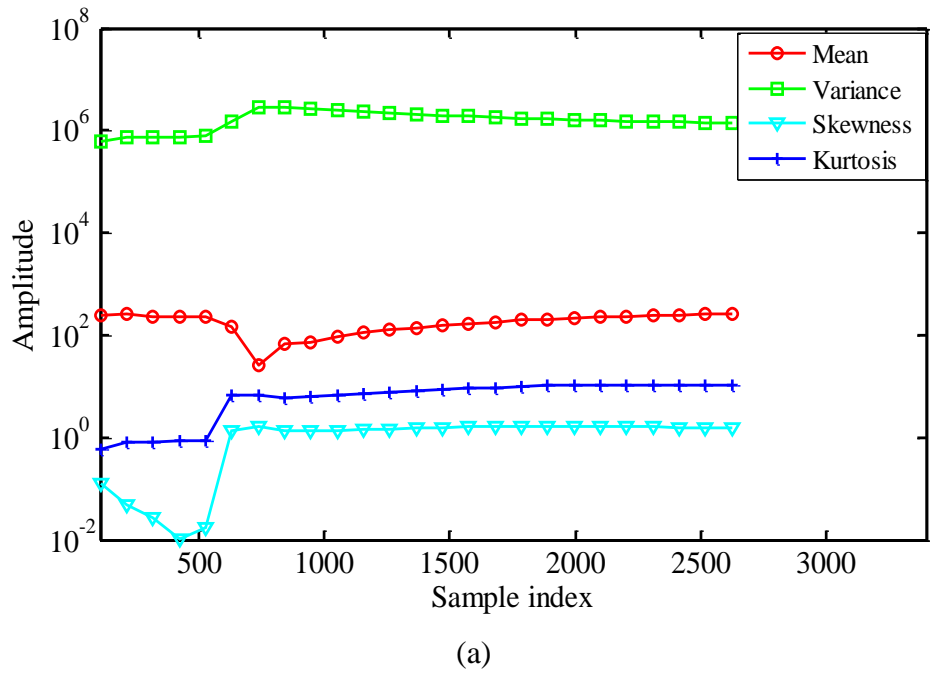
Figure 3.9 Performance of the mean, variance, skewness, kurtosis, and the standard STA/LTA on sample field data

The results obtained by these tests indicate that the presence of a phase arrival is usually characterized by changes in distribution from Gaussian (normal distribution) to non-Gaussian distributions (non-normal distribution). The use of these statistical functions, therefore, presents an opportunity for improving the detection and picking of event phase arrivals in AE/MS signal analysis. Based on the superior performance (determined based on the data tested) of the skewness and kurtosis based functions in enhancing changes in the character of the signals, the CF for this study shall be defined using the two functions. For the rest of this study, the use of the term CF will be in reference to skewness or kurtosis based function.

3.3.2. Phase/Arrival Time Picking Procedure. To ensure phase arrival picks obtained are reliable, the picking is done across at least three scales of the SDWT process. For each scale, the picking is done based on CFs defined by skewness and kurtosis. Since AE/MS data encompasses various forms of noise that may or may not always have a Gaussian distribution, phase picking performed with these two parameters in the time domain alone could lead to either high kurtosis or skewness values. This may result in false onset picks or a total failed pick. For this reason, the determination of these statistical parameters in the time-frequency domain presents an opportunity to avoid such problem. The time-frequency domain analysis ensures that the variations of the temporal and spectral characteristics of the AE/MS signal and background noise are properly accounted for. In fact, the effect of high-frequency noise and low-frequency trends is strongly reduced in the time-scale analysis. Again, in order to prevent false detection because of high kurtosis or skewness values due to secondary arrivals, the arrival-time pick analysis is performed on the rate of change of these parameters instead of using their maximum values.

For every selected scale, the statistical parameters are computed in a moving time window of length M. The window is moved one sample at a time. The most recent values of skewness and kurtosis in the window are stored at the end of the present window. A rate of change of skewness and kurtosis is then calculated at every point. The maximum slope of the series considered is then determined. After this determination, the sample index at which this maximum slope occurred and the corresponding stationary wavelet scale number are then recorded and saved to the results file. The maximum slopes among the

scales are further compared and the maximum determined. The results for the kurtosis-based and skewness-based criterion for each scale are then compared. If the difference in the sample index picked by the two criteria is more than a set threshold (Beta), the process is started by providing a new window size. Beta is obtained by first finding the difference between the maximum slope values determined across the scales for the kurtosis-based and skewness-based criterion. The resulting figure is then divided by the number of scales to give the final value of beta. The sample index corresponding to the maximum slope at which all conditions are satisfied then becomes the time at which the P-wave phase onset was detected and picked.

To test the suitability of the picking method described above, the method was applied to the data used in Figure 3.2. Sample results of the distribution of the slopes across selected scales for kurtosis-based and skewness-based pickers are shown in Figures 3.10, 3.11, and 3.12. For the particular data used in this test, the maximum slopes of kurtosis and skewness always occurred at sample number 550 for all scales (see Figures 3.10, 3.11, and 3.12). However, the maximum slope of kurtosis (0.326668) when compared across scales was obtained at Scale 5 (Figure. 3.12a). The maximum slope for the skewness-based picker, on the other hand, gave a value of 0.046587 with a corresponding sample index of 550. Again, this result was obtained in Scale 5 (Figure 3.12b). The two results, obtained by the skewness-based and kurtosis-based criterion, matched the manual readings and the results from Ge et al. [98] excellently. Therefore, it can be concluded that the method is reliable and efficient for detecting and picking the P-wave phase arrival onset for this particular case.

▇▇ PHASE ASSOCIATION AND RELIABILITY TEST

Automatic event phase onset detection and picking in the AE/MS field has mainly been done based on voltage threshold level crossing and event time window. In most cases, it is assumed that the picks made in these systems are solely P-wave arrivals, which in part are due to the absence of theories for the identification of arrival types in these algorithms. Incorrect arrival time picks resulting from such misidentifications leads to wrong source locations. In addressing this issue, this study adopted a phase association theory proposed by Ge and Kaiser [109] for the physical interpretation of arrival picks without waveforms.

The interpretation of the status according to Ge and Kaiser [109] is achieved in a two-step process: arrival time difference analysis and residual analysis. Since the present objective is not directly on source location but on accurate arrival time picks, the section of the theory dealing with arrival-time difference analysis is discussed and employed for analysis of the picks in this study to further enhance the reliability of the new method. Below is a detail discussion on the theoretical background of the phase association theory.

■ ARRIVAL TIME DIFFERENCE AND HYPERBOLOID

The idea underpinning the arrival time difference analysis is that there exist theoretical arrival time difference limits, which can be used for studying the type of arrival picks on AE/MS events [109]. The source location process is a very complex task and its accuracy is influenced by many factors. These factors include data gathering, processing, and interpretation [110]. This complexity can, however, be simplified by assuming a half-space velocity model to demonstrate its basic principles [109].

According to Ge and Kaiser [109], if a source is located in a three-dimensional space, it will be defined by four unknown parameters: x, y, z, and t. The unknown parameters x, y, and z represent the coordinates of the source, while the parameter t represents the event origin time. Assuming the stress wave propagation velocity is denoted by v, then the equation for source location based on the half-velocity model is given by Equation (3.12):

$$\sqrt{(x_i - x)^2 + (y_i - y)^2 + (z_i - z)^2} = v(t_i - t) \tag{3.12}$$

where x_i, y_i, and z_i are the i th transducer coordinated; and t_i the ith transducer arrival time.

Assuming one is interested in subtracting the jth transducer equation from the ith transducer equation, then Equation (3.12) can be rewritten as in Equation (3.13):

$$\sqrt{(x_i - x)^2 + (y_i - y)^2 + (z_i - z)^2} - \sqrt{(x_j - x)^2 + (y_j - y)^2 + (z_j - z)^2} = v(t_i - t_j) \tag{3.13}$$
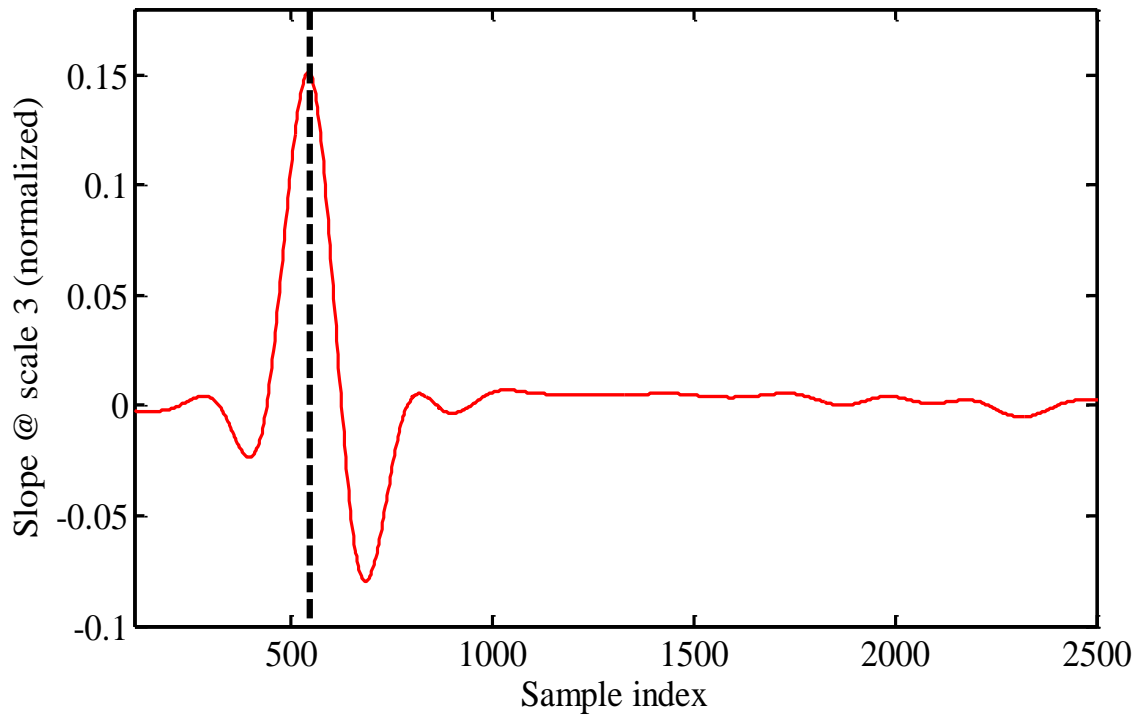
(a)
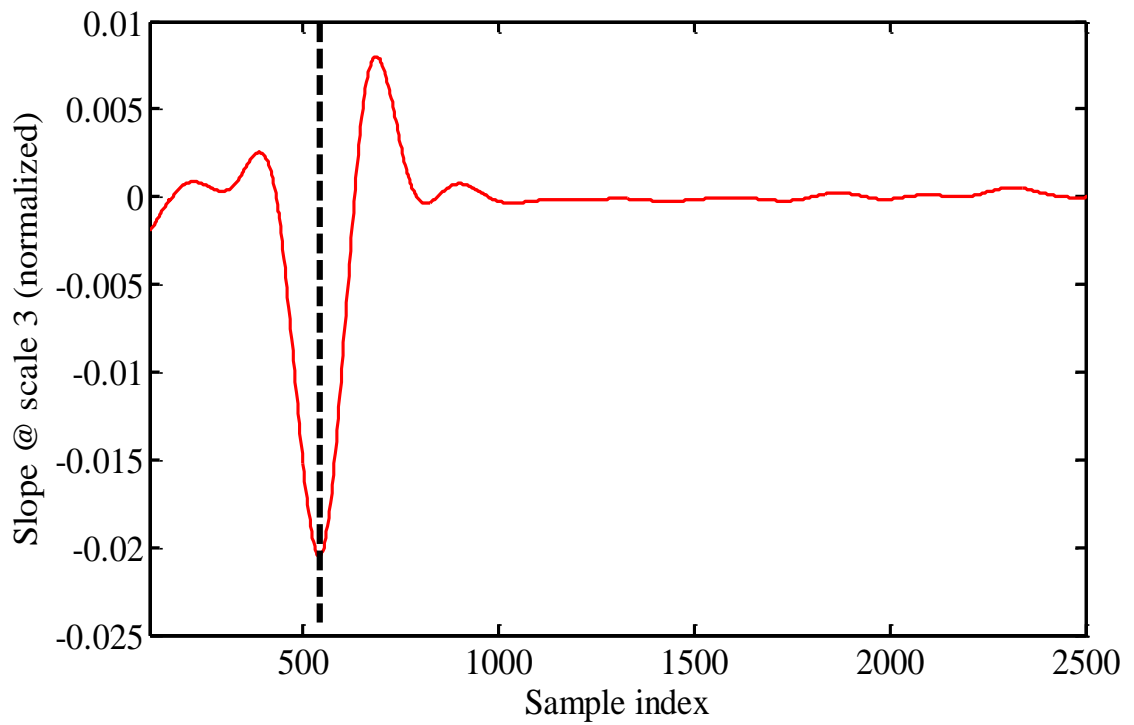
(b)

Figure 3.10 Slope of (a) kurtosis and (b) skewness on Scale 3 used for analysis
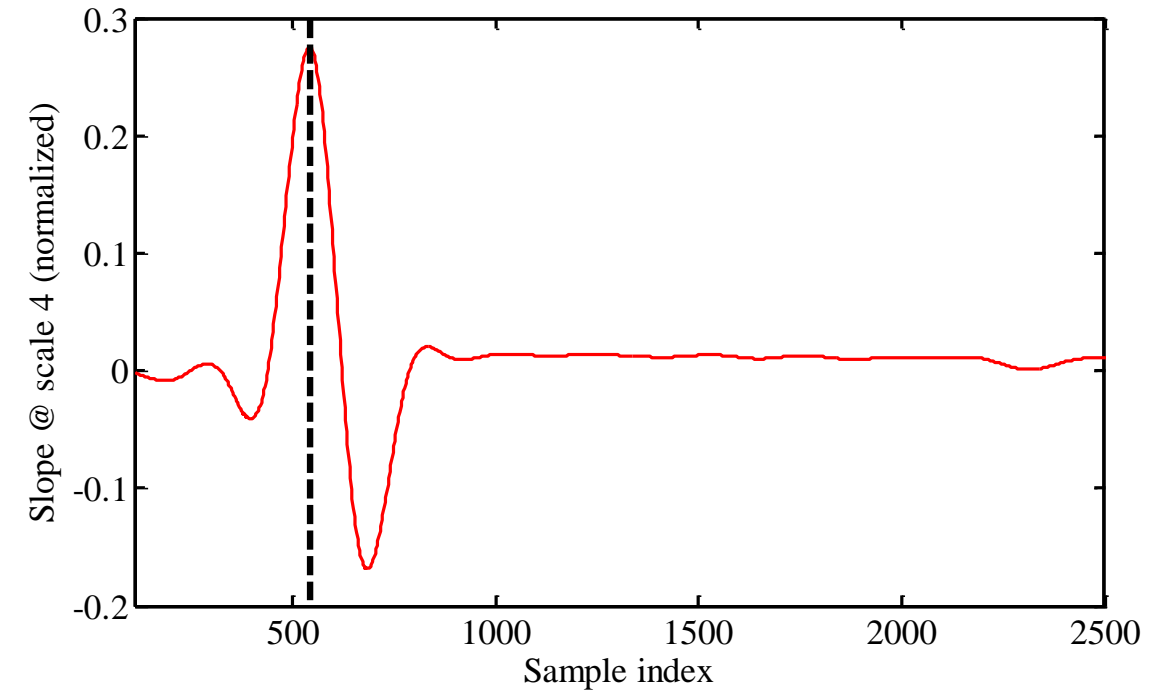
(a)
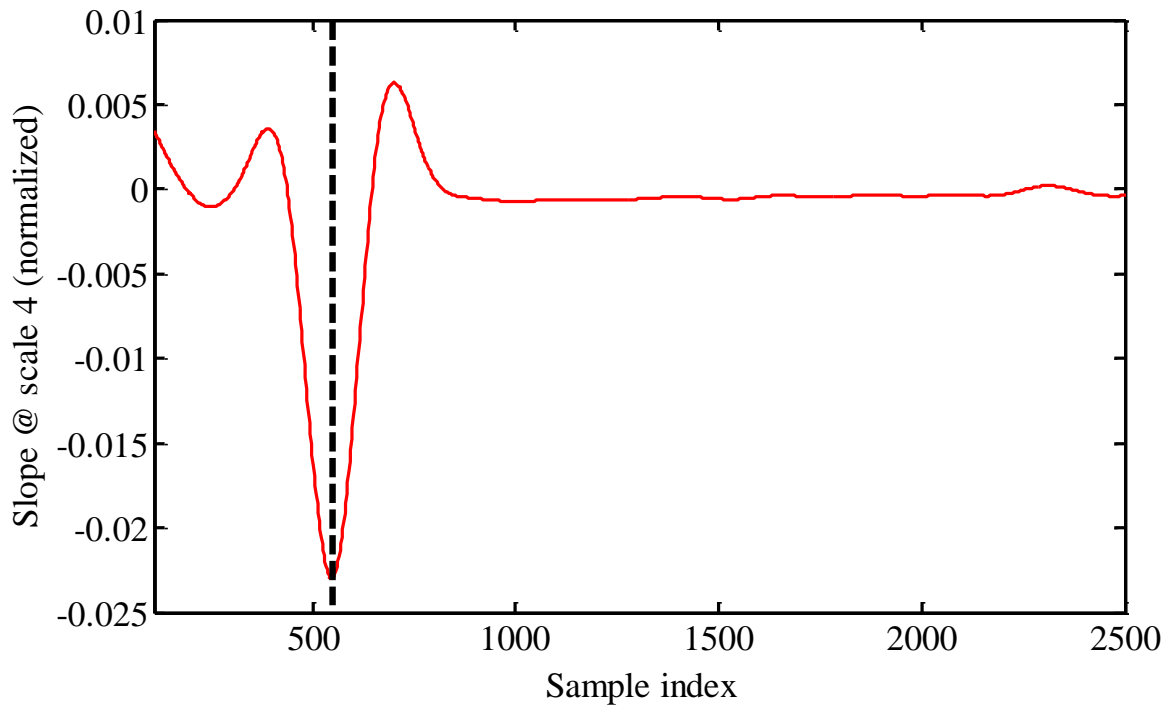
(b)

Figure 3.11 Slope of (a) kurtosis and (b) skewness on Scale 4 used for analysis
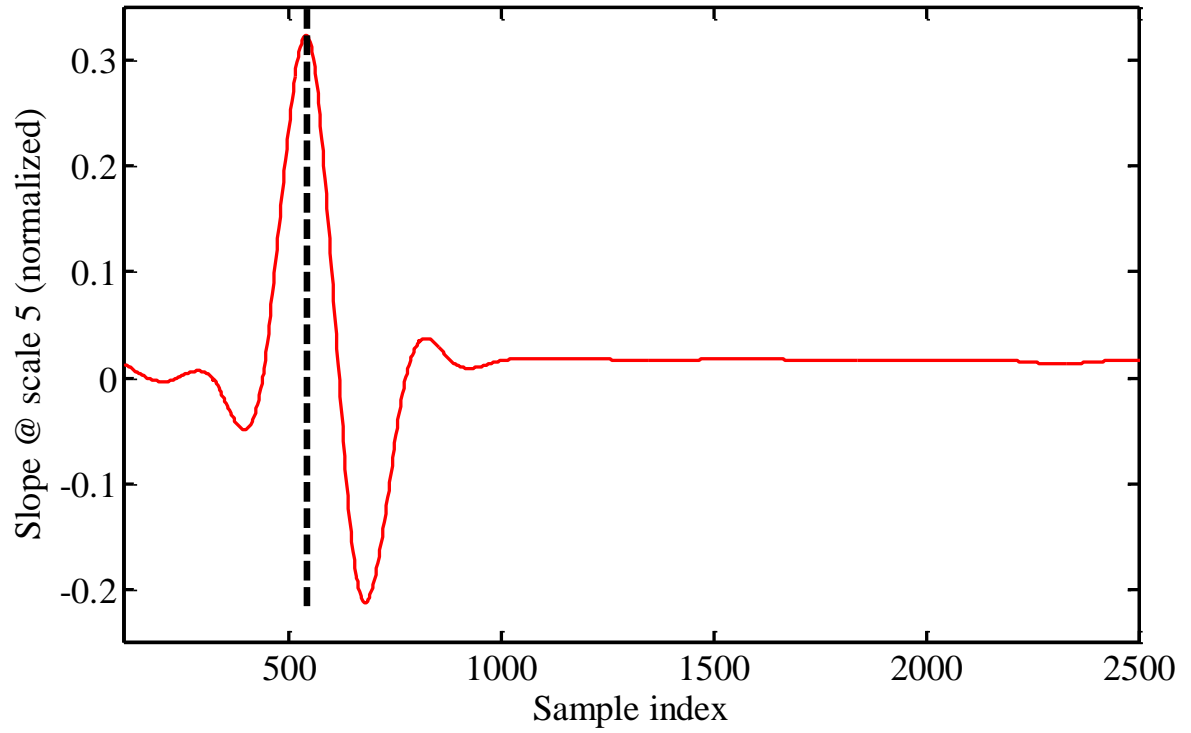
(a)
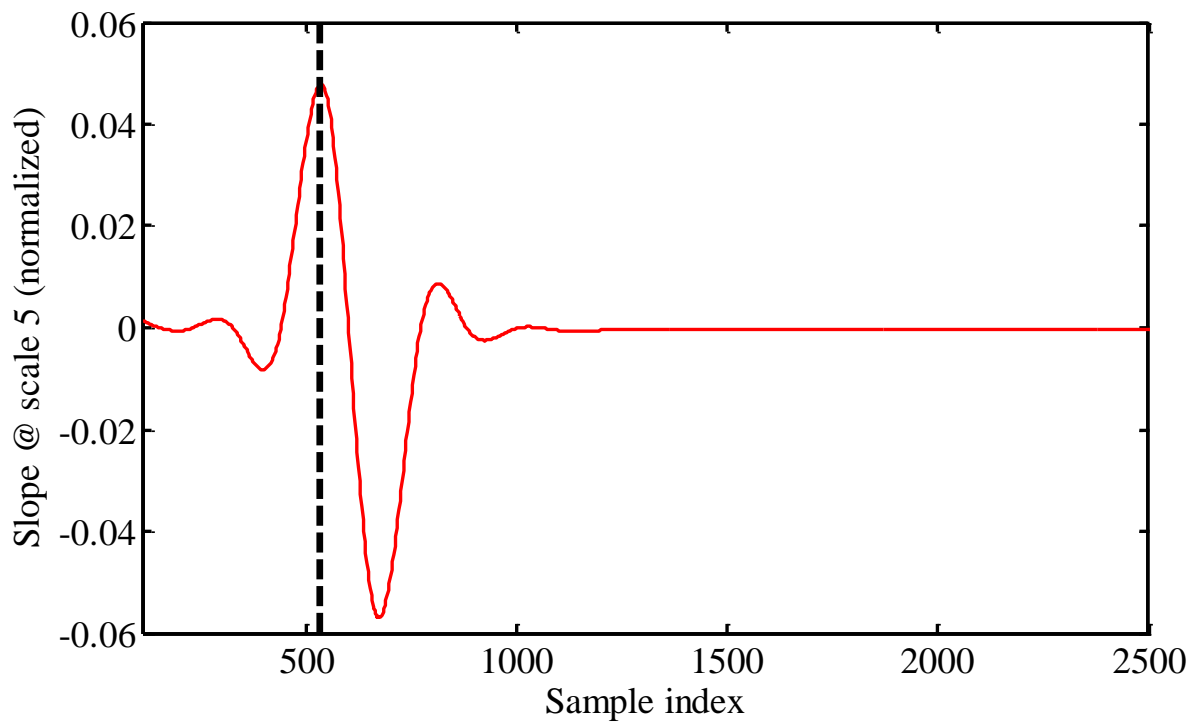
(b)

Figure 3.12 Slope of (a) kurtosis and (b) skewness on Scale 5 used for analysis

The resulting Equation (3.13), represents a hyperboloid and indicates that the use of the half-space velocity model for the determination of the source location is simply 'the process of finding the common intersection of hyperboloids" [109]. See Figure 3.13 for an illustration of the use of arrival time difference to determine a hyperbola.

From Equation (3.13), Ge and Kaiser [109] noted that the shape and position of the hyperboloid are solely dependent on the arrival time difference if the positions of the two transducers are known. It was also concluded that the range of the arrival time difference is given by Equation (3.14):

$$0 \leq \left| t_i - t_j \right| \leq \frac{2c}{v} \tag{3.14}$$

where $2c$ is the distance between the two transducers.

The following deductions can be derived from Equation (3.14) [109]:

I.   The source will be located on the mid-plane if the difference in arrival time is zero. That's the mid-plane will be located equal distance from the two transducers;

II.   A smaller arrival time difference is an indication that the source is closer to the mid-plane. See Figure 3.14 for an illustration of this point. In Figure 3.14, the mid-plane is represented by L_c. Higher arrival-time difference values are represented by hyperbolas that are further away from the mid-plane.

III. For a half-space velocity model, the theoretical limit of the arrival time difference is defined by $2c/v$. This implies:

$$\frac{2c}{v} \geq t_i - t_j \tag{3.15}$$

IV.   From Equation (3.15), it is impossible for a solution to be found based on the half-space velocity model if the arrival time difference is greater than the theoretical arrival time difference limit;

V.   It is only possible to reach the theoretical limit of $\frac{2c}{v}$, if the source is located at the first transducer or on an extension of a line connecting both transducers. However, such a situation is rare because it is very uncommon to have a source at transducer location.
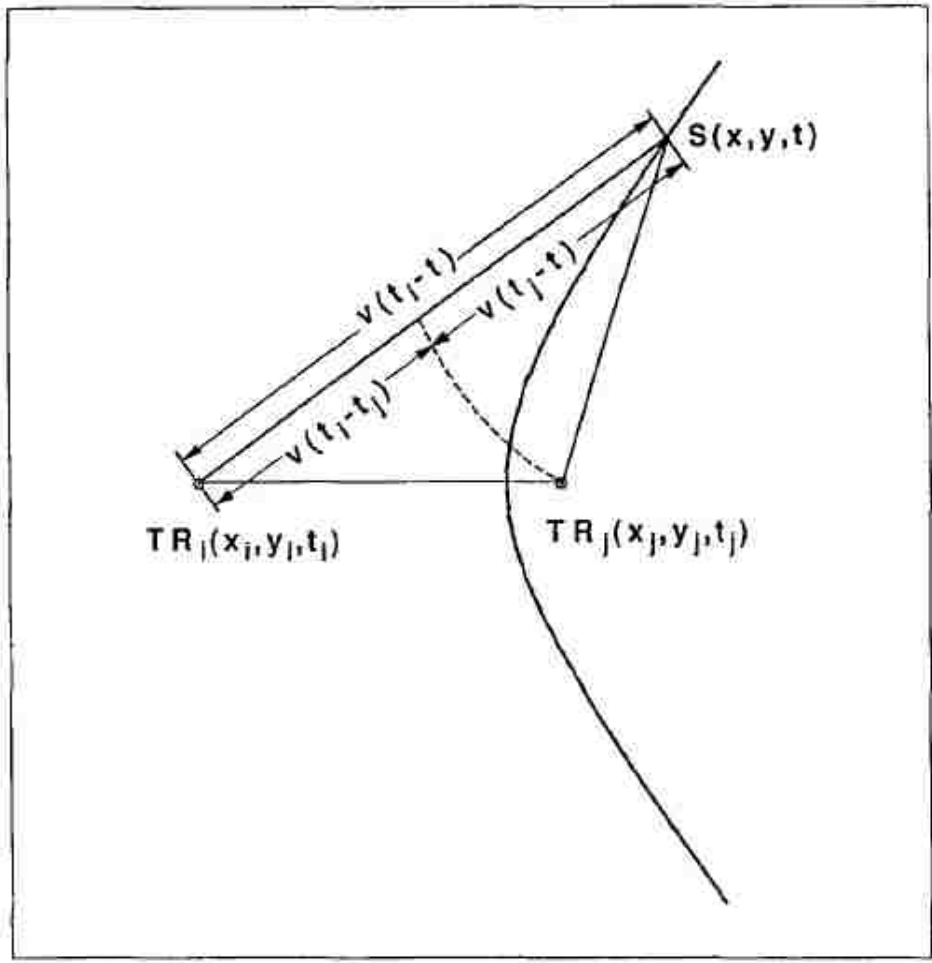
Figure 3.13 Use of arrival time difference at two transducers to determine a hyperbola (Ge [111])

From Equation (3.15), the authors noted that for a given velocity, the theoretical limit based on the half-space velocity model could be determined for different scenarios. Four of these limits applicable and relevant for AE/MS source locations are provided in Table 3.1. In the table, v_p and v_s represent the P- and S-waves velocities, respectively.
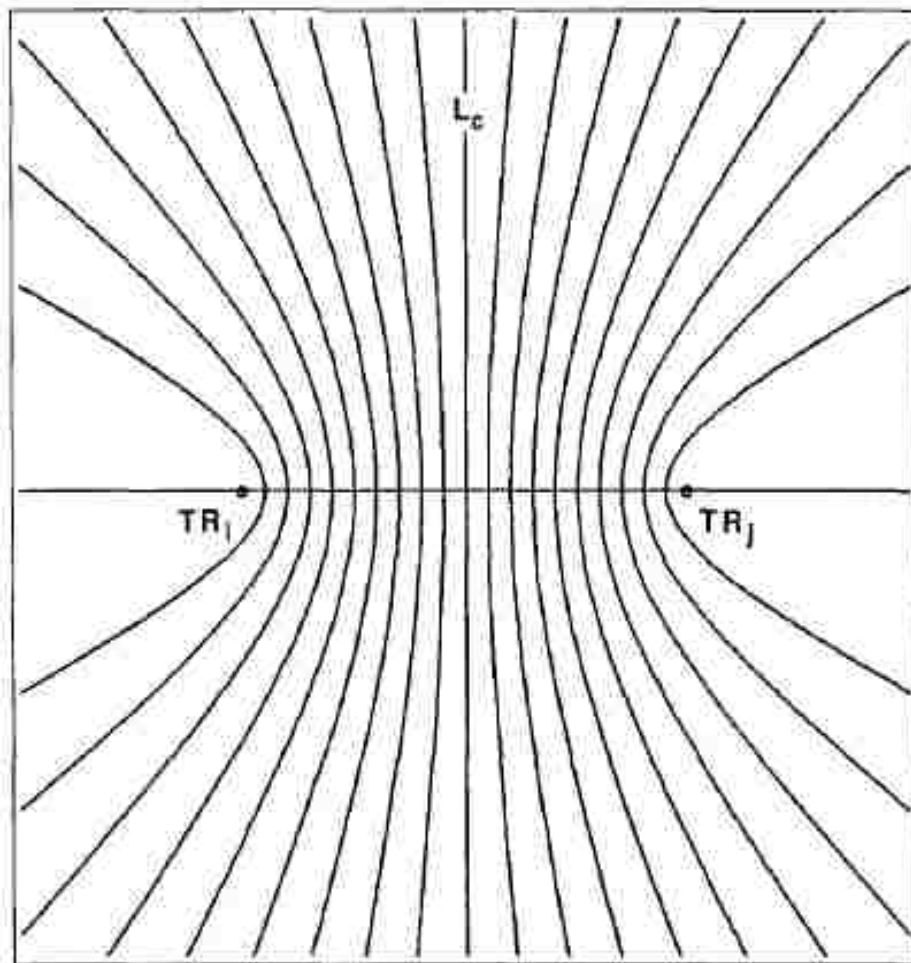
Figure 3.14 Two transducers illustrating a hyperbolic field with circles and L_c denoting positions of transducers and central line respectively (Ge and Hardy [112])

Table 3.1 Theoretical limits of arrival-time difference at two transducers for four wave-type combinations (Ge and Kaiser [109])

First Arrival	Second Arrival	Theoretical Limit
P	P	$2c/v_p$
S	S	$2c/v_s$
S	P	$2c/v_p$
P	S	∞

The detailed algorithm for computing and generating the arrival-time difference table for this study is provided in Figure 3.15. The major inputs for the algorithm include the number and coordinates of the transducers used in the data acquisition, approximate wave velocities for both P- and S-waves for the specific location and the arrival times picked using the automatic picking algorithm discussed in this study. With this information, the algorithm computes the theoretical arrival-time difference limit among all transducers and the reference transducer selected by the user. These difference limits are then compared with arrival time difference computed using the automatic algorithm proposed in this research to generate an arrival-time difference table for the appropriate decisions to be made by the user.
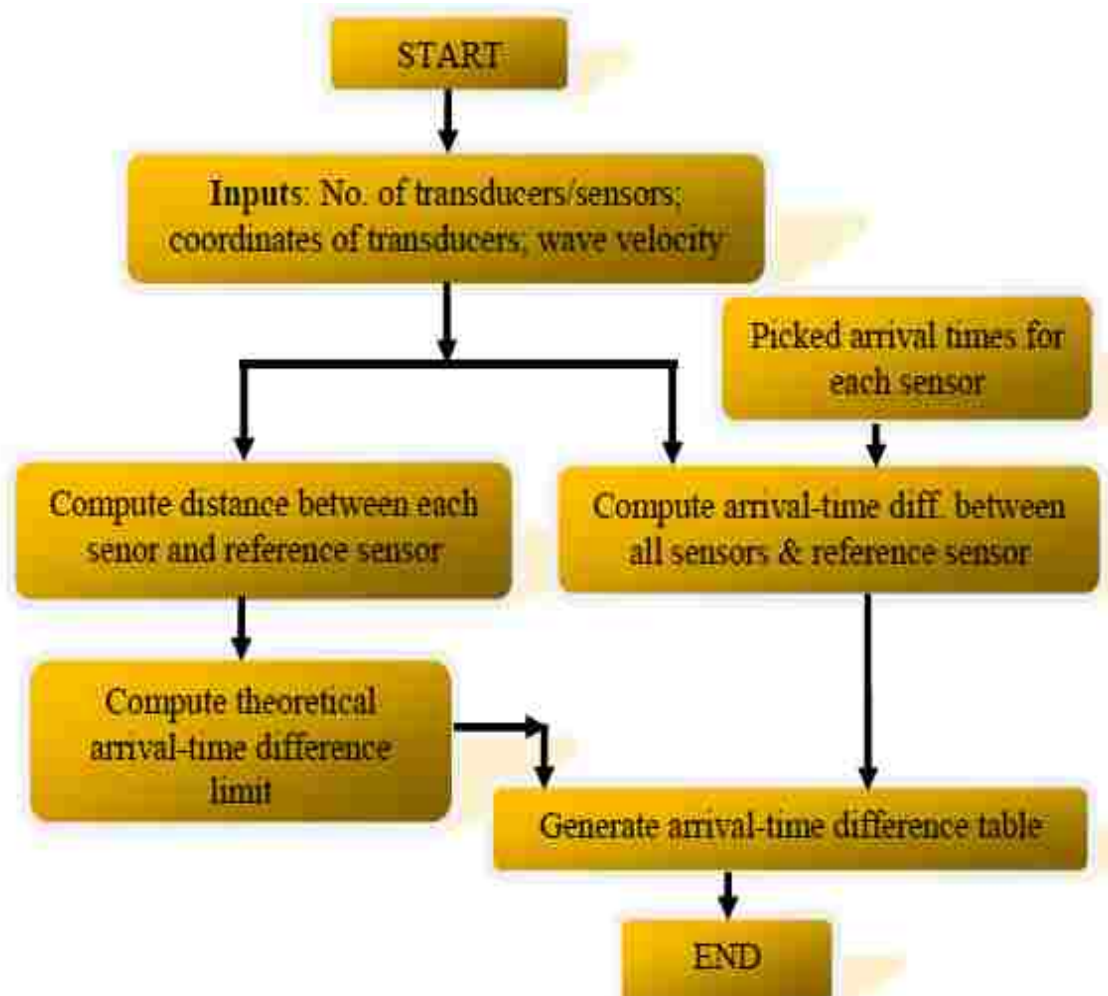
Figure 3.15 Phase association algorithm flow chart

SUMMARY OF THE PROPOSED ALGORITHM

The automatic picking method proposed in this dissertation can be grouped into four main stages: data filtering, CF function computation, phase identification and picking, and a reliability or phase association test. See Figure 3.16 for the flowchart of the proposed algorithm. A summary of the various stages of the process is provided below.

The first phase of the automatic data process involves the use of the SDWT filter and coefficient thresholding to improve the SNR of the AE/MS data. At this stage, the user provides a value for the number of decomposition levels (scales) desired. The effect of noise is generally observed to be higher at lower scales (typically the first and second scale base on the data used so far). As the number of scales increases, however, the impact of noise decreases while the emergence of the signal of interest becomes clearer. To ensure the SNR is further improved, the soft or hard thresholding algorithm is then applied to the coefficients at the scales to be selected for further analysis.

Phases two and three can be regarded as overlap processes. These processes involve the computation of the CFs (skewness and kurtosis) and using the changes in these parameters to pick arrival times. To ensure a computationally efficient automatic picking algorithm, three scales are used. A user can, however, choose to use less or more than three scales. For each selected scale, the skewness and kurtosis are calculated in a moving window of length M. The window is moved one sample at a time. The current value of the estimated value of the skewness and the kurtosis is then stored at the end of the present window. The rate of change of skewness and kurtosis is calculated as the slope at every point. The maximum slope for all cases of the series calculated is then found. The sample index at which this maximum slope occurred and the corresponding stationary wavelet scale number is then picked. The maximum slopes among the scales are further compared and the maximum determined. The results for the kurtosis-based and skewness-based criterion are then compared. If the difference in the sample index picked by the two criterions is more than a set threshold (Beta), the process is started by providing a new window size. Beta is obtained by first finding the difference between the maximum slope values determined across the scales for the kurtosis-based and skewness-based criterion. The resulting figure is then divided by the number of scales to give the final value of beta. If the difference in sample index is less or equal to the threshold, it proceeds to store the

sample index and other important information for further evaluation. The process is continued until all transducer records are evaluated.

To further validate the reliability of the arrival time picked on each transducer, the algorithm performs a phase association procedure to ensure that the picks are all coming from the same wave type and event. The detail discussion of the theory of the phase association is provided in Section 3.4. After performing the process of phase association, the sample index corresponding to the maximum slope at which all conditions are satisfied is then taken as the P-phase onset time. Once again, see Figure 3.16 for the complete flow chart of the algorithm.

■■■ SUMMARY

In this section, the fundamental theories and mathematical foundations for the various techniques employed in the proposed new data processing method were presented. The models developed for the various stages of the algorithm were tested on both synthetic and actual field data where necessary. The advantages and disadvantages of some specific techniques (for example, the SDWT) over other techniques were reviewed. Specifically, a detailed discussion on the choice of the SDWT as a filter is provided. The choice of the statistical parameters skewness and kurtosis over other parameters and their suitability for the processing of AE/MS were examined. The results obtained when these parameters were applied to both synthetic and field data showed superior performance in comparison the mean, variance, and the STA/LTA techniques. A phase association theory and its importance to enhancing the reliability of the proposed method were discussed. A summary of the proposed method is provided to conclude the section.
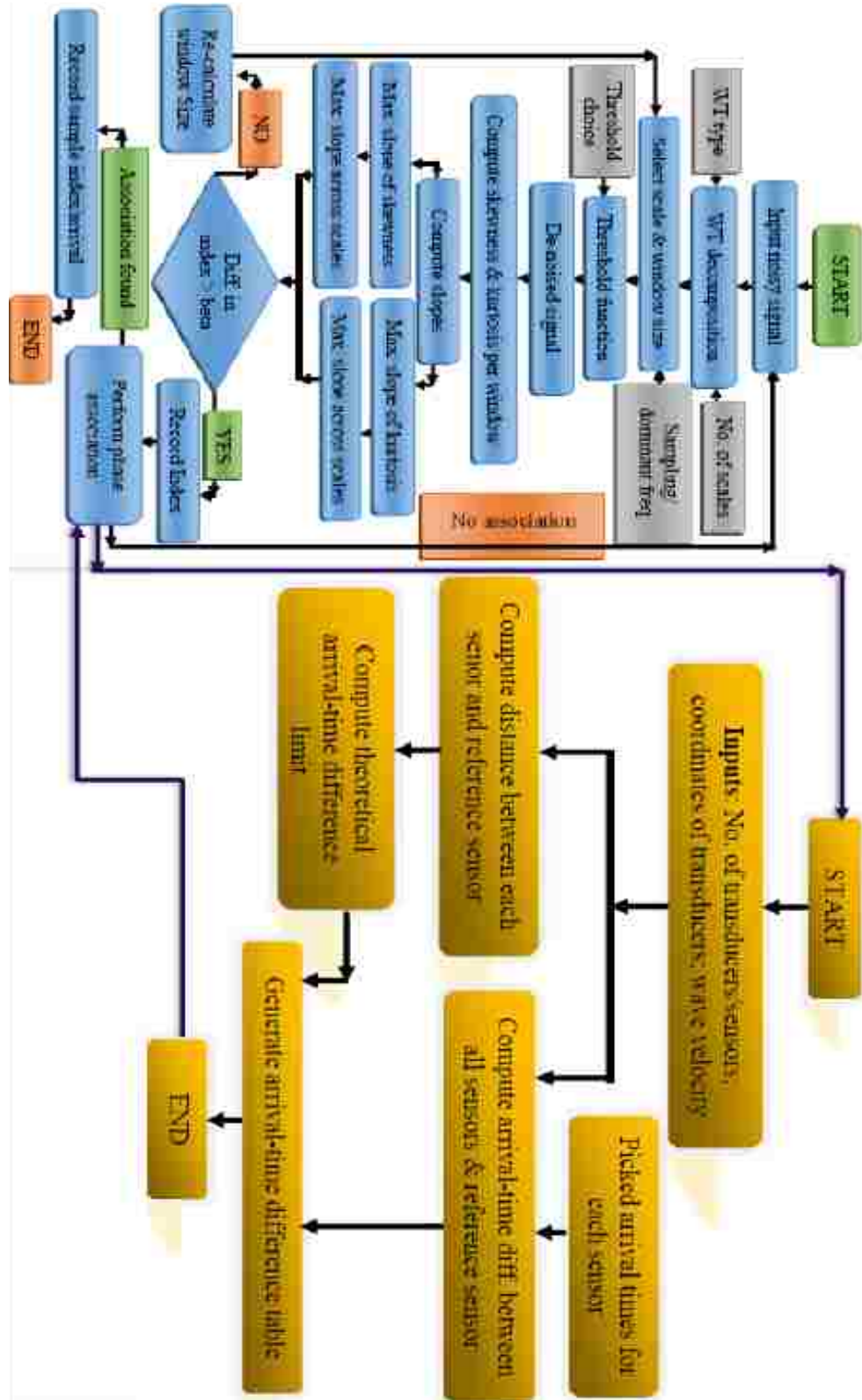
Figure 3.16 Flowchart of the proposed algorithm

4. MODEL PERFORMANCE TESTING AND VALIDATION

This section of the dissertation seeks to evaluate the performance of the newly proposed automatic picking algorithm discussed in Section 3. To achieve this objective, the algorithm is applied to AE/MS field data from a mine. The dataset consists of 43 AE/MS events with each acquired using a sixteen channel acquisition monitoring system. The acquisition system had a sampling frequency of 500 Hz. The P-wave velocity range was from 3800 to 4500 m/s, calculated from the field-blasting source locating experiment, and the average value of the measured wave velocity was 4000 m/s. The results and discussions for these tests are presented below.

▇ PARAMETRIC STUDIES ON AUTOMATIC PHASE PICKING

In this section, the impact of factors such as the CF, wavelet function, decomposition scale, and sample window size on picking accuracy of the automatic picking algorithm is examined. The results of these tests and the discussions are presented below.

4.1.1. Choice of WT Functions and Their Effects on Automatic Picking. The effectiveness of the WT algorithm is based on the type of the applied wavelet function. The particular wavelet function chosen for any particular application should therefore be able to effectively demonstrate the special features of the processed signal.

Several wavelet functions are available and have been widely used for different applications in the signal processing industry. For this study, to test the efficiency of the proposed method, the Haar, Daubechies (Db), Symmlet (Sym), and the Coiflets (Coif) wavelets were employed to examine their suitability for the present dataset. The different forms of these wavelet functions were applied to three events selected from the dataset (Figures 4.1, 4.2, and 4.3) for this study. The red vertical lines and the associated numbers on the figures represent the sample index at which the P-wave phase onset arrivals are located. The effects of these wavelet functions on the accuracy of the automatic arrival picks are shown in Table 4.1. In the table, the upper number represents picks obtained by kurtosis analysis, while the lower number represents picks based on skewness analysis. Analyses of the results indicate that the wavelet function type can greatly influence the

picking of the P-wave phase onset arrivals. For the cases considered, the most accurate results were obtained with the Db5 and Sym5 wavelet functions. The manual picks obtained across Scales 2 to 4 for Event 1 using the Db5 and Sym5 wavelet function are shown in Figure 4.4. The least effective wavelet function was the Haar wavelet (Table 4.1).

Table 4.1 Effects of wavelet function on the accuracy of automatic arrival picks

		Wavelet Function Type								
		Haar	Db3	Db5	Db7	Sym2	Sym3	Sym5	Coif2	Coif3
Event No.	1	500/ 550	550/ 550	576/ 569	550/ 600	550/ 700	550/ 550	576/ 512	550/ 800	550/ 850
	2	663/ 510	561/ 612	583/ 583	612/ 816	510/ 714	561/ 612	585/ 585	612/ 714	765/ 867
	3	612/ 663	663/ 765	535/ 535	663/ 816	612/ 612	663/ 765	540/ 540	663/ 714	714/ 918

The Db5 is used as the wavelet of choice for the study based on the results. The sample results, shown in Figure 4.4, illustrate that the wavelet coefficients provide a region of a P-phase arrival onset but does not provide the exact position of the P-phase arrival onset. This point is further highlighted by the automatic picking process for the four scales using the slopes of skewness and kurtosis for the three events (Figures 4.5 to 4.16). In Figure 4.5, the automatic pick based on both the slopes of skewness and kurtosis for Scale 1 is observed to be off the manual pick (Figure 4.1) by 64 sample points. However, as the number of scales increases, the variation between the manual and automatic picks decreases (Figures 4.6b and 4.7). It is also important to note that the variation between the manual and automatic picks begin to increase again at the very high scales (Figure 4.8). Similar trends are observed for Event 2 (Figures 4.9 to 4.12) and Event 3 (Figures 4.13 to 4.16). Phase onsets on Scales 4 are generally unclear (Figure 4.4). As such, picks on this scale could lead to pick errors. The characteristics demonstrated by these scales indicate that the four-scale decomposition will be enough for this dataset. However, to better understand the possible reason for these variations among the scales, a frequency content

analysis is performed for each of the four scales and for each of the three events. The results for the frequency content analysis is presented and discussed in Section 4.2.

(a)

(b)
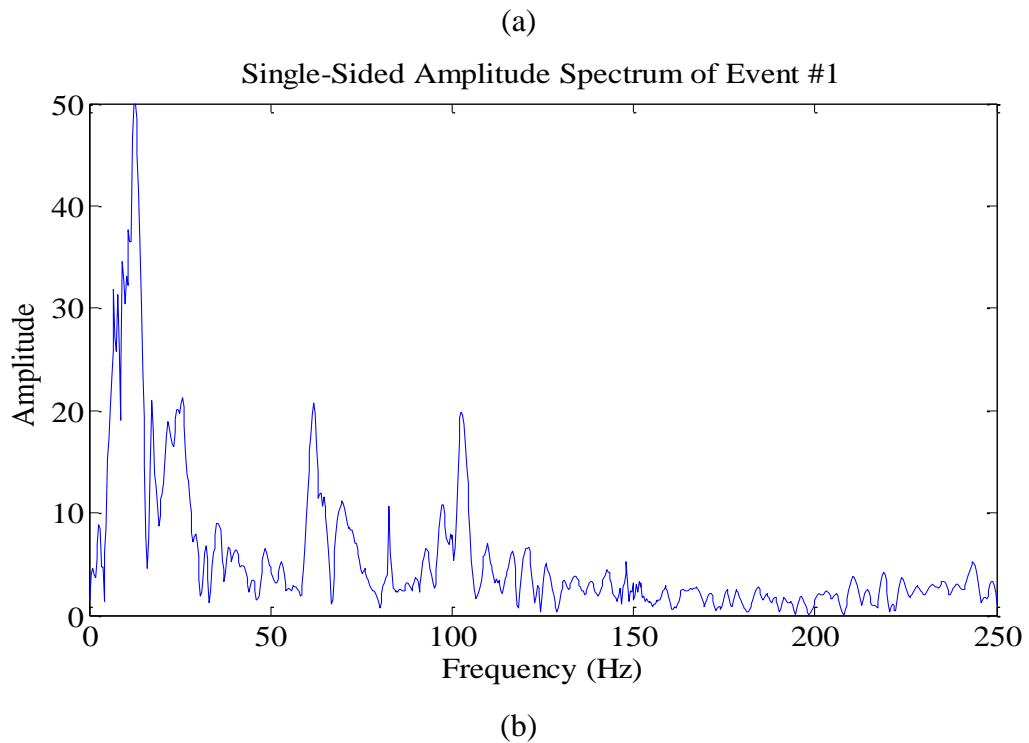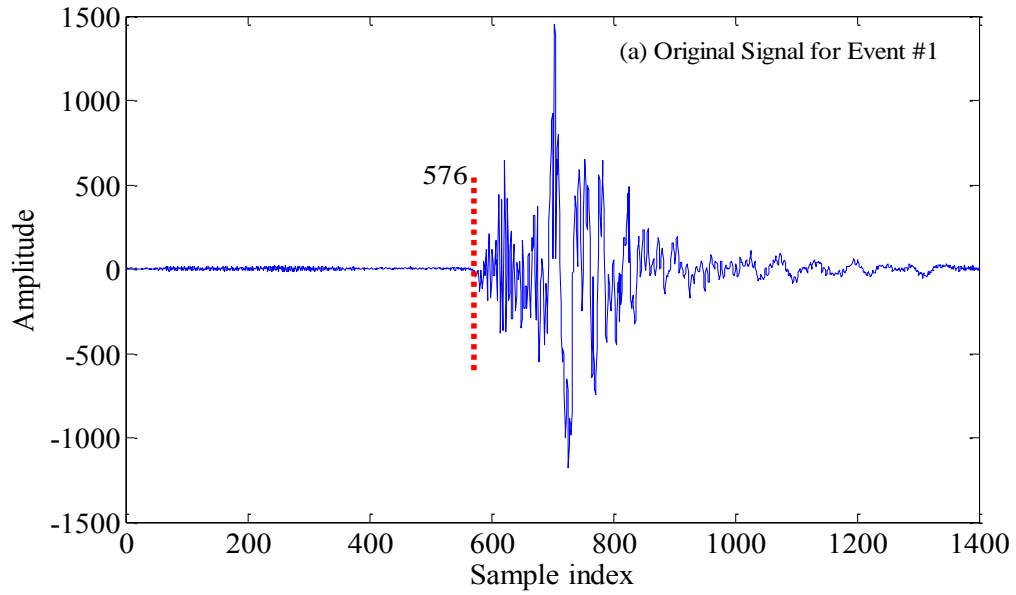
Figure 4.1 Original signals for (a) Event 1 and (b) corresponding amplitude spectrum by fast Fourier transform (FFT)

(a)

(b)
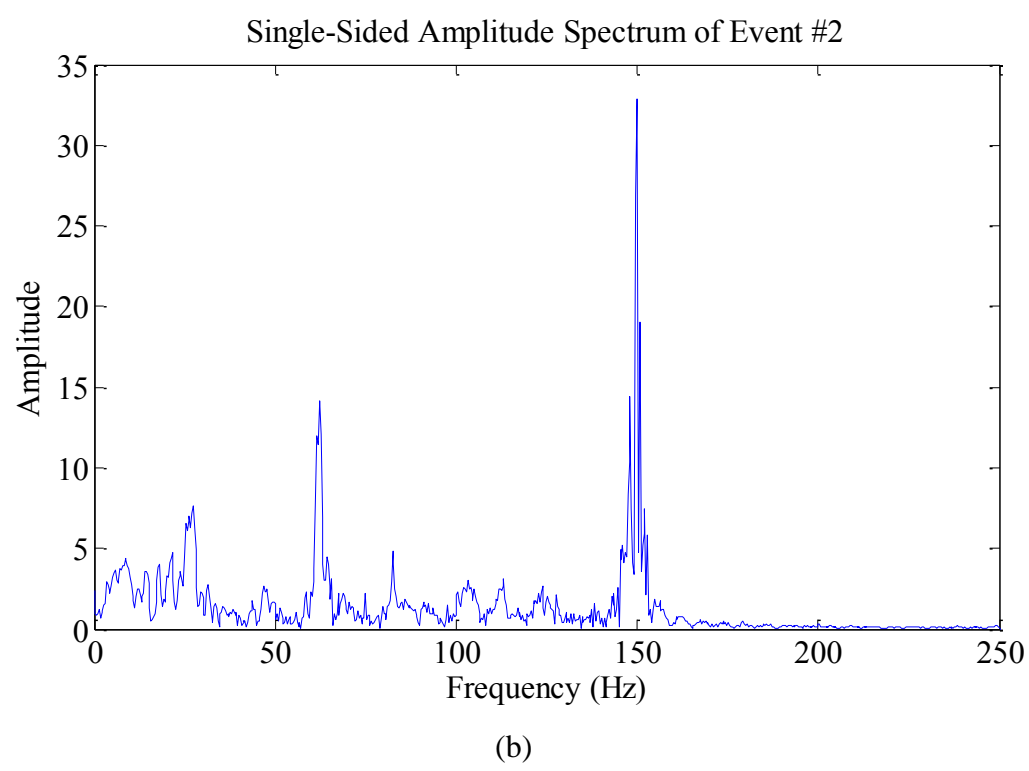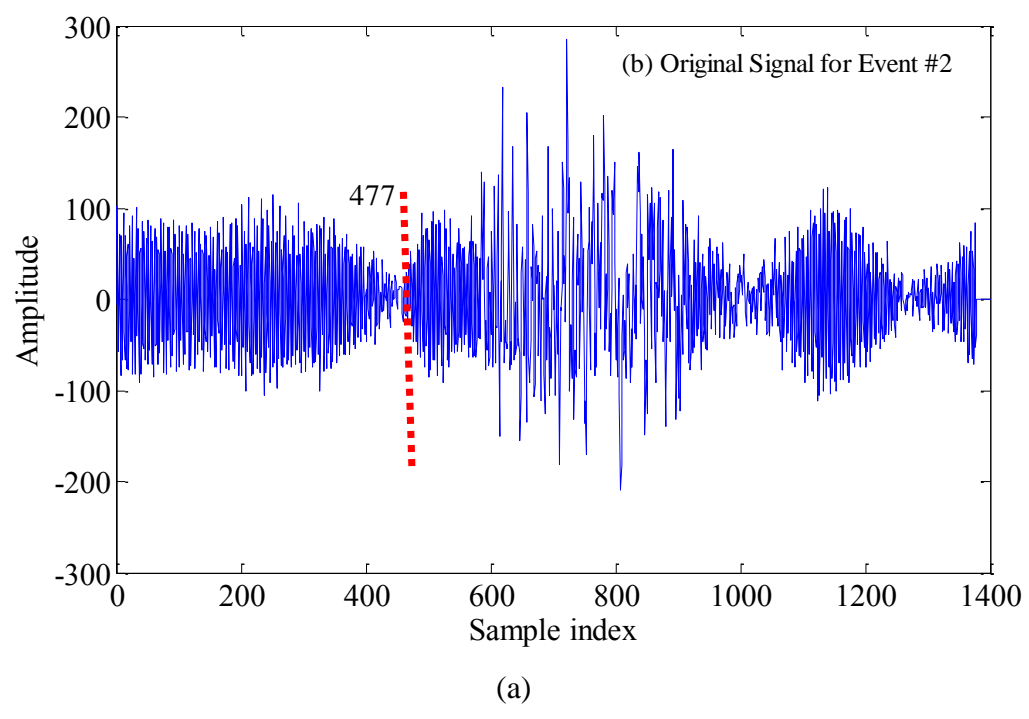
Figure 4.2 Original signals for (a) Event 2 and (b) corresponding amplitude spectrum by FFT

(a)

(b)
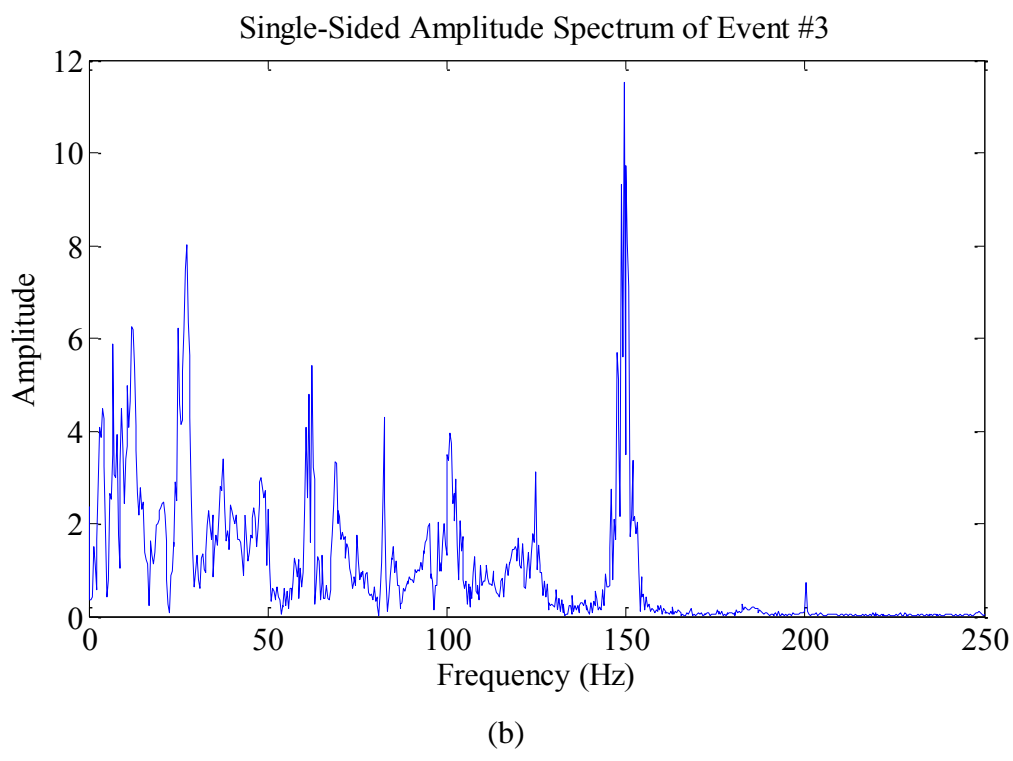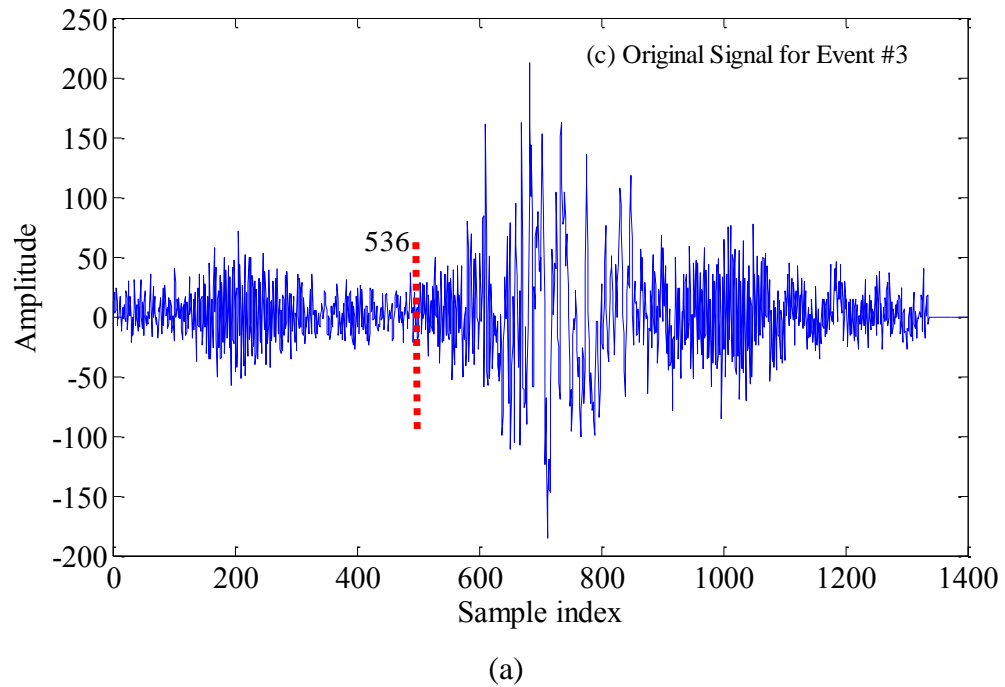
Figure 4.3 Original signals for (a) Event 3 and (b) corresponding amplitude spectrum by FFT
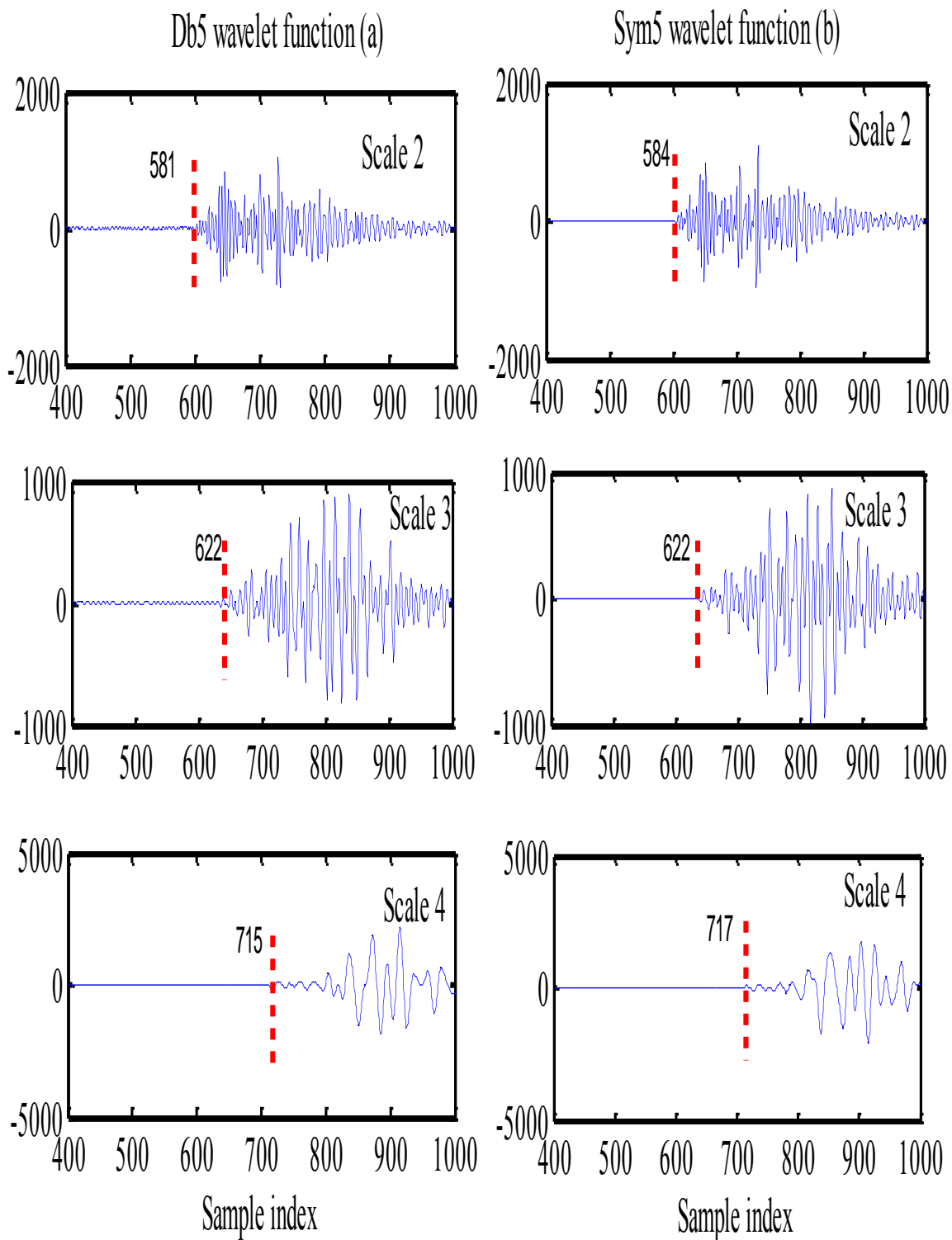
Figure 4.4 Manual picks for Event 1 based on filtering by (b) Db5 and (b) Sym5 wavelet functions
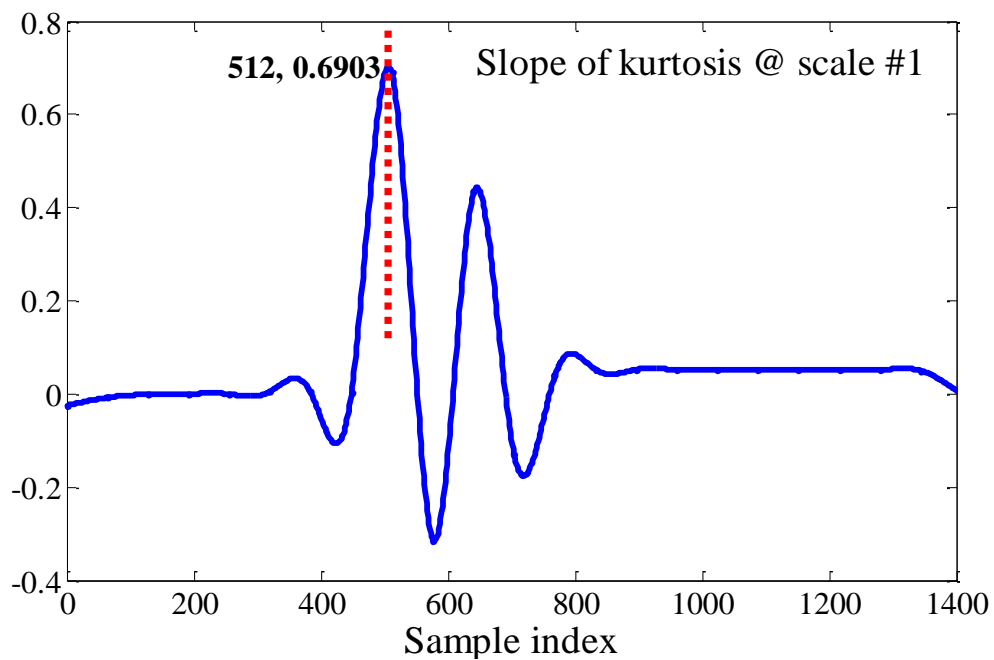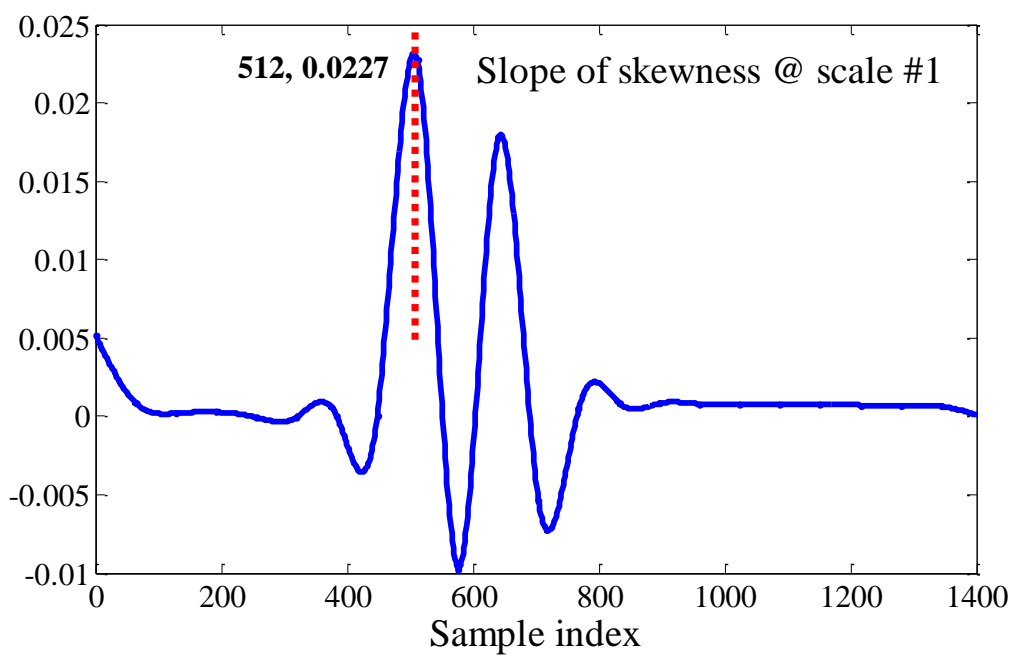
Figure 4.5 Automatic arrival picks on Scale 1 for Event 1 based on (a) slope of kurtosis and (b) slope of skewness
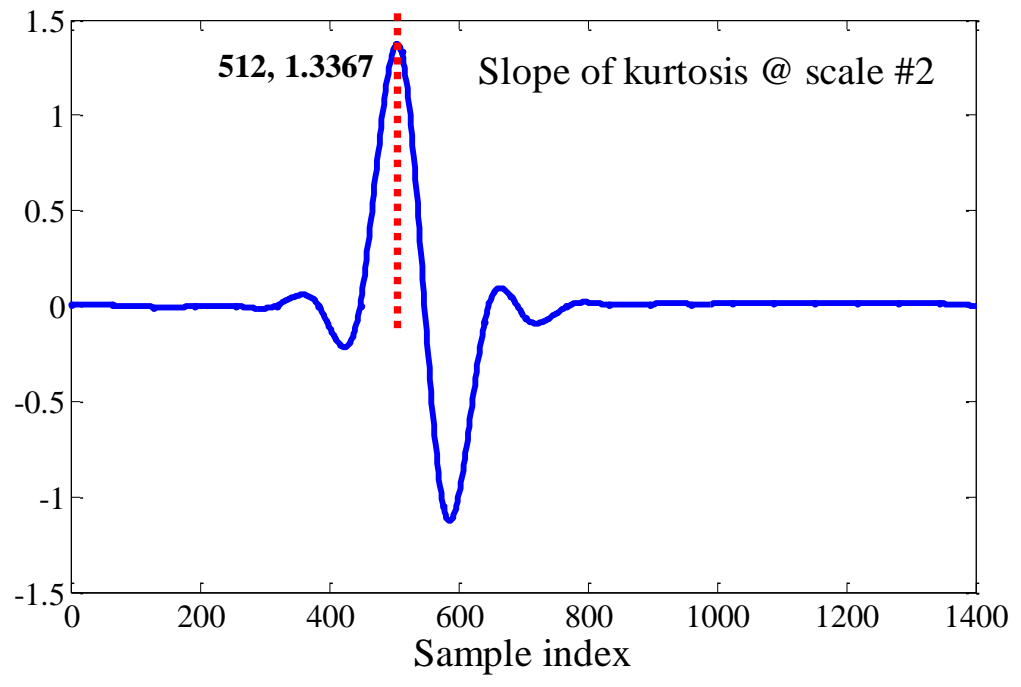
(a)
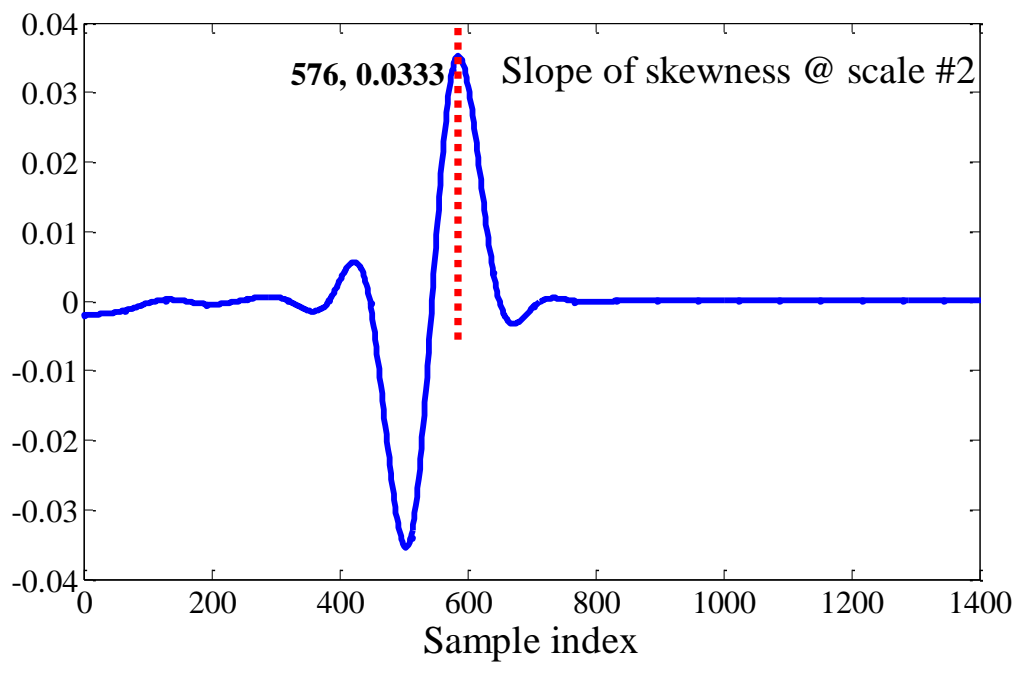
(b)

Figure 4.6 Automatic arrival picks on Scale 2 for Event 1 based on (a) slope of kurtosis
and (b) slope of skewness
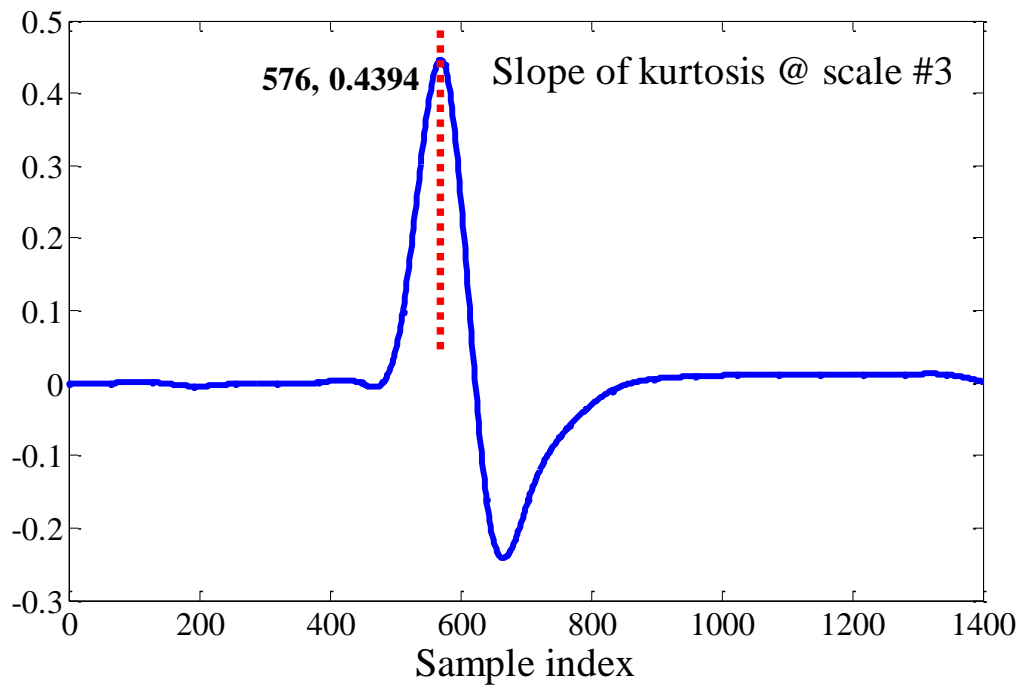
(a)
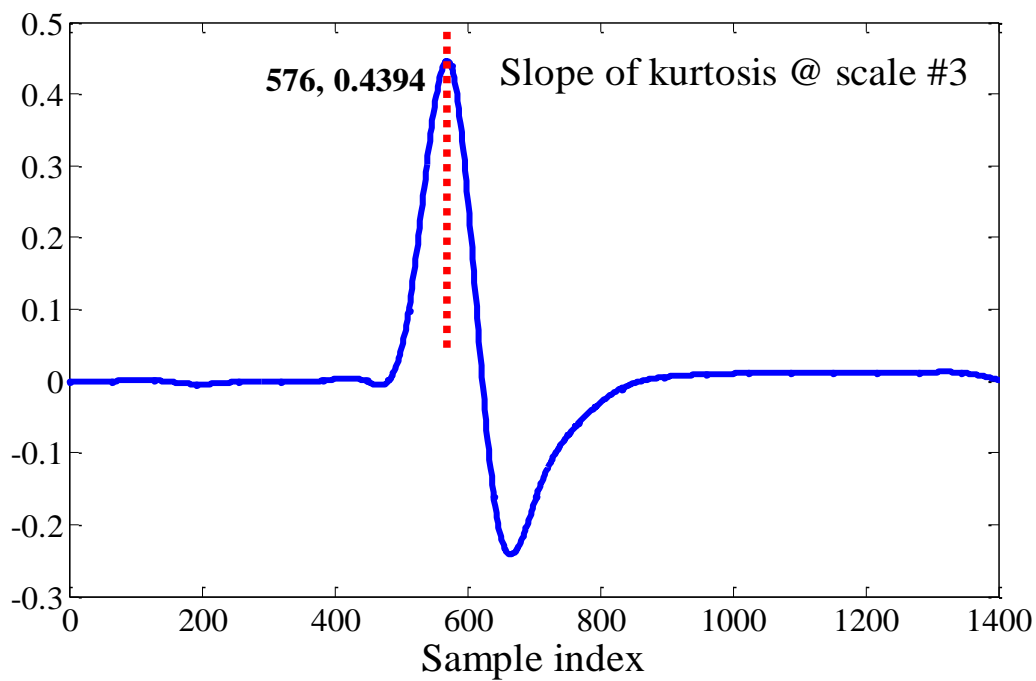
(b)

Figure 4.7 Automatic arrival picks on Scale 3 for Event 1 based on (a) slope of kurtosis
and (b) slope of skewness
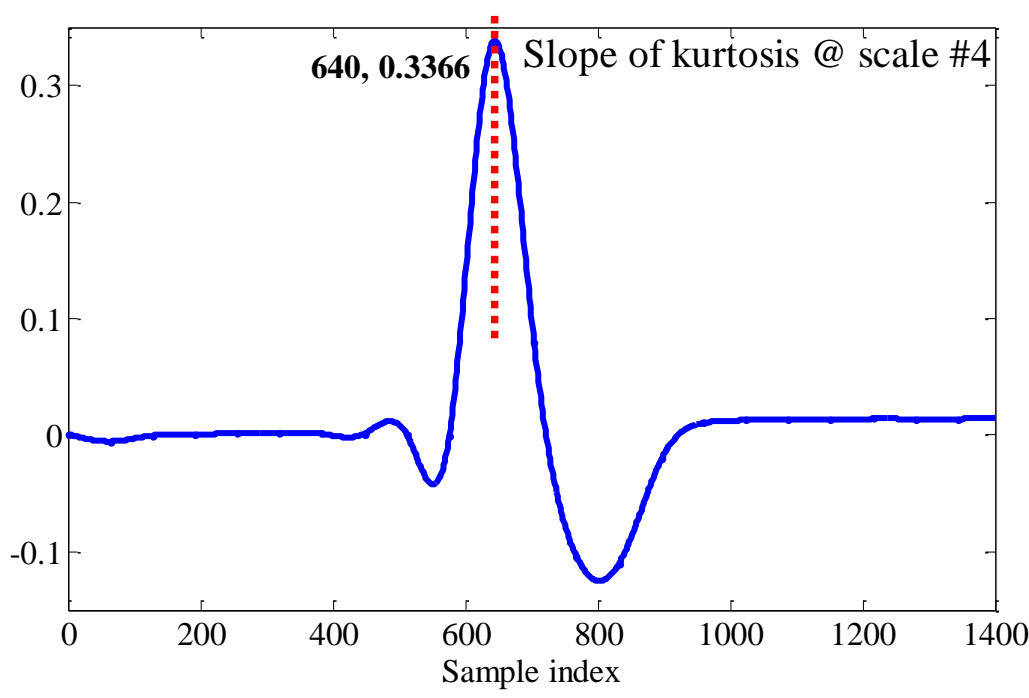
(a)
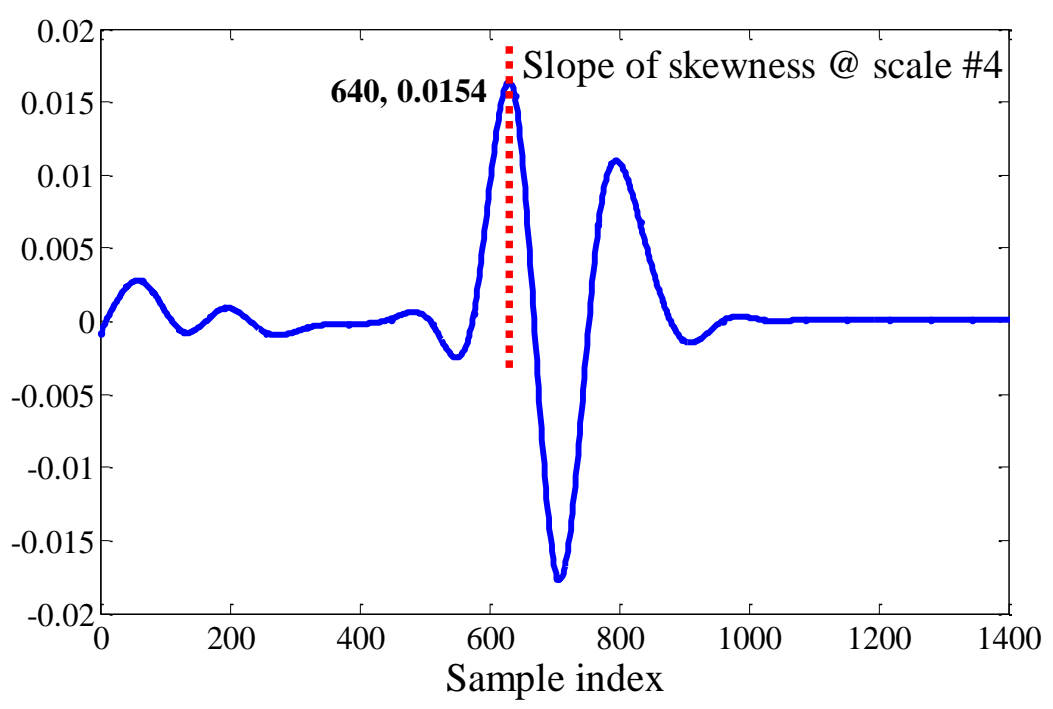
(b)

Figure 4.8 Automatic arrival picks on Scale 4 for Event 1 based on (a) slope of kurtosis and (b) slope of skewness
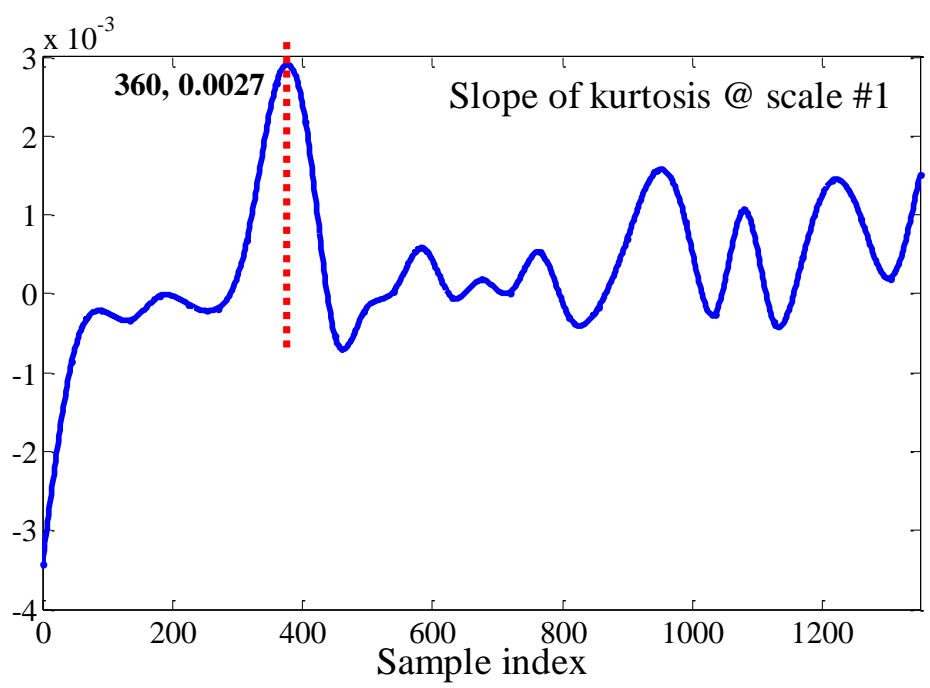
(a)
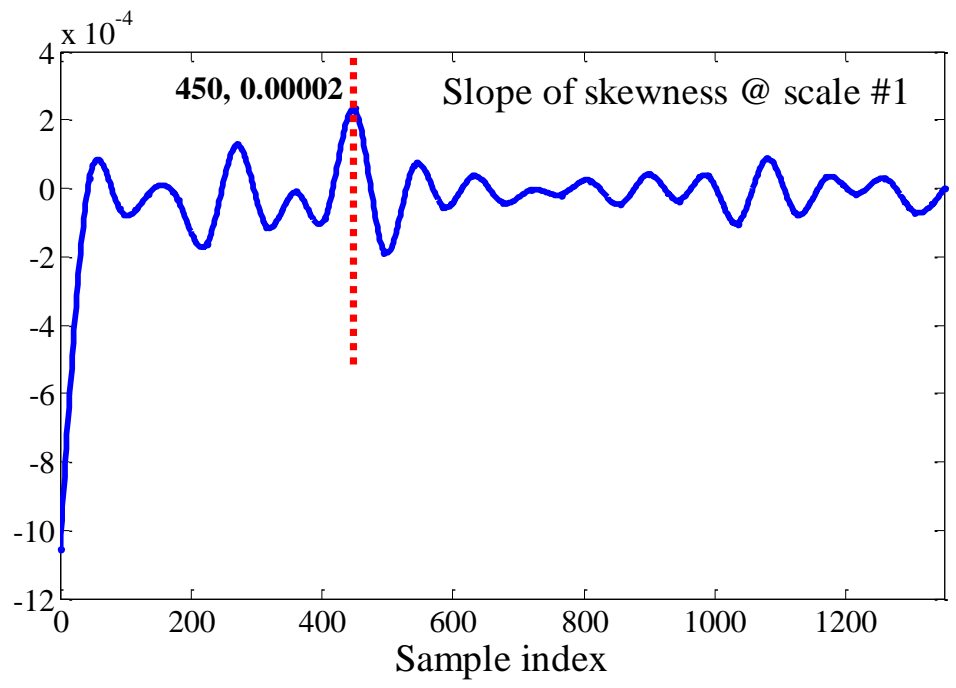
(b)

Figure 4.9 Automatic arrival picks on Scale 1 for Event 2 based on (a) slope of kurtosis and (b) slope of skewness
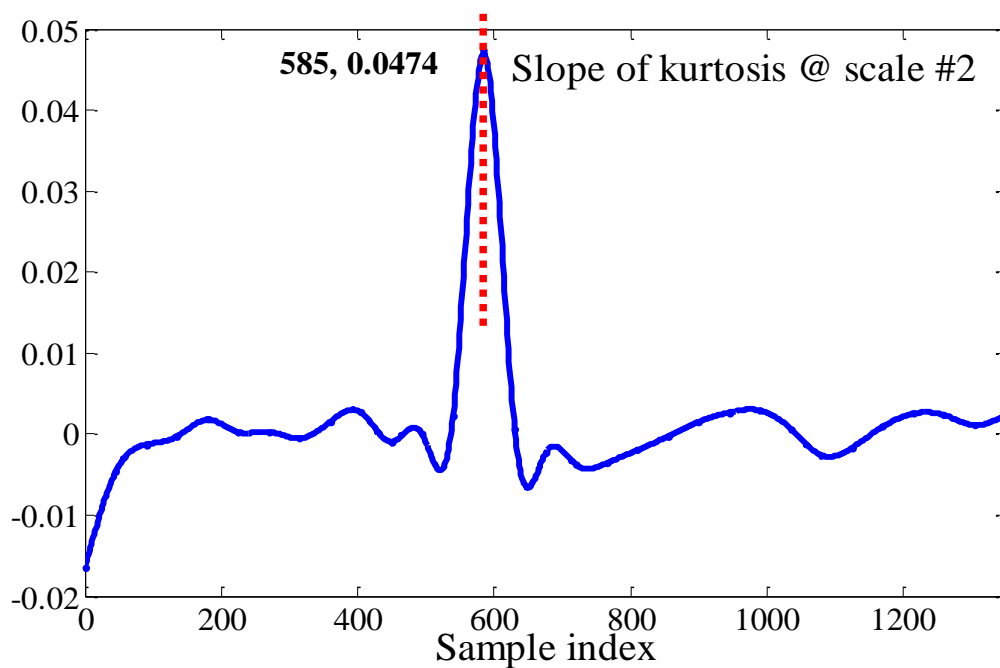
(a)
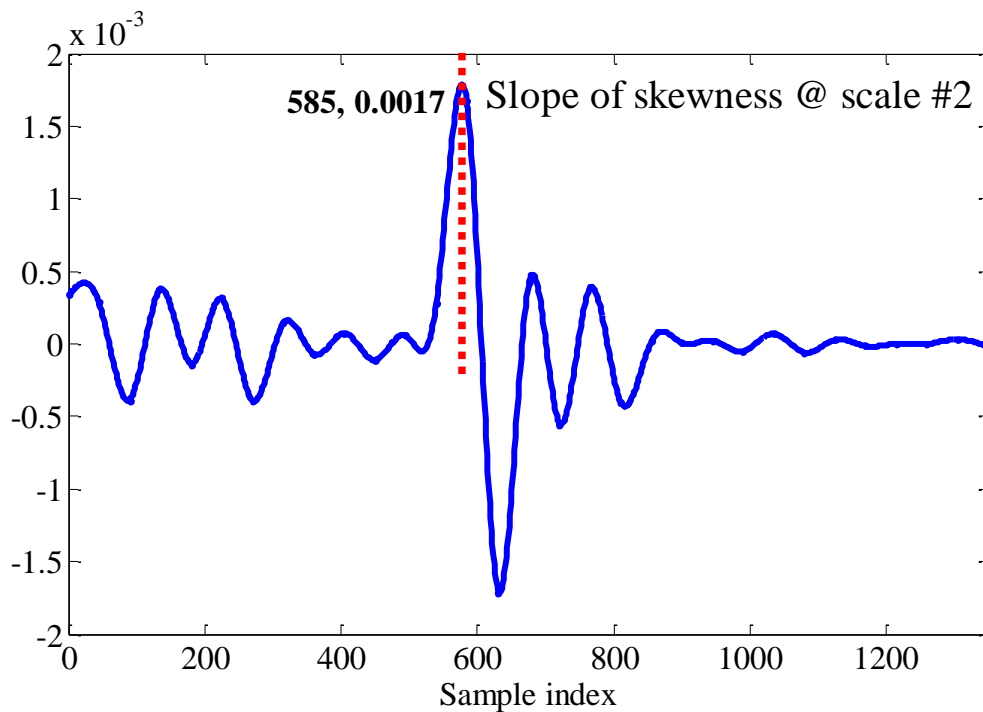
(b)

Figure 4.10 Automatic arrival picks on Scale 2 for Event 2 based on (a) slope of kurtosis and (b) slope of skewness
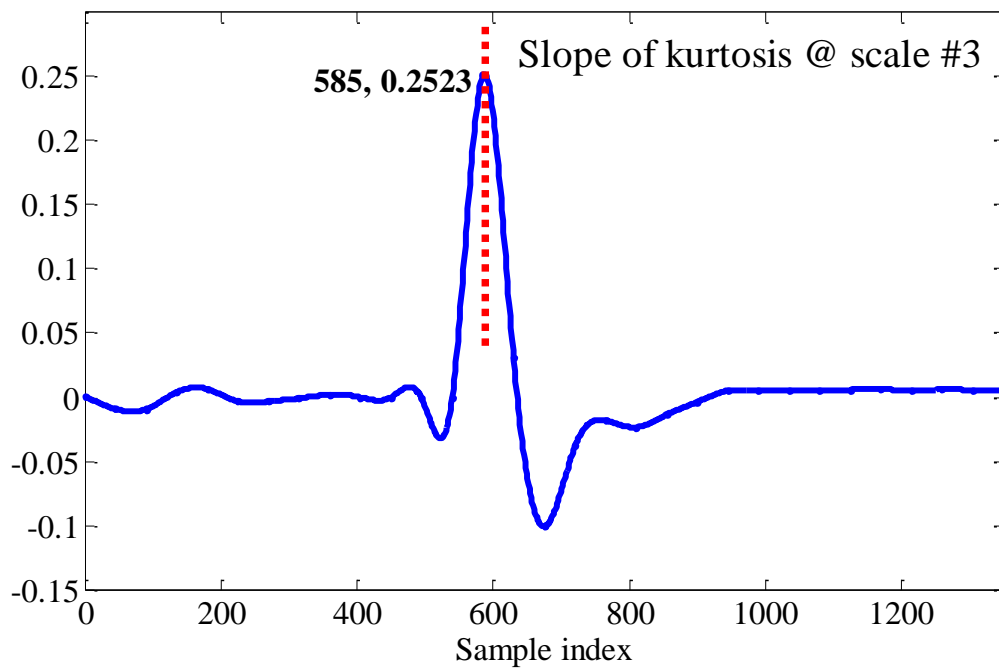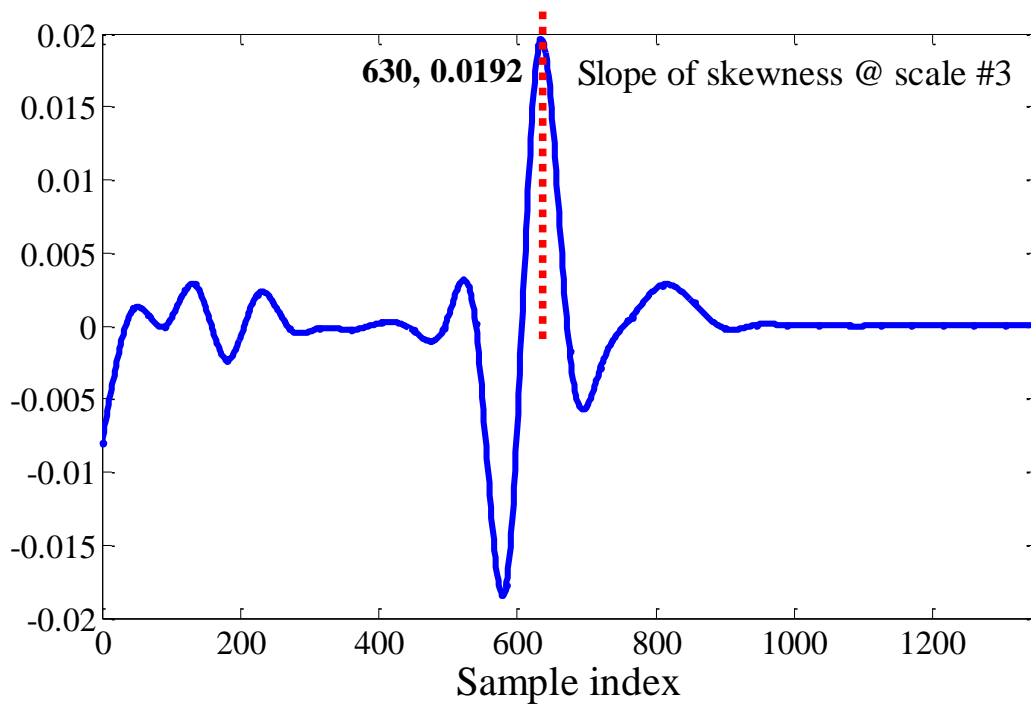
Figure 4.11 Automatic arrival picks on Scale 3 for Event 2 based on (a) slope of kurtosis and (b) slope of skewness
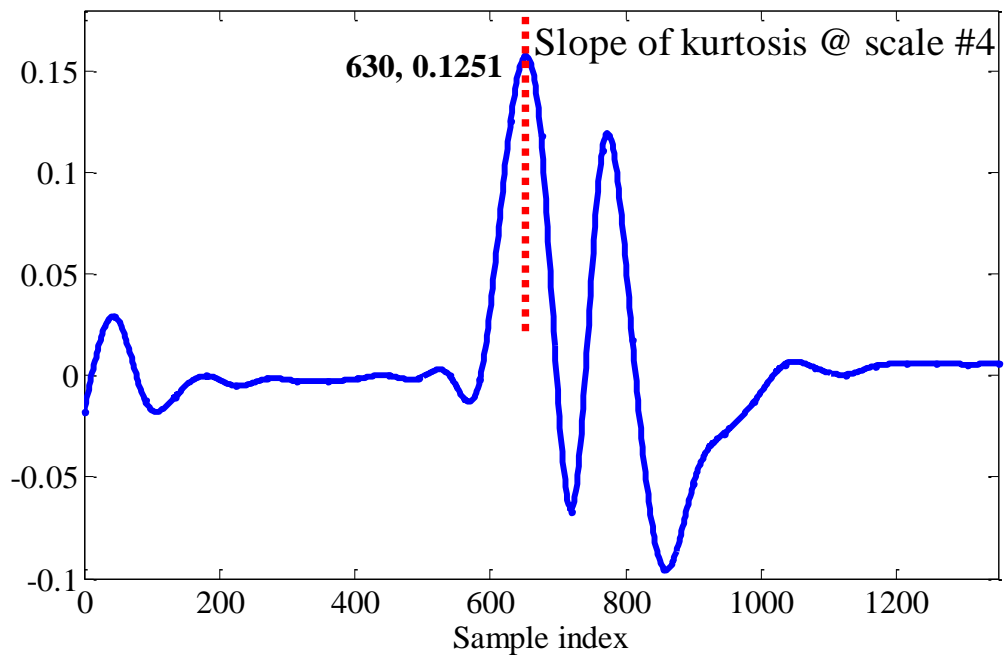
(a)
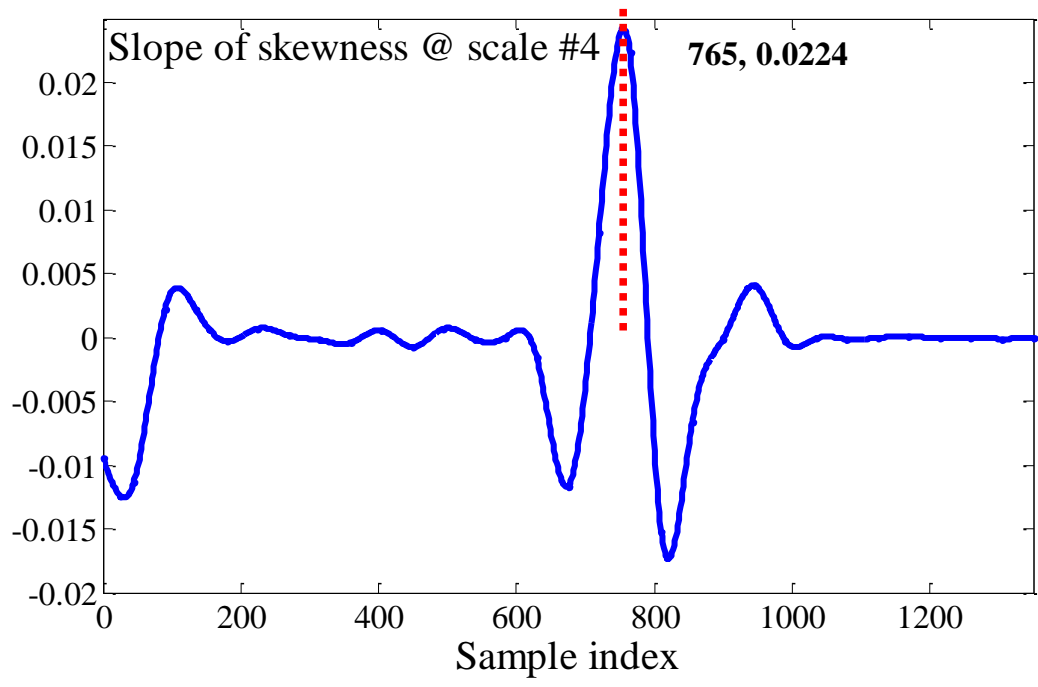
(b)

Figure 4.12 Automatic arrival picks on Scale 4 for Event 2 based on (a) slope of kurtosis and (b) slope of skewness
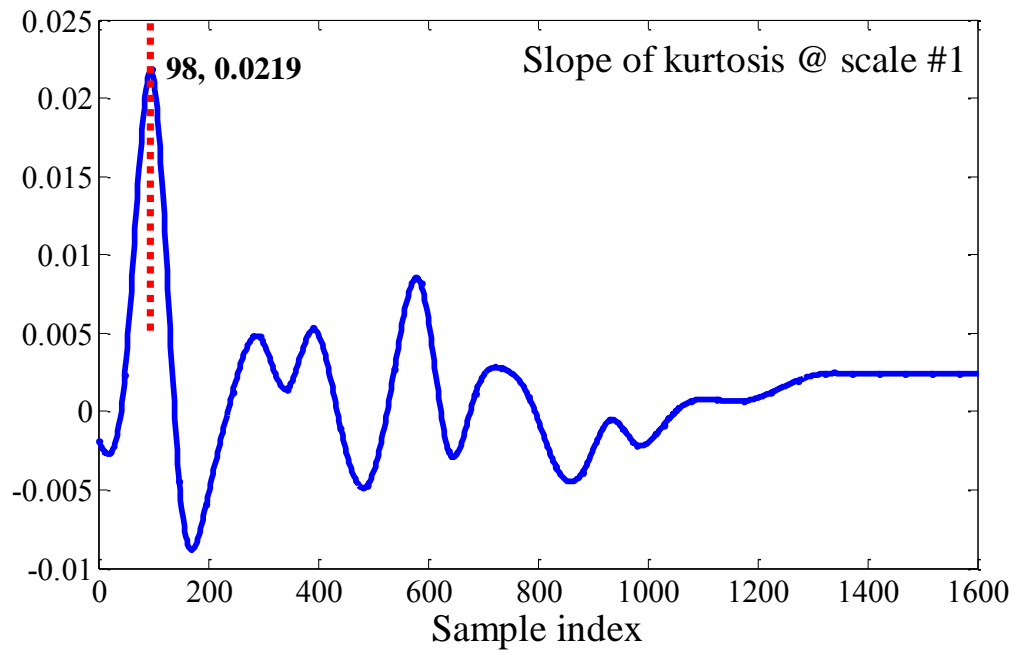
(a)
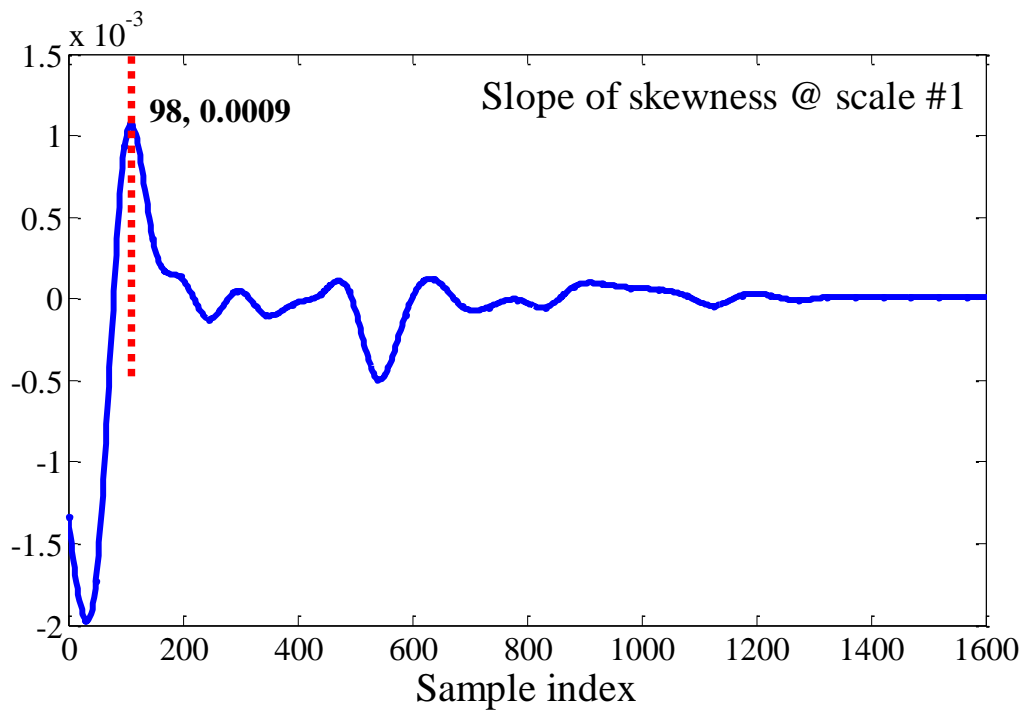
(b)

Figure 4.13 Automatic arrival picks on Scale 1 for Event 3 based on (a) slope of kurtosis and (b) slope of skewness
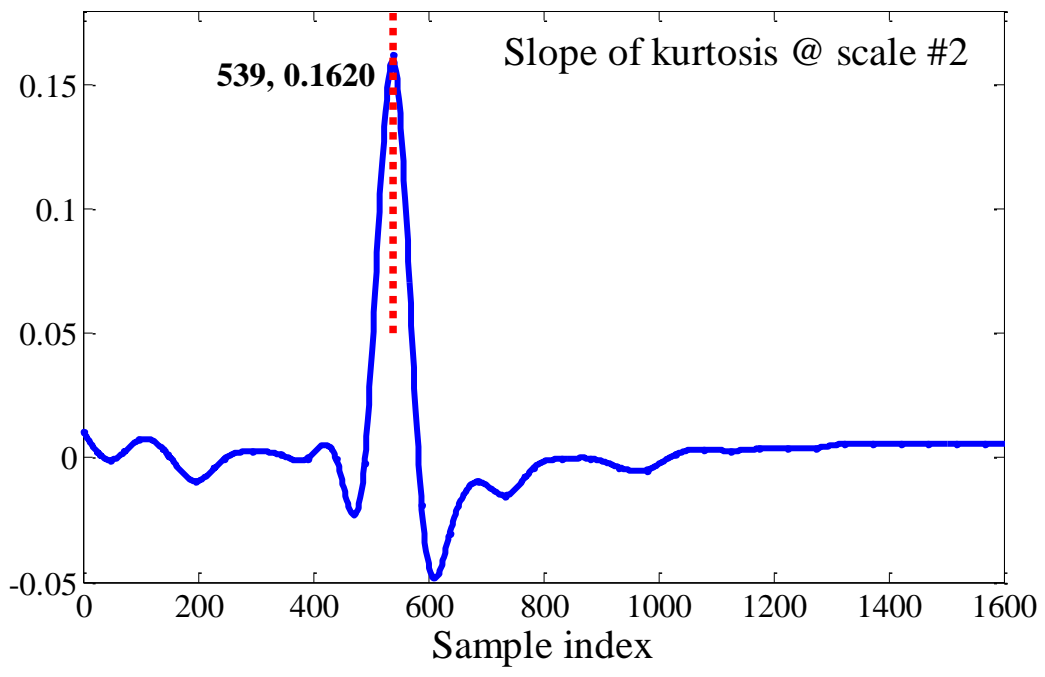
(a)
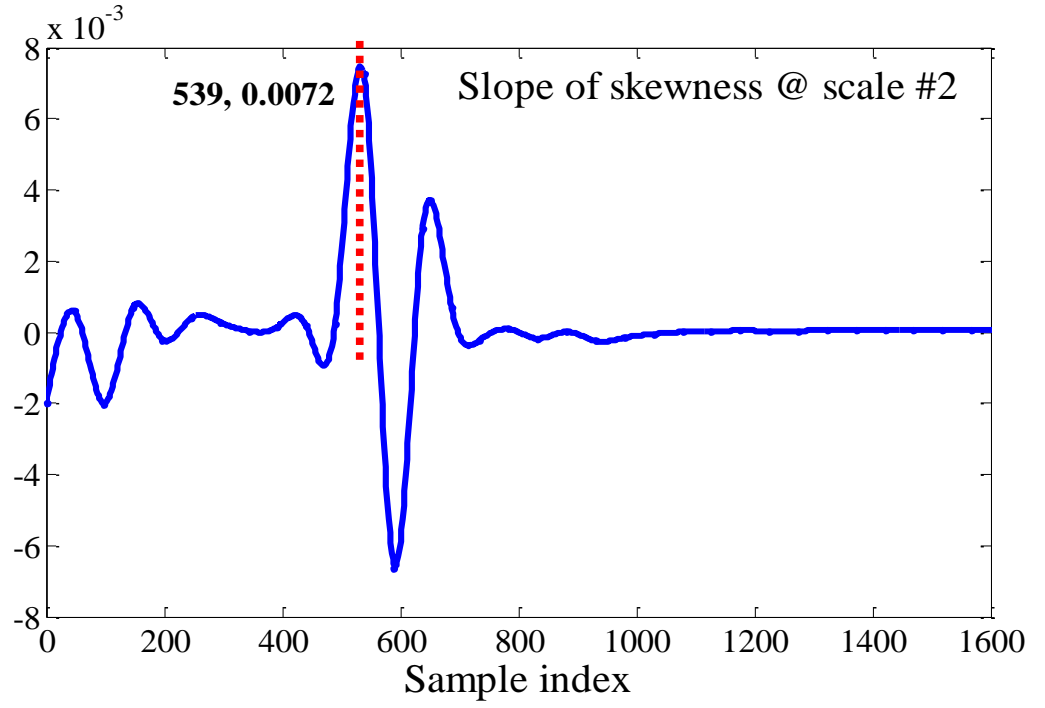
(b)

Figure 4.14 Automatic arrival picks on Scale 2 for Event 3 based on (a) slope of kurtosis and (b) slope of skewness
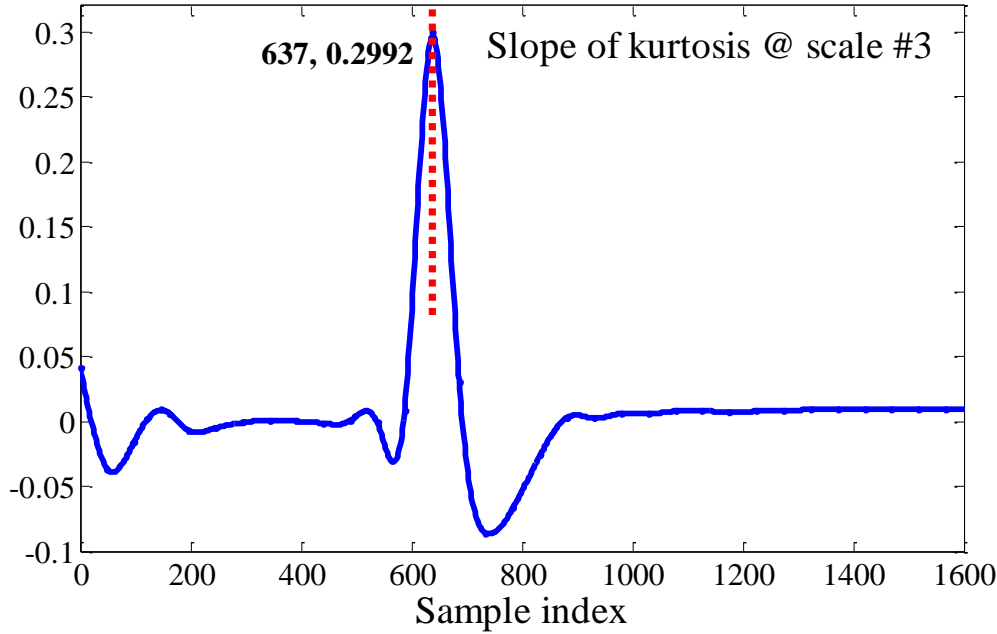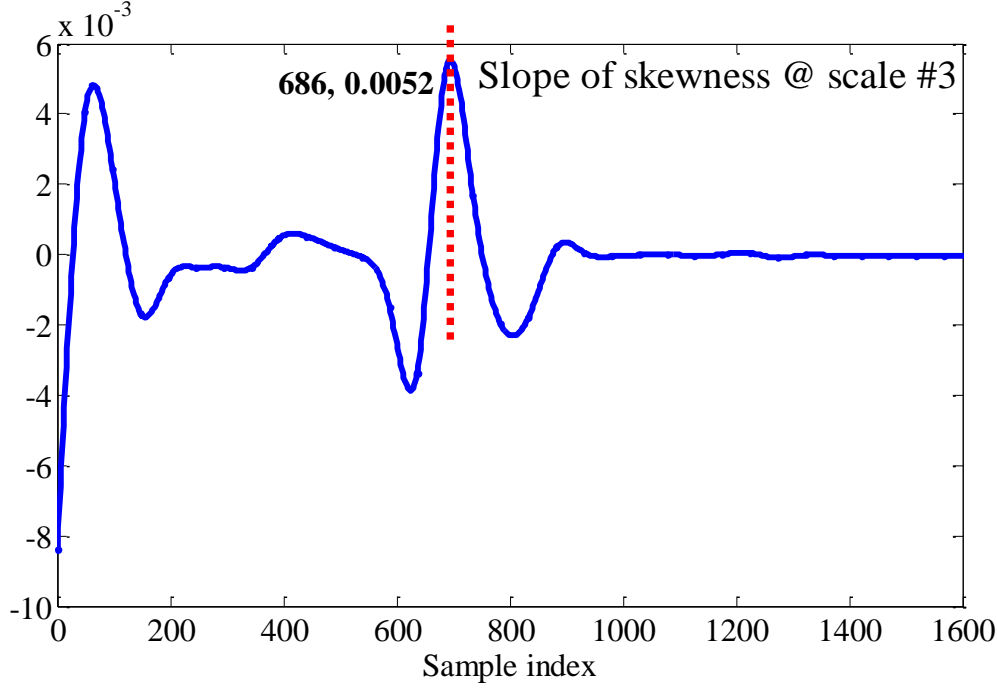
Figure 4.15 Automatic arrival picks on Scale 3 for Event 3 based on (a) slope of kurtosis and (b) slope of skewness
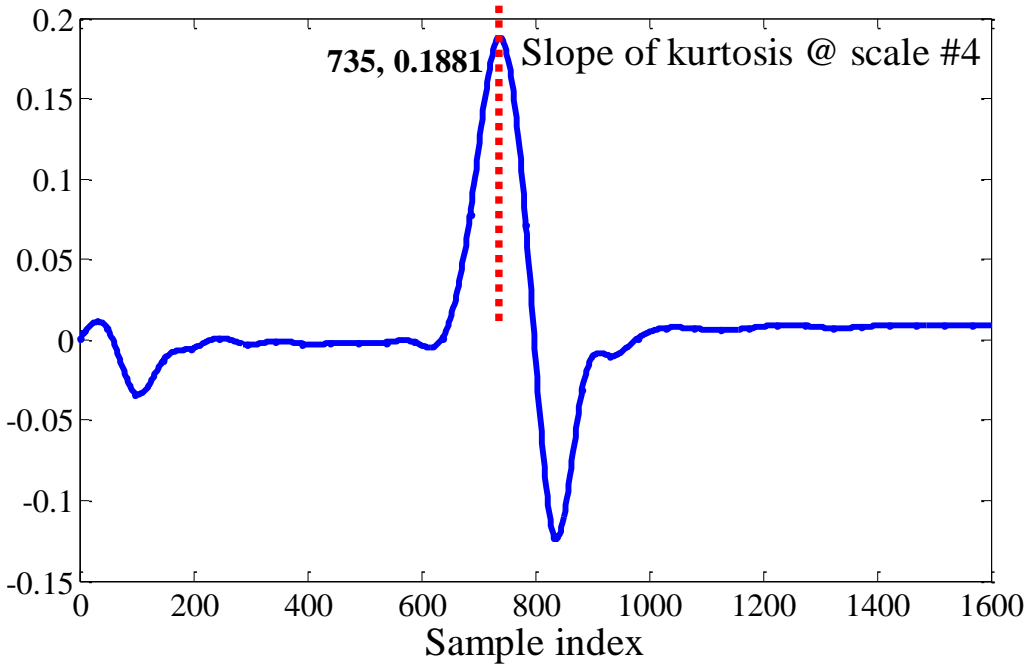
(a)
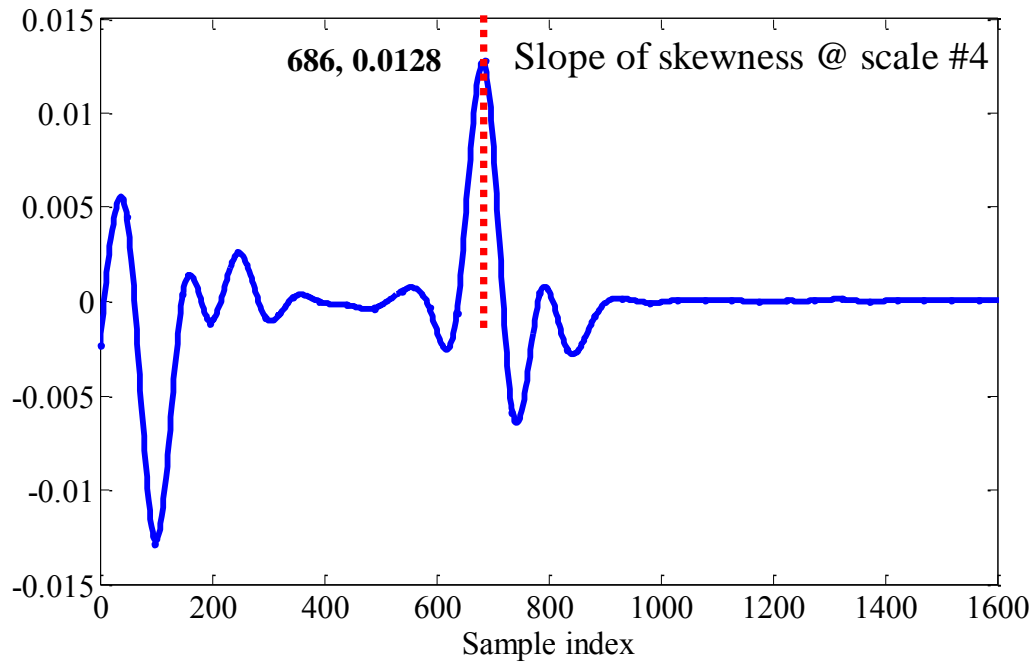
(b)

Figure 4.16 Automatic arrival picks on Scale 4 for Event 3 based on (a) slope of kurtosis and (b) slope of skewness

4.1.2. Window Size Effects on Automatic Picking. The number of samples used in the calculation of any statistical parameter intended for decision-making remains a critical component for the accuracy of such a decision. The proposed algorithm for P-wave phase onset detection and picking requires the computation of skewness and kurtosis in windows with a specified number of samples. It was important in this study to investigate the impact that the size of the window has on the picking accuracy of P-wave phase onset time.

Event 1 in Figure 4.1 was adopted as a case study to understand the impact of window size on the picking accuracy and reliability of the P-wave phase onset time. The results of the P-wave phase onset time picks across four scales for different window sizes are presented in Table 4.2. The results demonstrate that the window size had a great influence on the accuracy of the P-wave phase onset time picks. The impact of window size on picking accuracy was observed across all four scales. Higher residuals between the manual pick and the automatic picks were obtained for all the cases (Table 4.3). In Table 4.3, the observed general trend was that higher residuals were obtained in cases where the window sizes were either very small or very large. This phenomenon could be attributed to the biased estimation of skewness and kurtosis in these windows.

Table 4.2 Picking results for Event 1 for different window size

Window Size	Scale 1		Scale 2		Scale 3		Scale 4	
	Skew	Kurt	Skew	Kurt	Skew	Kurt	Skew	Kurt
5	625	700	600	595	675	640	720	705
8	616	608	632	590	640	640	712	704
10	620	580	630	590	630	630	710	700
15	615	570	630	585	810	630	705	690
20	600	560	620	580	660	620	700	680
25	600	550	625	575	600	600	750	675
30	600	540	690	570	600	600	690	660
40	560	520	600	560	640	600	680	640
50	550	500	600	550	550	550	750	650

Table 4.3 Picking residuals for Event 1 for different window sizes

Window Size	Scale 1		Scale 2		Scale 3		Scale 4	
	Skew	Kurt	Skew	Kurt	Skew	Kurt	Skew	Kurt
5	-49	-124	-24	-19	-99	-64	-144	-129
8	-40	-32	-56	-14	-64	-64	-136	-128
10	-44	-4	-54	-14	-54	-54	-134	-124
15	-39	6	-54	-9	-234	-54	-129	-114
20	-24	16	-44	-4	-84	-44	-124	-104
25	-24	26	-49	1	-24	-24	-174	-99
30	-24	36	-114	6	-24	-24	-114	-84
40	16	56	-24	16	-64	-24	-104	-64
50	26	76	-24	26	26	26	-174	-74

A more accurate result was obtained when the window size was adapted to the method proposed by Küperkoch et al. [50]. In this method, it is recommended that the frequency characteristics of the data be used as the main factor for the determination of the window size. Due to the reliable results obtained when this method was applied, the window size selection for data processing in this study is based on the Küperkoch et al. [50] method.

4.1.3. The Effects of CF on Automatic Picking. The CF remains the single most important parameter that determines the performance of an automatic detector or picker. Phase arrival is usually characterized by changes in the frequency content and amplitude of the seismic or AE/MS time series. Any good CF should, therefore, respond to this change and enhance the change in a timely manner [27].

The choice of this parameter is therefore critical in the design of any new detector or picker. The use of skewness and kurtosis functions for P-wave phase onset picking was first introduced by Saragiotis et al. [23, 67]. Generally, methods based on skewness and kurtosis estimate the P-wave phase onset as the global maximum kurtosis or skewness value in the series. This method of P-wave phase onset time picking was applied to Event

1 (Figure 4.1) and Event 2 (Figure 4.2) to assess the reliability of the automatic picks in comparison to manual picks. The automatic picks for Event 1 on Scales 2 and 3, which were based on maximum kurtosis and maximum skewness, are shown in Figures 4.17 and 4.18. Each figure shows the arrival times (sample index) and the corresponding maximum values for skewness and kurtosis. Compared to the manual pick for Event 1, a residual of 64 samples was obtained for both picking schemes on Scale 2. The residual on Scale 3, which was between the manual and automatic picks based on the skewness and kurtosis schemes, was 80 sample points. However, the picks on Scales 1 and 4 were off the manual pick in excess of 904 and 644 sample points, respectively. Figure 3.19 and Figure 3.20 show the automatic picking results for Event 2 on Scales 2 and 3, respectively. A comparison of these picking results with the manual picks showed that both picking algorithms completely missed the P-wave phase onset arrival.

The results obtained in this sensitivity analysis showed that the picking accuracy of the P-wave phase onset arrival was greatly dependent on the CF, as stated by Allen [27]. While both methods (maximum kurtosis and maximum skewness) performed fairly well with Event 1, which had high SNR, the P-wave phase onset arrival picks made on Event 2 (with a low SNR) were completely wrong in both cases. Also, the P-wave phase onset time picking based on both the maximum kurtosis and skewness shows to be after the actual phase onset. For pure noise, the values of skewness and kurtosis turn to zero or close to zero. However, as the sliding window reaches the P-wave phase onset arrival, the values of skewness and kurtosis increases and they only reach maximum values when a significant portion of the window contains the AE/MS event. These characteristics are observed to have caused delays in the picking of the P-wave phase onset time with the maximum kurtosis and skewness pickers. Hence, using the maximum values of kurtosis and skewness for the P-wave phase onset arrival picking could lead to significant errors in the determination of the source location of AE/MS events. The errors become more prominent, in cases where the AE/MS data is highly contaminated with background noise. High background noise leads to a low SNR, as was observed with Event 2 (Figure 4.2).

Due to the deficiencies associated with the method of maximum kurtosis and skewness, especially with signals with a low SNR, the method was not adopted in this

study. Instead, the P-wave phase onset arrival picking was performed using the slope of kurtosis and skewness as demonstrated in Section 4.1.1 (Figures 4.5 to 4.16).
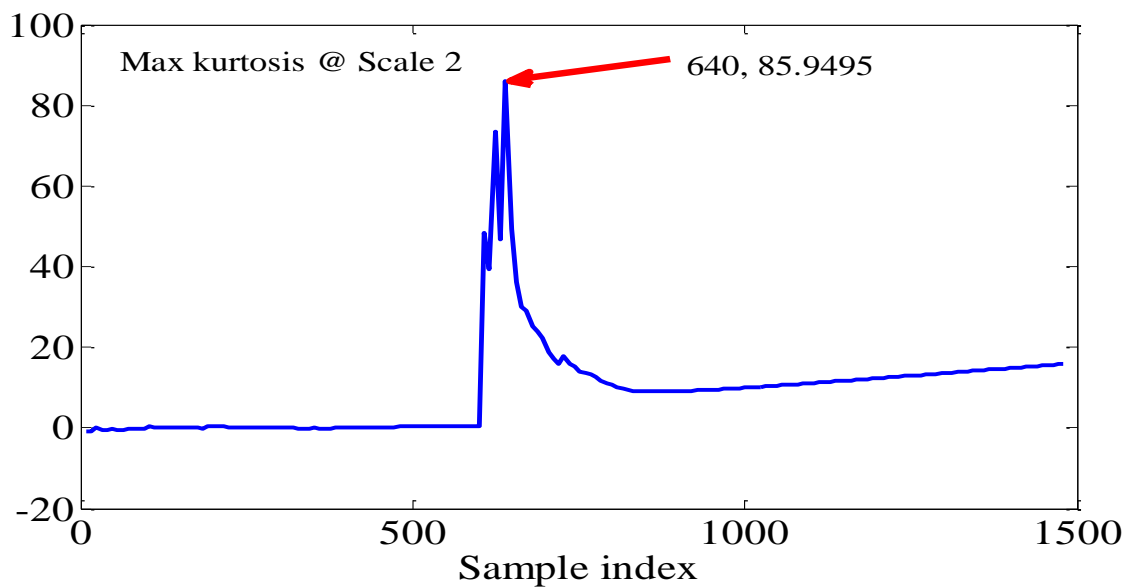
(a)
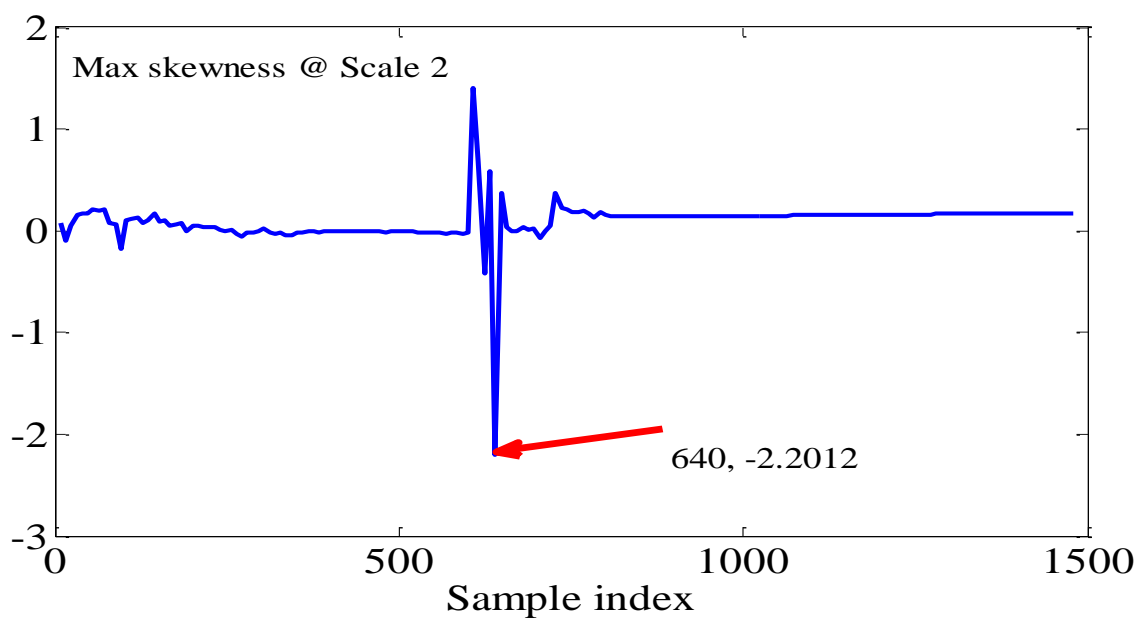
(b)

Figure 4.17 Automatic phase picking for Event 1 on Scale 2 using maximum skewness and kurtosis
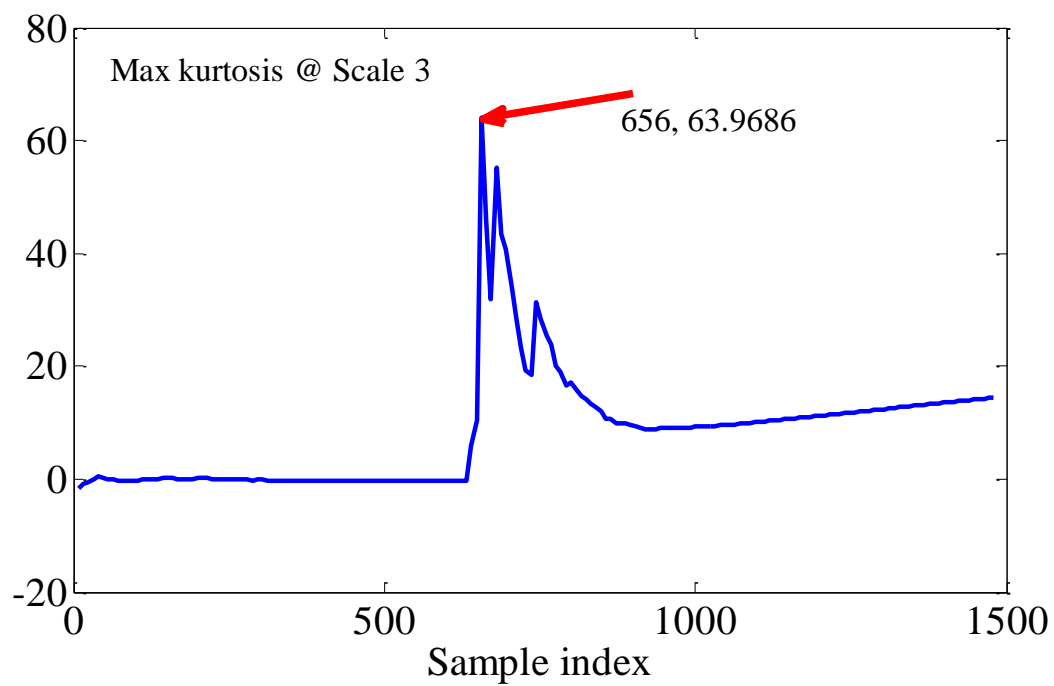
(a)
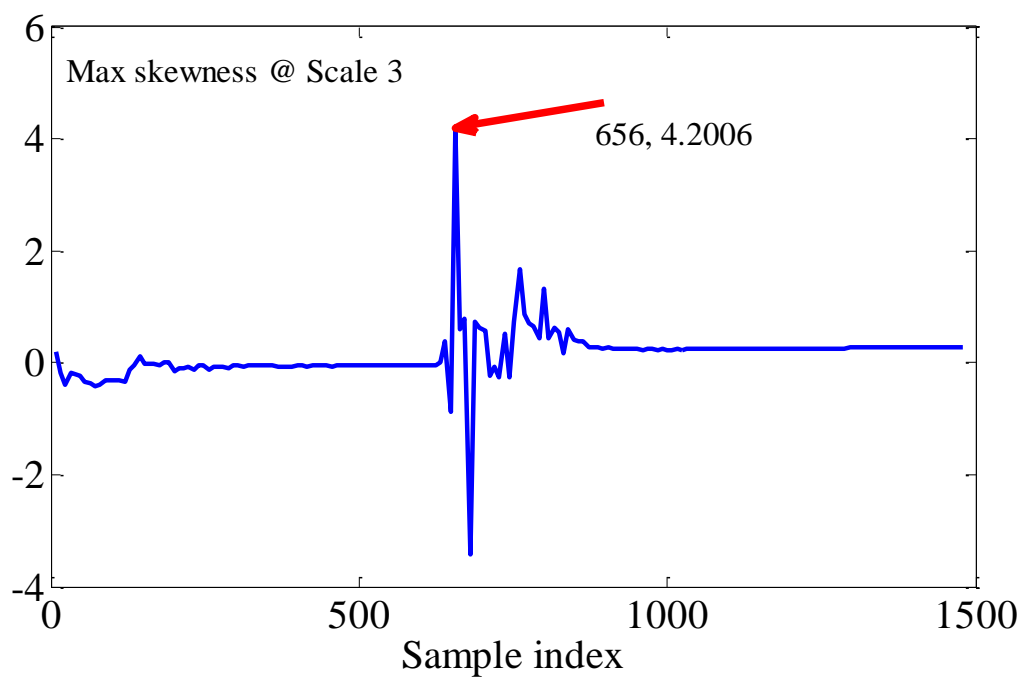
(b)

Figure 4.18 Automatic phase picking for Event 1 on Scale 3 using maximum skewness and kurtosis
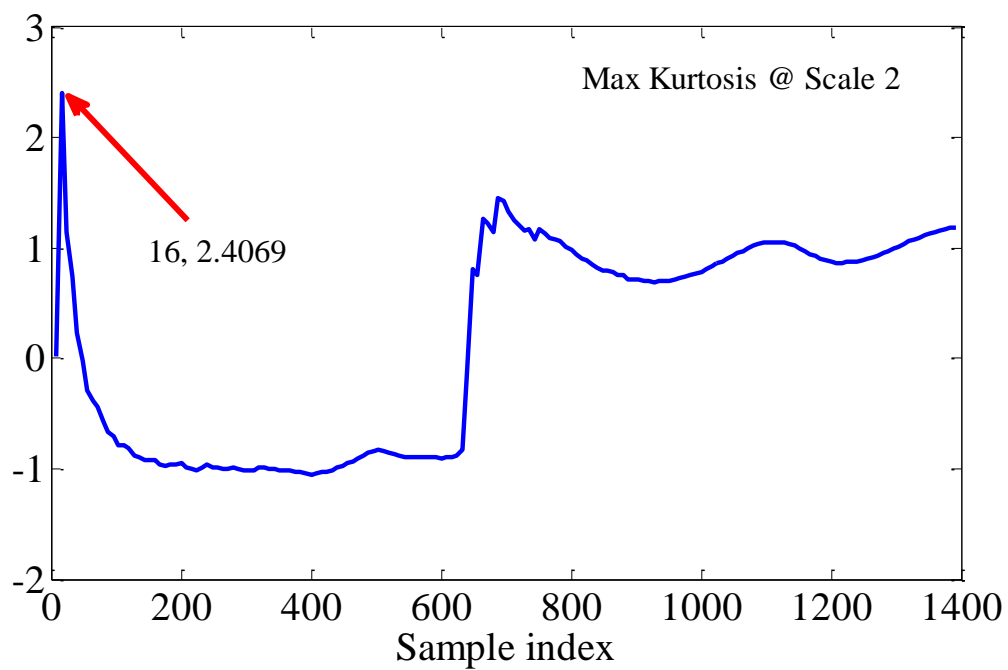
(a)
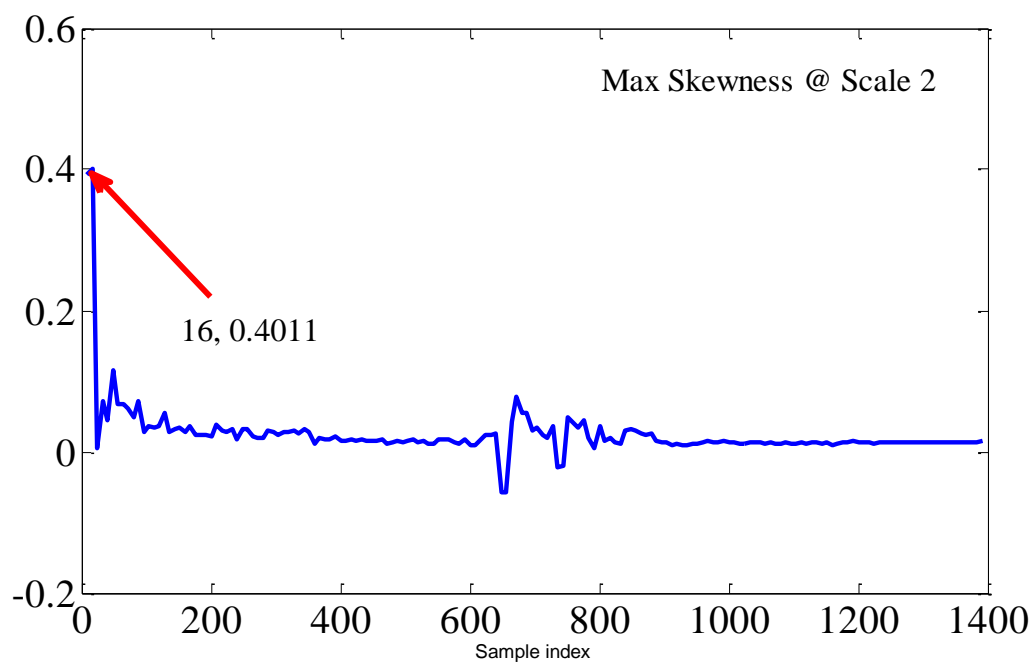
(b)

Figure 4.19 Automatic phase picking for Event 2 on Scale 2 using maximum skewness and kurtosis
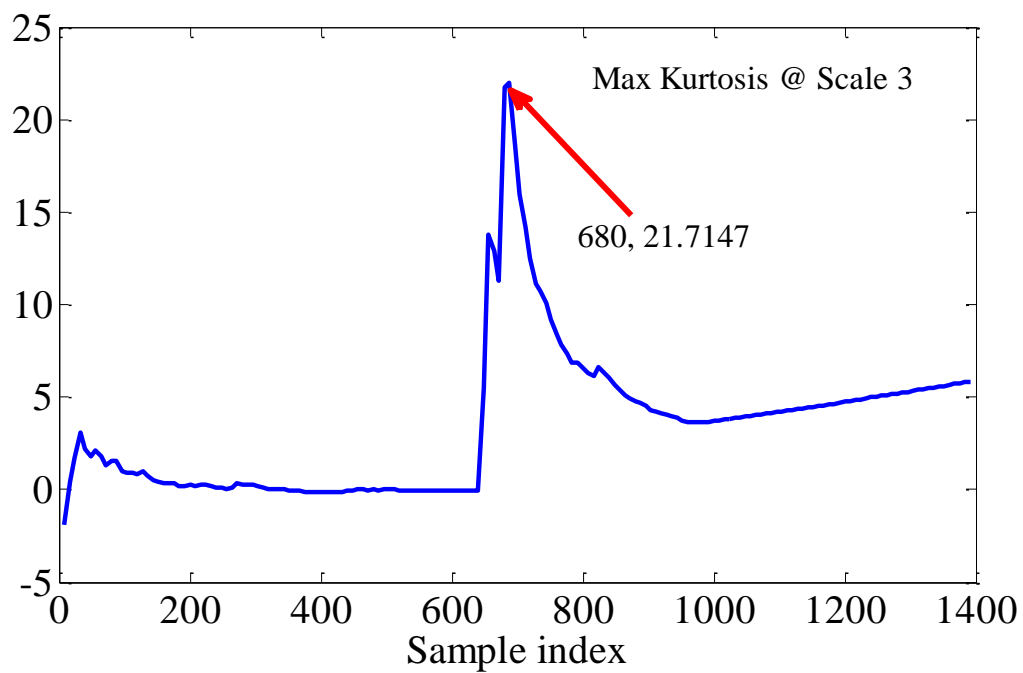
(a)
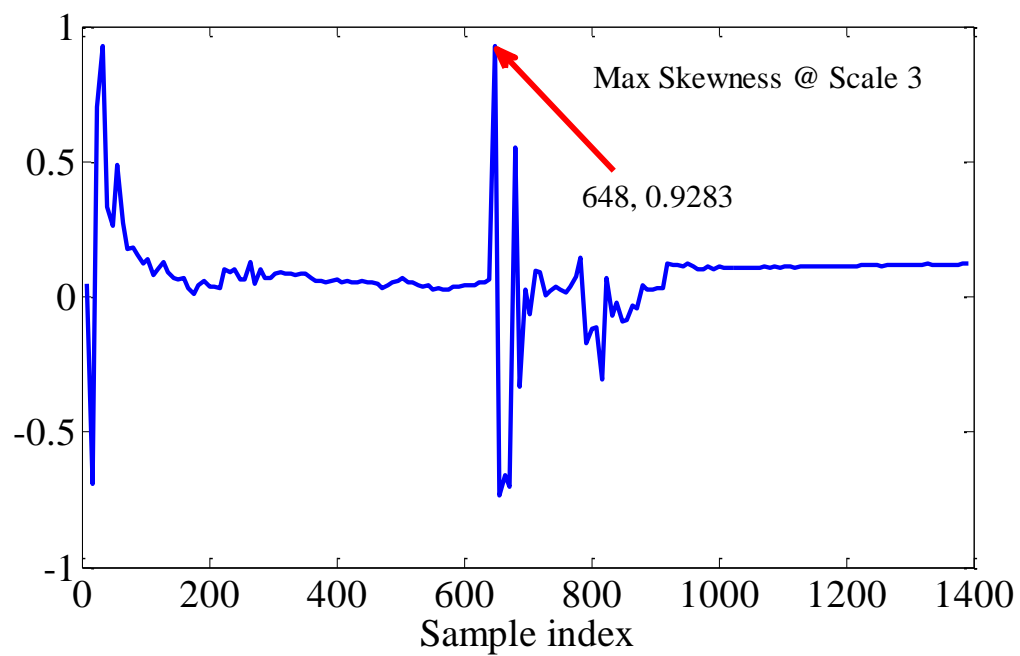
(b)

Figure 4.20 Automatic phase picking for Event 2 on Scale 3 using maximum skewness and kurtosis

■■■ FREQUENCY CONTENT ANALYSIS

To investigate why some scales provide better performance than others, a frequency content analysis was performed on the detail coefficients obtained at each scale for the three events shown in Figures 4.1, 4.2, and 4.3. As shown in Figures 4.1, 4.2, and 4.3, the FFT performed on the three signals indicated the presence of different frequency contents. However, it was impossible to identify which frequency content was associated with noise and which was for the signal of interest. Hence, to help distinguish noise from actual AE/MS signals, the FFT of the detail coefficients for each scale was performed.

Figures 4.21 to 4.24 represent the four-scale decomposition of the signal associated with Event 1 in Figure 4.1. Event 1 illustrates an event where there is less noise contamination, making it much easier to identify the onset of the P-phase arrival manually. Figures 4.21a, 4.22a, 4.23a, and 4.24a show the plots of the detail coefficients obtained over the four scales. The corresponding frequency distributions at these scales are shown in Figures 4.21b, 4.22b, 4.23b, and 4.24b. Very high frequency values are observed on Scale 1 (Figure 4.21). Scale 1 is generally the scale with high noise levels. Noises are usually characterized by high frequencies and hence provide a good justification for excluding Scale 1 in this study. On the other hand, as the number of scales increased from 2 to 4, the frequency distribution plots prominently showed the presence of low frequency compared to Scale 1. From the frequency distribution analysis, it is observed that the frequency content of Event 1 is approximately between 100 and 150 Hz, while that of the noise is approximately above 150 Hz.

The plots of the detail-coefficients and associated frequency distributions for Event 2 are shown in Figures 4.25 to 4.28. Unlike Event 1, Event 2 represents a case where the event is completely masked by noise. In this case, the P-phase arrival is preceded by noise spikes, which could be mistaken as the event onset for threshold technique. Once again, the first scale (Figure 4.25) showed a single major dominant frequency value centered on approximately 150Hz. However, as one follows the scales, the presence of other frequency content and the emergence of the P-phase arrival are observed (Figures 4.26 to 4.8). The frequency content of Event 2 can be approximated as being 115 Hz.
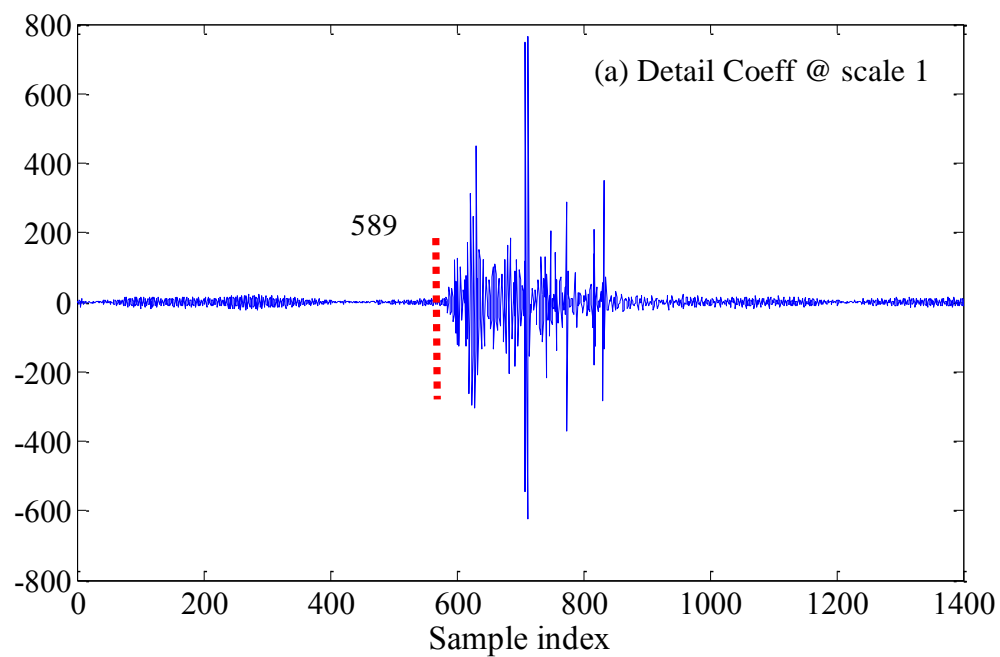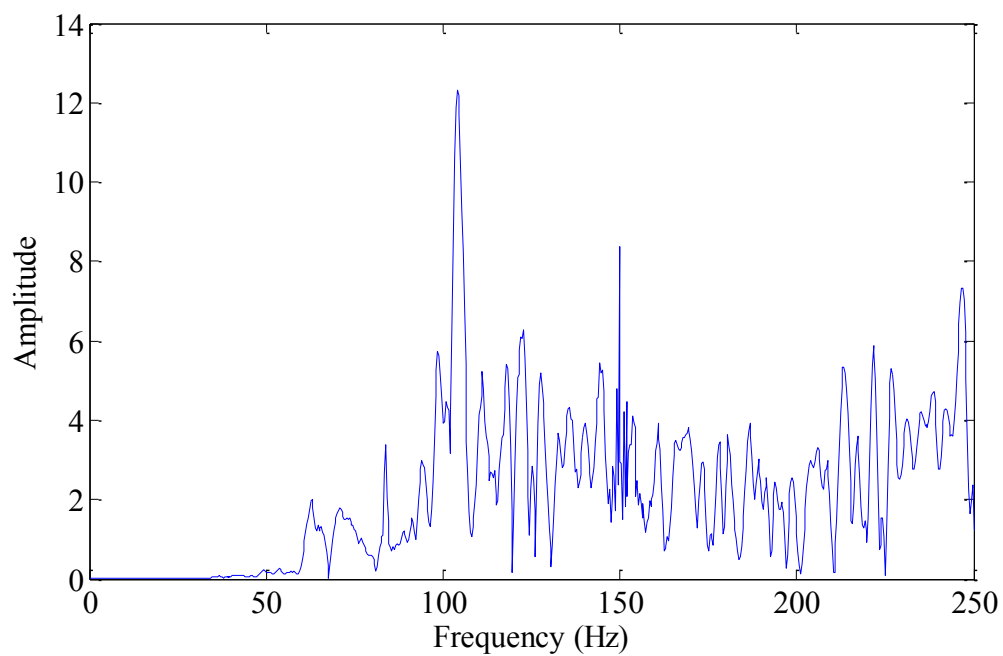
Figure 4.21 Manual picks for Event 1 on Scale 1 (a) after filtering by Db5 and (b) amplitude spectrum by FFT

(b) Detail Coeff @ scale 2

582

Sample index

(a)

Amplitude

Frequency (Hz)
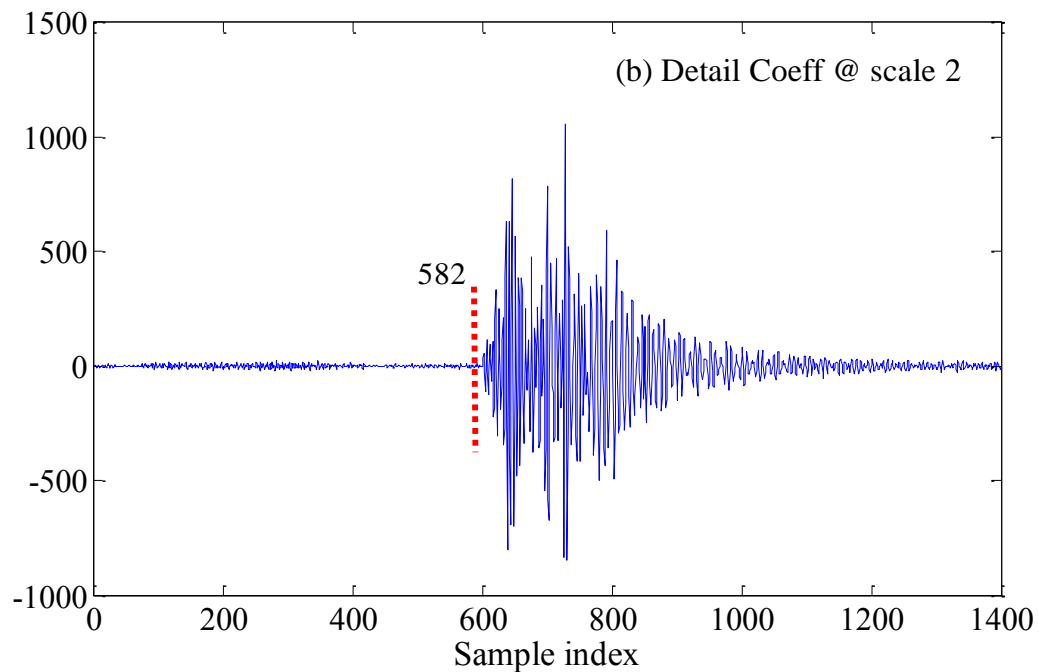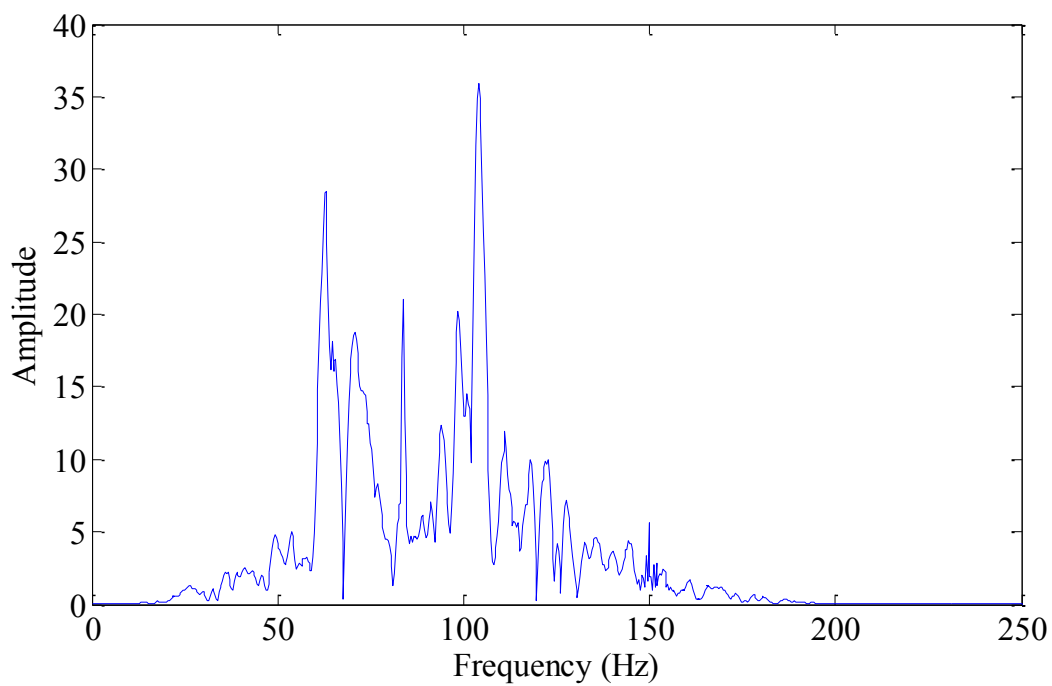
(b)

Figure 4.22 Manual picks for Event 1 on Scale 2 (a) after filtering by Db5 and (b) amplitude spectrum by FFT
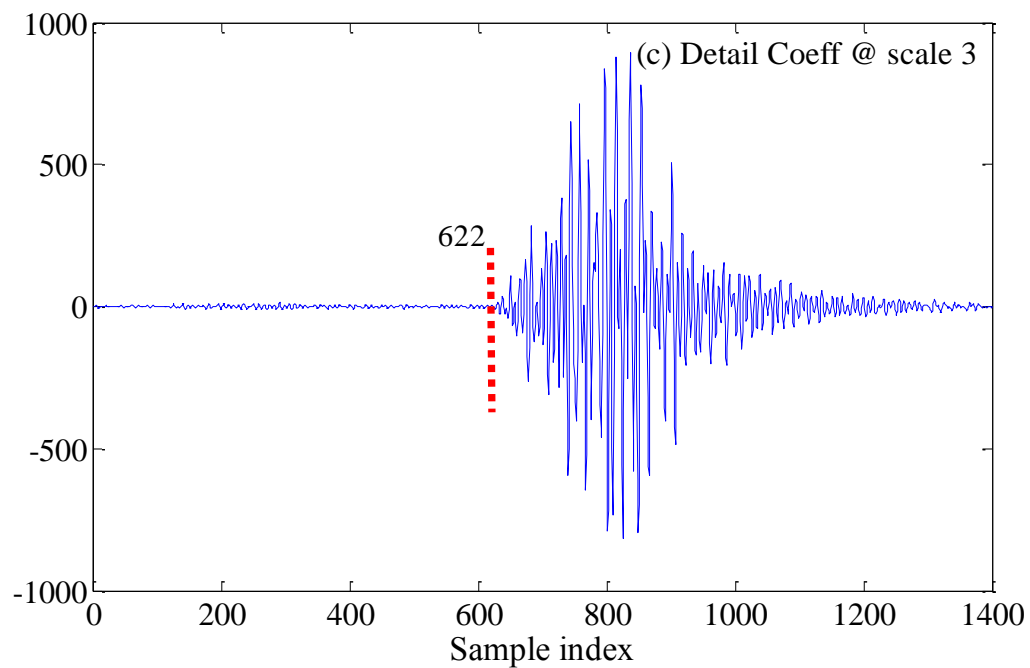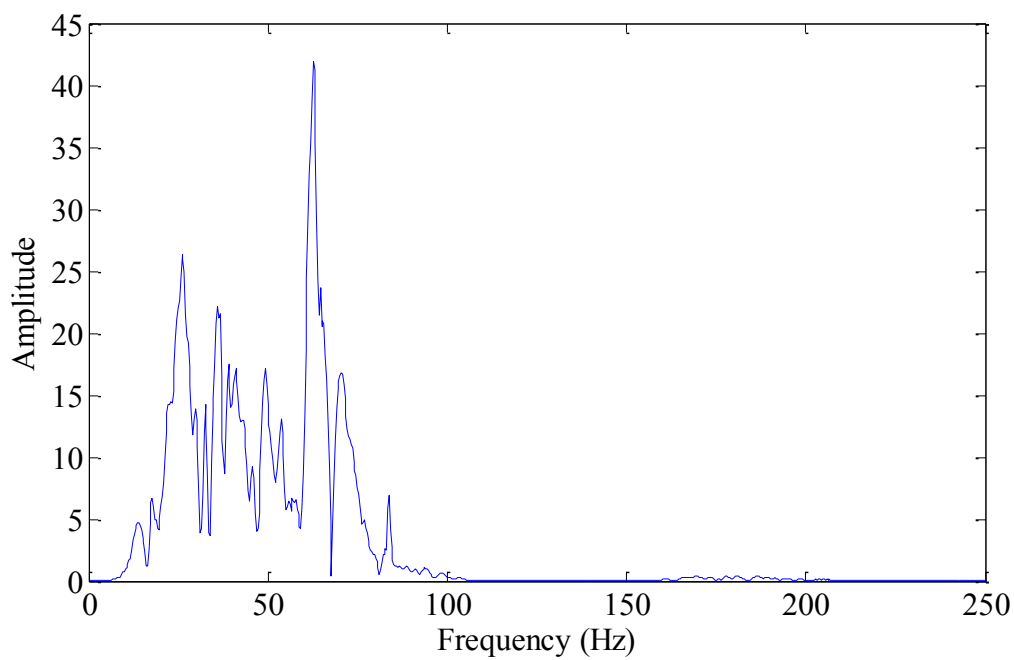
Figure 4.23 Manual picks for Event 1 on Scale 3 (a) after filtering by Db5 and (b) amplitude spectrum by FFT
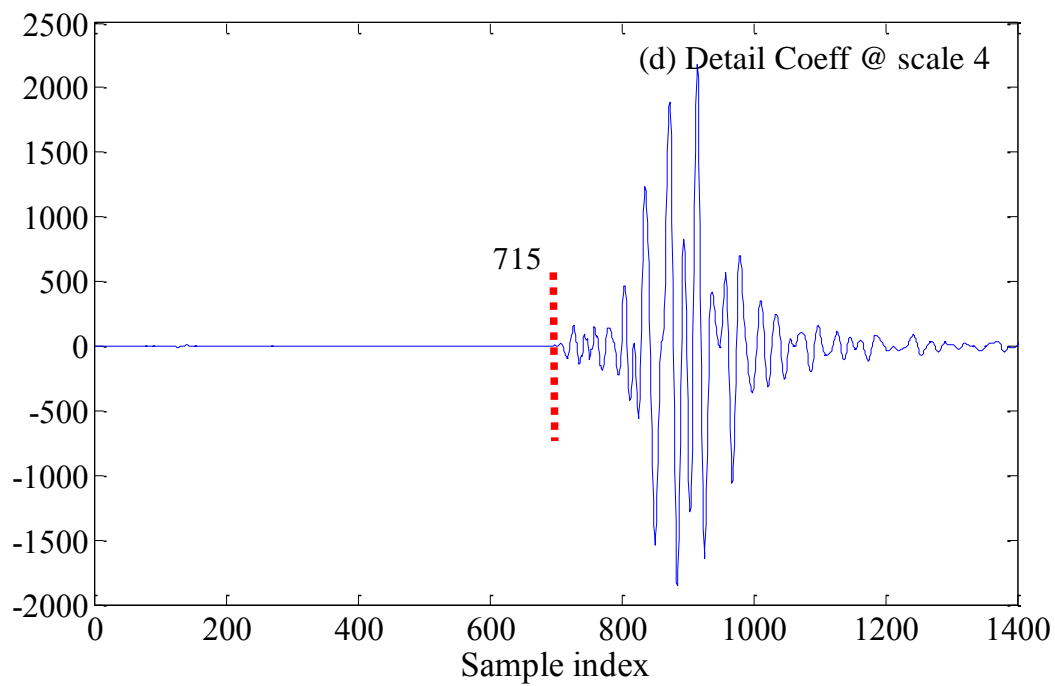
(a)
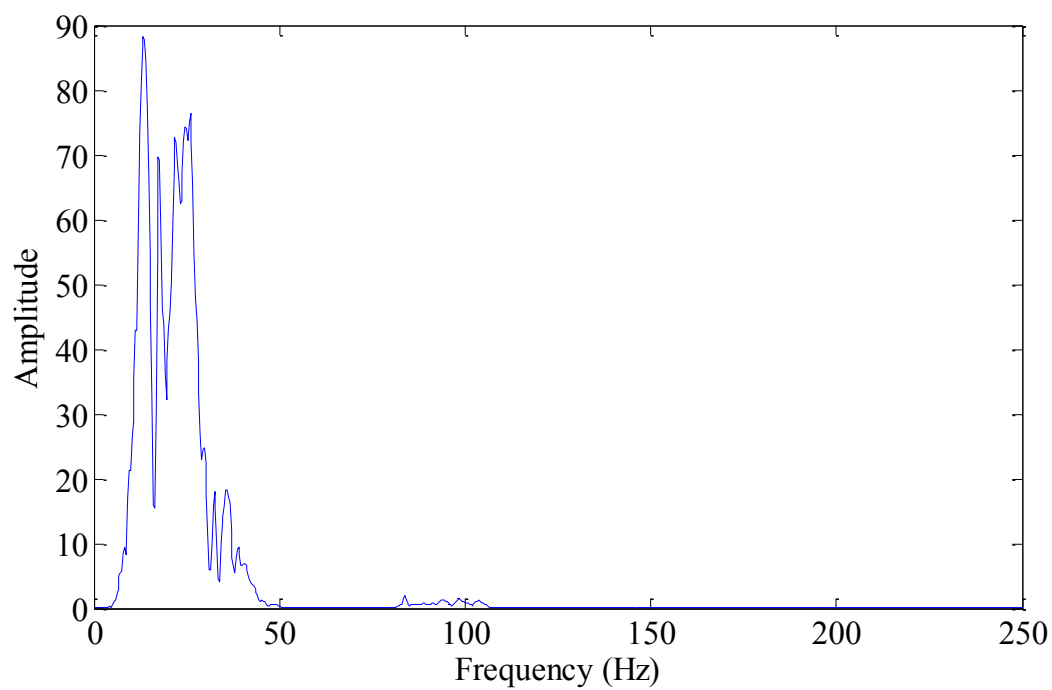
(b)

Figure 4.24 Manual picks for Event 1 on Scale 4 (a) after filtering by Db5 and (b) amplitude spectrum by FFT
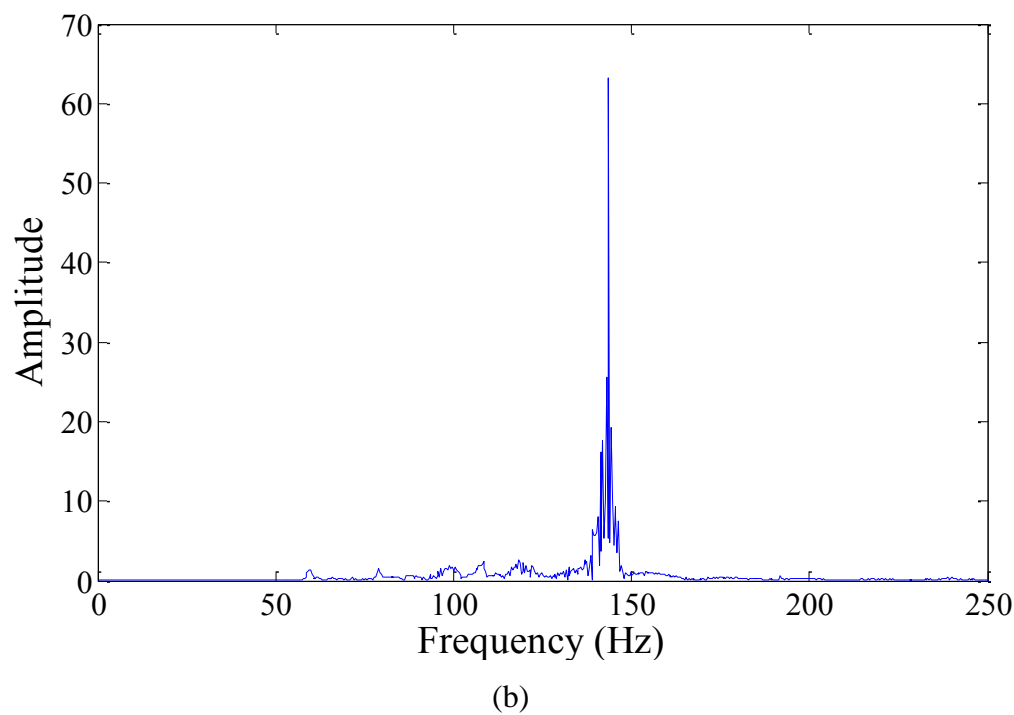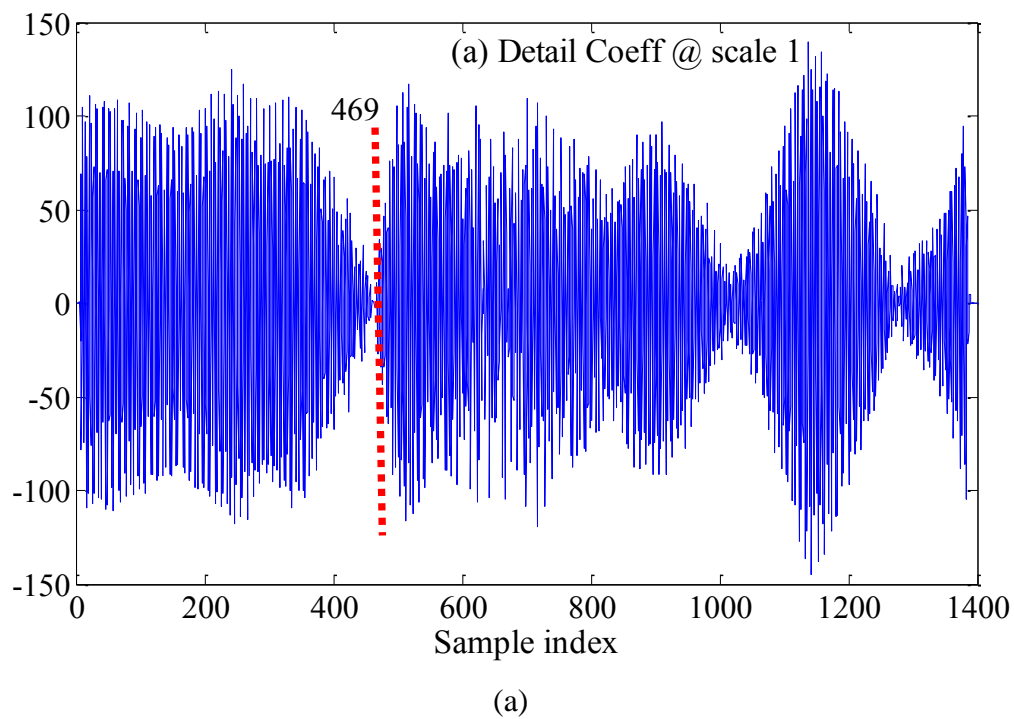
Figure 4.25 Manual picks for Event 2 on Scale 1 (a) after filtering by Db5 and (b) amplitude spectrum by FFT

(b) Detail Coeff @ scale 2

480

Sample index

(a)

Amplitude

Frequency (Hz)
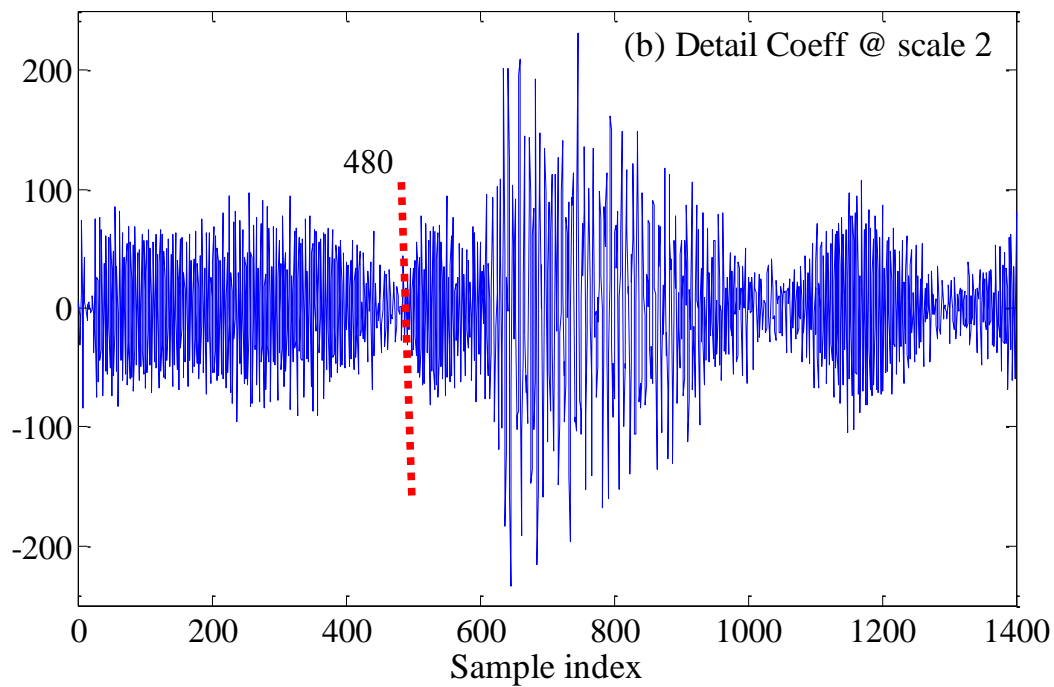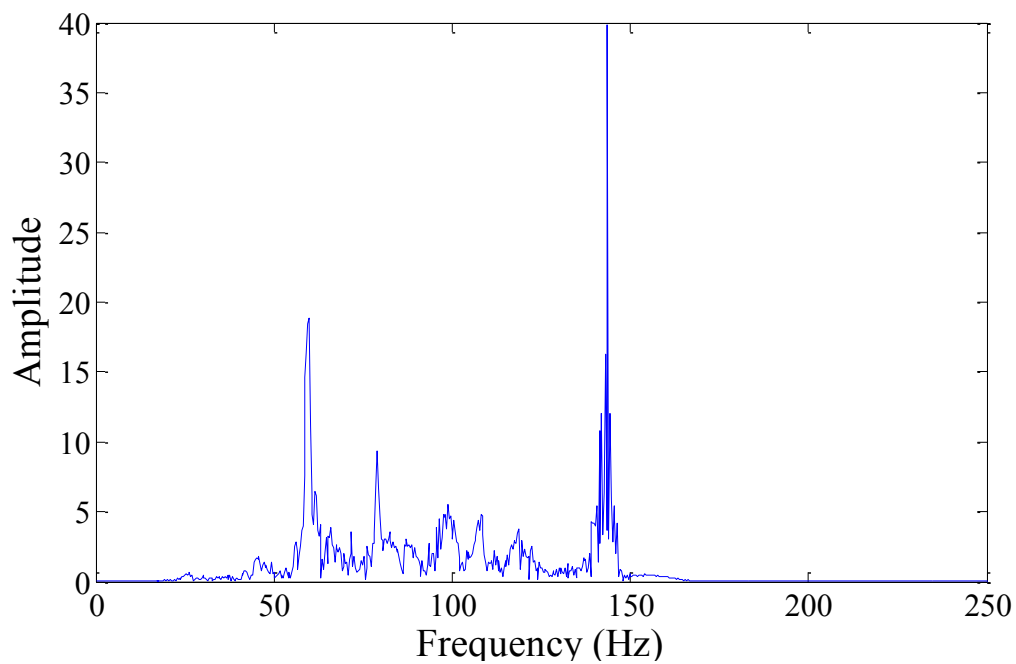
(b)

Figure 4.26 Manual picks for Event 2 on Scale 2 (a) after filtering by Db5 and (b) amplitude spectrum by FFT
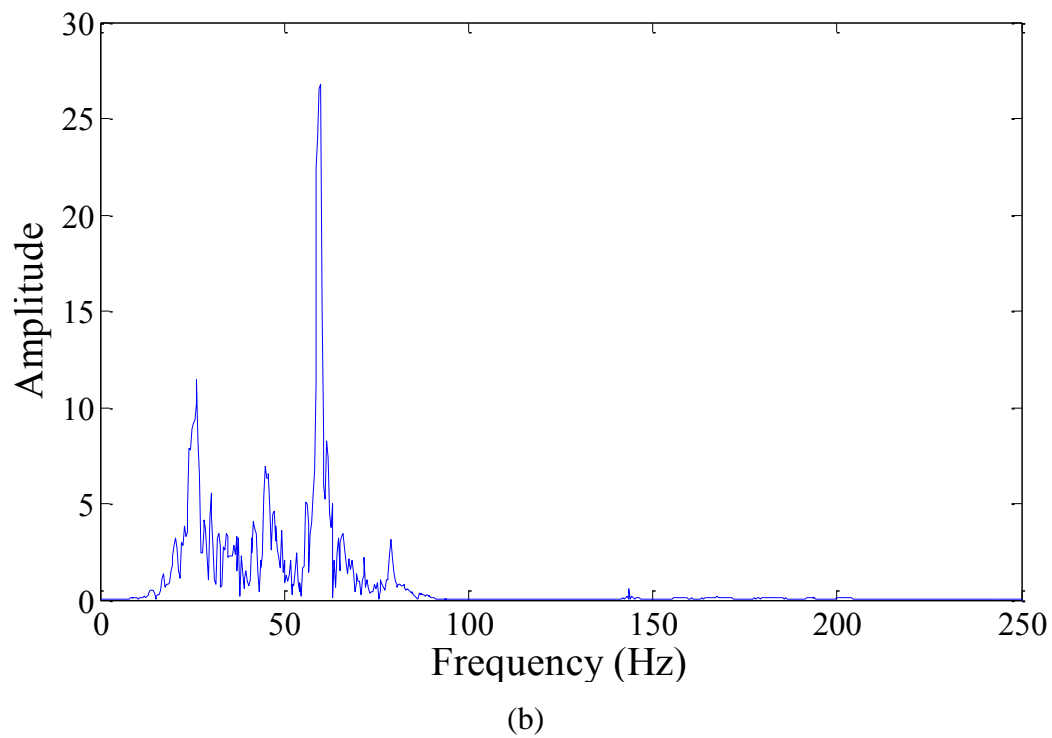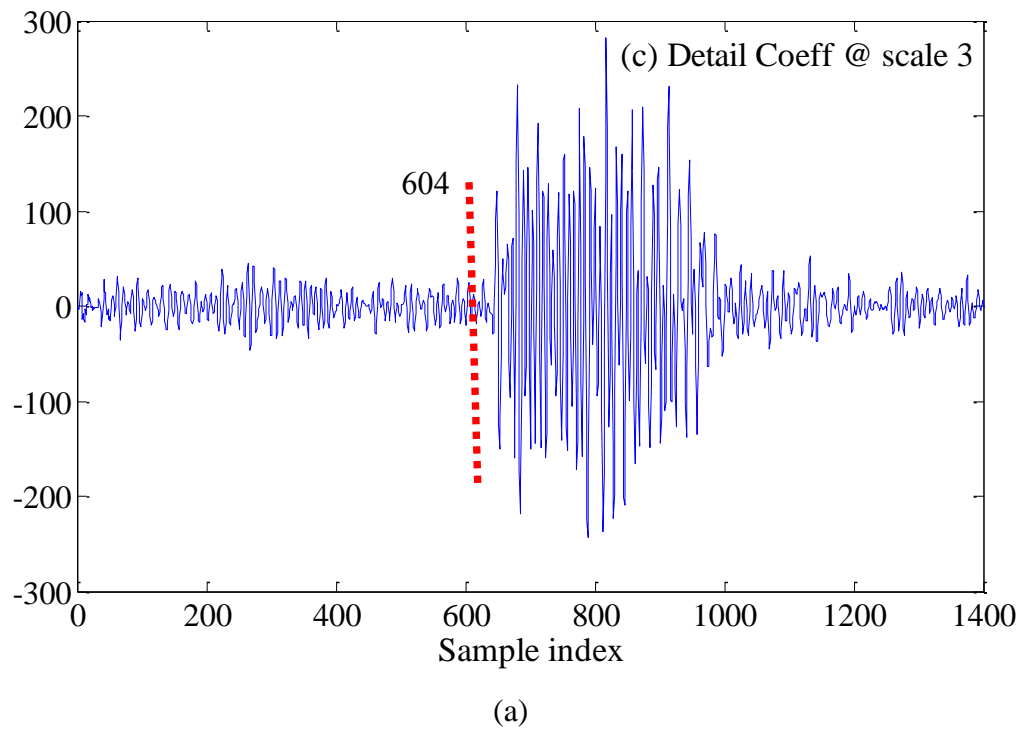
Figure 4.27 Manual picks for Event 2 on Scale 3 (a) after filtering by Db5 and (b)
amplitude spectrum by FFT

(a)

(b)
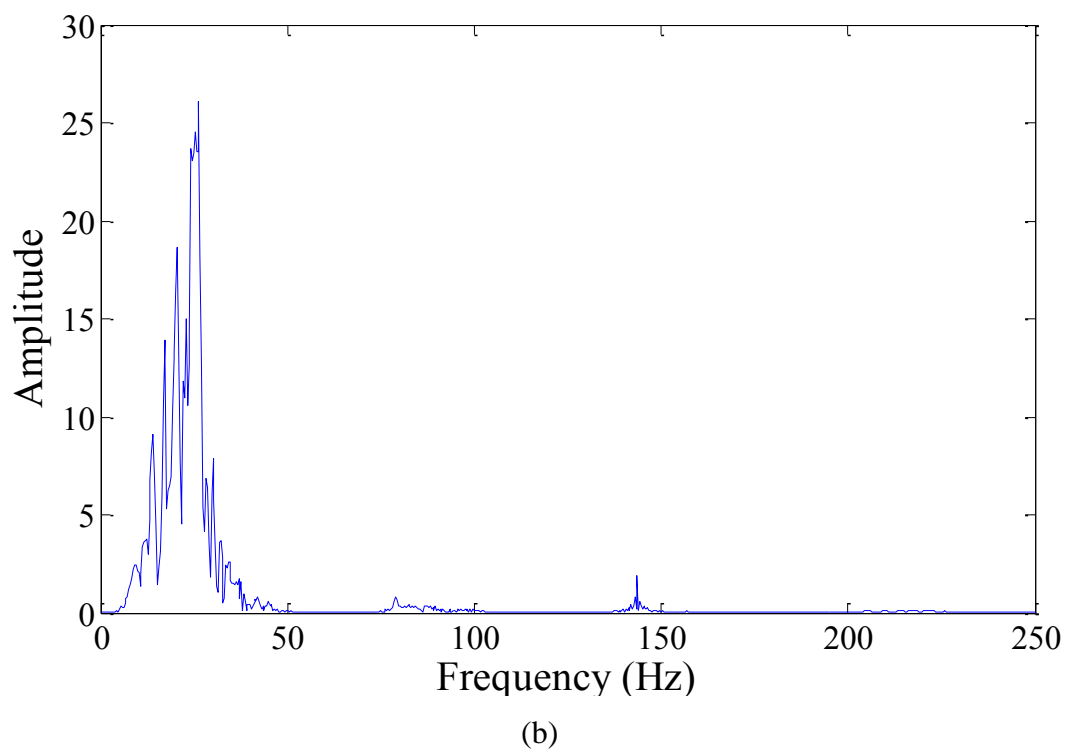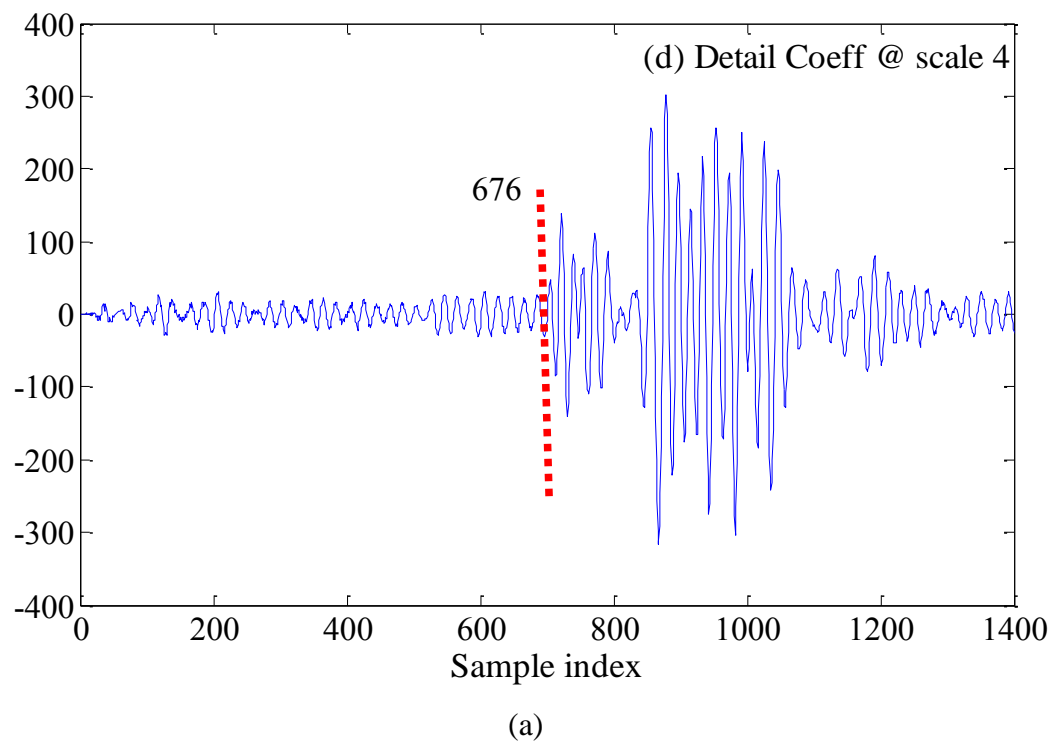
Figure 4.28 Manual picks for Event 2 on Scale 4 (a) after filtering by Db5 and (b) amplitude spectrum by FFT

As demonstrated in the cases of Event 1 (Figures 4.21 to 4.24) and Event 2 (Figures 4.25 to 4.28), Scale 1 of the detail coefficients of Event 3 is dominant by high frequency amplitudes centered on 150 Hz with some minor frequency amplitudes between the frequencies of 90 Hz and 130 Hz (Figures 4.29 to 4.32). However, at higher scales, which correspond to lower frequency bands, the hidden frequency bands that were not very visible on Scale 1 becomes more clear and visible. Associated with these frequency bands is the clear visibility of the emergence of the P-phase onset.

The frequency distribution analysis across the scales of decomposition performed in this section confirms and provides justification for the exclusion of Scale 1 detail coefficients for phase picking. As shown in Figures 4.21, 4.25 and 4.29, the detail-coefficients obtained from Scale 1 are usually dominated by high noise level. Therefore, using the Scale 1 detail coefficients for further analysis could lead to errors in arrival time picks.

■ PHASE ASSOCIATION TEST RESULTS

A phase association was performed to ensure the automatic phase arrival picks obtained are indeed those triggered by the presence of a P-wave onset. This was achieved by employing all the arrival picks obtained by each channel of the monitoring system used at the mine for recorded events. For each channel, the signal is decomposed across four scales, and then the automatic picking algorithm is applied to the second, third, and fourth scales. For each scale, the arrival picks is recorded for each channel. The phase association theory and algorithm discussed in Section 3.4 is then applied to determine if the picks were really due to a P-wave phase onset as assumed. In the phase association test, the arrival time difference computed from the automatic picks (observed arrival times) are compared to standard established theoretical arrival time equations developed based on the assumed type of arrival.

A comparison of the observed arrival times with the theoretical limits provides an opportunity for examining the validity of the assumption that the picks made by the automatic picker are all due to the onset of the P-wave. An arrival-time difference table was generated for each event. The results of this test for Event 1 discussed in Figure 4.1 are presented in appendix A in Tables A1 to A6 for Scales 2, 3, and 4 based on using

skewness and kurtosis. For each table, the numbers in first row and first column represent the transducer numbers in terms of triggering order. Also, each table has n columns and n double rows, with n being the number of transducers. For each row and column intersection, the upper number represents the observed arrival time difference while the lower number in italics represents the theoretical limit of the P-wave arrival time difference between the two transducers.

A look at the diagonal layout of the tables shows that the tables are symmetric. Sections highlighted in red and with one asterisk indicate instances for which the observed arrival time difference exceeded the theoretical limits. Regions with two asterisks indicate that the source of the event is located at the first transducer or on the extension of a line connecting the two transducers. Generally, the results from the tables show that many of the observed arrival time differences far exceeded the corresponding theoretical limits. However, instances such as these are not to be expected if the P-wave velocity used is correct (except for outlier arrivals) [109]. In other words, the results indicate that the assumption that all picks were due to the onset of the P-wave phase was incorrect. A careful examination of the transducer locations and the order in which they triggered, however, showed no arrivals for outliers. The assumption made in this case is that the source of the event is close to the first two to three transducers. A summary of the number of events flagged for misclassification on each scale and for each picking algorithm is presented in Figure 4.33. On Scale 2, thirty-five and forty-eight events were misclassified by the kurtosis-based and skewness-based methods, respectively. Fifty-one and fifty-two events were misclassified by the kurtosis-based method on Scale 3 and Scale 4 respectively. On the other hand, sixty-three events were misclassified by the skewness-based method on Scale 3 and Scale 4, respectively.

In light of the results obtained across all scales and the cases of excessive arrival time difference on some channels, it is reasonable to assume that the most reliable P-wave onset picks were obtained on channels one to eight. Generally, these channels showed either no case of observed arrival time difference exceeding the corresponding theoretical limit or one to three cases, depending on the used scale. On the other hand, channels nine, eleven, thirteen, fourteen, fifteen, and sixteen showed instances of four or more cases of observed arrival time difference exceeding the corresponding theoretical limits. It is

observed that on Scale 4, there are a large number of cases for which the observed arrival time difference exceed the corresponding theoretical limit. This trend confirms the initial observation that at higher scales, the onset of P-wave phase arrivals is usually unclear and could lead to pick errors.
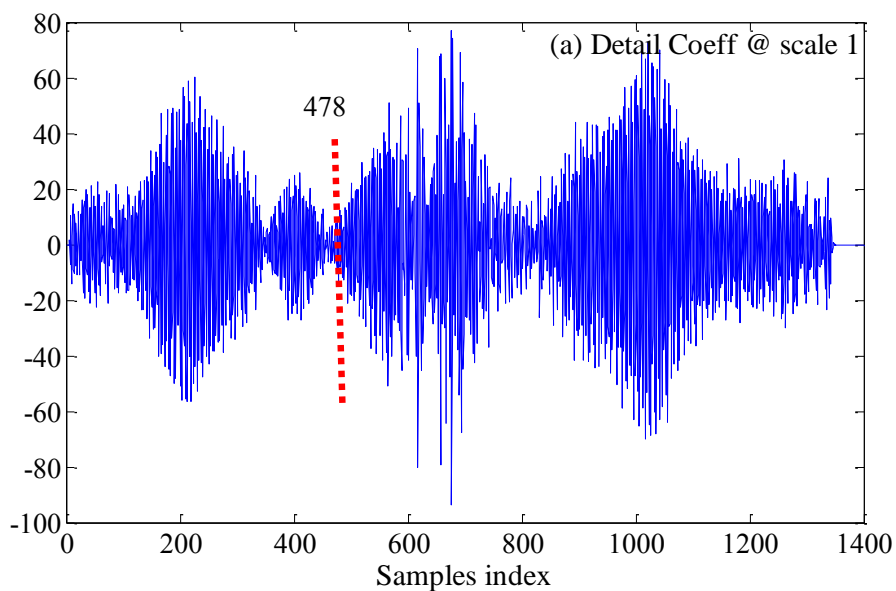
(a)
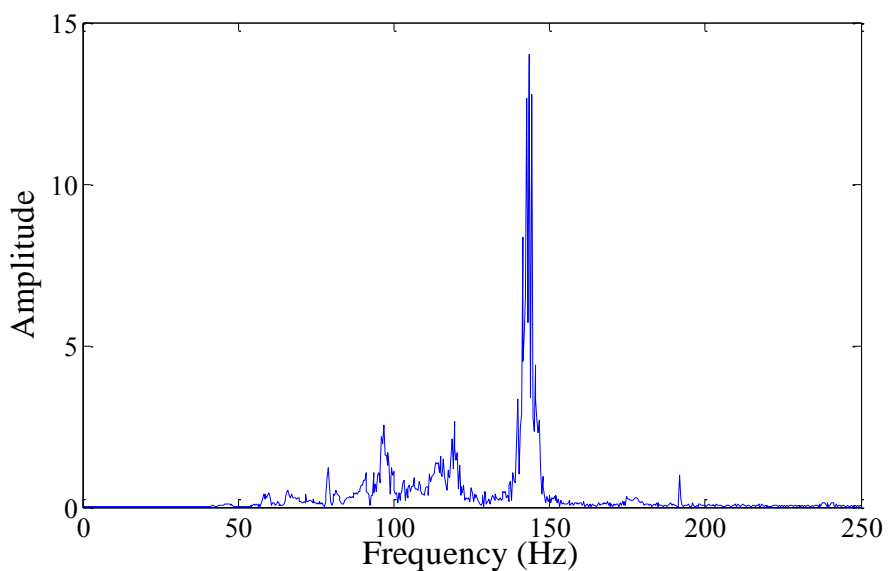
(b)

Figure 4.29 Manual picks for Event 3 on Scale 1 (a) after filtering by Db5 and (b) amplitude spectrum by FFT
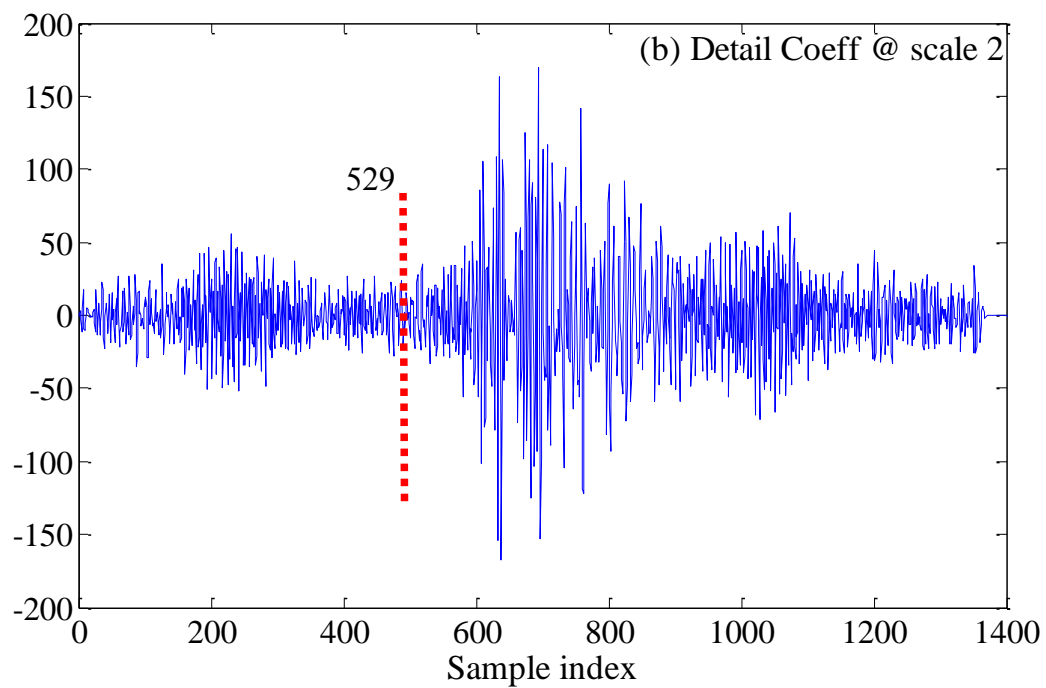
(a)
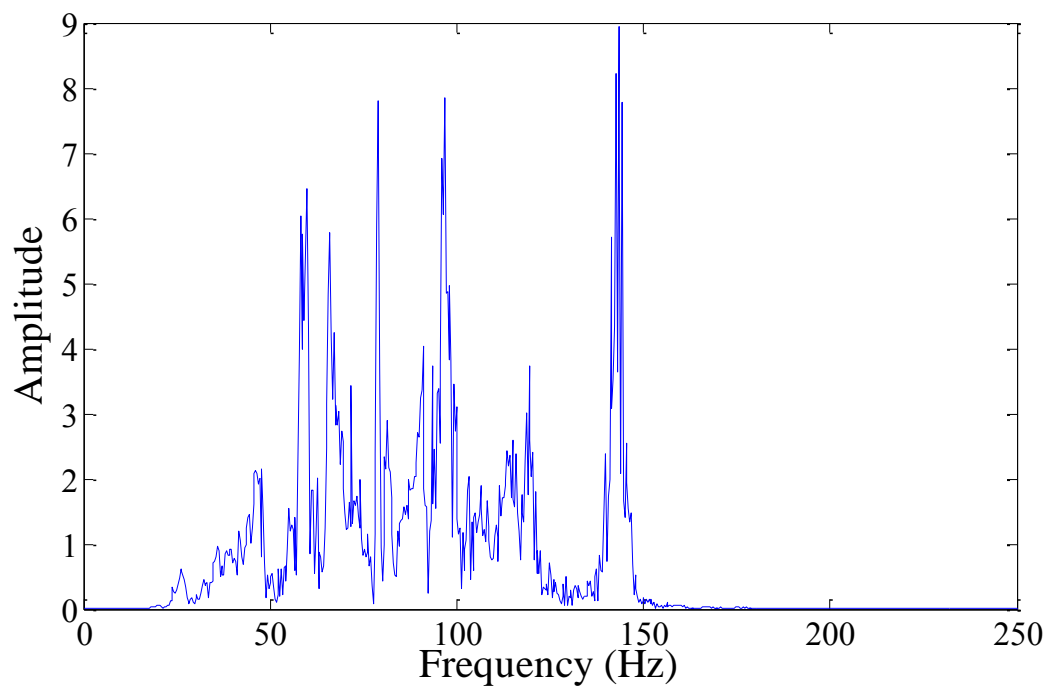
(b)

Figure 4.30 Manual picks for Event 3 on Scale 2 (a) after filtering by Db5 and (b) amplitude spectrum by FFT
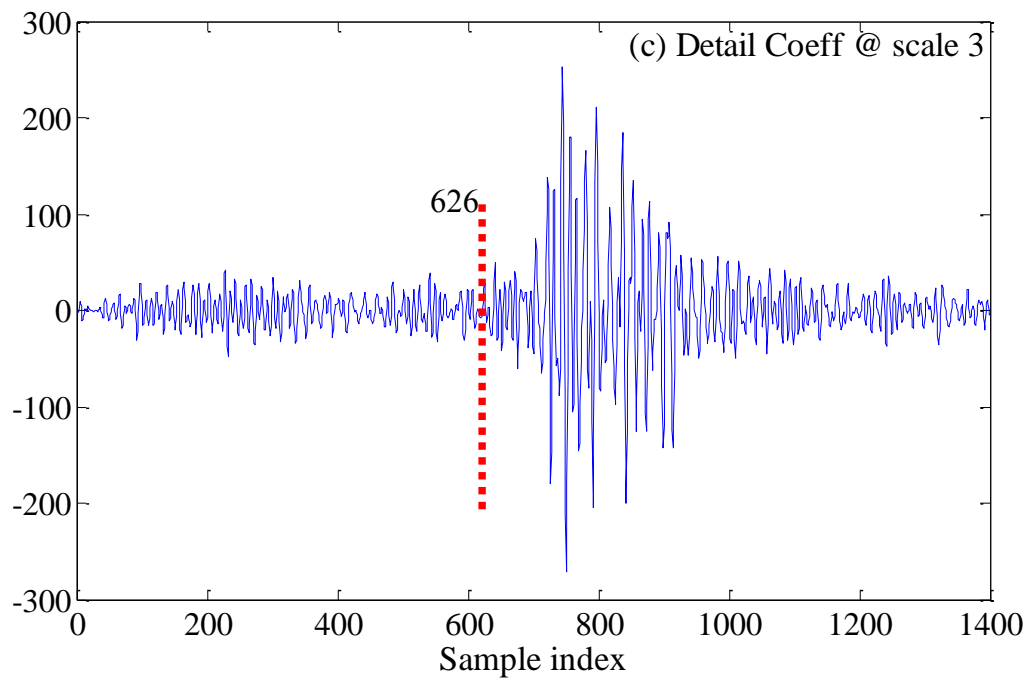
(a)
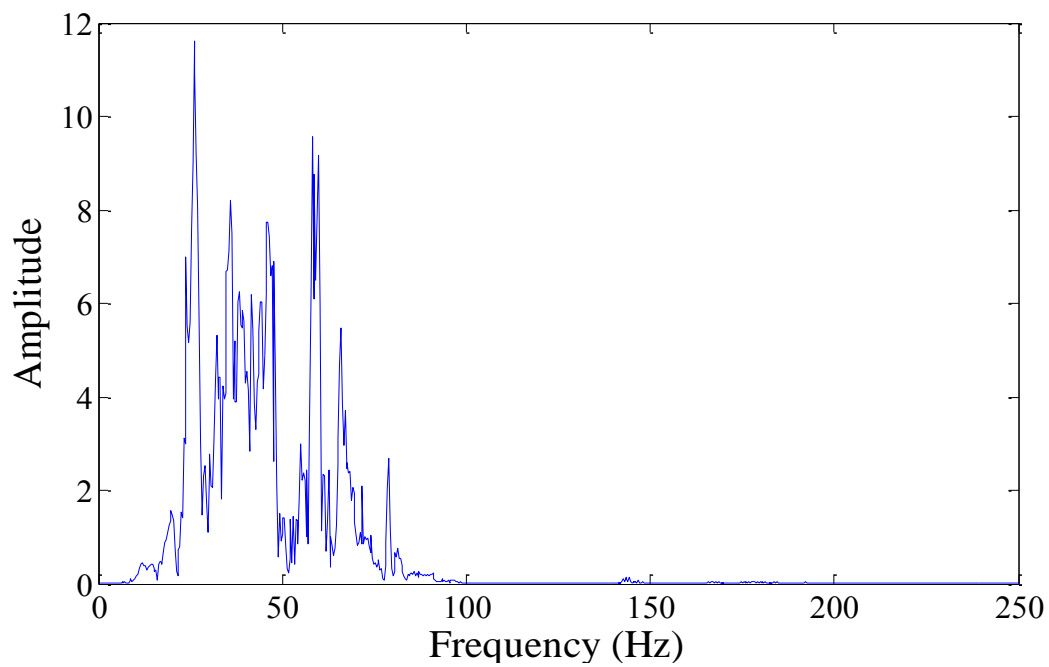
(b)

Figure 4.31 Manual picks for Event 3 on Scale 3 (a) after filtering by Db5 and (b) amplitude spectrum by FFT
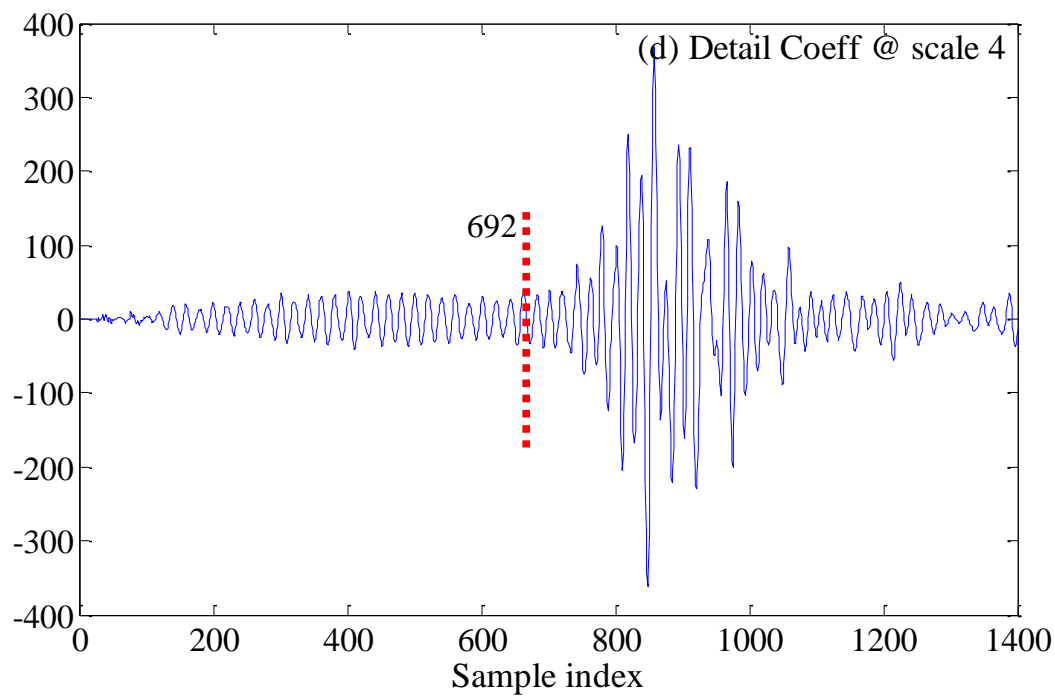
(a)
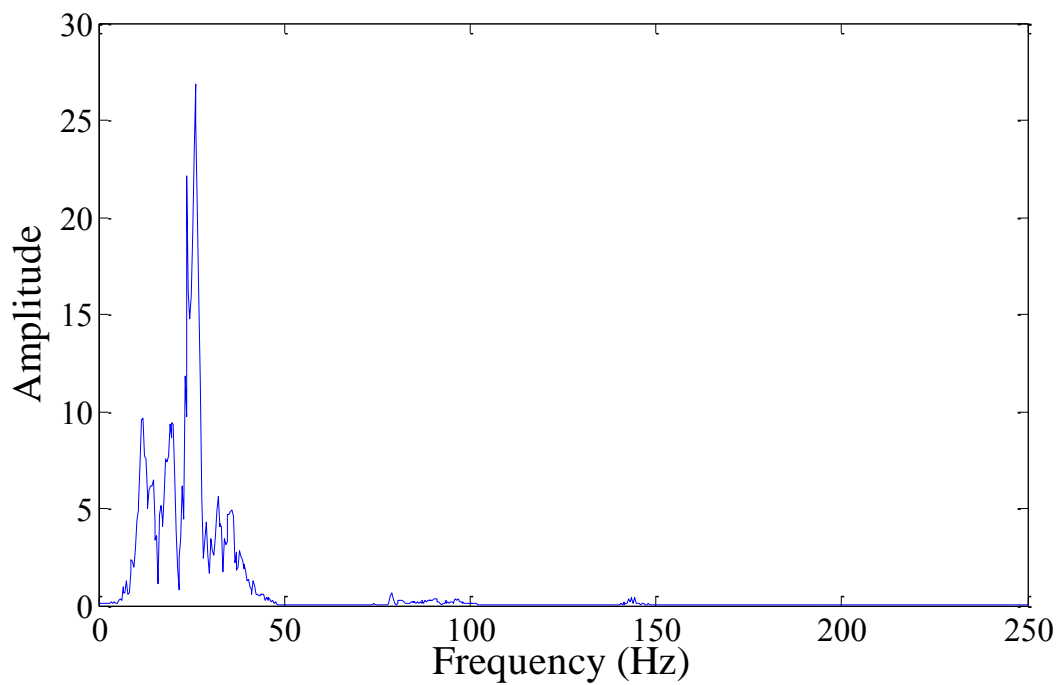
(b)

Figure 4.32 Manual picks for Event 3 on Scale 4 (a) after filtering by Db5 and (b) amplitude spectrum by FFT

The phase association test in this section provides evidence that the arrival picks obtained by the automatic picking algorithms are generally reliable. However, it is observed that picks based on kurtosis provide more reliable results compared to picks based on skewness. Also, picks on Scales 2 and 3 were observed to be more accurate compared to picks from Scales 1 and 4.
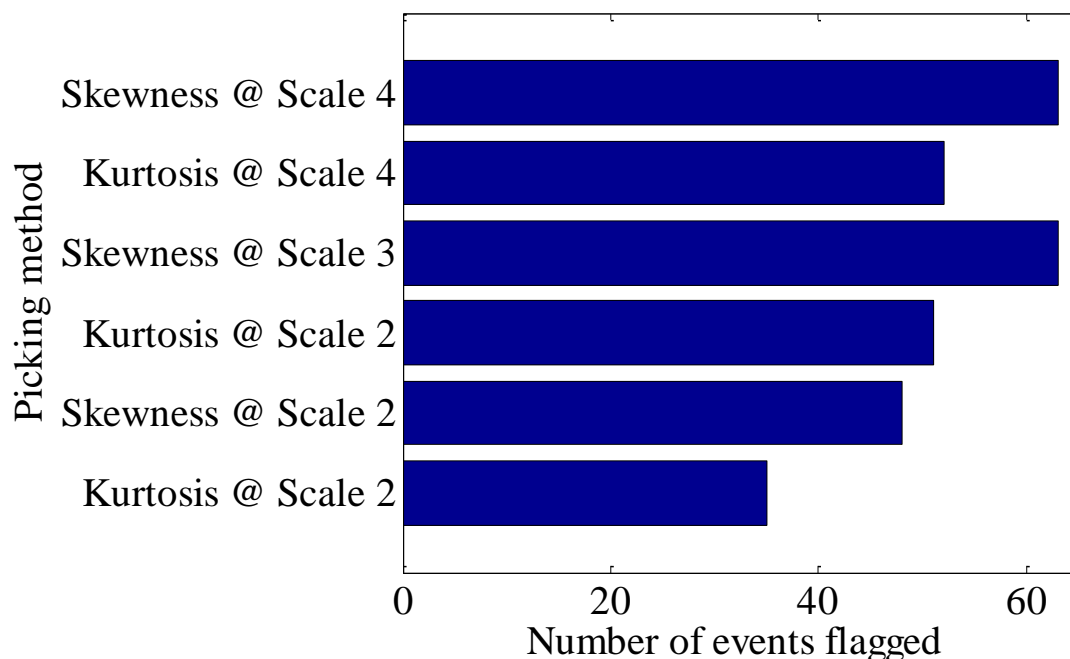
Figure 4.33 Summary of arrival-time difference picks for Event 1

SUMMARY

In this section, the proposed automatic picking algorithm was tested using three AE/MS events obtained from a dataset acquired at the Qianqiu Coal Mine, located at Yima County, Sanmenxia City, and Henan Province of China. The three events used were selected based on their exhibition of different noise levels, which highlighted the fundamental foundation of this research.

The first test performed involved the effect of wavelet function on the reliability of the picking accuracy of the automatic picker. The results showed that wavelet functions had influence on picking accuracy. The impact may be considered minimal; however, different wavelet functions resulted in the picking of different P-wave phase onset arrivals.

However, of the different types of wavelet functions tested, Db5 and Sym5 provided the most reliable results. The Db5 wavelet function was used as the wavelet of choice because it performed slightly better than Sym5.

The second test involved the automatic picking of phase arrivals using the slope of skewness and kurtosis across different scales of the filtered data. The automatic picking across the different scales showed that the wavelet coefficients provided a region of a P-wave phase arrival onset and not the exact position of the onset. It was observed, however, that the picking accuracy was more reliable on Scales 2 and 3 than on Scales 1 and 4. A frequency content analysis was performed to understand the possible cause of these phenomena. The results showed that Scale 1 is generally dominated by high frequency noises, making it difficult to distinguish the noise from the signal of interest. On the other hand, Scale 4 was associated with very low frequency content, which may be associated with later arrivals instead of the event onset.

The third test involved assessing the impact of window size on automatic picking of the P-wave phase onset arrivals. The results showed that, window size has a great influence on the accuracy of the P-wave phase onset time picks. The impact of window size on picking accuracy is observed across all the four scales. A more accurate result was obtained when the window size was adapted to the method proposed by Küperkoch et al. [50]. The results obtained in this sensitivity analysis showed that the picking accuracy of the P-wave phase onset arrival is indeed greatly dependent on the CF as stated by Allen [27].

Next was the assessment of the accuracy of P-wave phase onset picking based on the maximum kurtosis and skewness methods. The results showed that, the P-wave phase onset time picking based these methods turn to be after the actual phase onset. This behavior could be attributed to the fact that, the values of skewness and kurtosis turn to zero or close to zero for noise, but as the sliding window reaches the P-wave phase onset arrival, the values increases, reaching maximum values only when significant portions of the window contains the AE/MS event. Hence, using the maximum values of kurtosis and skewness for the P-wave phase onset arrival picking, could lead to significant errors in the determination of the source location of AE/MS events. Due to these deficiencies, in this

study, the P-wave phase onset determination is performed using the slope of kurtosis and skewness.

In the final test, phase associations of the arrival picks were performed across sixteen channels. For this test, the observed arrival-time difference table was constructed for each scale. The results were then compared with theoretical limits for a P-wave phase onset to validate the results from the automatic picks. The results showed that approximately 85% of cases had an observed arrival time difference less than the theoretical limit. Generally, the results showed that the P-wave phase onsets picked by the automatic picker were reliable and could be accurately used to determine the location of the source of those events.

5. SIMULATION RESULTS AND DISCUSSIONS

This section contains the results of two experimentation exercises using datasets from a coal mine and a laboratory test on 3-D concrete material. These experiments were performed to test the reliability of the newly proposed automatic picking algorithm. In these experiments, the datasets were first filtered using the SDWT algorithm to enhance the SNR of the signals. The picking algorithms based on the slope of skewness and kurtosis were then applied to pick the P-wave phase onset times. Using the arrival picks for each event and the coordinates of the transducers used in acquiring the data, a phase association was then performed to validate the accuracy and reliability of the picks. The results of the various tests are discussed below.

▉ APPLICATION OF THE ALGORITHM: CASE 1

To further illustrate the viability and efficiency of the automatic picker, the algorithm was first tested on a set of 43 AE/MS events obtained from a dataset acquired at the Qianqiu coal mine, located at Yima County in the city of Sanmenxia. The city of Sanmenxia is found in the Henan Province of China. The mine location is shown in Figure 5.1.

Figure 5.1 Location of the Qianqiu coal mine [113]

The Qianqiu coal mine was founded in 1956 and put into production in 1958. The production capacity of the mine is 2.1 million tons/year. The primary coal layer being mined is the coal seams 2-1. The angle of dip for these seams ranges from 3° to 13°. The general range of thickness is from 1.25 to 4.85 m, with an average thickness of 3.9 m. Most of the coal in these seams is exploitable. The immediate roof of the coal seams is composed of a 24 m thick mudstone. It has a homogeneous and dense lithology with undeveloped fissures. On the other hand, the main roof is multi-faceted, consisting of conglomerate, siltstone, mudstone, and clay rock. Shown in Figure 5.2 is the geological histogram of the mine [113].
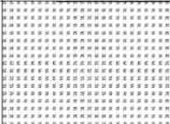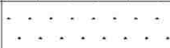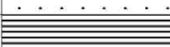
Lithology	Bore Illustrations		Thickness
Clay			120
Glutenite			100
Conglomerate			400
Siltstone			100
Mudstone			1.5
1-2 Coal seam			0.98
Siltstone			0.5
Mudstone			24
2-1 Coal seam			10
Conglomerate			8
Mudstone			>180

Figure 5.2 Geological histogram of the Qianqiu coal mine [113]

The 21,141 working face and the 21,121 goafs are situated in the west wing of mining area 21 and in the northern side of the face, respectively. The 21,161 virgin fields

are located in the southern side. The working face has a strike of length 15,000 m. The length of the slope, average seam thickness, and dip of the face are 130 m, 10.6 m, and 12° to 14° respectively. A diagram representing the working face is shown in Figure 5.3. The average thickness of the immediate roof of the working face consists of dark gray mudstone. The main roof has a thickness of 612 m and consists of mottled sand, conglomerates, and sandstone. The presence of the thick gravel roof provides an avenue for the accumulation of elastic energy. A sudden release of this energy during mining will lead to a coal bump or rockburst [113].
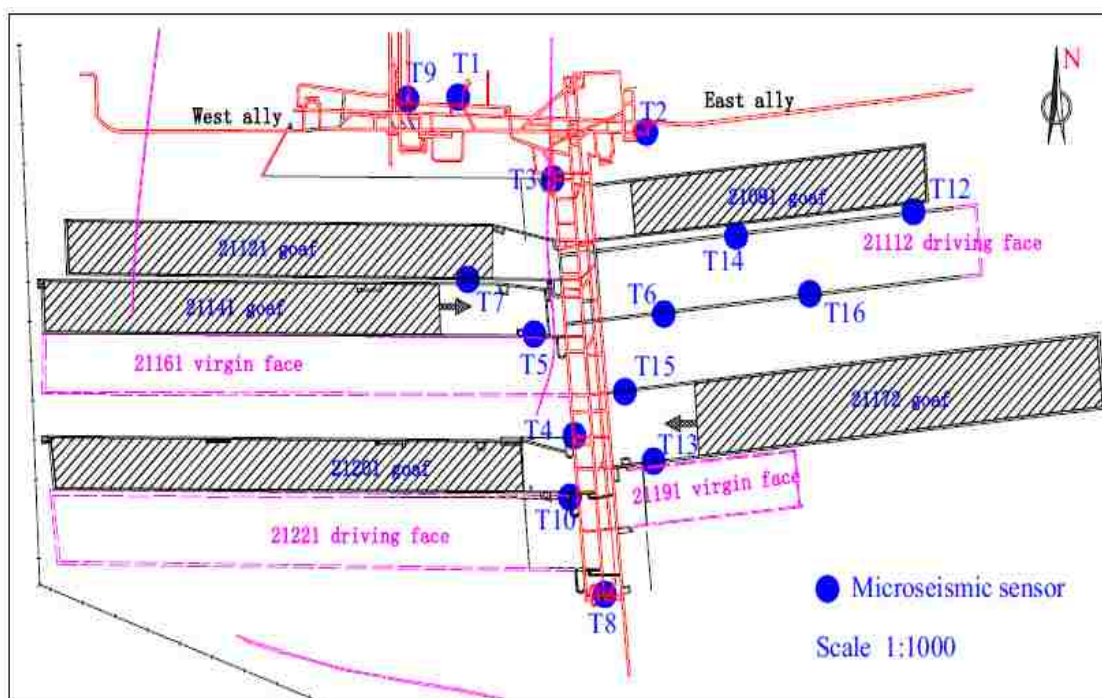
Figure 5.3 Mine working face and layout of AE/MS monitoring system [113]

Since the beginning of 2008, there have been more than 50-recorded accidents. Since the mining depth and mining intensity at the Qianqiu coal mine have been increasing, rockbursts and coal bumps have become important safety issues. It is expected that the impact of ground pressure and mine rock will become the main disaster of future coal mine production safety. Indeed, the impact of ground pressure, mine monitoring and forecasting, has become a major issue of health and development at the Qianqiu coal mine. Motivated

by the issues of health and safety, the mine installed an AE/MS monitoring system (Figure 5.3). The acquisition system has a sampling frequency of 500 Hz. The P-wave velocity range for the mine is from 3,800 to 4,500 m/s, which was calculated from the field-blasting source locating experiment. The average value of the measured wave velocity is 4,000 m/s [114].

5.1.1. Picking Results and Discussions. The algorithm was successfully applied to the 43 AE/MS event data acquired from the Qianqiu Coal Mine. Each AE/MS event signal was decomposed using the Db5 wavelet function. As was demonstrated in Section 4, Scales 2 to 4 of the wavelet decomposition provided the most reliable picks and are the scales used in this section (Table 5.1). For each event and for each case, the P-wave arrival phase onsets are picked based on the slopes of skewness and kurtosis. It was observed that for cases in which the phase onset is clear and the signal is not contaminated by much noise, both methods performed equally well (e.g., Event 1). However, a critical look at the overall performance of both picking methods showed that the kurtosis-based picker provided picks that were more reliable compared to the skewness-based method. A detailed analysis of the results showed that the more reliable picks were obtained on Scale 2. The percentage of reliable picks on Scale 2 for the 43 events was approximately 82%. The least number of accurately picked events (5%) were obtained on Scale 4 while 15% were correctly picked on Scale 3.

Figure 5.4 shows a residual plot of automatic and manual picks based on the kurtosis-picking algorithm. The residuals were obtained by a comparison of the automatic picks with the manual picks. Generally, manual picks by an analyst are found to be more reliable and therefore provides a qualitative evaluation of the performance of the algorithm. In addition, Figure 5.4 illustrates that the kurtosis-based algorithm was able to accurately pick 84% of the events with picking errors of less than 6 ms. These picking residuals are indicated by the two horizontal red lines. On the other hand, approximately 7% of the picks produced picking errors of above 10 ms, while 9% resulted in picking errors between 7 and 9 ms. Overall, the kurtosis-based algorithm was found to have reliably predicted about 93% of the considered events.
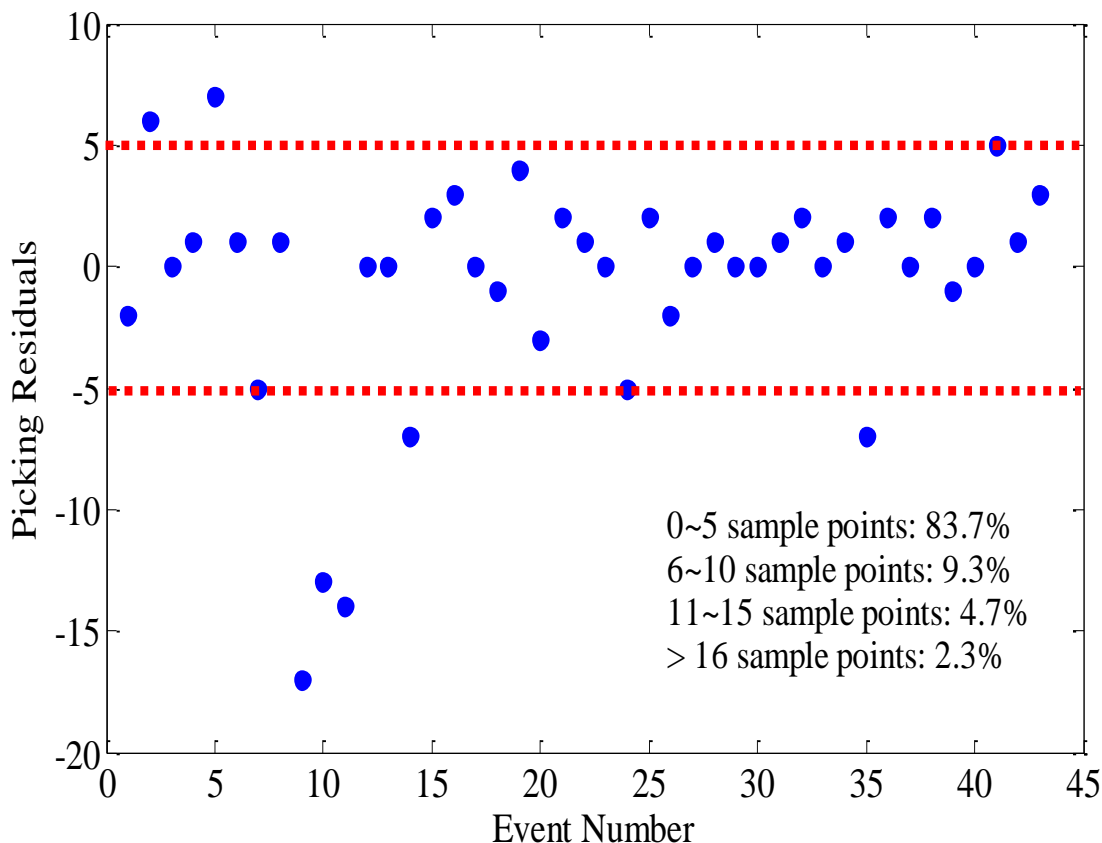
Figure 5.4 Residuals of automatic picks based on the kurtosis-picking algorithm and manual picks

5.1.2. Accuracy Comparison. The efficiency of the new picking algorithm was also tested by comparing its performance with some selected pickers. These pickers are the STA/LTA picker, the Baer and Kradolfer picker, the MER picker, and the S/L-Kurt picker. To evaluate the performance of the proposed picker in comparison to these pickers, 14 AE/MS events exhibiting different characteristics were randomly selected from the dataset from the Qianqiu Coal Mine (Table 5.2).

The specific characteristics of each event are provided in the comment section in Table 5.2. Generally, seven of the events had clear a P-wave phase onset, while the other seven had the P-wave phase onset partly masked by various degrees of noise. Table 5.3 provides the residual results obtained between each of these pickers and the manual picks.

Table 5.1 Automatic arrival picks based on kurtosis and skewness for scales 2, 3, and 4

Event No.	Scale # 2		Scale # 3		Scale # 4	
	Kurtosis	Skewness	Kurtosis	Skewness	Kurtosis	Skewness
1	512	576	576	576	640	640
2	585	585	585	630	630	765
3	539	539	637	686	735	686
4	576	576	576	640	768	832
5	576	704	704	704	768	832
6	552	576	576	704	640	640
7	572	576	640	704	704	704
8	520	64	640	704	704	704
9	512	512	704	256	704	704
10	542	566	640	640	704	768
11	512	64	576	704	704	704
12	704	640	704	768	768	832
13	576	640	640	832	704	896
14	512	512	576	64	704	192
15	517	517	576	128	704	768
16	512	512	576	576	640	640
17	582	576	512	576	640	576
18	512	512	576	0	704	768
19	502	128	640	0	704	704
20	576	0	640	640	704	640
21	640	640	640	64	768	64
22	576	64	704	768	704	704
23	64	128	704	640	768	832
24	512	512	576	128	768	768
25	576	320	640	0	64	0
26	512	640	640	704	704	768
27	768	832	768	832	832	1024
28	766	192	896	64	64	1024
29	512	576	704	704	768	832
30	512	576	576	0	768	0
31	640	704	704	64	832	0
32	512	512	576	704	640	640
33	512	576	512	576	768	0
34	576	448	640	0	768	768
35	512	576	576	640	640	640
36	511	192	576	640	640	704
37	448	0	704	0	768	0
38	576	64	640	704	768	768
39	592	576	576	640	704	768
40	519	512	704	512	704	704
41	576	576	640	640	704	768
42	704	576	1088	0	832	0

Table 5.2 Algorithms performance evaluation

Event No.	Manual Picking	Proposed Picker	STA/LTA Picker	Baer and Kradolfer Picker	MER Picker	S/L-Kurt Picker	General comments on signal characteristics
1	576	576/576	579	577	577	576	Clear P-wave arrival
2	477	585/585	602	588	591	586	P-wave arrival masked by high-frequency noise (HFN) and spikes
3	536	539/539	548	539	541	539	P-wave arrival masked by HFN and spikes
4	600	600/600	600	600	600	600	Clear P-wave arrival with heavy tails
5	567	560/560	523	558	558	559	P-wave onset masked by HFN
6	571	576/576	584	577	580	577	Clear P-wave arrival
7	560	565/565	567	566	566	565	Clear P-wave arrival with spikes
8	551	553/556	554	554	554	553	Clear P-wave arrival
9	566	590/591	601	591	595	590	P-wave onset masked by HFN
10	554	567/567	535	568	569	568	P-wave onset masked by HFN
11	582	586/589	570	587	588	586	P-wave onset masked by HFN
12	490	502/509	522	512	512	503	Clear P-wave arrival with spikes
13	660	660/660	660	660	660	660	Clear P-wave arrival
14	560	567/567	570	568	569	567	P-wave onset masked by HFN

The results in Table 5.2 and Table 5.3 show that for cases in which the P-wave phase onset is clear, all the pickers performed excellently when compared to the manual picks. For such cases, the resulting residuals were very small (Table 5.3). Classical examples include Events 1, 4, and 13, as shown in Table 5.3. However, for instances where the phase onset was masked by noise, the STA/LTA picker was observed to provide the least accurate results (example Events 2, 3, 9-12, and 14). These cases are highlighted by the high residuals in Table 5.3. On the other hand, the methods based on statistics (the proposed picker, the S/L-Kurt picker, Baer and Kradolfer Picker) provided results that were very close to the manual picks with, typical examples being Events 3 and 11. Although these signals had high-frequency noise, the residuals obtained between the pickers and the manual picks were very small compared to that between the STA/LTA picker and the manual picks. Based on the data used and the trends in Tables 5.2 and 5.3, it was observed that pickers based on statistical analysis provide reliable results in cases where the signal was masked by high noise levels. In addition, the results in Table 5.3 show that, for high noise level cases, the kurtosis-based picker performed better than the skewness-based picker. Typical cases include Events 9, 11, and 12, as shown by the residuals in Table 5.3.

Table 5.3 Residuals of automatic and manual picks

Event No.	Proposed Picker		STA/LTA Picker	Baer and Kradolfer Picker	MER Picker	S/L-Kurt Picker
	Kurtosis	Skewness				
1	0	0	3	1	1	0
2	108	108	125	111	114	109
3	3	3	12	3	5	3
4	0	0	0	0	0	0
5	7	7	44	9	9	8
6	5	5	13	6	9	6
7	5	5	7	6	6	5
8	2	5	3	3	3	2
9	24	25	35	25	29	24
10	13	13	19	14	15	14
11	4	7	12	5	6	4
12	12	19	32	22	22	13
13	0	0	0	0	0	0
14	7	7	10	8	9	7

■ APPLICATION OF ALGORITHM: CASE 2

To further test the reliability of the proposed picking algorithm, the algorithm was used to pick the P-wave onset on a dataset acquired during an experiment to determine the impact location of a three-dimensional structure. The experimentation was performed at the Smart Materials and Structure Laboratory at the Mechanical Engineering Department of the University of Houston. In total, 10 tests were performed at different locations, resulting in the acquisition of 100 events.

The experimental setup involved the creation of a model concrete pile with eight smart aggregates. The model concrete pile consisted of a commercial concrete mix with a diameter of 250 mm and height of 324 mm (Figure 5.5). Eight smart aggregates ($\varnothing 25.4 \times 20$ mm) were embedded in the concrete pile to measure the impact of excited P-waves. The coordinates of these sensors are provided in Table 5.4.

An NI PXI-5105 Digitizer was used as the data acquisition system (DAQ). The DAQ was triggered by the voltage signal of the designated smart aggregate, which was close to the impact location. The trigger level was set at 0.1 volts, and all the signals from the eight smart aggregates were recorded simultaneously at a sampling rate of 2 MS/s.

Figures 5.6 to 5.9 show one of the events recorded by the different sensors. Also shown in each figure are the manual arrival picks as indicated by the red vertical lines. On the other hand, Table 5.5 provides the arrival time picks for the event shown in Figures 5.6 to 5.9 for the eight sensors across Scales 2, 3, and 4. From Table 5.5, it was observed that the picks obtained by the kurtosis-based picking algorithm were more reliable compared to picks obtained from the skewness-based algorithm. This point is better illustrated by the table of residuals between each of the picking methods and the picks obtained manually (Table 5.6). In Table 5.6, a negative residual value indicates the automatic pick exceeded the manual picks by that amount of sample points. A positive value of residual indicates the picking algorithm underestimated the pick by that value of data points. Also, the results in Table 5.6 show that the kurtosis-based algorithm outperformed the skewness-based algorithm across all scales.

Figure 5.5 Model concrete pile submerged in water

Table 5.4 Location of smart aggregates in concrete pile

PZT sensor	Location of the center of the smart aggregate in 3-D
Sensor #1	(0, 76.2, 101.6)
Sensor #2	(0, 76.2, 254)
Sensor #3	(-76.2, 0, 101.6)
Sensor #4	(-76.2, 0, 254)
Sensor #5	(0, -76.2, 101.6)
Sensor #6	(0, -76.2, 254)
Sensor #7	(76.2, 0, 101.6)
Sensor #8	(76.2, 0, 254)

Table 5.5 Kurtosis and skewness based automatic arrival picks for scales 2, 3, and 4

Sensor #	Scale # 2		Scale # 3		Scale # 4	
	Skew-based picker	Kurt-based picker	Skew-based picker	Kurt-based picker	Skew-based picker	Kurt-based picker
1	4864	4840	4856	4848	4880	4864
2	5360	5360	5384	4936	5400	4952
3	5024	4920	4944	4912	4968	4912
4	5104	5000	5096	5000	5048	5024
5	5072	5072	5088	4920	5104	4944
6	5120	5024	5128	5024	5152	4960
7	5024	4981	5040	4986	5064	4952
8	5704	5000	5080	5008	5056	4968

Table 5.6 Picking residuals between manual and automatic picks

Sensor #	Scale # 2		Scale # 3		Scale # 4	
	Skew-based picker	Kurt-based picker	Skew-based picker	Kurt-based picker	Skew-based picker	Kurt-based picker
1	-32	-8	-24	-16	-48	-32
2	-3	3	-6	3	-65	-13
3	-122	-18	-42	-10	-66	-10
4	-85	19	-77	19	-29	-5
5	-83	-83	-99	69	-115	45
6	-137	-41	-145	-41	-169	23
7	-28	15	-44	10	-68	44
8	-690	14	-66	6	-42	46

An analysis of the complete dataset showed that the kurtosis-based algorithm reliably predicted 81% the P-wave onset time correctly compared to 69% by the skewness-based algorithm. In addition, approximately 78% of these events were correctly predicted on Scales 2 and 3. Seventy-five percent of the total picks that were considered reliable had arrival time pick errors of 3 to 10 sample points compared to the manual picks. This translates into arrival time errors between 0.00002 and 0.0001 s. These errors will have

little impact on the accuracy of source location if these arrival picks are used for such purposes. On the other hand, 54% of the wrongly picked arrival times were obtained on Scale 4.
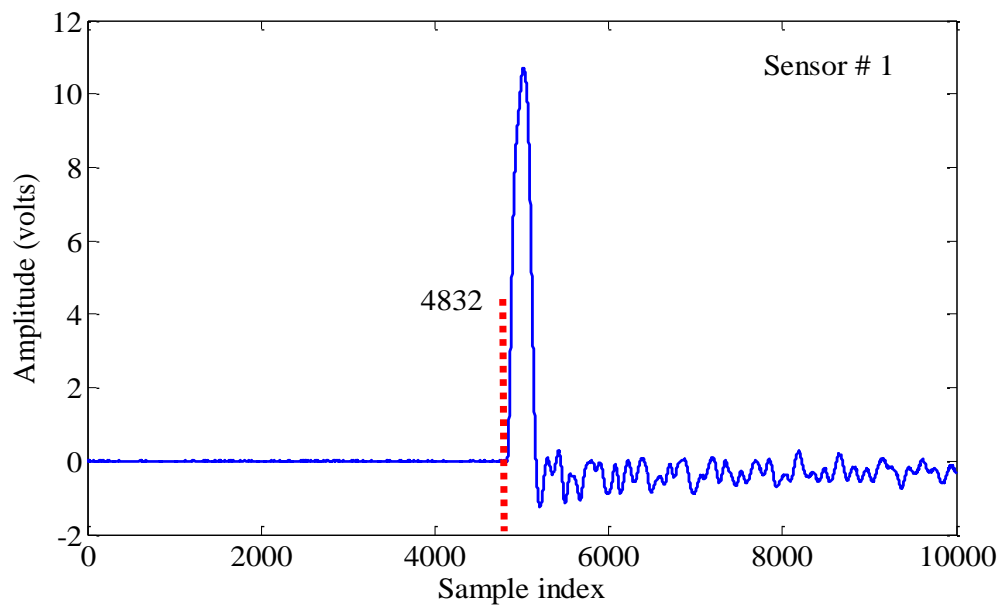
(a)
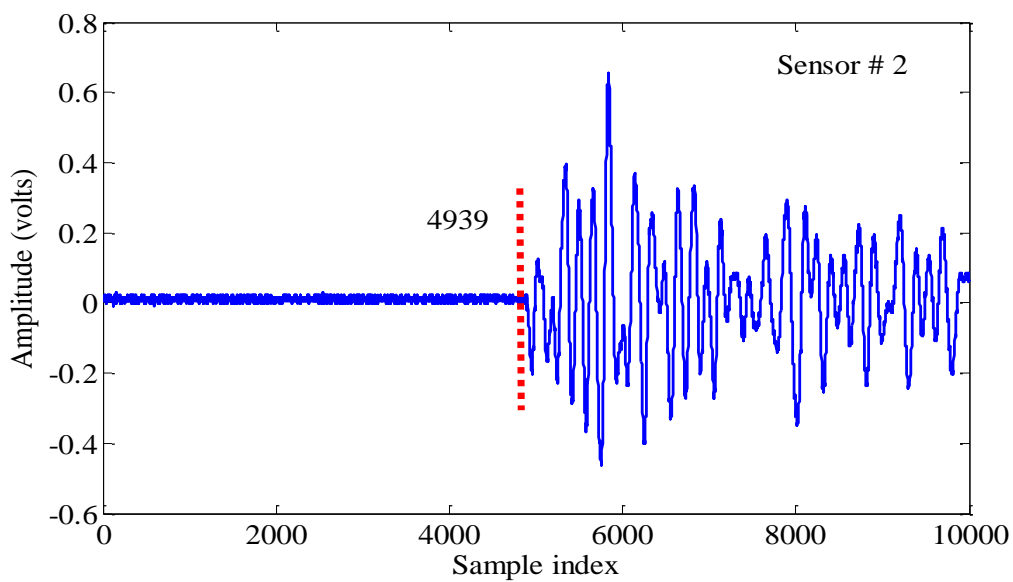
(b)

Figure 5.6 A sample event as recorded by (a) sensor 1 and (b) sensor 2
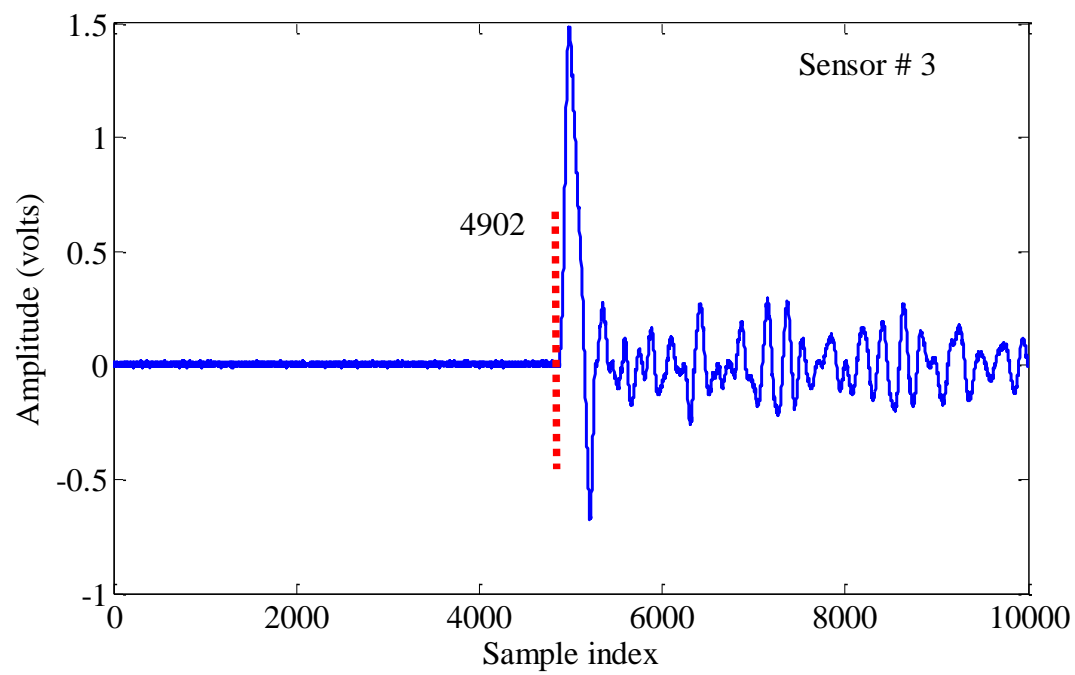
(a)
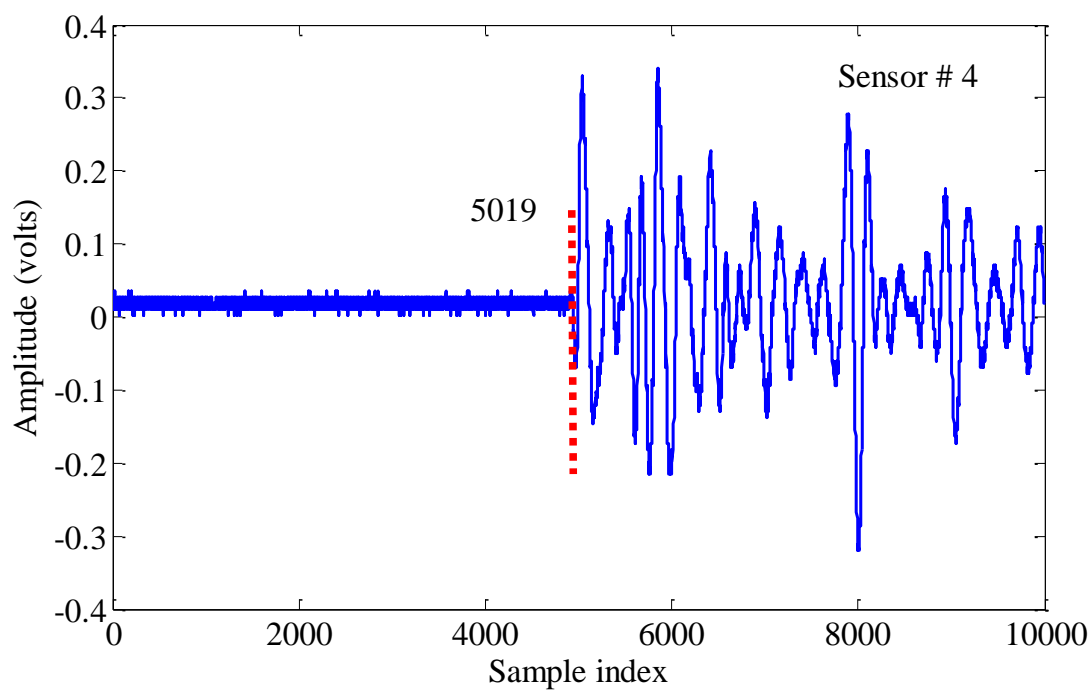
(b)

Figure 5.7 A sample event as recorded by (a) sensor 3 and (b) sensor 4
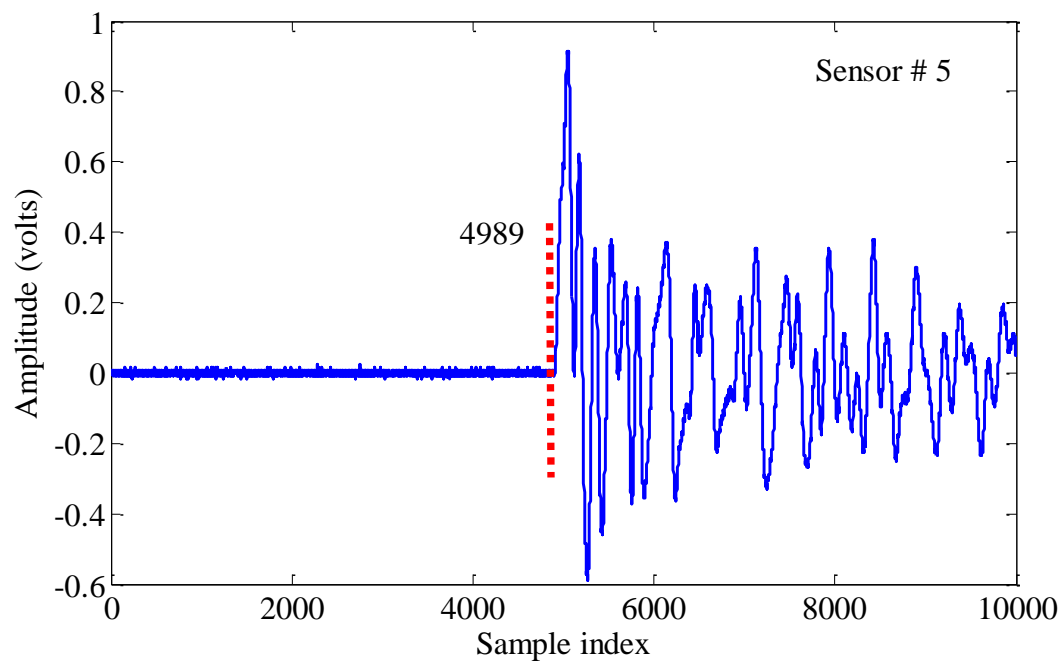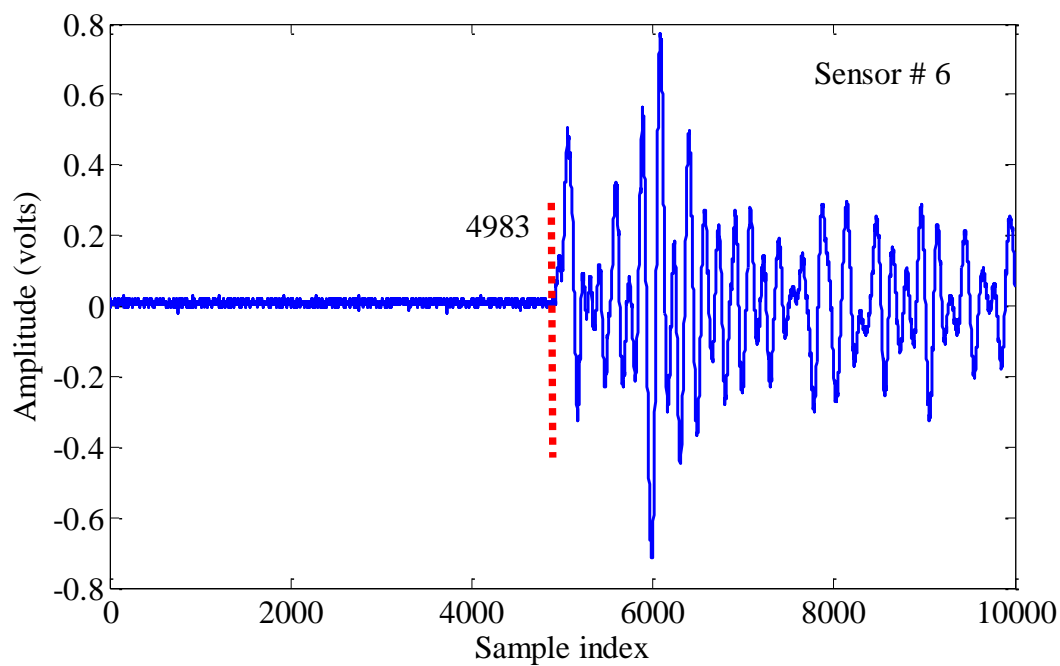
Figure 5.8 A sample event as recorded by (a) sensor 5 and (b) sensor 6
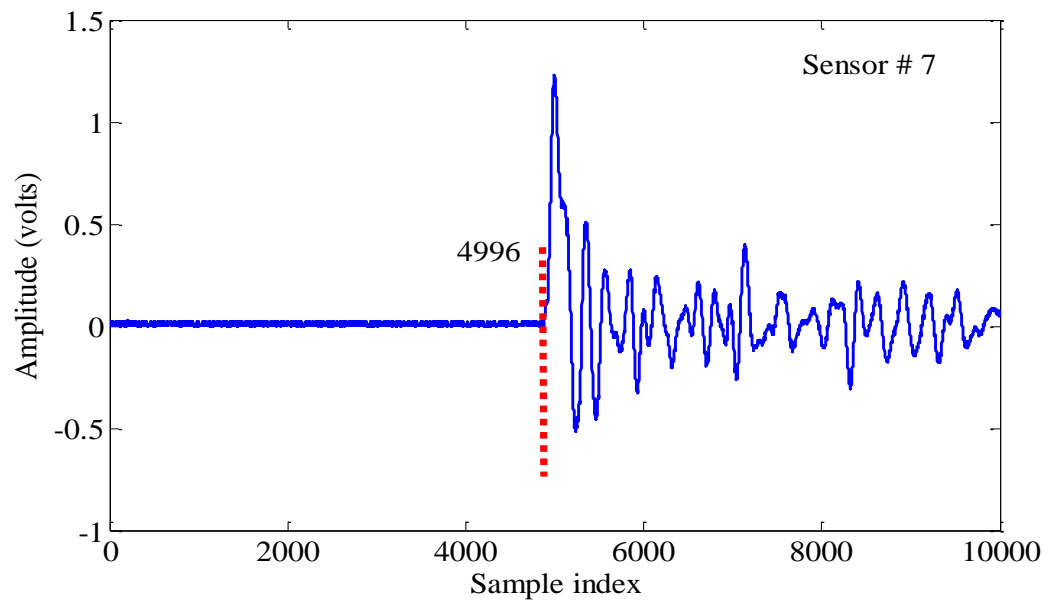
(a)
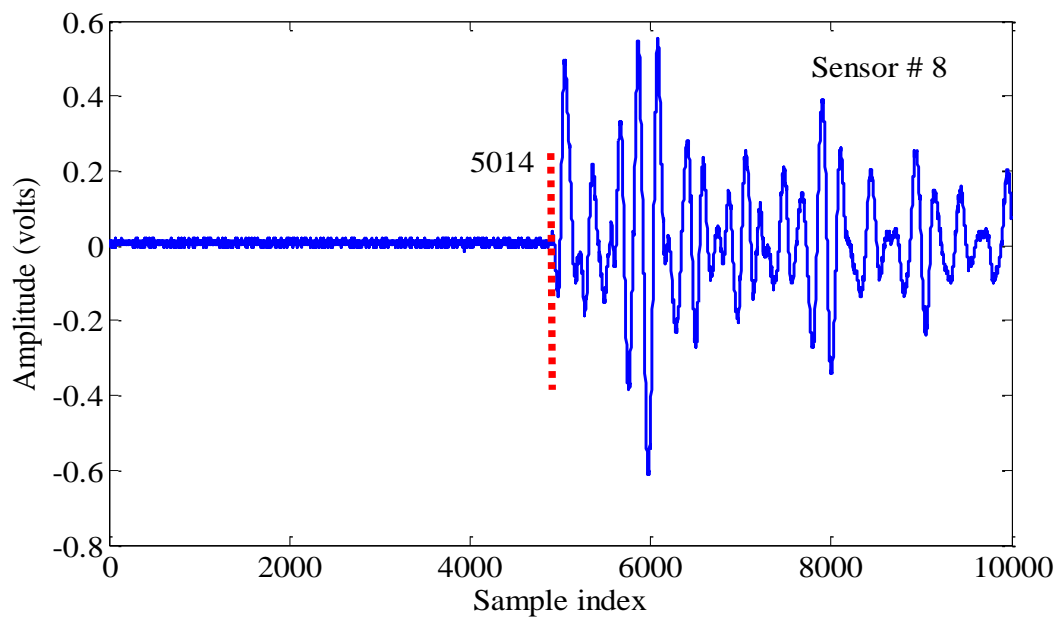
(b)

Figure 5.9 A sample event as recorded by (a) sensor 7 and (b) sensor 8

SUMMARY

In this section, the results of two experimentation exercises are presented using datasets from a coal mine and a laboratory test on a 3-D concrete material. An analysis of

the simulation results indicated that while the proposed picking algorithms for both skewness-based and kurtosis-based provided picking results within reasonable margins of error, the picks obtained by the kurtosis method were generally more accurate. For cases where there is less masking of the signal by noise, both methods achieved very accurate results with residuals between zero and three sample points (Table 5.3).

The study in the section also demonstrated that the wavelet components are capable of providing an estimation of the P-wave onset time across the different scales. However, the accuracy of these arrival picks can differ remarkably from scale to scale depending on the level of contamination of the signal by noise. Also, the main frequency for each scale is dependent on the signal sampling frequency. Therefore, for a given sampling frequency, the frequency band for each scale is confirmed [103]. However, due to issues of transformation of the original waveform by digitization, the accuracy of the arrival time picks across the different wavelet scales can be impacted. Consequently, by taking advantage of the phase association theory, the picking method proposed in this study enhanced the accuracy and reliability of P-wave phase onset picking.

The performance of the proposed algorithm has also been compared with the STA/LTA picker, the Baer and Kradolfer picker, the MER picker, and the S/L-kurt picker (Table 5.1 and Table 5.2). Generally, the proposed picker, the Baer and Kradolfer picker, the MER picker, and the S/L-kurt picker all outperformed the STA/LTA picker. However, for cases where the signal had less noise level, all the picking algorithms produced reliable results. On the other hand, for cases with high noise levels, the methods based on kurtosis (proposed kurtosis-based picker and S/L-kurt) were observed to be much more efficient compared to the other methods. In conclusion, it was observed that the use of the wavelet filter (SDWT) greatly improved the quality of the signal, especially if the data was highly corrupted by noise. Decomposing the signal over several scales provided an effective means to separate noise from the actual signal, thereby improving the picking accuracy. Also, the use of the phase association theory ensured elimination of picks that may have been triggered by arrivals other than the P-wave phase. This provided a more reliable means for assessing the quality of the phases picked.

6. SUMMARY, CONCLUSIONS, AND RECOMMENDATIONS

■ SUMMARY

Practically, event source location remains the most valuable feature of the AE/MS technique due to its ability to delineate the unstable areas of the monitored system. The accuracy and stability of the source location depends on many factors. If the reliable source location is to be achieved, then the quality of data used in the determination of the phase arrival remains one of the most important factors [1, 3, 4]. From a source location point of view, signal processing is comprised of two interrelated tasks: a rapid extraction of AE/MS events from the recorded data and the accurate timing of arrivals of the signals defining each event. The final goal is to provide a set of arrival times that can be used directly for the source location. Despite the fact that event extraction and timing are the first steps and also the foundation for signal processing, there is no efficient method for processing AE/MS data. The processes of extracting event arrivals have generally been performed by human analysts in this field.

In cases where automation had been employed, the widely used technique had been based on the simple amplitude-threshold signal detection method. In this technique, separation of the signal of interest ("useful" signal) from background noise ("useless" signal) is achieved by comparing the AE/MS amplitude with a predetermined threshold level. For cases where the signal to SNR is high, the technique has been found to be effective [5]. A major drawback with this method is the arbitrariness of the threshold choice, which could lead to errors in the accuracies of the AE/MS source location. If the AE/MS data is acquired in a noisy environment, the data can be severely affected by excessive background noise leading to low SNRs. This situation makes the automatic identification of phase arrival of incoming signals a major challenge in signal processing [3]. Thus, any effort toward improving the accuracy and reliability of seismic event phase extraction and timing must focus on these areas.

The reasons for the urgent need of automated systems have long been emphasized by Stewart [24]. A number of algorithms have been proposed for seismic event detection and picking of P- and S-waves onset time in the field of seismology and petroleum engineering [5, 25-34]. In the mining environment, however, little can be said in terms of

automation with regard to AE/MS event detection and arrival-time picking. In this research study, a new method was developed to resolve the problems of background noise and outburst activities characteristic of AE/MS data. The proposed method is a hybrid technique that encompasses four recent and sophisticated techniques, including the characteristic function, high order statistics, wavelet analysis, and a phase association theory. The information gained from this study will lead to a reduction of the human input and the time required for data processing and analysis in this modern world of digital data. It will also help promote health and safety in surface and underground mining, as well as the mechanical, electrical, civil, and geological engineering industries.

CONCLUSIONS

An extensive review of the literature relevant to the processes of improving and enhancing data quality, event phase arrival detection, and picking aimed at evaluating the contributions and limitations of the previous and current body of knowledge was carried out. While the traditional Fourier transform was identified as the main tool for frequency domain analysis, the STFT and the WT were identified as primary tools for time-frequency domain analysis. However, the reviewed literature showed that the STFT is fixed in time for any given window and is therefore not suitable for some applications. The WT, on the other hand, was found to be very reliable for time-frequency localization analysis of nonstationary signals such as AE/MS signals. The literature review also showed that most of the automatic phase arrival detection and picking algorithms available were developed for processing seismic data in the field of seismology. With various modifications, many of these algorithms are now being adopted for the processing of AE/MS data. In spite of the presence of these numerous algorithms, accurately detecting and picking phase arrival times on AE/MS data remains a major challenge. AE/MS data are generally characterized by low SNRs and complex waveforms, which makes automatic phase picking difficult. As was indicated by Sharma et al. [52], no arrival time picking algorithm is optimal under all conditions instead, they tend to become unstable under noisy conditions. Seismic event extraction with precise timing was identified as the most important step in AE/MS signal processing. Again, for cases where there was interference between the signals, the AE/MS signals themselves were found to present major challenges in processing. However, there

is no efficient method available in the literature that addresses these challenges. This realization makes the present research study relevant and critical in contributing to the knowledge bank of AE/MS signal processing.

Within the scope of this research, all the research objectives outlined in Section 1.3 have been achieved. The models for defining the CF, filtering AE/MS data, detecting and picking of P-wave phase arrivals, and correctly associating phases to wave types have been developed based on appropriate statistical and engineering principles. The CF model has been developed based on two HOS statistical parameters: skewness and kurtosis. The SDWT method has been developed as the model for AE/MS data filtering. Models based on the slopes of skewness and kurtosis over several scales of the SDWT filter have been developed for the identification and picking of P-wave phase onset arrivals, while theories on the theoretical limits of phase arrivals have been used to develop the models for phase association. These models have been combined in the C++ environment to develop an AE/MS data processing package.

Simulation trials have been used to determine optimal parameters for enhancing the accuracy and reliability of P-wave phase onset detection and picking. This optimization process involved the use of three AE/MS events with different SNRs. Wavelet function types, the SDWT decomposition scales, CF, window size, and proper phase association were identified as critical parameters required for accurate and reliable P-wave phase identification and picking. A combination of these parameters is capable of providing a good P-wave phase onset time and is considered critical for the optimal performance of the proposed picking algorithm.

From detailed mathematical formulation, numerical and simulation modeling, validation, and experimentation of the picking algorithm with AE/MS data from a coal mine and a 3-D concrete pile laboratory experiment, the following conclusions have been made:

1. The reliable detection and picking of P-wave phase onset are greatly improved, especially in cases where the SNR is low. For the AE/MS data from the coal mine, the kurtosis-based algorithm correctly picked 93% of P-wave phase arrivals, while the skewness-based algorithm, correctly picked 82% of the arrivals. The combined

effect was that the algorithm reliably picked 84% of all events with an error of less than 6 ms.

2. In the case of the 3-D concrete pile laboratory test, both the skewness-based and kurtosis-based algorithms correctly picked 69% and 81% of the P-wave onset arrival correctly. The signals in this case were less affected by the background noise and may have therefore contributed to the low percentages of correct picks.

3. Because of the phase association theory, phase arrival picks that were possibly triggered by S-wave, but were initially assumed to have been triggered by the P-wave, were identified, and classified for further investigation. This will lead to more confidence in the source location results when these arrival times are employed for such purposes.

4. Wavelet function type, the choice of the SDWT decomposition scales, CF, and the window size have been identified as having a great impact on the accuracy of the P-wave phase onset arrival picks.

5. The kurtosis-based picking algorithm provides more accurate picks compared to the skewness-based algorithm.

6. A comparative study with other algorithms showed that the algorithm outperformed the standard STA/LTA algorithm. Thus, the proposed algorithm is a good alternative to enhancing the processing of AE/MS data.

■ CONTRIBUTIONS OF PHD RESEARCH

This research advances and contributes to the body of knowledge on AE/MS signal processing and automatic picking of P-wave phase onset arrivals. The results from this work will go a long way to enhance the reliability of arrival picks and ensure an accurate location of events. In turn, this will provide critical information for planning and evaluating hazards associated with ground instability in mines. The following constitutes the major contribution of this research work:

1. The quality of data used for P-wave phase onset identification and picking was drastically improved by the utilization of the SDWT technique as a filter to remove background and culture noise characteristic of AE/MS data. Because the SDWT had no translation of the signal when decomposed compared to the DWT, no signal

information was lost. The resulting signal had the same length as the original signal, but with less noise present. This made both manual identification and automatic picking more efficient and reliable.

2. The introduction of the phase association theory, which was not present in previous algorithms, ensured noise due to the interference of outburst activities and late arrivals were not mistakenly classified as the first P-wave onset arrivals. The introduction of this ensured that the picks were correctly and accurately classified, thereby improving the reliability of the arrival pick times.

■ RECOMMENDATIONS

The body of knowledge in this research could significantly be improved in the following areas:

1. The algorithms have so far been tested and validated with two sets of data, from a coal mine and a lab test. Though the two datasets were acquired in different environments and with different noise levels, these datasets could not be considered adequate to replicate in all environments. Therefore, it is recommended that further studies be conducted using large datasets from multiple environments. For instance, monitoring conditions in an underground coal mine environment will be significantly different from that of a hard rock mine.

2. In order to make the algorithm a good candidate for online implementation, the run-time of the algorithm needs to be improved. Despite the efficiency of the SDWT algorithm in producing high-quality data, it is slow in its current form compared to the DWT algorithm. Future studies should interrogate how best the performance of the SDWT could be improved to make the algorithm a good online monitoring system.

APPENDIX A.

ARRIVAL-TIME DIFFERENCE TABLES

Table A1 Arrival time difference table of Event 1 for Scale 2 based on kurtosis picks (in seconds)

		Transducer No.															
		1	2	3	4	5	6	7	8	9	10	11	12	13	14	15	16
Transducer No.	1	0.00	0.00	0.13	0.13	0.13	0.00	0.13	0.00	1.02	0.00	1.02	0.13	0.26	0.00	0.13	0.00
		0.00	*0.30*	*0.30*	*0.46*	*0.30*	*0.48*	*0.38*	*0.74*	*0.13*	*0.60*	*0.53*	*0.71*	*0.61*	*0.50*	*0.50*	*0.63*
	2	0.00	0.00	0.13	0.13	0.13	0.00	0.13	0.00	1.02	0.00	1.02	0.13	0.26	0.00	0.13	0.00
		0.30	*0.00*	*0.20*	*0.35*	*0.31*	*0.25*	*0.34*	*0.61*	*0.40*	*0.48*	*0.70*	*0.41*	*0.43*	*0.21*	*0.35*	*0.34*
	3	0.13	0.13	0.00	0.00	0.00	0.13	0.00	0.13	0.89	0.13	0.89	0.26	0.38	0.13	0.26	0.13
		0.30	*0.20*	*0.00*	*0.18*	*0.12*	*0.21*	*0.14*	*0.45*	*0.43*	*0.32*	*0.80*	*0.52*	*0.31*	*0.28*	*0.20*	*0.39*
	4	0.13	0.13	0.00	0.00	0.00	0.13	0.00	0.13	0.89	0.13	0.89	0.26	0.38	0.13	0.26	0.13
		0.46	*0.35*	*0.18*	*0.00*	*0.18*	*0.20*	*0.10*	*0.28*	*0.59*	*0.14*	*0.97*	*0.54*	*0.16*	*0.32*	*0.07*	*0.38*
	5	0.13	0.13	0.00	0.00	0.00	0.13	0.00	0.13	0.89	0.13	0.89	0.26	0.38	0.13	0.26	0.13
		0.30	*0.31*	*0.12*	*0.18*	*0.00*	*0.30*	*0.08*	*0.44*	*0.43*	*0.30*	*0.83*	*0.63*	*0.34*	*0.39*	*0.23*	*0.49*
	6	0.00	0.00	0.13	0.13	0.13	0.00	0.13	0.00	1.02	0.00	1.02	0.13	0.26	0.00	0.13	0.00
		0.48	*0.25*	*0.21*	*0.20*	*0.30*	*0.00*	*0.26*	*0.39*	*0.61*	*0.28*	*0.94*	*0.35*	*0.20*	*0.13*	*0.15*	*0.19*
	7	0.13	0.13	0.00	0.00	0.00	0.13	0.00	0.13	0.89	0.13	0.89	0.26	0.38	0.13	0.26	0.13
		0.38	*0.34*	*0.14*	*0.10*	*0.08*	*0.26*	*0.00*	*0.36*	*0.51*	*0.23*	*0.90*	*0.61*	*0.27*	*0.37*	*0.16*	*0.45*
	8	0.00	0.00	0.13	0.13	0.13	0.00	0.13	0.00	1.02	0.00	1.02	0.13	0.26	0.00	0.13	0.00
		0.74	*0.61*	*0.45*	*0.28*	*0.44*	*0.39*	*0.36*	*0.00*	*0.87*	*0.14*	*1.25*	*0.66*	*0.19*	*0.50*	*0.26*	*0.50*
	9	1.02*	1.02*	0.89*	0.89*	0.89*	1.02*	0.89*	1.02*	0.00	1.02	0.00	1.15	1.28	1.02	1.15	1.02
		*0.13**	*0.40**	*0.43**	*0.59**	*0.43**	*0.61**	*0.51**	*0.87**	*0.00*	*0.73*	*0.40*	*0.80*	*0.74*	*0.61*	*0.63*	*0.74*
	10	0.00	0.00	0.13	0.13	0.13	0.00	0.13	0.00	1.02*	0.00	1.02	0.13	0.26	0.00	0.13	0.00
		0.60	*0.48*	*0.32*	*0.14*	*0.30*	*0.28*	*0.23*	*0.14*	*0.73**	*0.00*	*1.12*	*0.59*	*0.12*	*0.41*	*0.14*	*0.43*
	11	1.02*	1.02*	0.89*	0.89	0.89*	1.02*	0.89	1.02	0.00	1.02	0.00	1.15	1.28	1.02	1.15	1.02
		*0.53**	*0.70**	*0.80**	*0.97*	*0.83**	*0.94**	*0.90*	*1.25*	*0.40*	*1.12*	*0.00*	*1.03*	*1.10*	*0.90*	*1.00*	*1.02*
	12	0.13	0.13	0.26	0.26	0.26	0.13	0.26	0.13	1.15*	0.13	1.15*	0.00	0.13	0.13	0.00	0.13
		0.71	*0.41*	*0.52*	*0.54*	*0.63*	*0.35*	*0.61*	*0.66*	*0.80**	*0.59*	*1.03**	*0.00*	*0.48*	*0.24*	*0.49*	*0.17*

Table A1 Arrival time difference table of Event 1 for Scale 2 based on kurtosis picks (in seconds) continued

		Transducer No.															
		1	2	3	4	5	6	7	8	9	10	11	12	13	14	15	16
Transducer No.	13	0.26	0.26	0.38*	0.38*	0.38*	0.26*	0.38*	0.26*	1.28*	0.26*	1.28*	0.13	0.00	0.26	0.13	0.26
		0.61	0.43	0.31*	0.16*	0.34*	0.20*	0.27*	0.19*	0.74*	0.12*	1.10*	0.48	0.00	0.31	0.11	0.32
	14	0.00	0.00	0.13	0.13	0.13	0.00	0.13	0.00	1.02*	0.00	1.02*	0.13	0.26	0.00	0.13	0.00
		0.50	0.21	0.28	0.32	0.39	0.13	0.37	0.50	0.61*	0.41	0.90*	0.24	0.31	0.00	0.28	0.13
	15	0.13	0.13	0.26*	0.26*	0.26*	0.13	0.26*	0.13	1.15*	0.13	1.15*	0.00	0.13*	0.13	0.00	0.13
		0.50	0.35	0.20*	0.07*	0.23*	0.15	0.16*	0.26	0.63*	0.14	1.00*	0.49	0.11*	0.28	0.00	0.33
	16	0.00	0.00	0.13	0.13	0.13	0.00	0.13	0.00	1.02*	0.00	1.02**	0.13	0.26	0.00	0.13	0.00
		0.63	0.34	0.39	0.38	0.49	0.19	0.45	0.50	0.74*	0.43	1.02**	0.17	0.32	0.13	0.33	0.00

Table A2 Arrival time difference table of Event 1 for Scale 2 based on skewness picks (in seconds)

		Transducer No.															
		1	2	3	4	5	6	7	8	9	10	11	12	13	14	15	16
Transducer No.	1	0.00	0.00	0.00	0.26	0.13	0.13	0.26	0.13	0.90	0.26	1.15	0.13	1.02	0.13	0.00	0.13
		0.00	0.30	0.30	0.46	0.30	0.48	0.38	0.74	0.13	0.60	0.53	0.71	0.61	0.50	0.50	0.63
	2	0.00	0.00	0.00	0.26	0.13	0.13	0.26	0.13	0.90	0.26	1.15	0.13	1.02	0.13	0.00	0.13
		0.30	0.00	0.20	0.35	0.31	0.25	0.34	0.61	0.40	0.48	0.70	0.41	0.43	0.21	0.35	0.34
	3	0.00	0.00	0.00	0.26	0.13	0.13	0.26	0.13	0.90	0.26	1.15	0.13	1.02	0.13	0.00	0.13
		0.30	0.20	0.00	0.18	0.12	0.21	0.14	0.45	0.43	0.32	0.80	0.52	0.31	0.28	0.20	0.39
	4	0.26	0.26	0.26*	0.00	0.13	0.13	0.00	0.13	0.64	0.51	0.89	0.38	0.77	0.13	0.26	0.13
		0.46	0.35	0.18*	0.00	0.18	0.20	0.10	0.28	0.59	0.14	0.97	0.54	0.16	0.32	0.07	0.38
	5	0.13	0.13	0.13*	0.13	0.00	0.00	0.13	0.00	0.77	0.38	1.02	0.26	0.90	0.00	0.13	0.00
		0.30	0.31	0.12*	0.18	0.00	0.30	0.08	0.44	0.43	0.30	0.83	0.63	0.34	0.39	0.23	0.49
	6	0.13	0.13	0.13	0.13	0.00	0.00	0.13	0.00	0.77	0.38	1.02	0.26	0.90	0.00	0.13	0.00
		0.48	0.25	0.21	0.20	0.30	0.00	0.26	0.39	0.61	0.28	0.94	0.35	0.20	0.13	0.15	0.19

Table A2 Arrival time difference table of Event 1 for Scale 2 based on skewness picks (in seconds) continued

		Transducer No.														
		1	2	3	4	5	6	7	8	9	10	11	12	13	14	15	16
Transducer No.	7	0.26	0.26	0.26*	0.00	0.13*	0.13	0.00	0.13	0.64	0.51	0.89	0.38	0.77	0.13	0.26	0.13
		0.38	*0.34*	*0.14*￼*	*0.10*	*0.08*￼*	*0.26*	*0.00*	*0.36*	*0.51*	*0.23*	*0.90*	*0.61*	*0.27*	*0.37*	*0.16*	*0.45*
	8	0.13	0.13	0.13	0.13	0.00	0.00	0.13	0.00	0.77	0.38	1.02	0.26	0.90	0.00	0.13	0.00
		0.74	*0.61*	*0.45*	*0.28*	*0.44*	*0.39*	*0.36*	*0.00*	*0.87*	*0.14*	*1.25*	*0.66*	*0.19*	*0.50*	*0.26*	*0.50*
	9	0.90*	0.90*	0.90*	0.64*	0.77*	0.77*	0.64*	0.77	0.00	1.15	0.25	1.02	0.13	0.77	0.90	0.77
		0.13￼*	*0.40*￼*	*0.43*￼*	*0.59*￼*	*0.43*￼*	*0.61*￼*	*0.51*￼*	*0.87*	*0.00*	*0.73*	*0.40*	*0.80*	*0.74*	*0.61*	*0.63*	*0.74*
	10	0.26	0.26	0.26	0.51*	0.38*	0.38*	0.51*	0.38*	1.15*	0.00	1.41	0.13	1.28	0.38	0.26	0.38
		0.60	*0.48*	*0.32*	*0.14*￼*	*0.30*￼*	*0.28*￼*	*0.23*￼*	*0.14*￼*	*0.73*￼*	*0.00*	*1.12*	*0.59*	*0.12*	*0.41*	*0.14*	*0.43*
	11	1.15*	1.15*	1.15*	0.89	1.02*	1.02*	0.89	1.02	0.25	1.41*	0.00	1.28	0.13	1.02	1.15	1.02
		0.53￼*	*0.70*￼*	*0.80*￼*	*0.97*	*0.83*￼*	*0.94*￼*	*0.90*	*1.25*	*0.40*	*1.12*￼*	*0.00*	*1.03*	*1.10*	*0.90*	*1.00*	*1.02*
	12	0.13	0.13	0.13	0.38	0.26	0.26	0.38	0.26	1.02*	0.13	1.28*	0.00	1.15	0.26	0.13	0.26
		0.71	*0.41*	*0.52*	*0.54*	*0.63*	*0.35*	*0.61*	*0.66*	*0.80*￼*	*0.59*	*1.03*￼*	*0.00*	*0.48*	*0.24*	*0.49*	*0.17*
	13	1.02*	1.02*	1.02*	0.77*	0.90*	0.90*	0.77*	0.90*	0.13	1.28*	0.13	1.15*	0.00	0.90	1.02	0.90
		0.61￼*	*0.43*￼*	*0.31*￼*	*0.16*￼*	*0.34*￼*	*0.20*￼*	*0.27*￼*	*0.19*￼*	*0.74*	*0.12*￼*	*1.10*	*0.48*￼*	*0.00*	*0.31*	*0.11*	*0.32*
	14	0.13	0.13	0.13	0.13	0.00	0.00	0.13	0.00	0.77*	0.38	1.02*	0.26*	0.90*	0.00	0.13	0.00
		0.50	*0.21*	*0.28*	*0.32*	*0.39*	*0.13*	*0.37*	*0.50*	*0.61*￼*	*0.41*	*0.90*￼*	*0.24*￼*	*0.31*￼*	*0.00*	*0.28*	*0.13*
	15	0.00	0.00	0.00	0.26*	0.13	0.13	0.26*	0.13	0.90*	0.26*	1.15*	0.13	1.02*	0.13	0.00	0.13
		0.50	*0.35*	*0.20*	*0.07*￼*	*0.23*	*0.15*	*0.16*￼*	*0.26*	*0.63*￼*	*0.14*￼*	*1.00*￼*	*0.49*	*0.11*￼*	*0.28*	*0.00*	*0.33*
	16	0.13	0.13	0.13	0.13	0.00	0.00	0.13	0.00	0.77*	0.38	1.02**	0.26*	0.90*	0.00	0.13	0.00
		0.63	*0.34*	*0.39*	*0.38*	*0.49*	*0.19*	*0.45*	*0.50*	*0.74*￼*	*0.43*	*1.02**￼*	*0.17*￼*	*0.32*￼*	*0.13*	*0.33*	*0.00*

Table A3 Arrival time difference table of Event 1 for Scale 3 based on kurtosis picks (in seconds)

		1	2	3	4	5	6	7	8	9	10	11	12	13	14	15	16
								Transducer No.									
Transducer No.	1	0.00	0.13	0.13	0.13	0.26	0.00	0.26	0.00	1.15	0.00	1.15	0.13	0.26	0.00	0.00	0.38
		0.00	0.30	0.30	0.46	0.30	0.48	0.38	0.74	0.13	0.60	0.53	0.71	0.61	0.50	0.50	0.63
	2	0.13	0.00	0.26	0.26	0.38	0.13	0.38	0.13	1.28	0.13	1.28	0.00	0.13	0.13	0.13	0.26
		0.30	0.00	0.20	0.35	0.31	0.25	0.34	0.61	0.40	0.48	0.70	0.41	0.43	0.21	0.35	0.34
	3	0.13	0.26*	0.00	0.00	0.13	0.13	0.13	0.13	1.02	0.13	1.02	0.26	0.39	0.13	0.13	0.51
		0.30	0.20*	0.00	0.18	0.12	0.21	0.14	0.45	0.43	0.32	0.80	0.52	0.31	0.28	0.20	0.39
	4	0.13	0.26	0.00	0.00	0.13	0.13	0.13	0.13	1.02	0.13	1.02	0.26	0.39	0.13	0.13	0.51
		0.46	0.35	0.18	0.00	0.18	0.20	0.10	0.28	0.59	0.14	0.97	0.54	0.16	0.32	0.07	0.38
	5	0.26	0.38*	0.13*	0.13	0.00	0.26	0.00	0.26	0.89	0.26	0.89	0.38	0.51	0.26	0.26	0.64
		0.30	0.31*	0.12*	0.18	0.00	0.30	0.08	0.44	0.43	0.30	0.83	0.63	0.34	0.39	0.23	0.49
	6	0.00	0.13	0.13	0.13	0.26	0.00	0.26	0.00	1.15	0.00	1.15	0.13	0.26	0.00	0.00	0.38
		0.48	0.25	0.21	0.20	0.30	0.00	0.26	0.39	0.61	0.28	0.94	0.35	0.20	0.13	0.15	0.19
	7	0.26	0.38*	0.13	0.13*	0.00	0.26**	0.00	0.26	0.89	0.26	0.89	0.38	0.51	0.26	0.26	0.64
		0.38	0.34*	0.14	0.10*	0.08	0.26**	0.00	0.36	0.51	0.23	0.90	0.61	0.27	0.37	0.16	0.45
	8	0.00	0.13	0.13	0.13	0.26	0.00	0.26	0.00	1.15	0.00	1.15	0.13	0.26	0.00	0.00	0.38
		0.74	0.61	0.45	0.28	0.44	0.39	0.36	0.00	0.87	0.14	1.25	0.66	0.19	0.50	0.26	0.50
	9	1.15*	1.28*	1.02*	1.02*	0.89*	1.15*	0.89*	1.15*	0.00	1.15	0.00	1.28	1.41	1.15	1.15	1.53
		0.13*	0.40*	0.43*	0.59*	0.43*	0.61*	0.51*	0.87*	0.00	0.73	0.40	0.80	0.74	0.61	0.63	0.74
	10	0.00	0.13	0.13	0.13	0.26	0.00	0.26*	0.00	1.15*	0.00	1.15	0.13	0.26	0.00	0.00	0.38
		0.60	0.48	0.32	0.14	0.30	0.28	0.23*	0.14	0.73*	0.00	1.12	0.59	0.12	0.41	0.14	0.43
	11	1.15*	1.28*	1.02*	1.02*	0.89*	1.15*	0.89	1.15	0.00	1.15*	0.00	1.28	1.41	1.15	1.15	1.53
		0.53*	0.70*	0.80*	0.97*	0.83*	0.94*	0.90	1.25	0.40	1.12*	0.00	1.03	1.10	0.90	1.00	1.02
	12	0.13	0.00	0.26	0.26	0.38	0.13	0.38	0.13	1.2*8	0.13	1.28*	0.00	0.13	0.13	0.13	0.26
		0.71	0.41	0.52	0.54	0.63	0.35	0.61	0.66	0.80*	0.59	1.03*	0.00	0.48	0.24	0.49	0.17

Table A3 Arrival time difference table of Event 1 for Scale 3 based on kurtosis picks (in seconds) continued

							Transducer No.									
		1	2	3	4	5	6	7	8	9	10	11	12	13	14	15	16
Transducer No.	13	0.26	0.13	0.39*	0.39*	0.51*	0.26*	0.51*	0.26*	1.41*	0.26*	1.41*	0.13	0.00	0.26	0.26	0.13
		0.61	*0.43*	*0.31**	*0.16**	*0.34**	*0.20**	*0.27**	*0.19**	*0.74**	*0.12**	*1.10**	*0.48*	*0.00*	*0.31*	*0.11*	*0.32*
	14	0.00	0.13	0.13	0.13	0.26	0.00	0.26	0.00	1.15*	0.00	1.15*	0.13	0.26	0.00	0.00	0.38
		0.50	*0.21*	*0.28*	*0.32*	*0.39*	*0.13*	*0.37*	*0.50*	*0.61**	*0.41*	*0.90**	*0.24*	*0.31*	*0.00*	*0.28*	*0.13*
	15	0.00	0.13	0.13	0.13*	0.26*	0.00	0.26*	0.00	1.15*	0.00	1.15*	0.13	0.26*	0.00	0.00	0.38
		0.50	*0.35*	*0.20*	*0.07**	*0.23**	*0.15*	*0.16**	*0.26*	*0.63**	*0.14*	*1.00**	*0.49*	*0.11**	*0.28*	*0.00*	*0.33*
	16	0.38	0.26	0.51*	0.51*	0.64*	0.38*	0.64*	0.38	1.53*	0.38	1.53*	0.26*	0.13	0.38*	0.38*	0.00
		0.63	*0.34*	*0.39**	*0.38**	*0.49**	*0.19**	*0.45**	*0.50*	*0.74**	*0.43*	*1.02**	*0.17**	*0.32*	*0.13**	*0.33**	*0.00*

Table A4 Arrival time difference table of Event 1 for Scale 3 based on skewness picks (in seconds)

							Transducer No.									
		1	2	3	4	5	6	7	8	9	10	11	12	13	14	15	16
Transducer No.	1	0.00	0.38	0.00	0.00	0.00	0.00	0.13	0.26	1.02	0.26	1.02	0.26	0.90	0.13	0.26	0.51
		0.00	*0.30*	*0.30*	*0.46*	*0.30*	*0.48*	*0.38*	*0.74*	*0.13*	*0.60*	*0.53*	*0.71*	*0.61*	*0.50*	*0.50*	*0.63*
	2	0.38*	0.00	0.38	0.38	0.38	0.38	0.51	0.13	1.41	0.13	1.41	0.13	1.28	0.26	0.13	0.13
		*0.30**	*0.00*	*0.20*	*0.35*	*0.31*	*0.25*	*0.34*	*0.61*	*0.40*	*0.48*	*0.70*	*0.41*	*0.43*	*0.21*	*0.35*	*0.34*
	3	0.00	0.38*	0.00	0.00	0.00	0.00	0.13	0.26	1.02	0.26	1.02	0.26	0.90	0.13	0.26	0.51
		0.30	*0.20**	*0.00*	*0.18*	*0.12*	*0.21*	*0.14*	*0.45*	*0.43*	*0.32*	*0.80*	*0.52*	*0.31*	*0.28*	*0.20*	*0.39*
	4	0.00	0.38*	0.00	0.00	0.00	0.00	0.13	0.26	1.02	0.26	1.02	0.26	0.90	0.13	0.26	0.51
		0.46	*0.35**	*0.18*	*0.00*	*0.18*	*0.20*	*0.10*	*0.28*	*0.59*	*0.14*	*0.97*	*0.54*	*0.16*	*0.32*	*0.07*	*0.38*
	5	0.00	0.38*	0.00	0.00	0.00	0.00	0.13	0.26	1.02	0.26	1.02	0.26	0.90	0.13	0.26	0.51
		0.30	*0.31**	*0.12*	*0.18*	*0.00*	*0.30*	*0.08*	*0.44*	*0.43*	*0.30*	*0.83*	*0.63*	*0.34*	*0.39*	*0.23*	*0.49*
	6	0.00	0.38*	0.00	0.00	0.00	0.00	0.13	0.26	1.02	0.26	1.02	0.26	0.90	0.13	0.26	0.51
		0.48	*0.25**	*0.21*	*0.20*	*0.30*	*0.00*	*0.26*	*0.39*	*0.61*	*0.28*	*0.94*	*0.35*	*0.20*	*0.13*	*0.15*	*0.19*

Table A4 Arrival time difference table of Event 1 for Scale 3 based on skewness picks (in seconds) continued

		Transducer No.														
		1	2	3	4	5	6	7	8	9	10	11	12	13	14	15	16
7		0.13	0.51*	0.13	0.13*	0.13*	0.13	0.00	0.38	0.89	0.38	0.89	0.38	0.77	0.26	0.38	0.64
		0.38	0.34*	0.14	0.10*	0.08*	0.26	0.00	0.36	0.51	0.23	0.90	0.61	0.27	0.37	0.16	0.45
8		0.26	0.13	0.26	0.26	0.26	0.26	0.38*	0.00	1.28	0.00	1.28	0.00	1.15	0.13	0.00	0.26
		0.74	0.61	0.45	0.28	0.44	0.39	0.36*	0.00	0.87	0.14	1.25	0.66	0.19	0.50	0.26	0.50
9		1.02*	1.41*	1.02*	1.02*	1.02*	1.02*	0.89*	1.28*	0.00	1.28	0.00	1.28	0.13	1.15	1.28	1.53
		0.13*	0.40*	0.43*	0.59*	0.43*	0.61*	0.51*	0.87*	0.00	0.73	0.40	0.80	0.74	0.61	0.63	0.74
10		0.26	0.13	0.26	0.26*	0.26	0.26	0.38*	0.00	1.28*	0.00	1.28	0.00	1.15	0.13	0.00	0.26
		0.60	0.48	0.32	0.14*	0.30	0.28	0.23*	0.14	0.73*	0.00	1.12	0.59	0.12	0.41	0.14	0.43
11		1.02*	1.41*	1.02*	1.02*	1.02*	1.02*	0.89	1.28*	0.00	1.28*	0.00	1.28	0.13	1.15	1.28	1.53
		0.53*	0.70*	0.80*	0.97*	0.83*	0.94*	0.90	1.25*	0.40	1.12*	0.00	1.03	1.10	0.90	1.00	1.02
12		0.26	0.13	0.26	0.26	0.26	0.26	0.38	0.00	1.28*	0.00	1.28*	0.00	1.15	0.13	0.00	0.26
		0.71	0.41	0.52	0.54	0.63	0.35	0.61	0.66	0.80*	0.59	1.03*	0.00	0.48	0.24	0.49	0.17
13		0.90*	1.28*	0.90*	0.90*	0.90*	0.90*	0.77*	1.15*	0.13	1.15*	0.13	1.15*	0.00	1.02	1.15	1.41
		0.61*	0.43*	0.31*	0.16*	0.34*	0.20*	0.27*	0.19*	0.74	0.12*	1.10	0.48*	0.00	0.31	0.11	0.32
14		0.13	0.26*	0.13	0.13	0.13	0.13**	0.26	0.13	1.15*	0.13	1.15*	0.13	1.02*	0.00	0.13	0.38
		0.50	0.21*	0.28	0.32	0.39	0.13**	0.37	0.50	0.61*	0.41	0.90*	0.24	0.31*	0.00	0.28	0.13
15		0.26	0.13	0.26*	0.26*	0.26*	0.26*	0.38*	0.00	1.28*	0.00	1.28*	0.00	1.15*	0.13	0.00	0.26
		0.50	0.35	0.20*	0.07*	0.23*	0.15*	0.16*	0.26	0.63*	0.14	1.00*	0.49	0.11*	0.28	0.00	0.33
16		0.51	0.13	0.51*	0.51*	0.51*	0.51*	0.64*	0.26	1.53*	0.26	1.53*	0.26*	1.41*	0.38*	0.26	0.00
		0.63	0.34	0.39*	0.38*	0.49*	0.19*	0.45*	0.50	0.74*	0.43	1.02*	0.17*	0.32*	0.13*	0.33	0.00

Table A5 Arrival time difference table of Event 1 for Scale 4 based on kurtosis picks (in seconds)

		Transducer No.														
		1	2	3	4	5	6	7	8	9	10	11	12	13	14	15	16
Transducer No.	1	0.00	0.13	0.13	0.13	0.13	0.13	0.26	0.00	0.51	0.00	1.28	0.13	1.02	0.00	0.00	0.38
		0.00	*0.30*	*0.30*	*0.46*	*0.30*	*0.48*	*0.38*	*0.74*	*0.13*	*0.60*	*0.53*	*0.71*	*0.61*	*0.50*	*0.50*	*0.63*
	2	0.13	0.00	0.26	0.26	0.26	0.00	0.39	0.13	0.38	0.13	1.41	0.00	1.15	0.13	0.13	0.25
		0.30	*0.00*	*0.20*	*0.35*	*0.31*	*0.25*	*0.34*	*0.61*	*0.40*	*0.48*	*0.70*	*0.41*	*0.43*	*0.21*	*0.35*	*0.34*
	3	0.13	0.26*	0.00	0.00	0.00	0.26	0.13	0.13	0.64	0.13	1.15	0.26	0.90	0.13	0.13	0.51
		0.30	*0.20**	*0.00*	*0.18*	*0.12*	*0.21*	*0.14*	*0.45*	*0.43*	*0.32*	*0.80*	*0.52*	*0.31*	*0.28*	*0.20*	*0.39*
	4	0.13	0.26	0.00	0.00	0.00	0.26	0.13	0.13	0.64	0.13	1.15	0.26	0.90	0.13	0.13	0.51
		0.46	*0.35*	*0.18*	*0.00*	*0.18*	*0.20*	*0.10*	*0.28*	*0.59*	*0.14*	*0.97*	*0.54*	*0.16*	*0.32*	*0.07*	*0.38*
	5	0.13	0.26	0.00	0.00	0.00	0.26	0.13	0.13	0.64	0.13	1.15	0.26	0.90	0.13	0.13	0.51
		0.30	*0.31*	*0.12*	*0.18*	*0.00*	*0.30*	*0.08*	*0.44*	*0.43*	*0.30*	*0.83*	*0.63*	*0.34*	*0.39*	*0.23*	*0.49*
	6	0.13	0.00	0.26*	0.26*	0.26	0.00	0.39	0.13	0.38	0.13	1.41	0.00	1.15	0.13	0.13	0.25
		0.48	*0.25*	*0.21**	*0.20**	*0.30*	*0.00*	*0.26*	*0.39*	*0.61*	*0.28*	*0.94*	*0.35*	*0.20*	*0.13*	*0.15*	*0.19*
	7	0.26	0.39*	0.13	0.13*	0.13*	0.39*	0.00	0.26	0.77	0.26	1.02	0.39	0.77	0.26	0.26	0.64
		0.38	*0.34**	*0.14*	*0.10**	*0.08**	*0.26**	*0.00*	*0.36*	*0.51*	*0.23*	*0.90*	*0.61*	*0.27*	*0.37*	*0.16*	*0.45*
	8	0.00	0.13	0.13	0.13	0.13	0.13	0.26	0.00	0.51	0.00	1.28	0.13	1.02	0.00	0.00	0.38
		0.74	*0.61*	*0.45*	*0.28*	*0.44*	*0.39*	*0.36*	*0.00*	*0.87*	*0.14*	*1.25*	*0.66*	*0.19*	*0.50*	*0.26*	*0.50*
	9	0.51*	0.38	0.64*	0.64*	0.64*	0.38	0.77*	0.51	0.00	0.51	1.79	0.38	1.54	0.51	0.51	0.13
		*0.13**	*0.40*	*0.43**	*0.59**	*0.43**	*0.61*	*0.51**	*0.87*	*0.00*	*0.73*	*0.40*	*0.80*	*0.74*	*0.61*	*0.63*	*0.74*
	10	0.00	0.13	0.13	0.13	0.13	0.13	0.26*	0.00	0.51	0.00	1.28	0.13	1.02	0.00	0.00	0.38
		0.60	*0.48*	*0.32*	*0.14*	*0.30*	*0.28*	*0.23**	*0.14*	*0.73*	*0.00*	*1.12*	*0.59*	*0.12*	*0.41*	*0.14*	*0.43*
	11	1.28*	1.41*	1.15*	1.15*	1.15*	1.41*	1.02*	1.28*	1.79*	1.28*	0.00	1.41	0.25	1.28	1.28	1.66
		*0.53**	*0.70**	*0.80**	*0.97**	*0.83**	*0.94**	*0.90**	*1.25**	*0.40**	*1.12**	*0.00*	*1.03*	*1.10*	*0.90*	*1.00*	*1.02*
	12	0.13	0.00	0.26	0.26	0.26	0.00	0.39	0.13	0.38	0.13	1.41*	0.00	1.15	0.13	0.13	0.25
		0.71	*0.41*	*0.52*	*0.54*	*0.63*	*0.35*	*0.61*	*0.66*	*0.80*	*0.59*	*1.03**	*0.00*	*0.48*	*0.24*	*0.49*	*0.17*

Table A5 Arrival time difference table of Event 1 for Scale 4 based on kurtosis picks (in seconds) continued

		Transducer No.														
		1	2	3	4	5	6	7	8	9	10	11	12	13	14	15	16
Transducer No.	13	1.02*	1.15*	0.90*	0.90*	0.90*	1.15*	0.77*	1.02*	1.54*	1.02*	0.25	1.15*	0.00	1.02	1.02	1.41
		0.61*	0.43*	0.31*	0.16*	0.34*	0.20*	0.27*	0.19*	0.74*	0.12*	1.10	0.48*	0.00	0.31	0.11	0.32
	14	0.00	0.13	0.13	0.13	0.13	0.13	0.26	0.00	0.51	0.00	1.28*	0.13	1.02*	0.00	0.00	0.38
		0.50	0.21	0.28	0.32	0.39	0.13	0.37	0.50	0.61	0.41	0.90*	0.24	0.31*	0.00	0.28	0.13
	15	0.00	0.13	0.13	0.13*	0.13	0.13	0.26*	0.00	0.51	0.00	1.28*	0.13	1.02*	0.00	0.00	0.38
		0.50	0.35	0.20	0.07*	0.23	0.15	0.16*	0.26	0.63	0.14	1.00*	0.49	0.11*	0.28	0.00	0.33
	16	0.38	0.25	0.51*	0.51*	0.51*	0.25*	0.64*	0.38	0.13	0.38	1.66*	0.25*	1.41*	0.38*	0.38*	0.00
		0.63	0.34	0.39*	0.38*	0.49*	0.19*	0.45*	0.50	0.74	0.43	1.02*	0.17*	0.32*	0.13*	0.33*	0.00

Table A6 Arrival time difference table of Event 1 for Scale 4 based on skewness picks (in seconds)

		Transducer No.														
		1	2	3	4	5	6	7	8	9	10	11	12	13	14	15	16
Transducer No.	1	0.00	0.13	0.00	0.13	0.13	0.26	0.13	0.00	1.28	0.13	1.28	0.51	1.15	0.38	0.00	0.38
		0.00	0.30	0.30	0.46	0.30	0.48	0.38	0.74	0.13	0.60	0.53	0.71	0.61	0.50	0.50	0.63
	2	0.13	0.00	0.13	0.00	0.26	0.13	0.26	0.13	1.41	0.26	1.41	0.38	1.28	0.25	0.13	0.25
		0.30	0.00	0.20	0.35	0.31	0.25	0.34	0.61	0.40	0.48	0.70	0.41	0.43	0.21	0.35	0.34
	3	0.00	0.13	0.00	0.13	0.13	0.26	0.13	0.00	1.28	0.13	1.28	0.51	1.15	0.38	0.00	0.38
		0.30	0.20	0.00	0.18	0.12	0.21	0.14	0.45	0.43	0.32	0.80	0.52	0.31	0.28	0.20	0.39
	4	0.13	0.00	0.13	0.00	0.26	0.13	0.26	0.13	1.41	0.26	1.41	0.38	1.28	0.25	0.13	0.25
		0.46	0.35	0.18	0.00	0.18	0.20	0.10	0.28	0.59	0.14	0.97	0.54	0.16	0.32	0.07	0.38
	5	0.13	0.26	0.13*	0.26*	0.00	0.38	0.00	0.13	1.15	0.00	1.15	0.64	1.02	0.51	0.13	0.51
		0.30	0.31	0.12*	0.18*	0.00	0.30	0.08	0.44	0.43	0.30	0.83	0.63	0.34	0.39	0.23	0.49
	6	0.26	0.13	0.26*	0.13	0.38*	0.00	0.38	0.26	1.53	0.38	1.53	0.26	1.41	0.13	0.26	0.13
		0.48	0.25	0.21*	0.20	0.30*	0.00	0.26	0.39	0.61	0.28	0.94	0.35	0.20	0.13	0.15	0.19

Table A6 Arrival time difference table of Event 1 for Scale 4 based on skewness picks (in seconds) continued

Transducer No.		1	2	3	4	5	6	7	8	9	10	11	12	13	14	15	16
Transducer No.	7	0.13	0.26	0.13	0.26*	0.00	0.38*	0.00	0.13	1.15	0.00	1.15	0.64	1.02	0.51	0.13	0.51
		0.38	0.34	0.14	0.10*	0.08	0.26*	0.00	0.36	0.51	0.23	0.90	0.61	0.27	0.37	0.16	0.45
	8	0.00	0.13	0.00	0.13	0.13	0.26	0.13	0.00	1.28	0.13	1.28	0.51	1.15	0.38	0.00	0.38
		0.74	0.61	0.45	0.28	0.44	0.39	0.36	0.00	0.87	0.14	1.25	0.66	0.19	0.50	0.26	0.50
	9	1.28*	1.41*	1.28*	1.41*	1.15*	1.53*	1.15*	1.28*	0.00	1.15	0.00	1.79	0.13	1.66	1.28	1.66
		0.13*	0.40*	0.43*	0.59*	0.43*	0.61*	0.51*	0.87*	0.00	0.73	0.40	0.80	0.74	0.61	0.63	0.74
	10	0.13	0.26	0.13	0.26*	0.00	0.38*	0.00	0.13	1.15*	0.00	1.15	0.64	1.02	0.51	0.13	0.51
		0.60	0.48	0.32	0.14*	0.30	0.28*	0.23	0.14	0.73*	0.00	1.12	0.59	0.12	0.41	0.14	0.43
	11	1.28*	1.41*	1.28*	1.41*	1.15*	1.53*	1.15*	1.28*	0.00	1.15*	0.00	1.79	0.13	1.66	1.28	1.66
		0.53*	0.70*	0.80*	0.97*	0.83*	0.94*	0.90*	1.25*	0.40	1.12*	0.00	1.03	1.10	0.90	1.00	1.02
	12	0.51	0.38	0.51	0.38	0.64*	0.26	0.64*	0.51	1.79*	0.64*	1.79*	0.00	1.66	0.13	0.51	0.13
		0.71	0.41	0.52	0.54	0.63*	0.35	0.61*	0.66	0.80*	0.59*	1.03*	0.00	0.48	0.24	0.49	0.17
	13	1.15*	1.28*	1.152*	1.28*	1.02*	1.41*	1.02*	1.15*	0.13	1.02*	0.13	1.66*	0.00	1.54	1.15	1.54
		0.61*	0.43*	0.31*	0.16*	0.34*	0.20*	0.27*	0.19*	0.74	0.12*	1.10	0.48*	0.00	0.31	0.11	0.32
	14	0.38	0.25*	0.38*	0.25	0.51*	0.13**	0.51*	0.38	1.66*	0.51*	1.66*	0.13	1.54*	0.00	0.38	0.00
		0.50	0.21*	0.28*	0.32	0.39*	0.13**	0.37*	0.50	0.61*	0.41*	0.90*	0.24	0.31*	0.00	0.28	0.13
	15	0.00	0.13	0.00	0.13*	0.13	0.26*	0.13	0.00	1.28*	0.13	1.28*	0.51*	1.15*	0.38*	0.00	0.38
		0.50	0.35	0.20	0.07*	0.23	0.15*	0.16	0.26	0.63*	0.14	1.00*	0.49*	0.11*	0.28*	0.00	0.33
	16	0.38	0.25	0.38	0.25	0.51*	0.13	0.51*	0.38	1.66*	0.51*	1.66*	0.13	1.54*	0.00	0.38*	0.00
		0.63	0.34	0.39	0.38	0.49*	0.19	0.45*	0.50	0.74*	0.43*	1.02*	0.17	0.32*	0.13	0.33*	0.00

APPENDIX B.

ALGORITHMS

HEADER FILES

****

WAVELET FUNCTIONS

B1.   class discrete_stationary_wavelet {

public:

//Default Constructor

discrete_stationary_wavelet() { };

//Overload Constructor

discrete_stationary_wavelet(vector<double>   &signal,   string   &wavelet_name,   int decomp_level);

//Destructor

~discrete_stationary_wavelet() { };

//Main DSWT function

vector< vector<double> > compute_DSWT_output();

//Function to compute filter coefficients

int   compute_filt_coeff(string   name,   vector<double>   &low_pass1,   vector<double> &high_pass1, vector<double> &low_pass2, vector<double> &high_pass2);

//Periodic Extension Function. It extends the signal by some specified value in either direction

void compute_periodic_extension(vector<double> &signal, int x);

//Upsampling function

Void   compute_upsample(vector<double>&signal_upsampled,   int   upsample_factor, vector<double> &upsampled_signal);

//Perform the convolution of the signal and the filter

```
Double                perform_conv(vector<double>&conv_signal,vector<double>&vec2,
vector<double> &result);


//Get the length of the signal
int get_signal_length() {return m_length;};
vector< vector<double>>get_approx_coeff() {return m_approx_coef_last_level;};


private:
vector<double> m_signal; int m_decomp_level, m_length;  string m_wavelet_name;
vector< vector<double> > m_approx_coef_last_level; };#endif //DSWT_h


B2.    class Signal_Denoising {
public:
//Default Constructor
Signal_Denoising() {for(unsigned int i=0; i < m_signal.size(); i++)        m_signal[i]   =
0.000; };


//Overload Constructor
Signal_Denoising(vector<double> &signal, int threshold_choice);


//Destructor
~Signal_Denoising() { };


//Denoising Function
vector<double>  Denoised_DSWT(int j);


//Function to find maximum kurtosis
double maximum(vector<double> list, int &index);


//Function to find the slopes of Kurtosis
```

vector<double> slope(vector<double> list, int window_length_M); double Find_sign(double x);

private:

vector<double> m_signal; int m_threshold_choice;};

****

B3.   STATISTICAL FUNCTIONS

template<int N, class T>T nthPower(T x) {T ret = x; for (int i=1; i < N; ++i){ret *= x;} return ret;}

template<class T, int N>struct SumDiffNthPower { SumDiffNthPower(T x) : mean_ (x){};

T operator()(T sum, T current) {return (sum + nthPower<N>(current - mean_)); }

template<class T, int N, class Iter_T>T nthMoment(Iter_T first, Iter_T last, T mean) {size_t cnt = distance(first, last); return (accumulate(first, last, T(), SumDiffNthPower<T, N>(mean)) / cnt);}

template<class T, class Iter_T>T computeVariance(Iter_T first, Iter_T last, T mean){return (nthMoment<T, 2>(first, last, mean));   }

template<class T, class Iter_T>T computeStdDev(Iter_T first, Iter_T last, T mean) {return sqrt(computeVariance(first, last, mean));}

template<class T, class Iter_T>T computeSkew(Iter_T begin, Iter_T end, T mean) {T m3 = nthMoment<T, 3>(begin, end, mean); T m2 = nthMoment<T, 2>(begin, end, mean); return (m3 / (m2 * sqrt(m2))); }

template<class T, class Iter_T> T computeKurtosisExcess(Iter_T begin, Iter_T end, T mean) {T m4 = nthMoment<T, 4>(begin, end, mean); T m2 = nthMoment<T, 2>(begin, end, mean); return ((m4 / (m2 * m2)) - 3);}

```cpp
template<class T, class Iter_T> void computeStats(Iter_T first, Iter_T last, T& sum, T&
mean, T& var, T& std_dev, T& skew, T& kurt)
{size_t cnt = distance(first, last); sum = accumulate(first, last, T()); mean = sum / cnt; var
= computeVariance(first, last, mean); std_dev = sqrt(var); skew = computeSkew(first, last,
mean); kurt = computeKurtosisExcess(first, last, mean); }#endif //statistical_functions_h
```

B4.   PHASE ASSOCIATION

```cpp
Function to read data and perform arrival time difference for automatic picks
vector<vector<double>>get_auto_arrival_time_difference(string
auto_arrival_time_file_name);


Function to read sensor coordinates and perform theoritical arrival time difference
vector<double> get_theoritical_arrival_time(string file_name, double wave_velocity);


int main()
{
/* User Required Input Parameters*/
cout << "Enter the P-wave velocity value :" << endl;
double wave_velocity = 4000;
cin >> wave_velocity;
cout <<" "<< endl;


cout << "Enter the name of file containing the coordinates of the sensors :" << endl;
string coordinate_file_name = "sensor coordinates.txt";
cin >> coordinate_file_name;
cout <<" "<< endl;
cout << "Enter the name of file containing the automatic arrival times :" << endl;
string auto_arrival_time_file_name = "auto_arrival_time.txt";
cin >> auto_arrival_time_file_name;
cout <<" "<< endl;
cout <<"You will be prompted when the program is complete"<< endl;
```

```cpp
cout <<" "<< endl;

vector declarations for storing arrival time difference results
vector<double> limit_vector; //Output for theoritical arrival time
vector<vector<double>> auto_arrival_time_difference; //Output for automatic arrival time diff

//Ouputs for Automatic and Theoretical Arrival Time Difference Values
auto_arrival_time_difference=
get_auto_arrival_time_difference(auto_arrival_time_file_name);
limit_vector = get_theoritical_arrival_time(coordinate_file_name, wave_velocity);

//Output file name for results and writing of results
ofstream auto_arrival_time_L1s("auto_arrival_time_L1s.txt");
ofstream auto_arrival_time_L1k("auto_arrival_time_L1k.txt");
ofstream auto_arrival_time_L2s("auto_arrival_time_L2s.txt");
ofstream auto_arrival_time_L2k("auto_arrival_time_L2k.txt");
ofstream auto_arrival_time_L3s("auto_arrival_time_L3s.txt");
ofstream auto_arrival_time_L3k("auto_arrival_time_L3k.txt");
ofstream theoritical_arrival_time("theoritical_arrival_time.txt");

//Results for theoretical arrival time difference
for (unsigned int i = 0; i < limit_vector.size(); i++){theoritical_arrival_time << limit_vector[i] << endl;}

//Results for automatic arrival time difference
for (unsigned int i = 0; i < auto_arrival_time_difference.size(); i++){if( i == 0)
{
        for(unsigned int j = 0; j < auto_arrival_time_difference[i].size(); j++)
        {
        auto_arrival_time_L1s << auto_arrival_time_difference[i][j] << endl;
```

```cpp
        }
    }
        if( i == 1)
        {
                for(unsigned int j = 0; j < auto_arrival_time_difference[i].size(); j++)
                {
                auto_arrival_time_L1k << auto_arrival_time_difference[i][j] << endl;
                }
        }
        if( i == 2)
        {
                for(unsigned int j = 0; j < auto_arrival_time_difference[i].size(); j++)
                {
                        auto_arrival_time_L2s  <<  auto_arrival_time_difference[i][j]  <<
                        endl;
                }
        }
        if( i == 3)
        {
                for(unsigned int j = 0; j < auto_arrival_time_difference[i].size(); j++)
                {
                        auto_arrival_time_L2k  <<  auto_arrival_time_difference[i][j]  <<
                        endl;
                }
        }
        if( i == 4)
        {
                for(unsigned int j = 0; j < auto_arrival_time_difference[i].size(); j++)
                {
                        auto_arrival_time_L3s  <<  auto_arrival_time_difference[i][j]  <<
                        endl;
```

```
                }
        }
        if( i == 5)
        {
                for(unsigned int j = 0; j < auto_arrival_time_difference[i].size(); j++)
                {
                        auto_arrival_time_L3k  <<  auto_arrival_time_difference[i][j]  <<
                        endl;
                }
        }
}
        cout <<"Program is complete, enter any integer to exit"<< endl;
        int a;
        cin >> a;
        return 0;
}
```

REFERENCES

[1]   H. R. Hardy Jr, *Acoustic emission/microseismic activity: volume 1: principles, techniques and geotechnical applications* vol. 1: CRC Press, 2005.

[2]   M. Ge, "Microseismic Monitoring in Mines," in *Extracting the Science - A Century of Mining Research*, ed: Society for Mining, Metallurgy, and Exploration (SME), 2010, pp. 277-283.

[3]   M. Ge, "Efficient mine microseismic monitoring," *International Journal of Coal Geology,* vol. 64, pp. 44-56, 2005.

[4]   H. Hardy, "Acoustic Emission Microseismic Activity Volume 1: Principles, Techniques and Geotechnical Applications, vol. 1," ed: New York: Taylor & Francis, 2003.

[5]   M. Baer and U. Kradolfer, "An automatic phase picker for local and teleseismic events," *Bulletin of the Seismological Society of America,* vol. 77, p. 1437, 1987.

[6]   W. Blake and D. G. Hedley, *Rockbursts: case studies from North American hard-rock mines*: SME, 2003.

[7]   J. S. Monroe and R. Wicander, *The changing earth: exploring geology and evolution*, Sixth Edition ed.: Cengage Learning, 2011.

[8]   NIOSH. Distribution of Fatalities by Accident Class, Underground Mining Operations [Online].

[9]   I. G. Wong, "Recent developments in rockburst and mine seismicity research," in *The 33th US Symposium on Rock Mechanics (USRMS)*, 1992.

[10]   D. Heal, M. Hudyma, and Y. Potvin, "Evaluating rockburst damage potential in underground mining," in *Golden Rocks 2006, The 41st US Symposium on Rock Mechanics (USRMS)*, 2006.

[11]   H. S. Hasegawa, R. J. Wetmiller, and D. J. Gendzwill, "Induced seismicity in mines in Canada—an overview," *pure and applied geophysics,* vol. 129, pp. 423-453, 1989.

[12] P. Zhang, T. Yang, Q. Yu, T. Xu, W. Zhu, H. Liu, *et al.*, "Microseismicity Induced by Fault Activation During the Fracture Process of a Crown Pillar," *Rock Mechanics and Rock Engineering,* vol. 48, pp. 1673-1682, 2015.

[13] L. Obert, "The microseismic method: discovery and early history," in *First conf. on acoustic emission/microseismic activity in geologic structures and materials*, 1977, pp. 11-12.

[14] N. Cook, "The seismic location of rockbursts," in *Proceedings of the Fifth Rock Mechanics Symposium*, 1963.

[15] F. Leighton and W. I. Duvall, "Least squares method for improving rock noise source location techniques," Bureau of Mines, Washington, DC (USA)1972.

[16] F. Leighton and W. Blake, "Rock noise source location techniques," 1970.

[17] J. Ellenberger, K. Heasley, P. Swanson, and J. Mercier, "Three dimensional microseismic monitoring of a Utah longwall," in *DC Rocks 2001, The 38th US Symposium on Rock Mechanics (USRMS)*, 2001.

[18] W. Gale, K. Heasley, A. Iannacchione, P. Swanson, P. Hatherly, and A. King, "Rock damage characterisation from microseismic monitoring," in *DC Rocks 2001, The 38th US Symposium on Rock Mechanics (USRMS)*, 2001.

[19] M. Kelly, W. Gale, X. Luo, P. Hatherly, R. Balusu, and G. LeBlanc, "Longwall caving process in different geological environments better understanding through the combination of modern assessment methods," in *Proceedings, international conference on geomechanics/ground control in mining and underground construction*, 1998, pp. 573-89.

[20] X. Luo, P. Hatherly, and M. Gladwin, "Application of microseismic monitoring to longwall geomechanics and safety in Australia," in *Paper in Proceedings: 17th International Conference on Ground Control in Mining. August*, 1998, pp. 4-6.

[21] M. Cai, P. K. Kaiser, H. Morioka, M. Minami, T. Maejima, Y. Tasaka, *et al.*, "FLAC/PFC coupled numerical simulation of AE in large-scale underground excavations," *International Journal of Rock Mechanics and Mining Sciences,* vol. 44, pp. 550-564, 2007.

[22] H. Wang and M. Ge, "Acoustic emission/microseismic source location analysis for a limestone mine exhibiting high horizontal stresses," *International Journal of Rock Mechanics and Mining Sciences,* vol. 45, pp. 720-728, 2008.

[23] C. D. Saragiotis, L. J. Hadjileontiadis, I. T. Rekanos, and S. M. Panas, "Automatic P phase picking using maximum kurtosis and κ-statistics criteria," *IEEE Geoscience and Remote Sensing Letters,* vol. 1, pp. 147-151, 2004.

[24] S. W. Stewart, "Real-time detection and location of local seismic events in central California," *Bulletin of the Seismological Society of America,* vol. 67, p. 433, 1977.

[25] R. Allen, "Automatic earthequake recognition and timing from single traces," *Bulletin of the seismological society of America,* vol. 68, pp. 1521-1532, 1978.

[26] A. Ahmed, M. L. Sharma, and A. Sharma, "Wavelet Based Automatic Phase Picking Algorithm for 3-Component Broadband Seismological Data," *Journal of Seismology and Earthquake Engineering,* vol. 9, p. 15, 2007.

[27] R. Allen, "Automatic phase pickers: Their present use and future prospects," *Bulletin of the Seismological Society of America,* vol. 72, p. S225, 1982.

[28] C.-y. Bai and B. L. N. Kennett, "Automatic Phase-Detection and Identification by Full Use of a Single Three-Component Broadband Seismogram," *Bulletin of the Seismological Society of America,* vol. 90, pp. 187-198, 2000.

[29] S. V. Baranov, "Application of the wavelet transform to automatic seismic signal detection," *Izvestiya, Physics of the Solid Earth,* vol. 43, pp. 177-188, 2007.

[30] F. Boschetti, M. Dentith, and R. List, "A fractal-based algorithm for detecting first arrivals on seismic traces," *Geophysics,* vol. 61, pp. 1095–1102, 1996.

[31] F. Botella, J. Rosa-Herranz, J. J. Giner, S. Molina, and J. J. Galiana-Merino, "A real-time earthquake detector with prefiltering by wavelets," *Computers and Geosciences,* vol. 29, pp. 911-919, 2003.

[32] C. Capilla, "Application of the Haar wavelet transform to detect microseismic signal arrivals," *Journal of Applied Geophysics,* vol. 59, pp. 36-46, 2006.

[33] A. Cichowicz, "An automatic S-phase picker," *Bulletin of the Seismological Society of America,* vol. 83, pp. 180-189, 1993.

[34] Z. Chen and R. R. Stewart, "A multi-window algorithm for real-time automatic detection and picking of P-phases of microseismic events," 2006.

[35] C. D. Saragiotis, L. J. Hadjileontiadis, A. S. Savvaidis, C. B. Papazachos, and S. M. Panas, "Automatic S-phase arrival determination of seismic signals using nonlinear filtering and higher-order statistics," in *Geoscience and Remote Sensing Symposium, 2000. Proceedings. IGARSS 2000. IEEE 2000 International*, 2000, pp. 292-294.

[36] P. Bormann, "New manual of seismological observatory practice (NMSOP-2). IASPEI, GFZ German Research Centre for Geosciences, Potsdam," ed, 2012.

[37] T. Elboth, I. Vik Presterud, and D. Hermansen, "Time-frequency seismic data de-noising," *Geophysical Prospecting,* vol. 58, pp. 441-453, 2010.

[38] D. Gabor, "Theory of communication. Part 1: The analysis of information," *Journal of the Institution of Electrical Engineers-Part III: Radio and Communication Engineering,* vol. 93, pp. 429-441, 1946.

[39] K. Zhu, Y. San Wong, and G. S. Hong, "Wavelet analysis of sensor signals for tool condition monitoring: A review and some new results," *International Journal of Machine Tools and Manufacture,* vol. 49, pp. 537-553, 2009.

[40] A. C. To, J. R. Moore, and S. D. Glaser, "Wavelet denoising techniques with applications to experimental geophysical data," *Signal Processing,* vol. 89, pp. 144-160, 2009.

[41] P. Goupillaud, A. Grossmann, and J. Morlet, "Cycle-octave and related transforms in seismic signal analysis," *Geoexploration,* vol. 23, pp. 85-102, 1984.

[42] F. Yan and Z. Chunqin, "A New Seismic Data De-Noising Method Based on Wavelet Transform," 2008, pp. 92-96.

[43] P. Gendron, J. Ebel, and D. Manolakis, "Rapid Joint Detection and Classification with Wavelet Bases via Bayes Theorem," *Bulletin of the Seismological Society of America,* vol. 90, pp. 764-774, 2000.

[44] H. Zhang, C. Thurber, and C. Rowe, "Automatic P-Wave Arrival Detection and Picking with Multiscale Wavelet Analysis for Single-Component Recordings," *Bulletin of the Seismological Society of America,* vol. 93, pp. 1904-1912, 2003.

[45] S. Mallat, *A wavelet tour of signal processing*: Academic press, 1999.

[46] O. Rioul and M. Vetterli, "Wavelets and signal processing," *IEEE signal processing magazine,* vol. 8, pp. 14-38, 1991.

[47]   M. Vetterli and J. Kovacevic, *Wavelets and subband coding*: Prentice-Hall, 1995.

[48]   W. F. Freiberger, "AN APPROXIMATE METHOD IN SIGNAL DETECTION," *Quarterly of Applied Mathematics,* vol. 20, pp. 373-378, 1963.

[49]   T. O. M. Goforth and E. Herrin, "An automatic seismic signal detection algorithm based on the Walsh transform," *Bulletin of the Seismological Society of America,* vol. 71, p. 1351, 1981.

[50]   L. Küperkoch, T. Meier, J. Lee, W. Friederich, and E. W. Grp, "Automated determination of P-phase arrival times at regional and local distances using higher order statistics," *Geophysical Journal International,* vol. 181, pp. 1159-1170, 2010.

[51]   A. Trnkoczy, "Understanding and parameter setting of STA/LTA trigger algorithm," *In: Bormann, P. (Ed.), New Manual of Seismological Observatory Practice 2 (NMSOP-2)* 2012.

[52]   B. K. Sharma, A. Kumar, and V. M. Murthy, "Evaluation of seismic events detection algorithms," *Journal of the Geological Society of India,* vol. 75, pp. 533-538, 2010.

[53]   J. I. Sabbione and D. Velis, "Automatic first-breaks picking: New strategies and algorithms," *Geophysics,* vol. 75, pp. XV67-V76, 2010.

[54]   J. R. Evans and S. S. Allen, "A teleseism-specific detection algorithm for single short-period traces," *Bulletin of the Seismological Society of America,* vol. 73, p. 1173, 1983.

[55]   Z. Chen and R. R. Stewart, "A multi-window algorithm for real-time automatic detection and picking of P-phases of microseismic events," CREWES research report2006.

[56]   M. Withers, R. Aster, C. Young, J. Beiriger, M. Harris, S. Moore*, et al.*, "A comparison of select trigger algorithms for automated global seismic phase and event detection," *Bulletin of the Seismological Society of America,* vol. 88, pp. 95-106, 1998.

[57]   T. Takanami and G. Kitagawa, "A new efficient procedure for the estimation of onset times of seismic waves," *Journal of Physics of the Earth,* vol. 36, pp. 267-290, 1988.

[58]   M. Leonard and B. L. N. Kennett, "Multi-component autoregressive techniques for the analysis of seismograms," *Physics of the Earth and Planetary Interiors,* vol. 113, pp. 247–263, 1999.

[59]   R. Sleeman and T. van Eck, "Robust automatic P-phase picking: An online implementation in the analysis of broadband seismogram recordings," *Physics of Earth and Planet Interiors,* vol. 113, pp. 265–275, 1999.

[60]   T. Takanami and G. Kitagawa, "Estimation of the arrival times of seismic waves by multivariate time series model," *Annals of the Institute of Statistical Mathematics,* vol. 43, pp. 407-433, 1991.

[61]   M. Leonard, "Comparison of Manual and Automatic Onset Time Picking," *Bulletin of the Seismological Society of America,* vol. 90, pp. 1384-1390, 2000.

[62]   T. Diehl, N. Deichmann, E. Kissling, and S. Husen, "Automatic S-Wave Picker for Local Earthquake Tomography," *Bulletin of the Seismological Society of America,* vol. 99, pp. 1906-1920, 2009.

[63]   M. D. McCormack, D. E. Zaucha, and D. W. Dushek, "First-break refraction event picking and seismic data trace editing using neural networks," *Geophysics,* vol. 58, pp. 67-78, 1993.

[64]   H. Dai and C. MacBeth, "Automatic picking of seismic arrivals in local earthquake data using an artificial neural network," *Geophysical Journal International,* vol. 120, pp. 758-774, 1995.

[65]   S. Gentili and A. Michelini, "Automatic picking of P and S phases using a neural tree," *Journal of Seismology,* vol. 10, pp. 39-63, 2006.

[66]   S. E. J. Nippress, A. Rietbrock, and A. E. Heath, "Optimized automatic pickers: Application to the ANCORP data set," *Geophysical Journal International,* vol. 181, pp. 911-925, 2010.

[67]   C. D. Saragiotis, L. J. Hadjileontiadis, and S. M. Panas, "PAI-S/K: A robust automatic seismic P phase arrival identification scheme," *IEEE Transactions on Geoscience and Remote Sensing,* vol. 40, pp. 1395-1404, 2002.

[68]   S. K. Yung and L. T. Ikelle, "An example of seismic time-picking by third-order bicoherence," *Geophysics,* vol. 62, pp. 1947–1952, 1997.

[69]   J. C. Vandecar and R. S. Crosson, "Determination of teleseismic relative phase arrival times using multi-channel cross-correlation and least squares," *Bulletin of the Seismological Society of America,* vol. 80, pp. 150-169, 1990.

[70]   J. B. Molyneux and D. R. Schmitt, "Compressional-wave velocities in attenuating media: A laboratory physical model study," *Geophysics,* vol. 65, pp. 1162-1167, 2000.

[71]   D. Raymer, J. Rutledge, and P. Jaques, "Semi-automated relative picking of microseismic events," *SEG Annual Meeting,* pp. 1411-1414, 2008.

[72]   J. B. Molyneux and D. R. Schmitt, "First-break timing: Arrival onset times by direct correlation," *Geophysics,* vol. 64, pp. 1492–1501, 1999.

[73]   N. Rawlinson and B. L. N. Kennett, "Rapid estimation of relative and absolute delay times across a network by adaptive stacking," *Geophysical Journal International,* vol. 157, pp. 332-340, 2004.

[74]   K. Plenkers, J. R. Ritter, and M. Schindler, "Low signal-to-noise event detection based on waveform stacking and cross-correlation: application to a stimulation experiment," *Journal of seismology,* vol. 17, pp. 27-49, 2013.

[75]   C. Rivero-Moreno and B. Escalante-Ramirez, "Seismic signal detection with time-frequency models," in *Time-Frequency and Time-Scale Analysis, 1996., Proceedings of the IEEE-SP International Symposium on*, 1996, pp. 345-348.

[76]   S. Gabarda and G. Cristóbal, "Detection of events in seismic time series by time-frequency methods," *IET Signal Processing,* vol. 4, pp. 413-420, 2010.

[77]   L. Han, J. Wong, and J. Bancroft, "Time picking and random noise reduction on microseismic data," 2009.

[78]   L. Jiao and W. M. Moon, "Detection of seismic refraction signals using a variance fractal dimension technique," *Geophysics,* vol. 65, pp. 286-292, 2000.

[79]   T. D. Mikesell, K. Van Wijk, E. Ruigrok, A. Lamb, and T. E. Blum, "A modified delay-time method for statics estimation with the virtual refraction," *Geophysics,* vol. 77, pp. A29-A33, 2012.

[80]   S. Gaci, "The Use of Wavelet-Based Denoising Techniques to Enhance the First-Arrival Picking on Seismic Traces," *IEEE Transactions on Geoscience and Remote Sensing,* vol. 52, pp. 4558-4563, 2014.

[81]   F. Li, J. Rich, K. J. Marfurt, and H. Zhou. Automatic event detection on noisy microseismograms [Online].

[82]   J. Tronicke, "The influence of high frequency uncorrelated noise on first-break arrival times and crosshole traveltime tomography," *Journal of Environmental & Engineering Geophysics,* vol. 12, pp. 173-184, 2007.

[83]   A. J. Mendecki, G. V. Aswegen, and P. Mountfort, "A Guide to Routine Seismic Monitoring in Mines," in *A Handbook on Rock Engineering Practice for Tabular Hard Rock Mines*, A. J. Jager and J. A. Ryder, Eds., ed Cape Town: Creda Communications, 1999, pp. 3 - 35.

[84]   R. F. Poplawski, "Seismic parameters and rockburst hazard at Mt Charlotte mine," *International Journal of Rock Mechanics and Mining Sciences,* vol. 34, pp. 1213-1228, 1997.

[85]   A. Iannacchione, G. Esterhuizen, T. Bajpayee, P. Swanson, and M. Chapman, "Characteristics of mining-induced seismicity associated with roof falls and roof caving events," in *Alaska Rocks 2005, The 40th US Symposium on Rock Mechanics (USRMS)*, 2005.

[86]   J. F. Archibald, P. N. Calder, K. Bullock, and D. Madsen, "Development of in-situ rockburst precursor warning systems," *Mining Science and Technology,* vol. 11, pp. 129-152, 1990.

[87]   T. I. Urbancic and C.-I. Trifu, "Recent advances in seismic monitoring technology at Canadian mines," *Journal of Applied Geophysics,* vol. 45, pp. 225-237, 2000.

[88]   P. Hayes, "Moonee Colliery: renewing the economic viability of a mine using microseismic and hydraulic fracturing techniques in massive roof conditions," in *Proceedings of the 19th International Conference on Ground Control in Mining, Morgantown, WV, 8-10 August 2000*, 2001, pp. 38-44.

[89]   K. Mills and R. Jeffrey, "Development of hydraulic fracturing to control windblast," Australian Coal Association Research Program Project C9024 Final Report ACA 1787November 30, 2001 2001.

[90]   J. L. Edwards, "Seismic monitoring for windblast prediction," in *Proceedings of the Seminar on Mine Seismicity and Rockburst Management in Underground Mines, Australian Centre of Geomechanics*, 1998, pp. 2-4.

[91]   V. Brink and A. Newland, "Automatic real time assessment of windblast risk," ACARP End of Grant Report No. C80262002.

[92]   S. Q. Nan, "Investigation on the stability of boundary pillar and mining technology in transition open-pit to underground mine," Northeastern University, Ghina, unpublished|.

[93]   N. Xu, C. Tang, L. Li, Z. Zhou, C. Sha, Z. Liang, *et al.*, "Microseismic monitoring and stability analysis of the left bank slope in Jinping first stage hydropower station in southwestern China," *International Journal of Rock Mechanics and Mining Sciences,* vol. 48, pp. 950-963, 2011.

[94]   K. Tezuka and H. Niitsuma, "Stress estimated using microseismic clusters and its relationship to the fracture system of the Hijiori hot dry rock reservoir," *Engineering Geology,* vol. 56, pp. 47-62, 2000.

[95]   F. Aminzadeh, T. A. Tafti, and D. Maity, "An integrated methodology for sub-surface fracture characterization using microseismic data: A case study at the NW Geysers," *Computers & Geosciences,* vol. 54, pp. 39-49, 2013.

[96]   H. Akaike, "Autoregressive model fitting for control," *Annals of the Institute of Statistical Mathematics,* vol. 23, pp. 163-180, 1971.

[97]   W. H. Lee and S. W. Stewart, *Principles and Applications of Microearthquake Networks*. New York Academic Press, 1981.

[98]   M. Ge, M. Mrugala, and A. T. Iannacchione, "Microseismic Monitoring at a Limestone Mine," *Geotechnical and Geological Engineering,* vol. 27, pp. 325-339, 2009.

[99]   G. P. Nason and B. W. Silverman, "The stationary wavelet transform and some statistical applications," in *Wavelets and statistics*, ed: Springer, 1995, pp. 281-299.

[100]   S. Mallat, "Wavelets for a vision," *Proceedings of the IEEE,* vol. 84, pp. 604-614, 1996.

[101]   S. G. Mallat and S. Zhong, "Characterisation of signals from multiscale edges," *IEEE Transactions on Pattern Analysis and Machine Intelligence,* vol. 14, pp. 710-732, 1992.

[102]   A. P. Bradley, "Shift-invariance in the discrete wavelet transform," *Proceedings of VIIth Digital Image Computing: Techniques and Applications. Sydney,* 2003.

[103]   S. G. Mallat, "A theory for multiresolution signal decomposition: the wavelet representation," *IEEE Transactions on Pattern Analysis and Machine Intelligence,* vol. 11, pp. 674-693, 1989.

[104] D. L. Donoho and I. M. Johnstone, "Adapting to unknown smoothness via wavelet shrinkage," *Journal of the american statistical association,* vol. 90, pp. 1200-1224, 1995.

[105] C. Mborah and M. Ge, "Improving the first-arrival picking in mine microseismic data using a stationary discrete wavelet denoising technique " in *Proceedings of the 1st Int. Conference on Risk and Resilience Mining Solutions 2016*, ed. Vancouver, Canada: InfoMine, 2016, pp. 271-282.

[106] F. J. Gravetter and L. B. Wallnau, *Statistics for the behavioral sciences*: Cengage Learning, 2016.

[107] K. Pearson, "Contributions to the mathematical theory of evolution," *Philosophical Transactions of the Royal Society of London. A,* vol. 185, pp. 71-110, 1894.

[108] K. Pearson, "" Das Fehlergesetz und Seine Verallgemeinerungen Durch Fechner und Pearson." A Rejoinder," *Biometrika,* vol. 4, pp. 169-212, 1905.

[109] M. Ge and P. Kaiser, "Interpretation of physical status of arrival picks for microseismic source location," *Bulletin of the Seismological Society of America,* vol. 80, pp. 1643-1660, 1990.

[110] G. Maochen, "Analysis of source location algorithms Part I: Overview and non~ iterative methods, J," *Acoustic Emission,* vol. 21, pp. 14-24, 2003.

[111] M. Ge, "Optimization of transducer array geometry for acoustic emission/microseismic source location," Ph.D., Department of Mineral Engineering, Pennsylvania State University, Pennsylvania State University, 1988.

[112] M. Ge and H. R. Hardy, "The mechanism of array geometry in the control of AE/MS source location accuracy," in *The 29th US Symposium on Rock Mechanics (USRMS)*, 1988.

[113] B. Li, N. Li, E. Wang, X. Li, Y. Niu, and X. Zhang, "Characteristics of coal mining microseismic and blasting signals at Qianqiu coal mine," *Environmental Earth Sciences,* vol. 76, p. 722, October 28 2017.

[114] N. Li, "Research on Mechanisms of Key Factors and Reliability for Microseismic Source Location[D]," PhD, State Key Laboratory of Coal Resources and Safe Mining, China university of mining and technology, China university of mining and technology, 2014.

VITA

Charles Mborah was born in Akwatia, Ghana. He obtained his Bachelor of Science in mechanical engineering from Kwame Nkrumah University of Science and Technology, Ghana, in 2005. After obtaining his Bachelor's degree, Charles worked for a year as a Teaching Assistant at the University of Mines and Technology (UMaT), Ghana, from August 2005 to August 2006. In September 2006, he accepted admission offer to pursue a Master of Philosophy (MPhil) in mechanical engineering at UMaT. During the study for his MPhil, he obtained admission into Montana Tech. of the University of Montana, USA in 2007 as a short-term scholar. In his career pursuits, Charles worked as a lecturer, assistant lecturer, graduate research assistant and a teaching assistant in the Mechanical Engineering Department of the University of Mines and Technology, Ghana between November 2006 and January 2013. During these periods, he supervised, and also served as an external examiner for many undergraduate research projects in the department. In 2013, he accepted an admission offer to pursue his PhD in mining engineering at Missouri University of Science and Technology (Missouri S&T). However, upon admission, he also enrolled in a Master's Degree (MS) program in geology and geophysics. Charles eventually graduated with an MS degree in geology and geophysics in May 2017 and received his Ph.D. in mining engineering in May 2018.

While at Missouri S&T, Charles worked as a graduate research assistant, teaching assistant and received the award for outstanding graduate research in 2016. Charles was fortunate to have been part of the team of teaching fellows who taught at Saudi Mining Polytechnic (SMP) in the 2013/2014 academic year. On this program, Charles also served as a member of the Curriculum Advisory Steering Committee (CASC) for SMP. On this committee, Charles worked with the sub-committees on SImMentor and Curriculum Integration.